Role of Coxsackie- and adenovirus receptor (CAR) genetic variants, CAR- and adenovirus-based synthetic peptides, and CAR-shedding in CAR-mediated virus entry

Dissertation zur Erlangung des akademischen Grades
Doctor rerum naturalium (Dr. rer. nat.)
der Fakultät für Biologie der Universität Bielefeld

vorgelegt von
Leonie Herrmann

Erstbetreuer: Prof. Dr. rer. nat. Karsten Niehaus

Teile dieser Arbeit wurden veröffentlicht oder zur Veröffentlichung eingereicht:

Herrmann, L., Filip, A., Lapuente, D., Tenbusch, M., Niehaus, K., Rudolph, V., Farr, M. (2020). Naturally occurring variants in the transmembrane and cytoplasmic domains of the human Coxsackie- and adenovirus receptor have no impact on virus internalisation. Biochemical and Biophysical Research Communications *527*, 401–405.
doi: 10.1016/j.bbrc.2020.03.082

Herrmann, L., Schelletter, L., Hoffrogge, R., Niehaus, K., Rudolph, V., Farr, M. Human Coxsackie- and adenovirus receptor is a putative target of neutrophil elastase-mediated shedding. (eingereicht bei Biochimie)

TABLE OF CONTENTS

LIST OF ABBREVIATIONS

A549	carcinoma cells from human lung
ABC	ammonium bicarbonate
ACMG	American college of medical genetics
ACN	acetonitrile
Ad	adenovirus
ADAM	a disintegrin and metalloproteinase
ANOVA	analysis of variance
AP	alkaline phosphatase
A-particle	altered particle
AV	atrioventricular
BCA	bicinchoninic acid
BSA	bovine serum albumin
BT-IgSF	brain- and testis-specific immunoglobulin superfamily protein
CAM	cell adhesion molecule
CAR	Coxsackie- and adenovirus receptor
CDS	coding sequence
CG	cathepsin G
CHL1	close homolog of L1
CHO-CAR	Chinese hamster ovary cells expressing human CAR
CHO-K1	Chinese hamster ovary cells clone K1
CLMP	CXADR-like membrane protein
COI	cytochrome C oxidase 1
CPD	cytoplasmic domain
CREB	c-AMP responsive element binding protein
CREB	cAMP response element-binding protein
CTX	cortical thymocyte marker in *Xenopus*
CVA, B	Coxsackievirus A, B
CXADR	CAR-coding gene
Cy3, Cy7	cyanine 3 and cyanine 7
DAF	decay accelerating factor
DAPI	4′,6-diamidino-2-phenylindole
DCM	dilated cardiomyopathy
DMEM	Dulbecco's modified Eagle medium
DMSO	dimethyl sulphoxide
Dnp	2, 4-dinitrophenyl
Dpa	N-3-(2, 4-dinitrophenyl)-L-2,3-diaminopropionyl
DTT	dithiothreithol
E2F	E2 promotor binding factor
ECD	extracellular domain
ECM	extracellular matrix
EDTA	ethylenediaminetetraacetic acid disodium
ERK	extracellular-signal-regulated kinase
ESAM	endothelial cell selective adhesion molecule
ETS	E26 transformation-specific
FACS	fluorescence-activated cell sorting
FBS	fetal bovine serum
FITC	fluorescein isothiocyanate
FixVi	fixable viability dye
FS	forward scatter
GFP	green fluorescent protein
gnomAD	genome aggregation database

GPI	glycoslphosphatidylinositol
HEK-293	carcinoma cells from human embryonic kidney
HeLa	adenocarcinoma cells from human cervix
hepaCAM	hepatic and glial cell adhesion molecule
HEPES	4-(2-hydroxyethyl)-1-piperazineethanesulfonic acid
HepG2	human hepatocellular carcinoma cells
HIV	human immunodeficiency virus
HRP	horseradish peroxidase
HUVEC	human umbilical vein endothelial cells
ICAM-1	intracellular adhesion molecule 1
IgG1-Fc	immunoglobulin G1 fragment crystallisable region
IgSF	immunoglobulin superfamily
IL-8	interleukin 8
INF-γ	interferon-γ
IPTG	isopropyl β-d-1-thiogalactopyranoside
JAM-A, -B, -C	junctional adhesion molecule A, B, C
JAML	junctional adhesion molecule-like
JNK	c-Jun N-terminal kinase
KO	knockout
LB medium	lysogeny broth medium
LDS	lithium dodecyl sulfate
MAF	minor allele frequency
MAGI-1b	membrane-associated guanylate kinase inverted 1b
MAPK	mitogen-activated protein kinase
Mca	(7-methoxycoumarin-4-yl)acetyl
MEK	mitogen-activated protein kinase kinase
MeOSuc	methoxysuccinyl
MES	2-(N-morpholino)ethanesulfonic acid
MMP	matrix metalloproteinase
MOI	multiplicity of infection
MTT	3-(4,5-dimethylthiazol-2-yl)-2,5-diphenyltetrazolium bromide
MUPP-1	multi-PDZ domain protein 1
NCAM-1	neural adhesion molecule 1
NE	neutrophil elastase
NFκB	nuclear factor 'kappa-light-chain-enhancer' of activated B-cells
NiNTA	nickel nitrilotriacetic acid
nLC-MS/MS	nano liquid chromatography tandem mass spectrometry
Nval	norvaline
PAGE	polyacrylamide gel electrophoresis
PBS	phosphate buffered saline
PDB	protein data bank
PDZ	PSD95/Disc-large/ZO-1
PE	phycoerythrin
PECAM-1	platelet endothelial adhesion molecule 1
PFA	paraformaldehyde
PI3K	phosphoinositide 3-kinases
PICK1	protein interacting with C kinase 1
PIPES	piperazine-N,N′-bis(2-ethanesulfonic acid)
PISA	proteins, interfaces, structures, and assemblies
PMN	polymorphonuclear neutrophils
PMSF	phenylmethylsulfonyl fluoride
pNA	p-nitroanilide
PR3	proteinase 3
PSD-95	postsynaptic density protein 95

PSM	peptide spectrum match
PVDF	polyvinylidene fluoride
PVR	poliovirus receptor
Raf	rapidly accelerated fibrosarcoma
RIP	regulated intramembrane proteolysis
S.O.C.	super optimal broth with catabolite repression
sCAR-Fc	soluble CAR fused to immunoglobulin Fc portion
SDS	sodium dodecyl sulfate
SEM	standard error of the mean
SH3	Src-homology 3
SLAM	signalling lymphocytic activation molecule
Sp1	signal protein 1
SPR	surface plasmon resonance
SS	side scatter
STAT	signal transducer and activator of transcription
Suc	succinyl
SW13	small cell carcinoma cells from human adrenal gland
TBST	Tris-buffered saline with Tween20
TFA	trifluoroacetic acid
TGFβ	transforming growth factor β
TMD	transmembrane domain
TNFα	tumour necrosis factor α
VCAM-1	vascular cell adhesion protein 1
WT	wild type
ZEB1	zinc finger E-box-binding homeobox 1
ZO-1	zonula occludens 1

LIST OF FIGURES

LIST OF TABLES

ABSTRACT

The Coxsackie- and adenovirus receptor (CAR) is a transmembrane cell adhesion molecule with two extracellular immunoglobulin domains. It is located at cell-cell contacts, for example at intercalated discs between cardiomyocytes or at tight junctions in lung and intestines. CAR forms homodimers with its membrane-distal immunoglobulin domain D1 and is involved in cell adhesion, proliferation, and migration. It acts as a pathfinder protein during embryogenesis and during tissue remodelling after injuries. Next to its physiological functions, CAR aroused interest due to its role in cell entry and attachment of Coxsackie- and adenoviruses. Both viruses use CAR D1 as binding site and are a major cause for viral-induced myocarditis.

I investigated three different mechanisms that might influence CAR´s interaction with viruses. First, five genetic variants in the CAR-coding gene that are most frequent in human population were analysed regarding their influence on cell adhesion and proliferation as well as on virus internalisation. No differences were observed among the variants compared to wild type CAR. This gives further evidence to the idea of CAR as an indispensable protein during embryogenesis, for which until now no pathogenic genetic variant has been described.

Second, I designed peptides to use them as virus entry inhibitors. Synthetic peptides that inhibit virus-receptor interactions have not been described for adenoviruses yet. In this work, peptides based on known interaction motifs either of CAR D1 or of adenovirus binding knob were used. No peptide inhibited adenovector cell entry significantly. Probably, peptide binding was too weak to compete with virus-CAR interaction.

Third, several soluble proteases that are secreted by immune cells during myocarditis were tested for their ability to shed CAR, i.e. to release its extracellular domain through proteolysis. Soluble CAR extracellular domain could function as a virus trap and inhibit ongoing viral infections. I used human soluble or membranous CAR expressed by *E. coli* or mammalian cells to screen for potential ectodomain sheddases. For neutrophil elastase, both incubation time and protease concentration comply with a physiologically relevant process. CAR cleavage products comprise complete D1 domain, which could make them biologically active virus traps. Thus, CAR-shedding through neutrophil elastase, which is described here for the first time, might be a host defense mechanism against Coxsackie- and adenoviruses.

1 INTRODUCTION

1.1 The Coxsackie- and adenovirus receptor (CAR)

1.1.1 Protein structure

1.1.1.1 Protein family

CAR is a transmembrane protein with two extracellular immunoglobulin domains (Figure 1). Premature CAR contains a 19 amino acid long signal peptide at its N-terminus, which mediates correct transmembrane localisation (COYNE & BERGELSON 2005). Mature CAR has a size of about 40 kDa, but in a polyacrylamide gel it migrates at a height of about 46 kDa due to N-glycosylation of two residues (EXCOFFON ET AL. 2007; HONDA ET AL. 2000; TOMKO, XU, & PHILIPSON 1997).

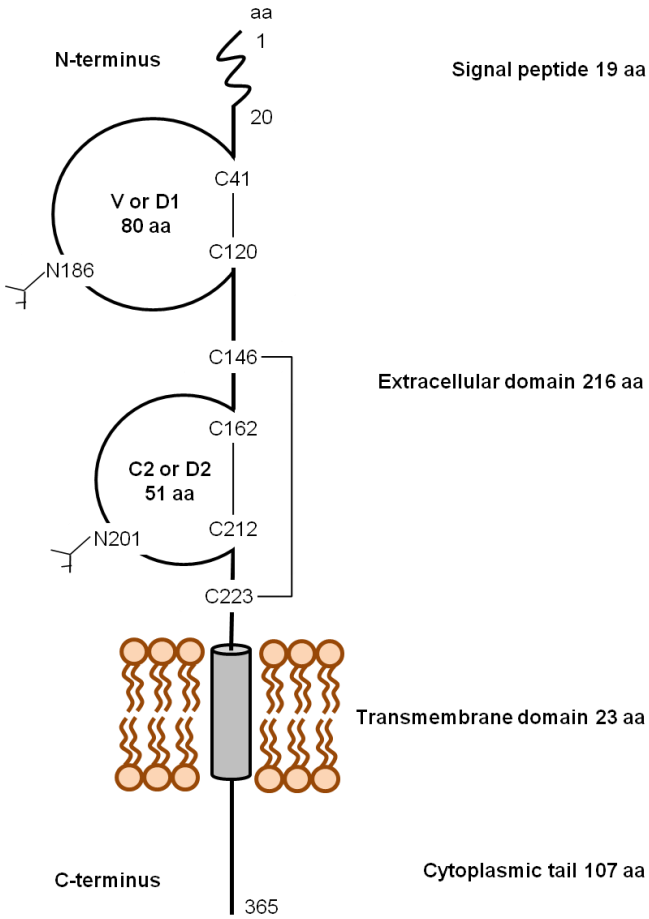

Figure 1: CAR protein structure. CAR is a transmembrane protein with two immunoglobulin domains (V- and C2-type or D1 and D2, respectively) in its extracellular domain (ECD). The N-terminal signal peptide is cleaved off during protein maturation. CAR builds three disulfide bonds and is N-glycosylated at two sites. CAR´s transmembrane domain (TMD) comprises 23 amino acids (aa) and CAR´s C-terminal cytoplasmic domain (CPD) is 107 amino acids long.

CAR is a cell adhesion molecule (CAM) and belongs to the highly conserved cortical thymocyte marker in *Xenopus* (CTX) subfamily of the immunoglobulin superfamily (IgSF) (CHRÉTIEN ET AL. 1996). All CTX proteins display the same protein structure: a signal peptide adjacent to two immunoglobulin-like domains, a type-I transmembrane domain, and a long cytoplasmic tail. The extracellular domain comprises a variable (V) and a constant (C2)-type immunoglobulin domain. C2 domain is defined by an extra pair of cysteines resulting in a second disulfide bonds.

Until now, ten CTX family members have been described and many of them promote cell adhesion and are localised in tight junctions: A33 antigen (HEATH ET AL. 1997), brain- and testis-specific immunoglobulin superfamily protein (BT-IgSF) (SUZU ET AL. 2002), CAR (TOMKO, XU, & PHILIPSON 1997), CAR-like membrane protein (CLMP) (RASCHPERGER ET AL. 2004), CTH (human CTX) (CHRÉTIEN ET AL. 1998), endothelial cell selective adhesion molecule (ESAM) (HIRATA ET AL. 2001), hepatic and glial cell adhesion molecule (hepaCAM) (CHUNG MOH, HOON LEE, & SHEN 2005), and junctional adhesion molecules (JAM-A, -B, and -C) (EBNET ET AL. 2004).

Next to CAR, other IgSF members are exploited as virus receptors: HIV binds CD4; murine hepatitis virus binds carcinoembryonic antigen-related cell adhesion molecule (CEACAM1); herpes simplex virus receptors are nectin-1 and -2; CD46 and signalling lymphocyte-activation molecule (SLAM) are receptors for measles; poliovirus uses poliovirus receptor (PVR); rabies bind neural adhesion molecule (NCAM-1); JAM-A is the reovirus receptor, and intracellular adhesion molecule (ICAM-1) is used by rhinoviruses (DERMODY ET AL. 2009).

CAR homologues are expressed in mammals like mouse (BERGELSON ET AL. 1998; TOMKO, XU, & PHILIPSON 1997), cow (THOELEN ET AL. 2001A), rat, dog, pig (FECHNER ET AL. 1999), and other non-mammalian vertebrates like chicken (PATZKE ET AL. 2010) and zebrafish (PETRELLA ET AL. 2002). In nematodes or *Drosophila*, no homologous protein was identified (COYNE & BERGELSON 2005).

1.1.1.2 Extracellular domain (ECD)

CAR´s immunoglobulin domains are designated D1 and D2. Each domain is important for proper localisation of CAR at cell junctions (EXCOFFON, TRAVER, & ZABNER 2005).

Membrane-distal D1 or V domain mediates homodimer formation, but also virus binding (FREIMUTH ET AL. 1999; HE ET AL. 2001; VAN RAAIJ ET AL. 2000). It displays

one disulfide bond between cysteines 41 and 120 (JIANG ET AL. 2004) and CAR D1 dimer has a dissociation constant of 16±7 µM (VAN RAAIJ ET AL. 2000). Dimerisation (Figure 2) can occur in a head-to-head manner with the CAR monomers localised at one cell (parallel; in cis) or in an anti-parallel manner with CAR monomers expressed on different cells (in trans). Models and binding residues were deduced for both interactions (PATZKE ET AL. 2010; VAN RAAIJ ET AL. 2000). Glycosylation of N106 in D1 domain has no influence on adenovirus or Coxsackievirus binding (EXCOFFON ET AL. 2007; PINKERT ET AL. 2016).

Membrane-proximal D2 or C2 domain contains two disulfide bonds (cysteines 146 and 223, 162 and 212) (JIANG & CAFFREY 2007). It ensures correct orientation and distance to the cell membrane of D1 domain, which is important for Coxsackie- and adenovirus infection (EXCOFFON, TRAVER, & ZABNER 2005). Deglycosylation of N201 resulted in increased Coxsackie- and adenovirus infections (EXCOFFON ET AL. 2007; PINKERT ET AL. 2016).

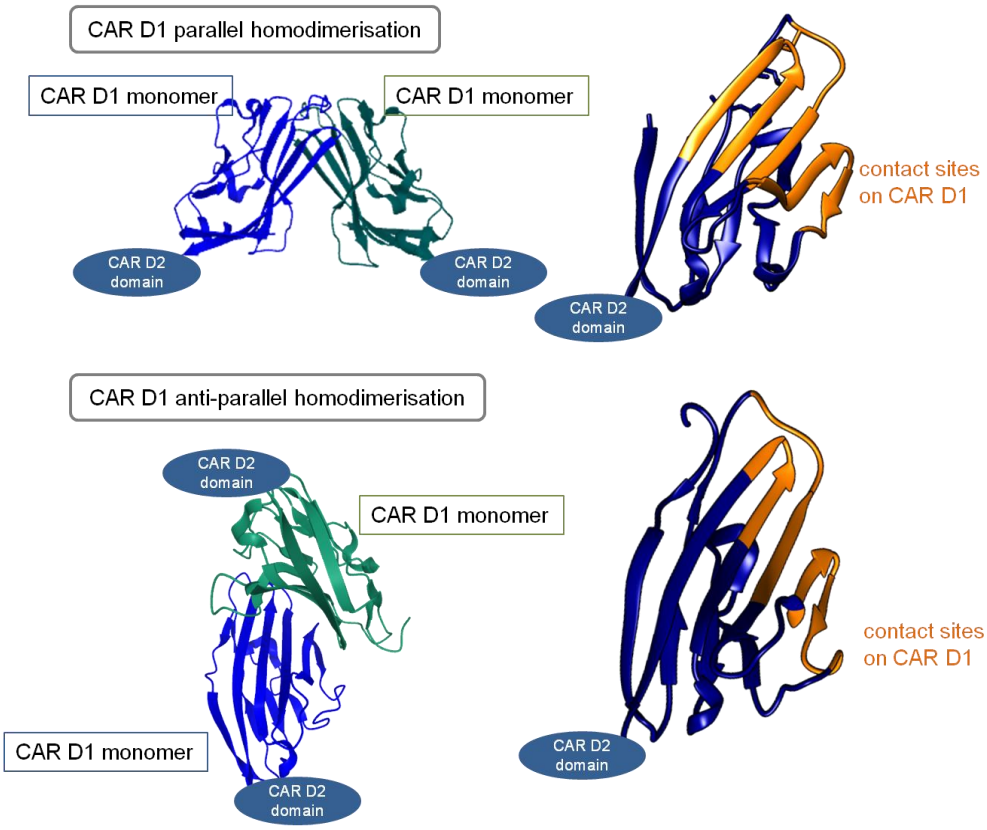

Figure 2: Models of CAR-CAR homodimerisation. Two CAR D1 monomers dimerise either in a parallel (top, PDB ID: 3JZ7, (PATZKE ET AL. 2010)) or anti-parallel manner (bottom, PDB ID: 1EAJ, (VAN RAAIJ ET AL. 2000)). Contact sites on D1 are coloured in orange. CAR D2 domain is added to show orientation of the complexes.

1.1.1.3 Transmembrane and cytoplasmic domain (TMD and CPD)

Neither the transmembrane nor the cytoplasmic domain is necessary for mediating Coxsackie- or adenovirus infection as was shown with two CAR constructs. The first construct lacks CAR´s CPD except for the cysteines at positions 259 and 260. The second construct is a fusion protein of CAR´s ECD fused to a glycosylphosphatidylinositol (GPI)-anchor, which mediates plasma membrane localisation. Both constructs facilitated Coxsackie- and adenovirus infections *in vitro* and *in vivo* (VAN'T HOF & CRYSTAL 2001; NALBANTOGLU ET AL. 1999; OKEGAWA ET AL. 2001; TALLONE ET AL. 2001; WALTERS ET AL. 2001; WAN ET AL. 2000; WANG & BERGELSON 1999).

CAR´s CPD is crucial for correct localisation at cell-cell contacts in non-polarised cells (COHEN ET AL. 2001A; EXCOFFON, MONINGER, & ZABNER 2003) and at the basolateral site of polarised cells (COHEN ET AL. 2001B; WALTERS ET AL. 2001). Furthermore, CAR lacking its CPD mislocalised in an *in vivo* model (RASCHPERGER ET AL. 2006). Total protein expression level was increased for CAR missing its TMD or its CPD (VAN'T HOF & CRYSTAL 2001) and the growth inhibitory effect of CAR (see 1.1.3.1) was lost for CAR without TMD and CPD (OKEGAWA ET AL. 2000, 2001).

CAR´s CPD displays several functional motifs (Figure 3). Two membrane-proximal cysteines (positions 259 and 260) are posttranslationally palmitylated, which is important for correct CAR membrane localisation, but not for adenovirus binding (VAN'T HOF & CRYSTAL 2002). CAR phosphorylation mediated by TNFα-signalling and PKCδ is necessary for CAR-dependent epithelial junction stability (MORTON ET AL. 2013). Upon lung inflammation in a murine model, level of phosphorylated CAR increased (MORTON ET AL. 2016). Regions for basolateral targeting in polarised epithelial cells (318-321 and 345-349) were defined by site-directed mutagenesis (CARVAJAL-GONZALEZ ET AL. 2012; COHEN ET AL. 2001B). Amino acids 333-337 are an SH3 domain recognition motif (COHEN ET AL. 2001A) and CAR´s most C-terminal amino acids are a PSD-95/Disc-large/ZO-1 (PDZ)-binding domain that is important for CAR-mediated cell adhesion (EXCOFFON ET AL. 2004). Several interaction partners containing a PDZ domain were identified: LNX1, LNX2, MAGI-1b, MUPP-1, PICK1, PSD-95, and ZO-1 (COHEN ET AL. 2001B; COYNE ET AL. 2004; EXCOFFON ET AL. 2004; MIRZA ET AL. 2005; SOLLERBRANT ET AL. 2003). Other CAR intracellular interaction partners are actin (HUANG ET AL. 2007) and microtubules (FOK ET AL. 2007). CAR is part of a multiprotein complex

that contains ZO-1, β-catenin, and connexin 45 *in vivo* (LIM ET AL. 2008). Figure 3 shows localisation of amino acids that were investigated in this study (see 1.4.1).

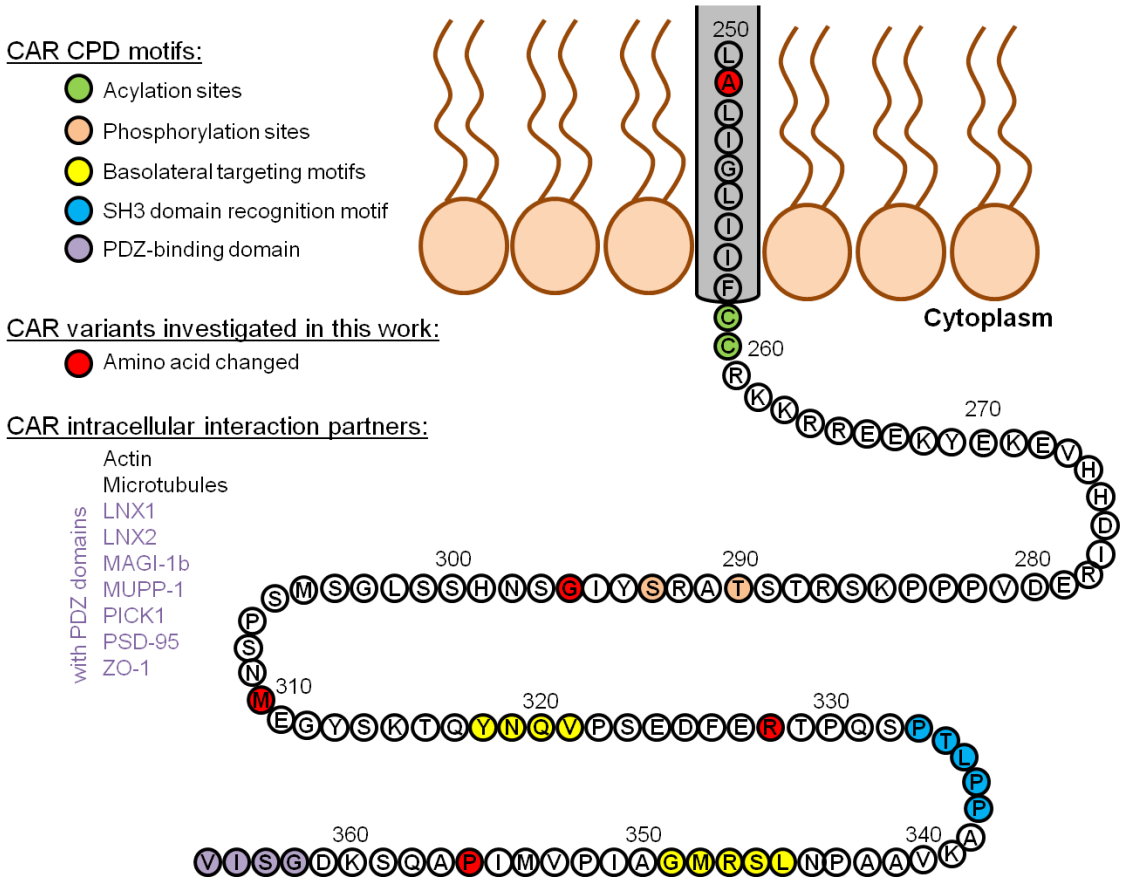

Figure 3: Schematic representation of CAR´s TMD and CPD. Residues that are post-translationally modified as well as motifs important for intracellular interaction and protein localisation are coloured. Amino acids that were changed via site-directed mutagenesis and investigated in this work (Table 1) are depicted in red. Known intracellular interaction partners of CAR are listed.

1.1.2 *CXADR* gene structure

1.1.2.1 Alternative splicing

CAR-coding gene *CXADR* is located on human chromosome 21. Four pseudogenes were identified on chromosomes 15, 18, and 21 (BOWLES ET AL. 1999). Several CAR mRNA species were found in human tissues with sizes ranging from 1.3 to 7 kb (FECHNER ET AL. 1999; TOMKO, XU, & PHILIPSON 1997).

CAR´s main splice isoform (CAREx7) comprises seven exons with a coding DNA sequence of 1098 bp (Figure 4). Exon 1 codes for most of CAR´s signal peptide. Rest of the signal peptides and the two immunoglobulin domains are encoded by exons 2-5.

Exon 6 encodes the TMD and the first part of the CPD. Remaining CPD is encoded by exon 7 (BOWLES ET AL. 1999).

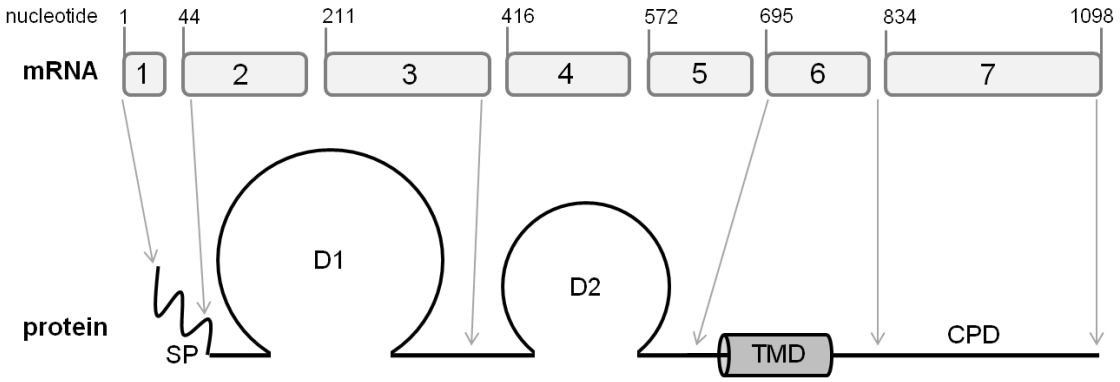

Figure 4: *CXADR* exons with nucleotide numbering and corresponding CAR protein domains. Exon 1 and part of exon 2 code for the signal sequence. Extracellular D1 domain originates from the rest of exon 2 and exon 3 and D2 domain is coded by exons 4 and 5. Exon 6 gives rise to the transmembrane domain (TMD) and the first part of the cytoplasmic domain (CPD). Rest of CPD is encoded by exon 7. Compare Figure 1 in Appendix for correlation between *CXADR* exons and CAR´s amino acid sequence.

CXADR is alternatively spliced resulting in another membranous isoform and three soluble isoforms lacking TMD (Figure 5). CAREx7 is encoded by exons 1 to 7, whereas in CAREx8, exon 8 is spliced to the first 183 bp of exon 7. Thereby, CAREx7 and CAREx8 differ only in their last amino acids at the C-terminus (BERGELSON ET AL. 1998). In men, CAREx7 is also called hCAR1, CARα or SIV (last C-terminal amino acids) and CAREx8 is also named hCAR2 or TVV. In mice, the nomenclature is interchanged by naming the shorter isoform mCAR1 and the longer one mCAR2. For clarification, I will use the terms CAREx7 and CAREx8. Isoforms β or CAR4/7, γ or CAR2/7, and δ or CAR3/7 are soluble (DÖRNER ET AL. 2004; THOELEN ET AL. 2001B). Splicing results in premature stop codons due to frameshifts. Isoforms CAR4/7 and CAR 2/7 use the canonical splice sites, whereas in CAR3/7, the first 21 nucleotides of exon 3 are fused to the last 97 nucleotides of exon 7.

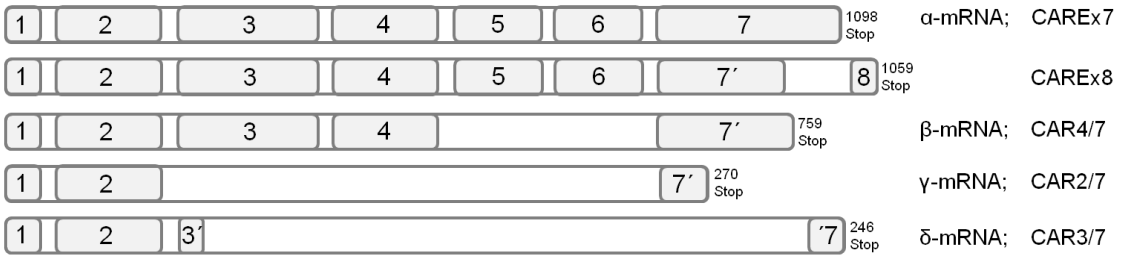

Figure 5: *CXADR* splice isoforms. Two protein isoforms are membrane-bound (CAREx7 and CAREx8) and three are soluble (CAR2/7, CAR3/7, and CAR4/7).

CAREx7 and CAREx8 mRNA species were found in human brain, heart, kidney, liver, lung, pancreas, placenta, and spleen (ANDERSSON ET AL. 2000; THOELEN ET AL. 2001B). In mice, both protein isoforms co-express at most epithelial contacts of the body cavities (RASCHPERGER ET AL. 2006). Since the extracellular domains of the isoforms are identical, both serve as virus receptors. However, in polarised airway epithelium, CAREx8 is expressed apically, whereas CAREx7 is located basolaterally. Thereby, only CAREx8 may be accessible for viruses *in vivo* (EXCOFFON ET AL. 2010). In other tissues and cells like endometrium, spermatozoa, skeletal and cardiac muscle, CAREx7 and CAREx8 expression pattern also differs, indicating varying functions (BEAUPARLANT, READ, & DI CRISTOFANO 2004; MIRZA ET AL. 2006; SHAW ET AL. 2004).

Soluble isoforms bind CAR ECD and Coxsackieviruses via their D1 domain (DÖRNER ET AL. 2004) and mRNA species were identified in several human tissues (THOELEN ET AL. 2001B). Proteins of the soluble isoforms are differentially regulated in ovarian and breast cancer and upon development of human preimplantation embryos (AUER ET AL. 2009; KRIVEGA, GEENS, & VAN DE VELDE 2014; REIMER ET AL. 2007). Nevertheless, the exact physiological function of the soluble isoforms is still unclear.

1.1.2.2 Expression regulation

CXADR transcription is initiated around 150 bp upstream of the ATG start codon and a promotor sequence is located at position -585 to -400 bp. A putative silencing region at -127 to -18 bp and binding sites for transcription binding factors Sp1, E2F, NFκB, STAT are also present (PONG ET AL. 2003; VINCENT ET AL. 2004). Lacher et al. located the *CXADR* core promotor within 291 bp upstream of the start codon and found putative binding sites for ETS and CREB transcription factors. In pancreatic and breast cancer cells, the E2 box-binding factor ZEB1 downregulated CAR expression (LACHER ET AL. 2011). Transcriptional complex Smad2/3/4 with transcription factor Snail1 interacts

with *CXADR* promotor and represses CAR levels (VINCENT ET AL. 2009). *CXADR* transcription seems to be regulated by epigenetic chromatin remodelling as CAR mRNA and protein levels were upregulated by several histone deacetylase inhibitors *in vitro* and *in vivo* (GOLDSMITH ET AL. 2007; KITAZONO ET AL. 2002; OKEGAWA ET AL. 2007; SEGURA-PACHECO ET AL. 2007). Furthermore, CAR expression regulation was linked to MAPK signalling cascades like the p38, Raf/MEK/ERK, and PI3K pathways. *In vivo*, a p38 inhibitor decreased CAR levels in mice infected with Coxsackieviruses (NIU ET AL. 2017). Inhibition of MEK activity led to elevated CAR levels in carcinoma cell lines (ANDERS ET AL. 2003; BAGHERI ET AL. 2011) and Raf activation as well as PI3K inhibition resulted in lower CAR levels (ANDERS ET AL. 2003).

Interestingly, CAR expression itself influences MAPK pathways as was shown *in vitro* and *in vivo*. CAR overexpression in murine adult heart and isolated cardiomyocytes led to JNK, p38, and ERK1/2 activation (YUEN ET AL. 2011). CAR overexpression activated AKT in developing mice heart (CARUSO ET AL. 2010) and upregulated ERK1/2 in epithelial cells (FARMER ET AL. 2009). CAR knockout (KO) in a human epidermal cell line resulted in Src and p38 activation (SU ET AL. 2016). The CAR-mediated intracellular signalling towards the MAPK pathways seems to be triggered by binding to its extracellular part. This was observed for homodimerisation *in cis* (FARMER ET AL. 2009) and junctional adhesion molecule-like protein (JAML) binding, which induced T cell activation (VERDINO ET AL. 2010; WEBER ET AL. 2014; WITHERDEN ET AL. 2010).

As MAPK pathways provide inflammatory signals, CAR signalling may be capable to induce an inflammatory response. Coxsackie- and adenovirus infections led to induction of the MAPK signal pathways (BRUDER & KOVESDI 1997; HUBER ET AL. 1999; OPAVSKY ET AL. 2002; TAMANINI ET AL. 2006), thereby triggering inflammatory responses as well as CAR upregulation.

The anti-inflammatory agent dexamethasone as well as cytokines TNFα, TGFβ, INF-γ and chemokine IL-8 influenced CAR levels (BRÜNING & RUNNEBAUM 2003; GAO & LUI 2014; KOTHA ET AL. 2015; LACHER ET AL. 2006, 2011; VINCENT ET AL. 2004). A drug against hypercholesterolemia and two anti-hypertensive drugs reduced CAR surface expression in human umbilical vein endothelia cells (HUVECs) (FUNKE ET AL. 2010; WERNER ET AL. 2014). CAR levels were upregulated with increasing confluency of HUVECs and cardiomyocytes (CARSON ET AL. 1999; ITO ET AL. 2000). Furthermore, fluid and heat stress influenced CAR levels (CHUNG ET AL. 2019; DENG ET AL. 2013).

1.1.3 Physiological functions and expression pattern

1.1.3.1 Cell adhesion molecule (CAM)

Until now, CAR´s physiological role is not completely understood. As it mediates cell adhesion, it is involved in multiple processes ranging from tumour growth and neutrophil transmigration to embryonic development.

CAR is a cell adhesion molecule and forms homodimers with its ECD. In cultured epithelial cells, CAR overexpression increases homophilic cell interactions (COHEN ET AL. 2001A). In human airway epithelia, transepithelial resistance correlates with CAR expression levels (EXCOFFON ET AL. 2004) and CAR is localised at the basolateral sites of polarised cells (EXCOFFON, TRAVER, & ZABNER 2005; PICKLES ET AL. 2000; WALTERS ET AL. 1999). *In vivo*, CAR protein is expressed in epithelial cells of all body tissues, the intercalated discs of cardiomyocytes, but not in the vasculature system or smooth muscle cells (KASHIMURA ET AL. 2004; RASCHPERGER ET AL. 2006). In adult human tissue, CAR mRNA was detected in heart, brain, pancreas, liver, lung, kidney, small intestine, testis, and prostate, but not in placenta, thymus, skeletal muscle, and spleen (BERGELSON ET AL. 1998; FECHNER ET AL. 1999; TOMKO ET AL. 2000; TOMKO, XU, & PHILIPSON 1997).

Probably due to its interaction with cytoskeleton proteins (FOK ET AL. 2007; HUANG ET AL. 2007), CAR influences cell properties like proliferation and migration. On the one hand, CAR overexpression in cell lines leads to increased cell aggregation, more cell-cell contacts, and growth inhibition (BRÜNING & RUNNEBAUM 2004; CHEN ET AL. 2013; OKEGAWA ET AL. 2000). CAR downregulation, on the other hand, enhances cell proliferation and migration and inhibits cell adhesion (COHEN ET AL. 2001A; STECKER ET AL. 2009). CAR KO results in increased wound healing *in vivo* (SU ET AL. 2016).

CAR is involved in T cell activation and polymorphonuclear neutrophils (PMN) transmigration through JAML interaction (WITHERDEN ET AL. 2010; ZEN ET AL. 2005). Besides, it forms the blood-testis-barrier (HUANG ET AL. 2019), and facilitates neurogenesis and synapse homeostasis (PATZKE ET AL. 2010; ZUSSY ET AL. 2016). CAR may also play a role in tumour progression. Tumour tissue displays both CAR upregulation and CAR downregulation in comparison to healthy tissues (REEH ET AL. 2013). It was suggested that CAR might be a tumour progression marker, but also a tumour suppressor depending on affected tissue and disease state. CAR downregulation decreases cell

adhesive properties of the tumour and results in metastasis formation. Metastasis cells might then upregulate CAR expression to facilitate colonisation (NOVAK 2002; STECKER ET AL. 2011).

CAR is essential for correct conduction in the heart, probably due to its adhesive role at intercalated discs and the atrioventricular (AV) node. Homozygous inducible CAR KO (germline and cardiomyocyte-specific) in adult mice results in AV block. Connexin 45, β-catenin, and ZO-1 are mislocalised in AV node and intercalated discs in CAR KO hearts. Affected mice develop cardiomyopathy (LIM ET AL. 2008; LISEWSKI ET AL. 2008; PAZIRANDEH ET AL. 2011). Mice with a heterozygous CAR KO show no spontaneous arrhythmias. However, sodium currents are reduced at intercalated discs. CAR immunoprecipitates with Nav1.5 sodium channel *in vitro* (MARSMAN ET AL. 2014). CAR overexpression (skeletal-muscle or cardiac-specific) in adult mice results in a lethal phenotype (CARUSO ET AL. 2010; SHAW ET AL. 2006), indicating that CAR is also important for tissue homeostasis.

1.1.3.2 Pathfinder protein during embryogenesis and in disease states

CAR´s spatiotemporal regulation (high levels during embryogenesis, decreasing expression in the adult, and upregulation during tissue disease) suggests that it might act as a pathfinder protein.

CAR KO models elucidate CAR´s involvement in morphogenesis and differentiation during embryogenic development. CAR KO mice die during midgestation at embryonic day E11.5 and suffer from cardiac defects including hyperplasia of left ventricular myocardium, pericardial oedema, and haemorrhages. Cardiomyocytes undergo apoptosis and have disorganised myofibrils. Cell-cell contacts between cardiomyocytes are short or even absent (ASHER ET AL. 2005; CHEN ET AL. 2006; DORNER ET AL. 2005). The important function of CAR for embryonic heart development is emphasised by cardiomyocyte-specific CAR KO at E9.5, which mimics the lethal phenotype observed for germline CAR KO. However, when CAR is deleted in cardiomyocytes at E11, mice survive to adulthood indicating a temporal window, in which CAR expression is crucial for heart development. CAR may regulate proliferation of cardiomyocytes (CHEN ET AL. 2006). Total CAR KO with CAR re-expression solely in the heart rescues mice (FREIBERG ET AL. 2014).

Next to CAR´s essential role in heart development, it is also involved in formation of other organ systems during embryogenesis: In a zebrafish CAR KO model, kidney development is impaired (RASCHPERGER ET AL. 2008). However, a murine podocyte-specific CAR KO model shows no influence on kidney formation (SCHELL ET AL. 2015). CAR KO in adult mice results in pancreas atrophy and enlarged intestines and thymus (PAZIRANDEH ET AL. 2011). CAR KO at E12.5 leads to insufficient separation of blood and lymphatic vessel systems resulting in embryonic death (MIRZA ET AL. 2012). In addition, CAR expression facilitates cell-cell contacts in pre-implantation blastocysts (JEONG ET AL. 2019; KWON, KIM, & CHOI 2016).

CAR is significantly downregulated postnatally, for example in brain (HOTTA ET AL. 2003), nervous system (AHN ET AL. 2008; PATZKE ET AL. 2010), lung (SUN ET AL. 2012), bladder (GYE ET AL. 2011), skeletal muscle (NALBANTOGLU ET AL. 1999), olfactory bulb (VENKATRAMAN ET AL. 2005), and heart (ITO ET AL. 2000). During differentiation of human embryonic stem cells and preimplantation embryos, CAR is downregulated (KRIVEGA, GEENS, & VAN DE VELDE 2014).

CAR is re-expressed during disease conditions. Upon differentiation, cells loose CAR (HIDAKA ET AL. 1999; HUNG ET AL. 2004; HUTCHIN, PICKLES, & YARBROUGH 2000; REBEL ET AL. 2000) and upregulation may facilitate tissue repair by recreating an embryonic expression pattern. This was observed in regenerating skeletal muscle fibers (SINNREICH ET AL. 2005) and heart muscle after myocardial infarction (FECHNER ET AL. 2003). When rat carotid arteries were injured, CAR expression in vascular smooth muscle cells increased (NASUNO ET AL. 2004). CAR is also upregulated in myocardial biopsy samples from patients with dilated cardiomyopathy, inflammatory cardiomyopathy, aortic valve disease, or mitral valve disease compared to samples from healthy donor hearts (NOUTSIAS ET AL. 2001; SASSE ET AL. 2003; TATRAI ET AL. 2011; TOIVONEN ET AL. 2010). In rats with experimental autoimmune myocarditis, CAR levels also increase (ITO ET AL. 2000).

1.1.4 Virus receptor

1.1.4.1 Accessibility for viruses

As CAR, many other CAMs act as virus receptors (see 1.1.1.1). Viruses take advantage of the adhesive properties of these proteins and benefit from the high evolutionary conservation of the extracellular domains. This is underlined by the observation that adeno-

viruses and picornaviruses of many species are able to bind murine or human CAR: dogs (SOUDAIS ET AL. 2000), fowl (TAN ET AL. 2001), chimpanzees (COHEN ET AL. 2002), bats (KOBAYASHI ET AL. 2019), and pigs (MARTINO ET AL. 2000). Both Coxsackie- and adenoviruses use CAR´s extracellular D1, which is important for homodimerisation (see 1.1.1.2). Mutations that reduce virus attachment could also affect CAR´s physiological function and are less likely to occur.

Generally, CAR expression levels correlate with susceptibility of cells or tissue towards virus infection. This was observed in cancer cells (OKEGAWA ET AL. 2000; QIN ET AL. 2003; YOU ET AL. 2001), cultured cardiomyocytes (FECHNER ET AL. 2007; NOUTSIAS ET AL. 2001), muscle fibers (NALBANTOGLU ET AL. 2001), and murine models, which overexpressed CAR in heart, pancreas, or T and B lymphocytes (KALLEWAARD ET AL. 2009; SCHMIDT ET AL. 2000; SHI ET AL. 2009).

The susceptibility of mouse and rat tissues towards adenovector transduction does not always correlate with CAR expression levels (FECHNER ET AL. 1999). As CAR localises at junctions between adjacent cells, it is normally inaccessible for viruses. In polarised epithelial cells and freshly excised human airway epithelium, CAR expression is limited to basolateral sites and adenovirus infections are inefficient from the apical site (COHEN ET AL. 2001A; PICKLES ET AL. 2000; SHIEH & BERGELSON 2002; WALTERS ET AL. 1999; ZABNER ET AL. 1997). When tight junctions were disrupted by addition of histamine, trypsin, or EDTA, CAR was accessible and virus infection was facilitated (BRÜNING & RUNNEBAUM 2003; COHEN ET AL. 2001A; SHARMA ET AL. 2012; WALTERS ET AL. 1999; ZABNER ET AL. 2003). *In vivo*, Coxsackie- and adenoviruses may overcome this constraint by binding their co-receptors, DAF and integrins, which are expressed apically (ANDERSON, JOHNSON, & HAGEMAN 1995; SHIEH & BERGELSON 2002). Furthermore, CAREx8 isoform localises at low expression levels at the apical surface of human airway epithelial cells and facilitates viral entry (EXCOFFON ET AL. 2010; KOLAWOLE ET AL. 2012). Once a tissue is infected, newly synthesised virions and adenovirus fibers are released on basolateral sites, where they bind CAR. This disrupts cell-cell contacts and allows virus spreading (WALTERS ET AL. 2002).

1.1.4.2 Coxsackievirus receptor

Human Coxsackieviruses belong to the family *Picornaviridae* and the genus *Enterovirus*. They are non-enveloped, icosahedral, positive-stranded RNA viruses and are classi-

fied in two groups A (CVA) and B (CVB). CVA mainly cause gastrointestinal illness, whereas CVB also infect respiratory tract, eyes, skin, pancreas, myocardium, or pericardium. Infections cause febrile illness, meningoencephalitis, myocarditis, pancreatitis, or hand, foot, and mouth disease. Several infections, however, are asymptomatic. Coxsackievirus transmission occurs mostly by faecal-oral route or by droplet inhalation (MUEHLENBACHS, BHATNAGAR, & ZAKI 2015).

CVB1, 3, and 5 serotypes use decay accelerating factor (DAF) for cell-attachment (SHAFREN ET AL. 1995) and all six CVB serotypes bind CAR for cell entry (MARTINO ET AL. 2000). CAR D1 domain binds mainly viral protein VP1 at the fivefold viral vertices (Figure 6). CVB contact sites on CAR D1 (Figure 2 in Appendix) differ from residues involved in homodimer and adenovirus binding (Figure 17). Affinity of D1 domain to CVB (K_d=0.25 µM) is lower than for adenovirus binding, but higher than for D1 homophilic interaction (GOODFELLOW ET AL. 2005). Upon CAR-interaction, CVB form altered (A)-particles. A-particles are a crucial intermediate for virus uncoating, but cannot bind to cells anymore (GOODFELLOW ET AL. 2005; MILSTONE ET AL. 2005). In contrast to CAR, DAF alone is insufficient for virus infection (SHAFREN, WILLIAMS, & BARRY 1997).

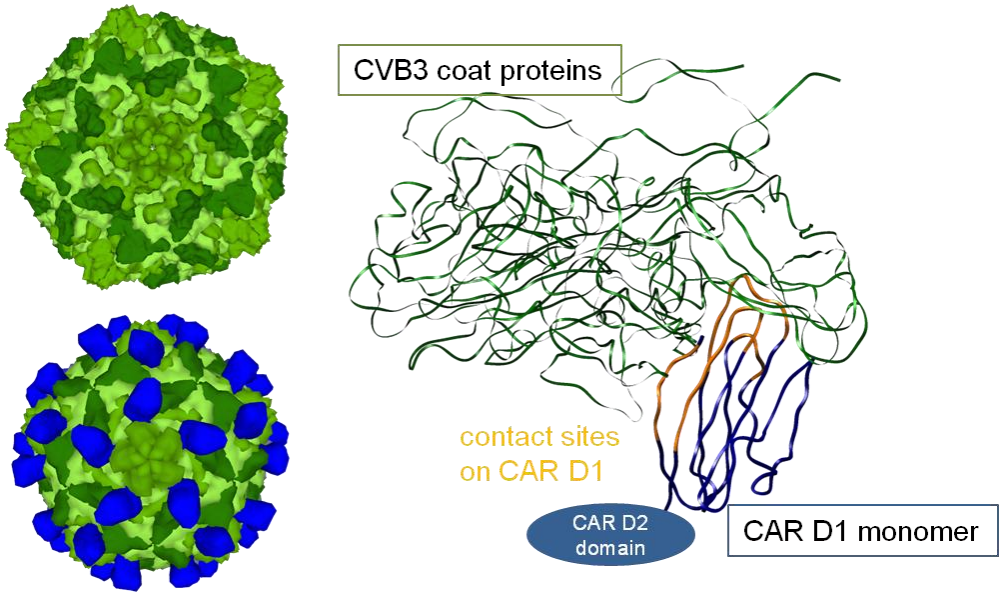

Figure 6: Coxsackievirus structure and model of CAR D1-CVB3 interaction. Left: Coxsackievirus icosahedral capsids comprise of four proteins (VP1-4) and have a diameter of about 30 nm (modified from PDB ID: 1COV (MUCKELBAUER ET AL. 1995)). Each depression (canyon) that surrounds the viral fivefold symmetry axes of CVB3 (green) interacts with a CAR D1 domain (blue). Right: Contact sites with CVB3 coat proteins on CAR D1 domain are coloured in orange (PDB ID: 1JEW; (HE ET AL. 2001)). CAR D2 domain is added to show orientation of the complex.

1.1.4.3 Adenovirus receptor

Human adenoviruses belong to the *Adenoviridae* family and consist of more than 50 types and 7 species (A-G). They have an icosahedral capsid comprising hexon and fiber proteins. Fibers protrude from each penton base of the twelve vertices (Figure 7). Adenoviruses are non-enveloped, double-stranded DNA viruses. Most frequently, adenoviruses infect the upper and lower respiratory tract, the conjunctiva, and the gastrointestinal tract. Febrile respiratory disease, keratoconjunctivitis, and diarrheal illness can ensue. More rarely, viruses cause encephalitis, myocarditis, and meningitis. Infections can also be asymptomatic. Adenoviruses are transmitted via faecal-oral route, inhalation of aerosols, and smear infections (LYNCH & KAJON 2016).

Adenoviruses of all species, except B, use CAR as attachment receptor. They bind to the D1 domain with their fiber knob domain (ARNBERG 2012). For cell entry, adenoviruses bind αv integrins with their penton base, which induces virus fiber shedding and uncoating (BURCKHARDT ET AL. 2011).

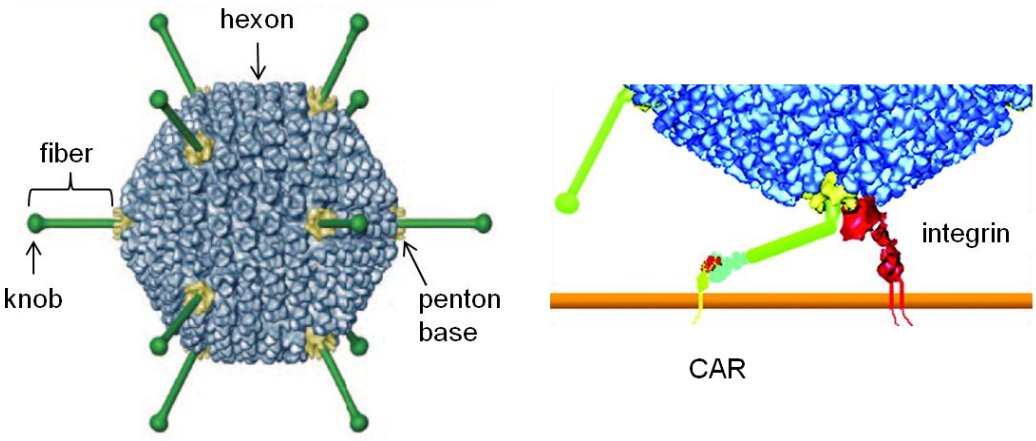

Figure 7: Adenovirus structure. Adenovirus icosahedral capsid has a diameter of about 100 nm and comprises hexon proteins and twelve fibers. Fiber proteins originate from the penton bases at the vertices and form a knob domain at their end. Adenoviruses use CAR and integrins as receptors (modified from (ZHANG & BERGELSON 2005)).

Adenovirus knob-CAR D1 interaction is visualised in Figure 8. Fiber knobs are homotrimers and each monomer binds one CAR D1 domain (BEWLEY ET AL. 1999). Residues on CAR D1 involved in homodimerisation overlap with residues involved in adenovirus binding (Figure 17). Thus, mutations in CAR that affect adenovirus attachment probably also alter CAR´s physiological function and occur less likely. Knob-D1 interaction displays a 1000-fold higher affinity (K_d=14.8±4.5 nM for adenovirus serotype 5) than

the homophilic CAR association (KIRBY ET AL. 2000). Two interfaces are involved in knob-D1 interaction. Contact sites on CAR D1 (BEWLEY ET AL. 1999; KIRBY ET AL. 2000; TOMKO ET AL. 2000) and on adenovirus knob (KIRBY ET AL. 2000; LAW & DAVIDSON 2005; NICKLIN ET AL. 2005; SANTIS ET AL. 1999) have been deduced from structure models and by site-directed mutagenesis.

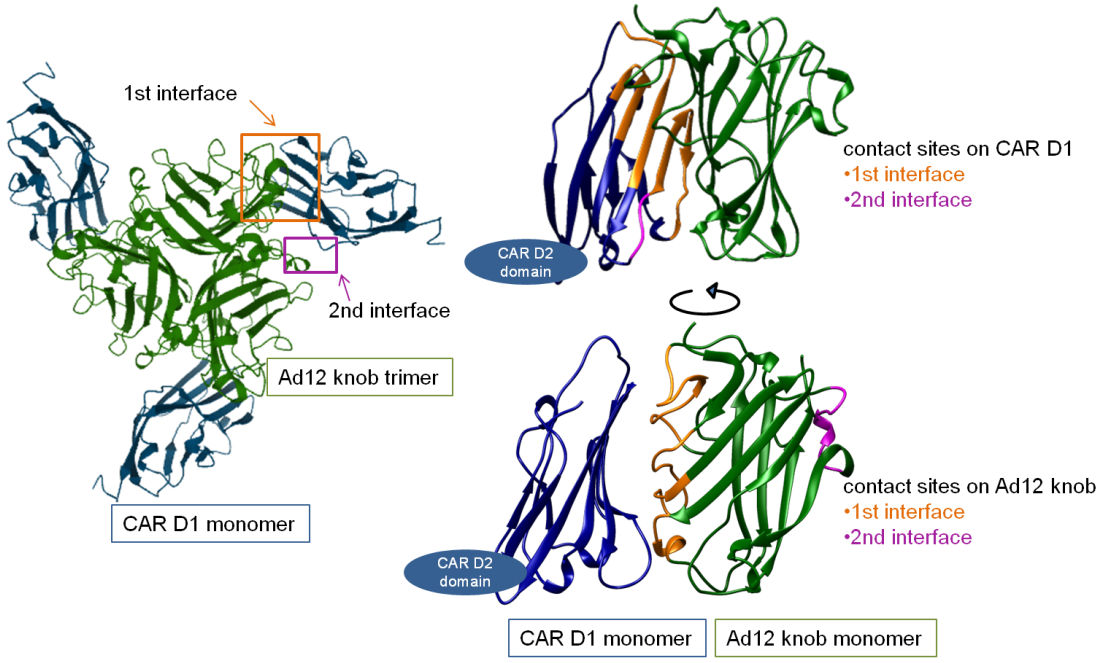

Figure 8: Model of CAR D1-Ad12 knob interaction. Left: Ad12 knob trimer (green) is able to interact with three CAR D1 monomers (blue) (PDB ID: 1KAC, (BEWLEY ET AL. 1999)). Contact is established via two interfaces. Right: Contact sites on CAR D1 (top) and on Ad12 knob (bottom) are coloured in orange and purple for the first and second interface, respectively. CAR D2 domain is added to show orientation of the complex.

1.1.4.4 Soluble ECD as antiviral decoy

CAR splice isoforms, recombinant CAR ECD, CAR D1, and CAR ECD fused to IgG1-Fc (sCAR-Fc) were used as soluble CAR proteins for virus inhibition experiments. Soluble CAR ECD prevents virus infections in two ways. Firstly, they function as virus traps by binding to viruses. Thereby, they block binding sites for membranous CAR and cause steric hindrance during uncoating and cell entry for those viruses, which still manage to bind to the cell (FECHNER ET AL. 2011). Secondly, soluble CAR forms homodimers with their membranous counterparts and block those for virus attachment. CVB are especially susceptible to CAR decoy, as they form A-particles upon interaction (GOODFELLOW ET AL. 2005; MILSTONE ET AL. 2005). A-particles are crucial in the virus uncoating process, but cannot infect cells anymore.

CAR decoys are effective competitors that impede CVB and Ad infections *in vivo* and *in vitro*. They inhibit CVB and Ad entry in various cell types (DÖRNER ET AL. 2004; FREIMUTH ET AL. 1999; LIM ET AL. 2006; ROELVINK ET AL. 1998). Treatment of CVB3-infected mice with soluble CAR reduces virus titer in the myocardium and pancreas, and reduced virus-induced mortality (YANAGAWA ET AL. 2004; ZHANG ET AL. 2013). Exogenous expression of sCAR-Fc by skeletal muscle inhibits CVB-induced myocarditis in mice (LIM ET AL. 2006). Liver and heart adenovirus infections are significantly inhibited in immunosuppressed mice expressing soluble CAR (RÖGER ET AL. 2015). Most *in vivo* studies did not reveal safety issues, but treatment with CAR splice isoform 4/7 increased myocardial inflammation and heart tissue damage in a murine CVB3 myocarditis model, when applied intraperitoneally. At the same time, CVB3 titer was reduced. CAR4/7 injection without subsequent virus infection elicited no immune reaction in mice (DÖRNER ET AL. 2006).

1.2 Viral-induced myocarditis

1.2.1 Symptoms, diagnosis, and treatment

Myocarditis is the most clinically relevant inflammatory cardiac disease (BLAUWET & COOPER 2010; CAFORIO ET AL. 2013). Most inflammations of the myocardium are a-symptomatic or patients shown mild symptoms like fever and fatigue. Therefore, the true incidence is unknown. However, it was estimated that 3.1 million myocarditis cases occurred worldwide in 2017 (JAMES ET AL. 2018). Severe symptoms vary from chest pain and palpitations to cardiogenic shock with arrhythmias and sudden cardiac death. Especially young victims of sudden cardiac death suffer from myocarditis (DOOLAN, LANGLOIS, & SEMSARIAN 2004; ECKART ET AL. 2004; MARON 2003). Chronic viral persistence can result in dilated cardiomyopathy (DCM), which is a leading cause for heart transplantation. For diagnosis of myocarditis, an endomyocardial biopsy is examined for inflammatory infiltrates and cardiomyocyte necrosis. Presence of viral genome in the sample can be determined and cardiac magnetic resonance imaging can be used for non-invasive diagnosis. Treatment of more severe cases targets arrhythmias or heart failure. Immunosuppressive therapy yields no benefit (MASON ET AL. 1995).

1.2.2 Virus aetiology

Myocarditis can be caused by drugs, toxins, autoimmune diseases, or infectious agents like viruses, bacteria, fungi, or protozoa. Viral infections are the most frequent aetiology in North America and Europe (BURIAN, BUSER, & ERIKSSON 2005). Adenoviruses and enteroviruses (e.g. Coxsackieviruses) are identified most frequently in myocarditis and DCM cases, among other viruses like influenza, Epstein-Barr, cytomegalo, hepatitis C, and parvovirus B19 (BOWLES ET AL. 2002, 2003; KINDERMANN ET AL. 2008; KÜHL ET AL. 2005; LIU ET AL. 2013).

Due to CAR´s role as virus receptor for both eponymous viruses, its role in viral-induced myocarditis and DCM has been studied extensively. Cardiomyocytes and cardiac fibroblasts are CAR-positive and thereby susceptible towards viral infections (LINDNER ET AL. 2014). Cardiac-specific CAR KO prevents coxsackieviral infection (KALLEWAARD ET AL. 2009; SHI ET AL. 2009), whereas upregulation in cardiomyocytes increases cells´ susceptibility towards viral infection (NOUTSIAS ET AL. 2001). CAR expression is upregulated in DCM and myocarditis (KAUR ET AL. 2012; LIU ET AL. 2013; NOUTSIAS ET AL. 2001; RUPPERT ET AL. 2008; SHARMA ET AL. 2016; TATRAI ET AL. 2011; TOIVONEN ET AL. 2010). This is probably a result of inflammation rather than a cause for initial virus infection, since CAR was found to be upregulated in several other disease states (see 1.1.3.2). Interestingly, forced cardiac-specific CAR upregulation in mice results in severe cardiac inflammation and cardiomyopathy without viral contribution, probably via MAPK signalling (CARUSO ET AL. 2010; YUEN ET AL. 2011). Therefore, high CAR levels in myocarditis and DCM may influence cardiac remodelling directly.

1.2.3 Phases and immune response

Myocarditis is defined by three different phases (LIU & MASON 2001; SHAUER ET AL. 2013): First, cardiomyocyte lysis occurs during viral replication in the acute phase. Consequently, the innate immune system is activated, chemokines and cytokines are expressed, and immune cells infiltrate. If immune response is adequate, myocarditis heals after this phase. During the second phase, the adaptive immune system activates antigen-presenting cells that are directed against both viral and cardiac epitopes. Massive inflammation and sustainable damage of myocardium ensue. Autoimmunity through molecular mimicry can exceed pathogenic effects of viral infection. Autoreactive T cells, high cytokine concentrations, and cross-reactive antibodies often have

detrimental consequences for heart function. In some cases, viral and autoimmune inflammatory processes can continue and a chronic DCM develops as a third possible phase of myocarditis. DCM is defined as chronic inflammation of the myocardium with dilated left ventricle and impaired contractibility.

Viral-induced tissue injury elicits inflammatory responses. A hallmark of inflammation is the recruitment of immune cells, which release reactive oxygen species and proteolytic enzymes. Matrix metalloproteinases (MMPs) cleave components of the extracellular matrix (ECM) as well as various other proteins (MITTAL ET AL. 2016A). Neutrophil serine proteases cathepsin G (CG), neutrophil elastase (NE), and proteinase 3 (PR3) cleave cell surface molecules and chemokines (PHAM 2006). MMP and NE activities increase in viral-induced myocarditis (CHEUNG ET AL. 2006; LEE ET AL. 1998; LI ET AL. 2002). Neutrophils express several soluble proteases in their granules: CG, NE, and PR3 in azurophilic (primary) granules, MMP-9 (gelatinase), and MMP-1, -8, and -13 (collagenases) in specific (secondary) granules, and MMP-9 in gelatinase (tertiary) granules (WRIGHT ET AL. 2010). Furthermore, other immune cells like phagocytes, natural killer cells, monocytes, macrophages, eosinophils, basophils, mast cells, and leukocytes all express serine proteases or MMPs (OWEN & CAMPBELL 1999). With the help of those proteases, immune cells migrate through ECM, kill pathogens, and facilitate cardiac remodelling. ECM turnover and reconstruction allow healing of the heart tissue after inflammation (MARCHANT & MCMANUS 2009; RUTSCHOW ET AL. 2006). Other sources of proteases in the myocardium are cardiomyocytes (COKER ET AL. 1999) and fibroblasts (CLEUTJENS ET AL. 1995).

1.3 Shedding

Ectodomain shedding is a posttranslational modification defined as limited proteolysis and release of an extracellular part of a transmembrane protein (HAYASHIDA ET AL. 2010). Shedding releases a soluble proteoform of the transmembrane protein, which can have biological functions. For example, it can act as agonist or antagonist for the remaining full-length receptor. By shedding, cell surface expression levels of the protein decrease independently from transcriptional regulation. Furthermore, shedding is often followed by regulated intramembrane proteolysis (RIP), which produces a cytoplasmic

fragment that can be involved in gene expression regulation. Shedding can be constitutive or induced by activators, e.g. phorbol esters.

Leukocytes migrate through epithelium to the sites of inflammation with the help of proteases that target CAMs. Ectodomain shedding of CAMs expressed by leukocytes or epithelial cells influences tethering and rolling of leukocytes (GARTON, GOUGH, & RAINES 2006). Besides, CAM shedding plays a major role in cell adhesiveness and migration and thereby also in cancer progression (VAN KILSDONK ET AL. 2010).

Sheddases (or secretases) can be membranous or soluble proteases, for example a disintegrin and metalloproteinases (ADAMs) (REISS & SAFTIG 2009), MMPs (PARKS, WILSON, & LÓPEZ-BOADO 2004), and serine proteases expressed by PMNs (GINZBERG ET AL. 2001). Several CAMs are shed by membranous or soluble proteases: CD44, JAM-A, JAM-C, and L1 are cleaved by ADAM10 and ADAM17 (KOENEN ET AL. 2009; MARETZKY ET AL. 2005; NAGANO ET AL. 2004; RABQUER ET AL. 2010). ICAM-1, E-cadherin, N-cadherin, NCAM-1, and PECAM-1 are shed by MMPs or NE (CONANT ET AL. 2017; GINZBERG ET AL. 2001; HÜBSCHMANN ET AL. 2005; ILAN ET AL. 2001; LYONS & BENVENISTE 1998; MCGUIRE, LI, & PARKS 2003). Nectin-4 and vascular cell adhesion protein 1 (VCAM-1) are digested by ADAM17 (FABRE-LAFAY ET AL. 2005; SINGH ET AL. 2005). Close homolog of L1 (CHL1) is proteolysed by ADAM8 (NAUS ET AL. 2004). Other target proteins or secreted proteases include growth factors, cytokines, chemokines, or growth factors (MURPHY, MURTHY, & KHOKHA 2008).

Membranous ADAM10 sheds murine CAR´s ECD and releases a soluble fragment of 32 kDa. After shedding, murine CAR is processed by RIP (HOURI, HUANG, & NALBANTOGLU 2013). Trypsin cleaved CAR´s ECD into fragments that can be visualised in a reducing gel and subsequent Western blot. HeLa cells treated with trypsin remained CVB-susceptible, probably because CAR fragments remained attached to the cells through disulfide bonds (CARSON 2000). Elastase, pancreatin, and chymotrypsin treatment of HeLa cells inhibited CVB attachment, which provided indirect evidence for a possible CAR-shedding (LEVITT & CROWELL 1967; ZAJAC & CROWELL 1965). High trypsin concentrations reduced CAR surface levels on Caco-2 cells (RIABI ET AL. 2014).

1.4 Scope of this study

1.4.1 CAR genetic variants

Due to CAR´s important role in embryogenesis and in remodelling following tissue injury (see 1.1.3.2), *CXADR* has been searched for pathogenic mutations. However, no missense or splice variants were found in patients suffering from ischemic or dilated cardiomyopathy (TATRAI ET AL. 2011), left ventricular non-compaction cardiomyopathy (HERRMANN 2016), myocarditis (BOWLES ET AL. 2002), myocardial infarction (BUGERT ET AL. 2011), myxoma (BISCHOF 2018), or usher syndrome (EXCOFFON ET AL. 2006). Variants in intron three and exon seven were characterised in patients suffering from chronic obstructive pulmonary disease, but they did not associate with adenoviral infection rates (KASUGA ET AL. 2009). A variant in exon seven, which results in a silent mutation in CAREx7 and in a missense mutation in CAREx8, was associated with increased blood pressure (SHETTY ET AL. 2012).

Sequencing of *CXADR* in 108 healthy individuals revealed no polymorphisms in D1 domain, indicating high conservation of CAR´s functional domain (THOELEN ET AL. 2002). CAR homologues are expressed in several species including mammalian and non-mammalian vertebrates, birds, and fish. Amino acid conservation in extracellular D1 domain and cytoplasmic part is very high (BERGELSON ET AL. 1997; FECHNER ET AL. 1999; PATZKE ET AL. 2010; PETRELLA ET AL. 2002; THOELEN ET AL. 2001A; TOMKO, XU, & PHILIPSON 1997).

The Genome Aggregation Database (gnomAD) (KARCZEWSKI ET AL. 2020) lists genetic variants in human population. By now, sequencing data of more than 140000 unrelated individuals from disease-specific and population genetic studies are loaded. Interestingly, *CXADR* has no variants with a minor allele frequency (MAF) above 1 % that would be considered as typical polymorphisms.

I was interested in the most frequent variants in human population (Table 1) and their influence on CAR-mediated virus uptake. Missense variant p.P356S was detected in a deaf patient, but no change of CAR´s *in vitro* characteristics was observed. Localisation, expression level, CAR-mediated adenovirus entry, and intracellular interaction with MAGI-1b did not differ from wild type CAR (EXCOFFON ET AL. 2006). The other four variants have not been described in the literature yet.

Table 1: Investigated point mutations in human *CXADR*. Most frequent missense mutations in the canonical transcript ENST00000284878 that are listed in gnomAD (last accessed on November 4th, 2020). Affected nucleotides are enumerated according to their position in the coding sequence (CDS). Variants are located in CAR´s transmembrane domain (TMD) or cytoplasmic domain (CPD).

Nr.	rs number	CDS nucleotide	Exon in *CXADR*	amino acid	Domain in CAR	MAF
1	148881358	c.752C>T	6	p.Ala251Val	TMD	0.0107%
2	372559893	c.886G>A	7	p.Gly296Ser	CPD	0.0115%
3	536246226	c.928A>G	7	p.Met310Val	CPD	0.0418%
4	143764073	c.983G>A	7	p.Arg328His	CPD	0.0941%
5	142651712	c.1066C>T	7	p.Pro356Ser	CPD	0.2570%

The five frequent variants are localised in CAR´s TMD or CPD, but do not affect known functional motifs directly (Figure 3). Nevertheless, those motifs may be influenced by the variants indirectly, for example by conformational changes. Since CAR´s cytoplasmic tail is important for intracellular signalling, has multiple interaction partners, and regulates CAR´s expression levels (see 1.1.1.3), it was tempting to speculate that variants in this domain might also alter virus internalisation.

Variants in the TMD and CPD of CAR may influence virus entry and attachment by altering the natural functions of those domains. Changes in CAR expression levels, CAR localisation, or CAR intracellular signalling as well as changes in cell migration, adhesion, or proliferation properties may all alter virus entry efficiency (Figure 9). I overexpressed five CAR missense variants that are most frequent in human population in Chinese hamster ovary (CHO) cells and determined their subcellular localisation, their influence on cell adhesion and proliferation, and their potential to mediate adenovector and Coxsackievirus internalisation.

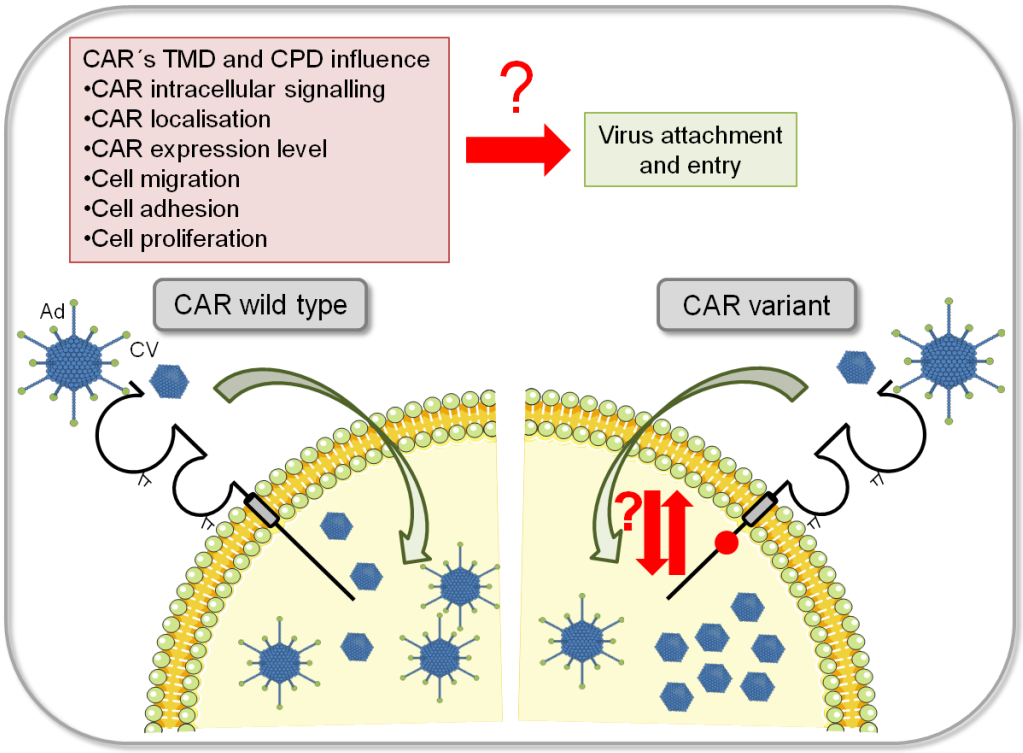

Figure 9: Hypothesis ´CAR genetic variants´. Transmembrane and intracellular CAR missense mutations may influence virus uptake by altering CAR´s localisation and expression level or its interaction with intracellular partners. Furthermore, CAR´s function in cell-cell interaction (cell migration, adhesion, and proliferation properties) may be influenced by the variants. Changing those characteristics of the virus receptor may also affect virus infection. It could be possible that virus attachment and entry are enhanced or decreased and that responses differ for Coxsackie- and adenoviruses. For localisation of variants in the amino acid sequence, see Figure 3.

1.4.2 Peptides as virus entry inhibitors

Several organisms including bacteria, plants, fish, birds, and mammals express short antimicrobial peptides as part of their defense system. Peptides expressed by vertebrates target bacteria, fungi, or viruses and are expressed in granules of circulating immune cells, the gastrointestinal tract, and epithelia (JENSSEN, HAMILL, & HANCOCK 2006). Some human defensins, a subgroup of antimicrobial peptides, inhibit infections with adenovirus (BASTIAN & SCHÄFER 2001; SMITH & NEMEROW 2008), HIV (WANG ET AL. 2003), or herpes virus (YASIN ET AL. 2004).

Synthetic antiviral peptides are designed to inhibit several phases of the viral life cycle. Enfuvirtide is a 20mer peptide and inhibits membrane fusion of host cell and HIV, which is necessary for infection (MURAKAMI ET AL. 1997). Other peptides inhibit adenovirus escape from endosomes (HORNE ET AL. 2005) or HIV DNA synthesis (COLE ET AL. 2002). Another interesting target for antiviral peptides is the virus-cell interaction.

Peptides that bind to the receptor or the virus to inhibit virus entry were designed for example for hepatitis C virus (YIN ET AL. 2017), HIV (FÄTKENHEUER ET AL. 2005; TAMAMURA ET AL. 1996), or dengue virus (ALHOOT ET AL. 2013). Arginine-glycine-asparagine (RGD) peptides, which target adenovirus-integrin interaction, inhibit adenovirus entry (WICKHAM ET AL. 1993). In the antiviral peptide database, no entry inhibitor peptide targeting adenovirus or Coxsackievirus entry via CAR are listed (QURESHI ET AL. 2014).

Both CAR D1 domain (FECHNER ET AL. 1999) and adenovirus fiber knob domain (PICKLES ET AL. 2000; ROELVINK ET AL. 1998) successfully inhibit adenovirus entry into cells. I designed peptides based on D1 or knob motifs to use them as entry inhibitors for adenovectors. Peptides may block binding sites either on CAR D1 or on adenovirus knob and thereby inhibit vector entry into host cells (Figure 10). I determined cytotoxicity of the synthetic peptides and tested their inhibitory efficiency towards adenovector entry in human lung epithelial cells.

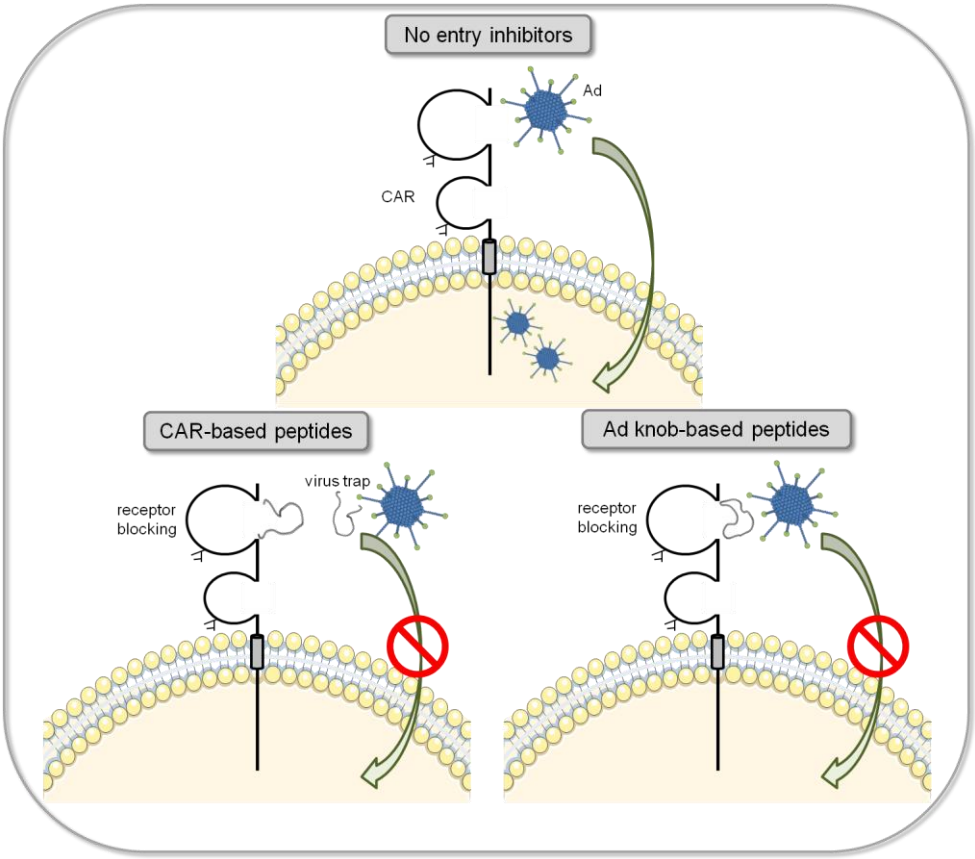

Figure 10: Hypothesis ´Synthetic peptides as adenovirus entry inhibitors´. Peptides corresponding to motifs from CAR D1 domain may block virus attachment either by binding to CAR or to virus knob. Peptides with amino acid sequences from the adenovirus knob may inhibit virus attachment by blocking CAR for upcoming viruses.

1.4.3 CAR-shedding

CAR-shedding may be a mechanism that limits ongoing virus infections, for example during myocarditis (Figure 11). Cardiac myocytes express CAR and are susceptible to Coxsackie- and adenovirus infections. After virus entry and replication, new virions escape from the host cells through lysis and infect neighbouring tissue. At the same time, the host´s immune system is activated leading to migration of immune cells towards the site of infection. Immune cells like neutrophils, natural killer cells, or macrophages secrete proteases. Those proteases facilitate migration through the tissue by cleaving adhesion molecules and ECM components. Main proteases secreted by neutrophils are MMPs and serine proteases (see 1.2.3). If those proteases that are present in the myocardium during virus infection would also cleave CAR´s extracellular domain, this would be a new immune defense mechanism against Coxsackie- and adenovirus infections. CAR-shedding would limit ongoing virus infections via three different mechanisms:

1) Loss of CAR´s ECD from the cardiomyocytes´ cell surface would reduce virus binding sites. CAR expression levels correlate with cells´ susceptibility towards virus infections *in vitro* and *in vivo* (see 1.1.4.1).

2) Shedding releases a soluble part of CAR´s ECD. This soluble fragment would be physiologically relevant, if it contained CAR´s membrane-distal D1 domain. Then, it would serve as a virus trap like recombinant proteins comprising CAR´s ECD *in vitro* and *in vivo* (see 1.1.4.4).

3) A soluble part of CAR´s ECD would dimerise with membranous CAR and block it for upcoming viruses (see 1.1.1.2).

I investigated the proteolysis of human CAR by proteases that are known to be secreted during myocarditis. Different *in vitro* models were applied to identify proteases that cleave CAR, to define mechanisms that facilitate or inhibit cleavage, and to determine proteolytic cleavage sites in CAR´s ECD. Recombinant human full-length CAR or CAR ECD expressed by prokaryotic or eukaryotic cells were cleaved with human serine proteases and MMPs. Furthermore, proteolysis of membrane-bound CAR of various mammalian cells was monitored.

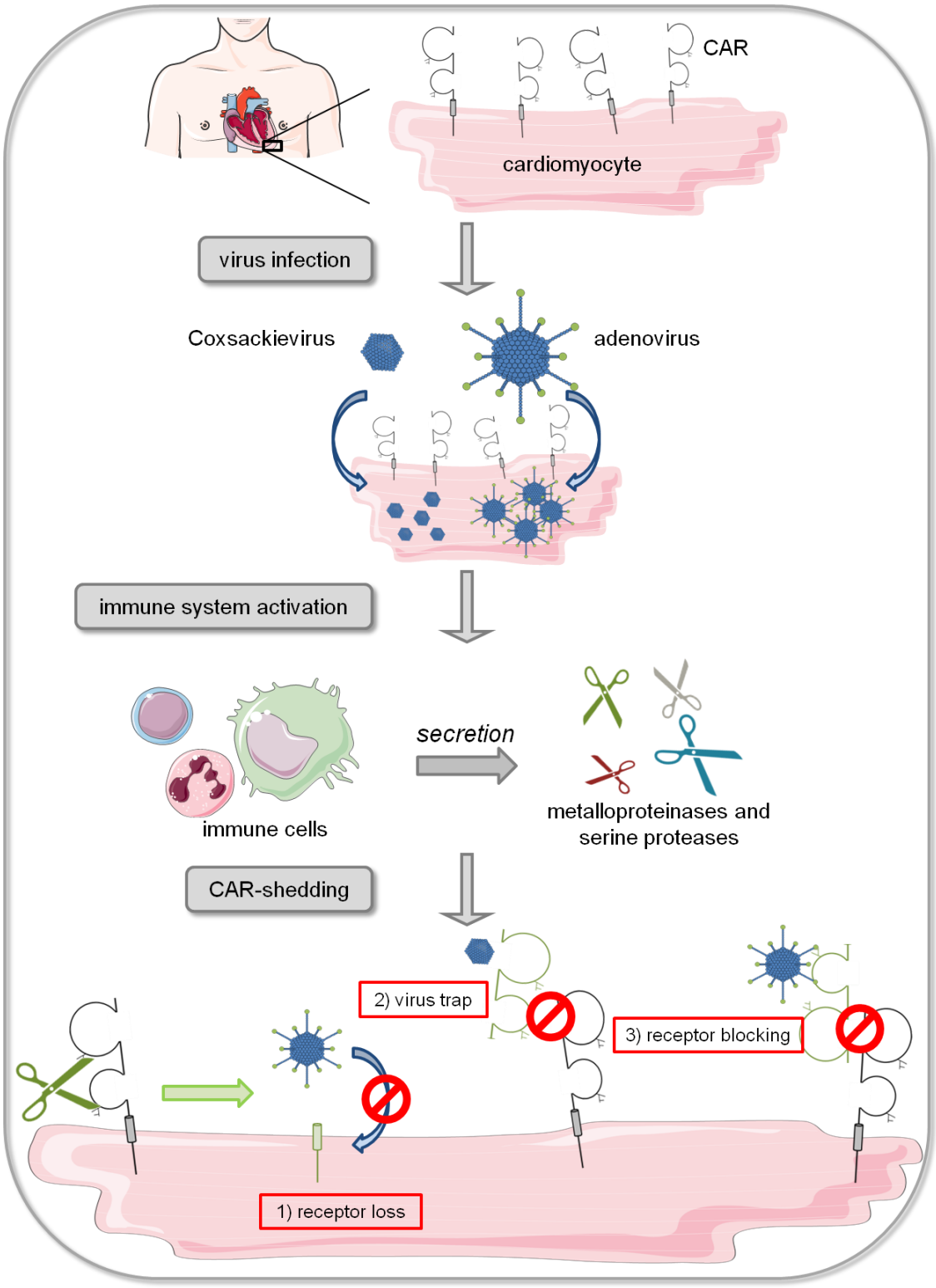

Figure 11: Hypothesis ´CAR-shedding`. Viral-induced myocarditis may be limited by CAR-shedding. Cardiomyocytes expressing CAR are susceptible to Coxsackie- and adenovirus infections. Upon immune system activation, immune cells migrate towards the site of infection and secrete proteases, which may act as sheddases for CAR. CAR-shedding would limit virus binding through three different mechanisms: 1) decreasing virus receptor levels, 2) providing a virus trap in form of released soluble ECD, and 3) blocking membranous CAR for virus by dimerisation of soluble and cell-bound ECD.

2 MATERIAL

2.1 Instruments

Table 2: Instruments

Instrument	Name	Supplier
Autoclave	2540 EL	Systec
Autoclave	5075 ELV	Tuttnauer
Cell culture hood		Binder
Centrifuge	5417C	Eppendorf
Centrifuge	Rotina 420 R	Hettich GmbH & Co. KG
CO_2 Incubator		Binder
Concentrator	5301	eppendorf
Electrophoresis chamber and blot module	Xcell Sure Lock ™	Invitrogen™ life technologies
ESI-OrbiTrap	QExactive Plus	ThermoFisherScientific
Flow cytometer	Cytomics FC500	Beckman Coulter
Flow cytometer	Attune Nxt	ThermoFisherScientific
Fluorescence confocal microscope	TCS SP8	Leica
Incubator		memmert
Incubator	innova 4230	New Brunswick Scientific
Incubator	Heraeus B15	ThermoFisherScientific
Inverted microscope	Eclipse TE 200-U	Nikon
Light microscope	CK2	Olympus
Magnetic mixer	MR3001	Heidolph
Micro scales		KERN ABJ
Microplate reader	Infinite® M1000 PRO	TECAN
pH meter	766	Knick Calimatic
Power supplier	PowerEase500	Invitrogen™ life technologies
Rocker	HS 260 basic	IKA Werke
Scales	BL1500S	Sartorius
Sequencer	ABI 3500 Genetic Analyzer	Applied Biosystems
Spectrophotometer	Nanodrop	ThermoFisherScientific
Surface plasmon resonance (SPR) system	Biacore™ T200	Cytiva
Suspension Mixer		Ratek Instruments
Thermocycler	T1	Biometra
Thermoshaker	MKR23	HLC
UHPLC$^+$	UltiMate 3000 RSLCnano	ThermoFisherScientific
Ultrasonic bath	RK100SH	Bandelin
Vortex	VortexGenie2	ScientificIndustries, Inc.™
Water bath		memmert
Western blot imaging system	ECL Chemostar	INTAS

2.2 Consumables

Table 3: Consumables

Consumable	Supplier
24 well cell culture plate cellstar	greiner bio-one
6 well cell culture plate cellstar	greiner bio-one
96 well cell culture plate cellstar	greiner bio-one
96 well cell culture plate Nunclon Delta	ThermoFisherScientific
96 well cell culture plate Nunclon Delta black	ThermoFisherScientific
96 well plate non-binding black	greiner bio-one
96-well Reaction Plate MicroAmp Fast Optical	ThermoFisherScientific
Acclaim™ PepMap™ 100 C18 LC-column	ThermoFisherScientific
Acclaim™ PepMap™ 100 C18 pre-column	ThermoFisherScientific
Cellstar cell culture flasks 75 cm^2	greiner bio-one
Cellstar serological pipets 25 mL, 10 mL, 5 mL	greiner bio-one
Centrifuge tubes, 15 ml, 50 ml	nerbeplus
Clear screw vial with screw cap and inlet	VWR
Cover glasses 13mm diameter, thickness 1.5	VWR
Cover slips 24x50 mm	VWR
Cryo vials	Nationallab
Glassware (flasks, beakers, measuring cylinders)	Schott DURAN
HisPur™ NiNTA Resin	ThermoFisherScientific
Multipette® plus	Eppendorf
Neubauer-improved counting chamber	Marienfeld superior
NTA series S chip	Cytiva
NuPAGE 4-12 % Bis-Tris Gel 0,1 mm x 15 well	Invitrogen™ life technologies
PCR Tube 0.2 mL	Eppendorf
Pipet Controler Easypet	Eppendorf
Pipet tips	Eppendorf
Pipets Reference	Eppendorf
PVDF membrane 0.2 mm pore size	Invitrogen™ life technologies
Reaction tubes 1.5 mL	Eppendorf
Sponge pads	Invitrogen™ life technologies
Syringe Filter Minisart 0.2 µm	Sartorius stedim
Syringe Luer-Lok Tip	BD Falcon
Tubes 15 mL, 50 mL	ThermoFisherScientific
Tubes 5 mL for flow cytometry	Sarstedt
UV cuvettes	Brand

2.3 Chemicals, reagents, and enzymes

Table 4: Chemicals, reagents, and enzymes

Chemical/reagent/enzyme	Supplier
Acetic acid	Sigma-Aldrich®
Acetone	ChemSolute
Ammonium bicarbonate (ABC)	Carl Roth® GmbH & Co. KG
Ampuwa® aqua ad injectabilia	Fresenius Kabi Austria GmbH

Aqua	B. Braun Melsungen AG
Bicinchoninic acid (BCA)	Sigma-Aldrich®
Bicine	Carl Roth® GmbH & Co. KG
BisTris	Carl Roth® GmbH & Co. KG
Bovine serum albumin (BSA)	Carl Roth® GmbH & Co. KG
Brij®35	Carl Roth® GmbH & Co. KG
Calcium chloride dihydrate	MERCK
Carbenicillin	ThermoFisherScientific
Collagen R solution 0.2 %	Serva
Copper(II) sulfate solution 4 % (w/v)	Sigma-Aldrich®
CoulterClenz® Cleaning Agent	Beckman Coulter
4′,6-diamidino-2-phenylindole (DAPI)	Carl Roth® GmbH & Co. KG
Digitonin	Sigma-Aldrich®
Dimethyl sulphoxide (DMSO)	Sigma-Aldrich®
Dimethylformamide	Carl Roth® GmbH & Co. KG
Dithiothreitol (DTT) 0.5 M	InvitrogenTM life technologies
Ethylenediaminetetraacetic acid disodium (EDTA)	Sigma-Aldrich®
EDTA UltraPure 0.5 M pH 8	ThermoFisherScientific
Ethanol	MERCK
Exo SAP-IT	USB
Fixable viability dye (FixVi)	ThermoFisherScientific
Fluorescence mounting medium	DAKO
Formaldehyde (16 % w/v), MeOH-free (PFA)	ThermoFisherScientific
Glucose	MERCK
Glycerol	MERCK
4-(2-hydroxyethyl)-1-piperazineethanesulfonic acid (HEPES)	Carl Roth® GmbH & Co. KG
HotStarTaq Master Mix	QIAGEN
Hydrochloric acid	Carl Roth® GmbH & Co. KG
Imidazole	Carl Roth® GmbH & Co. KG
IsoFlowTM Sheath Fluid	Beckman Coulter
Isopropyl β-d-1-thiogalactopyranoside (IPTG)	Carl Roth® GmbH & Co. KG
LB-Medium (Lennox)	InvitrogenTM life technologies
Lysozyme	Sigma-Aldrich®
Magnesium chloride hexahydrate	MERCK
Magnesium sulfate heptahydrate	MERCK
Methanol	Carl Roth® GmbH & Co. KG
Morpholinopropane sulfonic (MOPS)	MERCK
3-(4,5-dimethylthiazol-2-yl)-2,5-diphenyltetrazolium bromide (MTT)	Sigma-Aldrich®
Nonidet® P40 substitute	Sigma-Aldrich®
Novex® AP Chromogenic Substrate	InvitrogenTM life technologies
NuPAGE® Antioxidant	InvitrogenTM life technologies
NuPAGE® LDS Sample Buffer (4x)	InvitrogenTM life technologies
NuPAGE® MES running buffer (20x)	InvitrogenTM life technologies
Phenylmethylsulfonyl fluoride (PMSF)	Sigma-Aldrich
Phosphate buffered saline (PBS) pH 7.2 - $CaCl_2$ -$MgCl_2$	Carl Roth® GmbH & Co. KG
Piperazine-N,N′-bis(2-ethanesulfonic acid) (PIPES)	Carl Roth® GmbH & Co. KG
PNGase F (glycerol-free)	New England BioLabs®
PNGase F RapidTM (non-reducing format)	New England BioLabs®
Potassium chloride	MERCK
Potassium phosphate	MERCK

Powdered Milk Blotting Grade	Carl Roth® GmbH & Co. KG
PrestoBlue™ cell viability reagent	ThermoFisherScientific
Super optimal broth with catabolite repression (S.O.C.) medium	ThermoFisherScientific
Saponin	Sigma-Aldrich®
SeeBlue® Plus2 Pre-Stained Protein Standard	InvitrogenTM life technologies
Sodium acetate	MERCK
Sodium azide	Sigma-Aldrich®
Sodium chloride	Carl Roth® GmbH & Co. KG
Sodium dodecyl sulfate (SDS)	Carl Roth® GmbH & Co. KG
Sodium hydroxide	MERCK
Sucrose	Carl Roth® GmbH & Co. KG
Tris (hydroxymethyl)aminomethane	MERCK
Tris-HCl	Carl Roth® GmbH & Co. KG
Triton X-100	Carl Roth® GmbH & Co. KG
Tween® 20	Carl Roth® GmbH & Co. KG
Type G Immersion liquid	Leica
Urea	ICN Biomedicals, Inc.
WesternBright substrate	Biozym
Zinc chloride	Sigma-Aldrich®
β-mercaptoethanol	Sigma-Aldrich®

2.4 Kits

Table 5: Kits

Kit	Supplier	Application
BigDye® Terminator v1.1 Kit	Applied Biosystems	Sequencing PCR
DyeEx 2.0 Spin Kit	QIAGEN	PCR product purification
Novex Colloidal Blue Staining Kit	Invitrogen™ life technologies	Gel staining
NTA Reagent Kit	Cytiva	SPR assay
QIAamp® DNA Mini Kit	QIAGEN	Isolation of genomic DNA
Silver Stain Kit	Pierce	Gel staining

2.5 Recombinant proteins

CHO cells express human integrin αvβ5 as a heterodimer (αv: 31-992 (Uniprot P06756) with C-terminal 6xHis tag, β5: 24-719 (Uniprot P18084)). Lyophilised protein was reconstituted in PBS to a concentration of 200 µg/ml. Mouse myeloma cells express human DAF (35-353, Uniprot P08174) with C-terminal 6xHis tag. Lyophilised protein was reconstituted in PBS to a concentration of 200 µg/ml. HEK-293 cells express murine CAR extracellular domain (rmECD, 1-237, Uniprot P97792) with C-terminal 6xHis tag. Lyophilised protein was reconstituted in sterile deionised water to a concentration of 400 µg/ml. HEK-293 cells express human CAR extracellular domain

(rhECD, 20-237, Uniprot P78310) with C-terminal 6xHis tag. Lyophilised protein was reconstituted in sterile deionised water to a concentration of 400 µg/ml.

Table 6: Recombinant proteins

Recombinant protein	Cat.-No.	Supplier
Human Integrin αVβ5 (His tag)	2528-AV	R&D Systems
Human CD55/DAF (His tag)	2009-CD	R&D Systems
Murine Coxsackie- and adenovirus receptor (His tag)	50019-M08H	Biozol
Human Coxsackie- and adenovirus receptor (His tag)	ab168893	abcam

2.6 Human proteases, buffers, serine protease inhibitor, and artificial substrates

Used human matrix metalloproteinases (MMPs) and serine proteases neutrophil elastase (NE), proteinase 3 (PR3), and cathepsin G (CG) are listed in Table 7. MMPs were purchased as recombinant catalytic domains expressed by yeast (MMP-2) or *E. coli* (others): collagenases (MMP-1, -8, -13), gelatinases (MMP-2, -9), matrilysin (MMP-7), metalloelastase (MMP-12), and stromelysins (MMP-3, -10, -11).

Table 7: Proteases

Protease	Cat.-No.	Supplier
MMP MultiPack-2: active recombinant catalytic domains MMPs 3, 7, 10, 11, 12	BML-AK014	Enzo
MMP MultiPack-1: active recombinant catalytic domains MMPs 1, 2, 8, 9, 13	BML-AK013	Enzo
Neutrophil elastase isolated from human neutrophils	324681	MERCK
Proteinase 3 isolated from human neutrophils	BML-SE498	Enzo
Cathepsin G isolated from human neutrophils	BML-SE283	Enzo

Serine proteases were reconstituted in suitable reconstitution buffers (Table 8; CG and NE) or water (PR3) to a concentration of 500 ng/µl, as recommended by the manufacturers. MMPs were purchased in soluble form in reconstitution buffers.

Table 8: Protease buffer formulations

Buffer	Formulation (1-fold ion strength)
MMP-9 reconstitution buffer	50 mM Tris, 1 mM CaCl2, 300 mM NaCl, 5 µM ZnCl2, 15 % glycerol, 0.1 % Brij®-35, pH 7.5
MMP (except MMP-9) reconstitution buffer	50 mM Tris, 5 mM CaCl2, 300 mM NaCl, 20 µM ZnCl2, 30 % glycerol, 0.5 % Brij®-35, pH 7.5
MMP assay buffer	50 mM HEPES, 10 mM CaCl2, 0.05 % Brij-35, pH 7.0 (pH 6.0 for MMP-3)
NE reconstitution buffer	50 mM sodium acetate, 200 mM NaCl, pH 5.5
NE assay buffer	100 mM Tris-HCl, 500 mM NaCl, pH 7.5
PR3 assay buffer	100 mM MOPS, 500 mM NaCl, pH 7.5
CG reconstitution buffer	50 mM sodium acetate, 150 mM NaCl, pH 5.5
CG assay buffer	160 mM Tris-HCl, 1.6 M NaCl, pH 7.4

Phenylmethylsulfonyl fluoride (PMSF) is a serine protease inhibitor and was prepared as 100 mM solution in anhydrous ethanol, since it is unstable in water.

Artificial protease substrates are listed in Table 9. NE, PR3, and CG digest chromogenic substrates with p-nitroanilide (pNA) as chromophore and succinyl (Suc) or methoxysuccinyl (MeoSuc) to improve water solubility. Cleavage sites are phenylalanine in BML-P141 and valine in 324696. MMPs cleave fluorescent substrates with 2, 4-Dinitrophenyl (Dpn) and N-3-(2, 4-Dinitrophenyl)-L-2,3-diaminopropionyl (Dpa) as quenchers and (7-Methoxycoumarin-4-yl)acetyl (Mca) as fluorophore. Cleavage sites are the peptide bonds between glycine and leucine in ES010 and between glutamine and norvaline (Nval, non-proteinogenic amino acid) in ES002.

Table 9: Artificial peptide substrates

Substrate	Cat.-No.	Supplier
Suc-AAPF-pNA	BML-P141	Enzo
MeOSuc-AAPV-pNA	324696	MERCK
Mca-KPLGL-Dpa-AR-NH2	ES010	R&D Systems
Mca-RPKPVE-Nval-WRK(Dnp)-NH2	ES002	R&D Systems

2.7 Antibodies

Table 10: Antibodies

Antibody	Cat.-No.	Supplier
anti-CAR antibodies		
anti-N-terminal aa1-50	ab189216	abcam
anti-CXADR aa272-346	HPA030411	Sigma
3C100 aa1-300	sc-70493	SantaCruz
H-300 aa1-300	sc-15405	SantaCruz
RmcB	05-644	Merck
E1-1 PE	sc-56892 PE	SantaCruz
other antigens		
anti-vinculin	A14193	Abclonal
anti-vimentin antibody	ab92547	abcam
anti-6x His tag ® antibody HRP	ab1187	abcam
anti-enteroviral VP1 clone 5-D8/1	M7064	Dako
secondary antibodies		
anti-rabbit AP	D0487	DAKO
anti-rabbit HRP	NA934	Amersham
anti-mouse Cy3-conjugated	115-165-068	Jackson Immuno Research
anti-rabbit Alexa Fluor 488	A-11008	Invitrogen™ life technologies
anti-mouse FITC	554001	BD Pharmingen™
isotype control antibodies		
mouse IgG1kappa clone 1E2.2	CBL610	Merck
mouse IgG1 PE	sc-2866	SantaCruz

2.8 *E. coli* strain, Coxsackievirus, adenovector, human and Chinese hamster cell lines

E. coli strain OneShot® BL21 (DE3) from Invitrogen™ life technologies was used for expression of human CAR.

Coxsackieviruses B3 and adenovector based on serotype 5 coding for green fluorescent protein (Ad5-GFP) were kindly provided by Matthias Tenbusch.

All used cell lines were epithelial-like (Table 11). For Chinese hamster ovary (CHO-K1) epithelial cells from *Cricetulus griseus*, species speciation was performed by cytochrome C oxidase 1 (COI) DNA barcoding as offered by Leibniz-Institut Deutsche Sammlung von Mikroorganismen und Zellkulturen. For COI DNA barcoding, the 5´ coding region of the gene coding for COI is sequenced. The DNA sample prepared from the CHO-K1 cell line in question contained no human, mouse, rat, or Syrian hamster DNA, but was identified to stem from Chinese hamster as expected.

Table 11: Epithelial cell lines

Cell line	Species	Tissue	Disease	Literature
A549	human	lung	carcinoma	(LIEBER ET AL. 1976)
CHO-K1	Chinese hamster	ovary		(PUCK, CIECIURA, & ROBINSON 1958)
HEK-293	human	embryonic kidney	carcinoma	(GRAHAM ET AL. 1977)
HeLa	human	cervix	adenocarcinoma	(SCHERER, SYVERTON, & GEY 1953)
HepG2	human	liver	hepatocellular carcinoma	(ADEN ET AL. 1979)
SW13	human	adrenal cortex	small cell carcinoma	(LEIBOVITZ ET AL. 1973)

2.9 Primers

Sequencing primers were purchased from Invitrogen™ life technologies with a starting synthesis scale of 50 nM.

Table 12: Primers

Name	Sequence 5´→3´	Length (bp)
CMV for	CGCAAATGGGCGGTAGGCGTGT	22
BGH rev	TAGAAGGCACAGTCGAGG	18
CAR-in for	CTGGTAGTTCTTGTTAAGCCTTCAGG	26
CAR-in rev	GTACAGCTGTATGTCCCAGAGTAC	24
CAR-in for5	GATCAGTGCCTGTTGCGTCTA	21

2.10 Reagents for nLC-MS/MS

Table 13: Reagents for nLC-MS/MS

Reagent/protease/chemicals	Cat.-No.	Supplier
Acetonitrile, HPLC for Gradient Analysis	A/0627/17	ThermoFisherScientific
LiChroSolv water	1.153.332.500	Merck
Trifluoroacetic acid (TFA) for LC-MS	84868	VWR
Tris	37181.02	Serva
Trypsin Gold Mass Spectrometry Grade for MS	Promega	V5280

2.11 Reagents, media, and antibiotics for cell culture

Table 14: Reagents, media, and antibiotics for cell culture

Reagent/media/antibiotics	Supplier
Accutase®	Sigma-Aldrich®
Antibiotic antimycotic solution (100x)	Sigma-Aldrich®
Dimethyl sulphoxide (DMSO) Hybri-Max®	Sigma-Aldrich®
Dulbecco´s modified Eagle medium (DMEM)	Sigma-Aldrich®
EDTA UltraPure 0.5 M pH 8.0	ThermoFisherScientific
Fetal bovine serum (FBS) Superior	Sigma-Aldrich®
FuGENE® HD Transfection Reagent	Promega GmbH
Ham's F-12 with L-Glutamine	Lonza BioWhittaker™
Trypan blue solution 0.4%	Sigma-Aldrich®
Trypsin-EDTA (0.05%), phenol red Gibco®	Invitrogen™ life technologies
Zeocin™ 100 mg/ml	InvivoGen

2.12 Vectors

CAR mammalian cell expression vectors based on the high-copy pcDNA4/TO/myc-HisA vector (Invitrogen™ life technologies) with full-length *CXADR* insert (Figure 12). As part of my Master´s thesis (HERRMANN 2016), the stop codon was inserted to express CAR without *c-myc* epitope and His tag. Besides, the mock vector and five vectors containing one point mutation each were created by site-directed mutagenesis. See Table 1 for an overview of the variants.

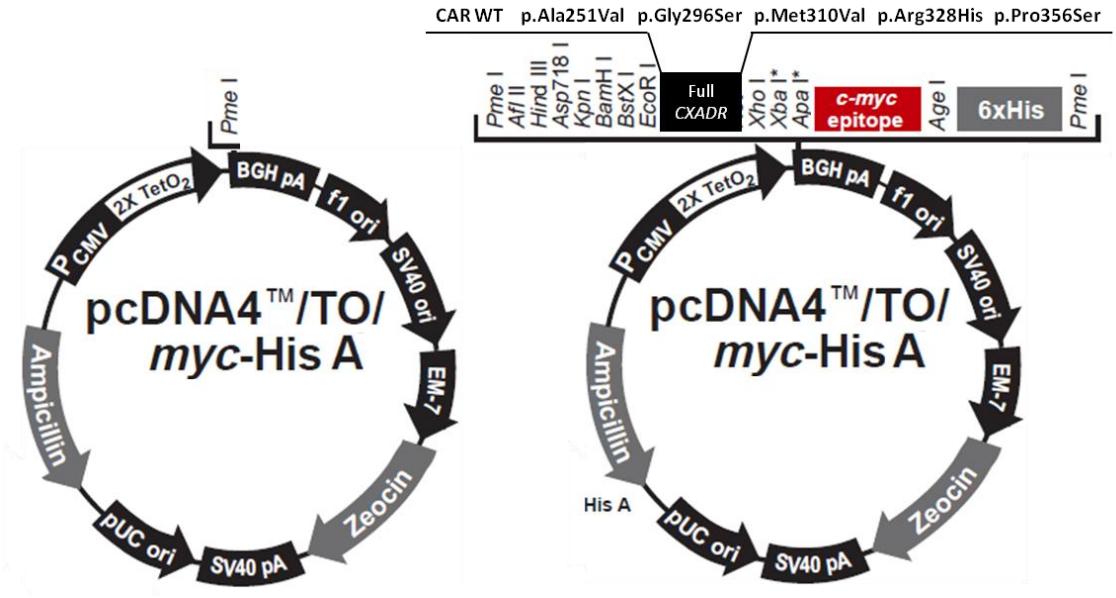

Figure 12: Maps of vectors used for shedding experiments and examination of the five CAR variants. pcDNA4/TO/myc-HisA (left; 4981 bp) was used as mock vector. pCXADR_pcDNA4/TO/myc-HisA coded either for wild type CAR or for one of the CAR variants (right; 6223 bp).

The *CXADR* sequence has been cloned into low-copy vector pET100/D-TOPO (Invitrogen) by V. Oberscheidt in 2014 (Figure 13). Resulting pCXADR_pET100/D-TOPO includes the *CXADR* sequence for mature CAR (without the signal peptide; 1041 bp) and was used for *E. coli* expression of CAR with N-terminal His tag.

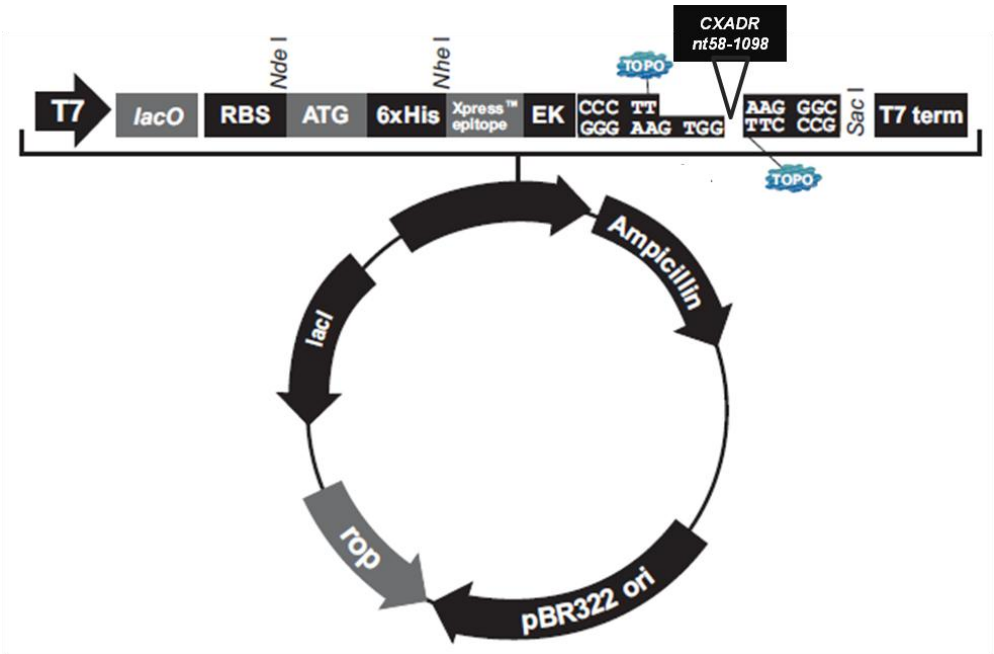

Figure 13: Map of pCXADR_pET100/D-TOPO (6856 bp) coding for mature CAR (nucleotides 58-1098, amino acids 20-365) (OBERSCHEIDT 2014).

2.13 Peptides

Peptides (1 mg freeze-dried TFA acid salts) were from JPT Peptide Technologies.

Table 15: Synthetic peptides. For each peptide, number of amino acids (aa), net molecular weight (average and as determined via MS), purity, and net charge are listed. Peptides Ad1, Ad2, and Ad3 were head-to-tail cyclised (marked with an asterisk).

Name	Sequence * head-to-tail cyclised	Length (#aa)	Net molecular weight [g/mol] (average)	MS [m/z] ESI	Purity [%] (HPLC 220 nm linear gradient)	Net charge
CAR1	H-EDQGPLDIEWIL-OH	11	1314.41	1315.8 [M+H]+	96.3	-4
CAR2	H-EDQGPLDIEWLISPAIGTYQTKVKKAPGVANKKIH-OH	35	3846.41	1923.8 [M+2H]2+, 1282.9 [M+3H]3+, 962.5 [M+4H]4+	94.6	+1
CAR3	H-EDQGPLDIEWLISPADNQKVDQVIILYS-OH	28	3199.56	1600.8 [M+2H]2+, 1067.6 [M+3H]3+	94.8	-5
CAR4	H-DQVIILYSGDKIYDDYYP-OH	18	2180.42	1091.0 [M+2H]2+	90.1	-3
CAR5	H-KVKKAPGVAN-OH	20	1011.22	1011.9 [M+H]+	97.0	+3
CAR6	H-IGTYQTKVKKAPGVANKKIHLV-OH	22	2393.87	1198.0 [M+2H]2+, 799.1 [M+3H]3+	95.7	+6
CAR7	H-DIGTYQTKVKKAPGVANKKIHLVVG-OH	25	2665.14	889.2 [M+3H]3+, 667.2 [M+4H]4+	93.8	+5
Ad1	H-TLWTTPAPSPNCRLNAEKDAKLTLVLTK-OH*	28	3082.58	1028.3 [M+3H]3+, 771.5 [M+4H]4+	90.9	+2
Ad2	H-WNFRNGDLTEGT-OH*	12	1391.46	1392.0 [M+H]+, 697.0 [M+2H]2+	90.3	-1
Ad3	H-AYPKSHGKTAKS-OH*	12	1256.44	629.0 [M+2H]2+, 419.6 [M+3H]3+	92.4	+4

2.14 Software and online programs

Table 16: Software

Name	Supplier	Application
CXP software	Beckman Coulter	Cytometer control software
Kaluza 1.2	Beckman Coulter	Flow cytometry data analysis
Attune NxT Software	ThermoFisherScientific	Flow cytometry data analysis
LasX	Leica	Fluorescence microscope software
LUCIA G S/W	Lucia	Light microscope software
FreeStyle™ 1.6	ThermoFisherScientific	MS raw data analysis
Proteome Discoverer 2.4	ThermoFisherScientific	MS database search
ImageJ		Size estimation of proteins in poly-acrylamide gels
Prism 6	Graph Pad	Statistics

The *in silico* prediction programs MutationTaster2 (SCHWARZ ET AL. 2014), PolyPhen-2 (ADZHUBEI ET AL. 2010), PROVEAN (CHOI ET AL. 2012), FATHMM (SHIHAB ET AL. 2013), and SNPs&GO (CAPRIOTTI ET AL. 2013) were used to assess pathogenicity of *CXADR* variants. Effect of a *CXADR* variant on splicing was assessed with the program Human Splicing Finder (DESMET ET AL. 2009).

3D models of crystallography data were obtained from Protein Data Bank (PDB) (BERMAN ET AL. 2000). Important sequences in 3D models were highlighted using Chimera 1.4 (PETTERSEN ET AL. 2004). Interaction sites were computed using Protein interfaces, surfaces and assemblies (PISA) (KRISSINEL & HENRICK 2007) with PBD IDs as input data.

Randomly shuffled sequences of human CAR and NE used for MS analysis were generated with online program Sequence Manipulation Suite Version 2, Paul Stothard, 2004.

3 METHODS

3.1 Mammalian cell culture techniques

3.1.1 Culture environment, passaging, cryopreservation, and thawing

Cells were grown as a monolayer at 37 °C with a 100 % humidified atmosphere and 5 % CO_2 in air. CHO-K1 cells were cultured in Ham´s F-12; all other cells were cultured in Dulbecco´s modified Eagle medium (DMEM). Both media were supplemented with antibiotic antimycotic solution and 10 % fetal bovine serum (FBS). Cultures were passaged when they reached 80 to 90 % confluency. Cells were washed with PBS and dissociated with 500 µM ethylenediaminetetraacetic acid (EDTA) in PBS. HepG2 cells were dissociated with 10 mM EDTA. Cells were pelleted for 4 min at 1100 x g and resuspended in medium. 5 x 10^5 to 7.5 x 10^5 cells were seeded per 75 cm^2 cell culture flask. If not stated otherwise, cells were harvested with EDTA in PBS as described above. However, to test influence of trypsin on CAR surface levels, cells were also harvested with trypsin-EDTA solution.

For cryopreservation, 1 x 10^6 cells were pelleted and resuspended in culture medium containing 10 % dimethyl sulphoxide (DMSO). 1 ml cell suspension was filled into a sterile cryovial and frozen overnight at –80 °C. The next day, the vial was transferred in liquid nitrogen for long-term storage. For freezing out, cells were thawed at room temperature and pelleted. Then, cells were resuspended in culture medium and seeded in a 75 cm^2 culture flask.

3.1.2 Stable transfection, selection and verification of monoclones

1.8 x 10^5 CHO-K1 cells were seeded per well of a 6-well plate, in order to obtain 80 % confluency after 24 h. Cells were transfected with pCXADR_pcDNA4.0/TO/myc-HisA vector as described in the FuGENE® 6 Transfection Reagent protocol. FuGENE® is a nonliposomal reagent that functions with serum-containing medium. 9 µl FuGENE® was added to Ham´s F-12 medium, mixed, and incubated for 5 min at room temperature. Afterwards, 3 µg plasmid DNA was added. The total volume of Ham´s F-12 medium plus plasmid DNA was 100 µl. The solution was mixed, incubated for 15 min at room temperature, and added to cells and culture medium. 48 h after transfection, CHO cells were passaged with culture medium containing 200 µg/ml Zeocin and medium was

refreshed every third day. After about twelve days, resistant cells formed foci and were expanded to a 75 cm^2 cell culture flasks.

Cells were plated into a 96-well plate in a serial dilution of 1:10 and wells with a single cell were determined with a light microscope. After one week, cells from one well were expanded to a well of a 6-well plate and subsequently to a 75 cm^2 cell culture flask. CAR expression of the monoclonal cell lines was determined by flow cytometry (3.1.5) and point mutations in *CXADR* sequence were verified by sequencing of genomic DNA (3.2).

3.1.3 Determination of cell proliferation properties

Cell proliferation of CHO-CAR cells was measured with PrestoBlue, a resazurin dye that is reduced to fluorescent resorufin by viable cells. In preliminary studies, cell number per well and incubation times were optimised. 1000 cells were seeded in 90 µl Ham´s F-12 medium containing FBS and antibiotics per well of a black 96-well plate. Per cell line, three wells were seeded and for each day of measurement (24, 48, 72, and 96 h after seeding), one plate was prepared. At the day of measurement, 10 µl PrestoBlue solution was added per well. Plate was mixed gently and incubated for 1 h at 37 °C with 5 % CO_2 and in humidified atmosphere. Fluorescence was measured with a TECAN plate reader with excitation at 560 nm and emission at 590 nm. Relative fluorescence units were normalised to time point day 1 for each cell line.

Furthermore, at every passaging day, cell number per millilitre medium was determined by counting viable cells with a hemocytometer. Cells were harvested, resuspended in 4 ml medium and dead cells were stained blue by mixing the cell suspension 1:1 with trypan blue solution.

3.1.4 Determination of cell adhesion properties

Cell adhesion properties of CHO-CAR cells were determined with a protocol derived from different publications (COHEN ET AL. 2001A; HONDA ET AL. 2000; OKEGAWA ET AL. 2001). Cells were harvested and 1 x 10^6 cells were resuspended in 1 ml Ham´s F-12 medium containing FBS and antibiotics. Cells were incubated at 37 °C with 5 % CO_2 and in humidified atmosphere. Every hour, suspension was mixed carefully by inverting, in order to maintain cell aggregates. 20 µl cell suspension was mixed very gently with 20 µl trypan blue solution and particles were counted with a hemocytometer. One

particle was defined either as a single cell or as a cell aggregate (single cells contacting each other). Particle number was normalised to time point 1 h for each cell line.

3.1.5 Flow cytometry for determination of CAR surface and vimentin expression levels

2.5×10^5 cells were resuspended in PBS containing anti-CAR antibody E1-1 PE-conjugated or isotype control antibody PE-conjugated (1:66) and incubated for 1 h at room temperature in the dark. This antibody concentration was titrated in preliminary studies using monoclonal CHO-CAR cells. Cells were washed with PBS, resuspended in 300 µl PBS, and analysed with a Cytomics FC500. As HepG2 cells form strong aggregates, PBS was supplemented with 10 mM EDTA in every step for this cell line.

To stain cells intracellularly for vimentin, they were fixed for 20 min in 2 % paraformaldehyde (PFA) in PBS at 4 °C and permeabilised for 15 min at 4 °C with 0.04 % saponin and 0.5 % bovine serum albumin (BSA) in PBS. Then, cells were indirectly stained with anti-vimentin antibody (1:66 in 100 µl PBS) for 1 h at room temperature and with anti-rabbit Alexa488-conjugated (1:1000 in PBS) for 30 min at room temperature in the dark.

For analysis of CHO-CAR variant cells, 1×10^4 events were counted. For analysis of CAR-shedding, events were counted for 6 min. For the forward scatter channel, pulse height as well as pulse area were measured. Side scatter and fluorescence channels were analysed as pulse areas. Gating strategies are visualised in Figure 17 in Appendix.

3.1.6 Immunofluorescence microscopy

Cover glasses were placed in wells of a 24-well cell culture plate and coated with 0.02 % collagen in water for a few seconds. Then, collagen solution was aspirated and glasses were dried and UV-radiated at room temperature.

Cells were either seeded or spotted on the collagen-coated cover glasses. When seeded, cells grew to a confluency of about 80 % in their appropriate cell culture medium. Then, medium was aspirated and cells were washed with PBS, fixed with methanol for 10 min at -20 °C and washed with PBS again. Cells that were in suspension after protease treatment (see 3.1.7) were spotted on cover glasses. Therefore, cells were washed with PBS, resuspended in methanol and fixed for 10 min at -20 °C. Cells were pelleted at 1100 x g for 4 min, resuspended in PBS and pipetted on the glasses. Liquid evapo-

rated by heating the glasses for 20 min at 65 °C. Adhered cells were washed once with water to remove salt crystals and kept in PBS afterwards.

For immunofluorescence staining, protocols differed for intracellular and extracellular target proteins. When staining only for extracellular proteins, cells were incubated with the primary antibody diluted in Ham´s F-12 medium at 4 °C for 1.5 h. For antibody dilutions refer to Table 17. Cells were washed with Ham´s F-12 medium two times and fixed with methanol as described above. After washing with blocking solution (1 % BSA in PBS), cells were stained with secondary antibody diluted in blocking solution for 2 h at room temperature in the dark. After washing with blocking solution, cells were stained with 4′,6-diamidino-2-phenylindole (DAPI) 1 µg/ml in blocking solution for 5 min at room temperature in the dark. Cells were washed twice with PBS and once with water. Cover glasses were placed on coverslips with mounting medium and sealed with fingernail polish. When cells were to be stained extra- and intracellularly, they were fixed and permeabilised by methanol as described above. Then, they were washed with PBS and blocked for 1 h in blocking solution at room temperature. Staining with primary antibody diluted in blocking solution was performed overnight at 4 °C. Incubation with secondary antibody and DAPI as well as cover glass mounting was performed as described above.

Table 17: Antibody dilutions used for immunofluorescence staining

Primary antibody	Dilution	Secondary antibody	Dilution
mouse anti-CAR N-term 3C100	1:500	goat anti-mouse Cy3	1:1000
mouse anti-CAR N-term RmcB	1:200		
rabbit anti-CAR N-term H-300	1:300	goat anti-rabbit Alexa488	1:1000
rabbit anti-vimentin	1:500		

Fluorescence confocal microscopy was performed with a TCS SP8. Excitation and emission wavelengths for different fluorophores were as follows: DAPI (405 nm, 430-465 nm); Alexa488 (488 nm, 510-545 nm), Cy3 (552 nm, 560-595 nm). Gain settings for each fluorophore were kept constant for specimens that had to be compared. For tile scans, 5 x 5 images were taken to obtain an 825 µm x 825 µm field. Analysis of fluorescence intensities was performed with the LasX software using the stack profile function that calculates mean grey scale values. Mean values of Cy3 signal (CAR staining) intensity were divided by mean values of DAPI signal (cell nuclei staining) intensity, in order to relate CAR signal to cell number.

3.1.7 NE treatment of mammalian cells

To observe, how NE detaches cells from the cell culture dish surface, cells were seeded in a 96-well plate and treated with NE (100 ng/µl) in Ham´s F-12 medium when reaching 90 % confluency. As control, NE reconstitution buffer was added instead of NE. Detachment over time was monitored with a light microscope.

To determine CAR levels of cells in dependency of NE treatment, 2.5 x 10^5 cells were pelleted at 1100 x g for 4 min and resuspended in 12.5 µl Ham´s F-12 medium including 100 ng/µl NE or NE reconstitution buffer. Digest was performed at 37 °C with shaking at 600 rpm and cells were washed with PBS subsequently. If cells were reduced after NE treatment, they were incubated for 15 min in 12.5 µl PBS containing 50 mM dithiothreitol (DTT) at room temperature and washed with PBS. Then, cells were either used for flow cytometric analysis (3.1.5), immunofluorescence staining (3.1.6), or differential detergent fractionation (3.1.9). Supernatants were collected and precipitated with acetone (3.4.6).

3.1.8 Cell lysis

5 x 10^5 cells were pelleted and lysed with 50 µl ice cold lysis buffer (50 mM Tris-HCl, 150 mM NaCl, 1 % Nonidet P40, pH 7.8) for 10 min at 4 °C. Then, solution was centrifuged for 10 min at 10000 x g and supernatant with whole cell lysate was analysed with BCA assay (3.4.8).

3.1.9 Differential detergent fractionation

Per 5 x 10^5 cells, 50 µl ice-cold buffer was added. Cell pellet was resuspended in digitonin buffer (0.15 mM digitonin, 10 µM piperazine-*N*,*N*′bis[2-ethanesulfonic acid] (PIPES), 0.3 mM sucrose, 100 µM NaCl, 1.5 µM $MgCl_2$, 5 mM EDTA) containing 1 mM PMSF. Solution was incubated on ice for 12 min at 350 rpm and centrifuged at 500 x g and 4 °C for 10 min. The supernatant with the cytosolic fraction was discarded. Pellet was resuspended in Triton buffer (0.5 % Triton X-100, 10 µM PIPES, 0.3 mM sucrose, 100 µM NaCl, 1.5 µM $MgCl_2$, 3 mM EDTA) containing 1 mM PMSF and incubated for 30 min on ice. Solution was pelleted at 5000 x g and 4 °C for 10 min. Supernatant contained membranous fraction and protein concentration was analysed with BCA assay (3.4.8) and 5 µg total protein were loaded for LDS-PAGE and subsequent Western blot analysis (3.4.9).

3.2 Molecular biology techniques

3.2.1 Genomic DNA isolation from CHO-CAR cells

Point mutations in *CXADR* were verified by sequencing genomic DNA of CHO-CAR cells. Therefore, DNA was purified according to the manual of the QIAamp® DNA Mini kit. 1 x 10^6 cells were harvested and resuspended in 200 µl PBS. Then, 20 µl QIAGEN proteinase K and 200 µl AL buffer were added and sample was heated for 10 min at 56 °C. 200 µl ethanol was added and mixture was applied to QIAamp® Mini spin column. Column was centrifuged at 6000 x g for 1 min and flow-through was discarded. 500 µl buffer AW1 was added, column was centrifuged, and 500 µl AW2 buffer was added. Column was centrifuged at 20000 x g for 3 min and incubated for 5 min with 50 µl distilled water. After centrifugation at 6000 x g for 1 min, flow-through with genomic DNA was collected.

3.2.2 Cycle sequencing PCR, PCR product purification, and Sanger sequencing

Cycle sequencing reaction was performed as described in the BigDye® Terminator v1.1 Cycle Sequencing Kit protocol. Reaction mix included 100 ng genomic CHO DNA, 10 µM primer, 2.5 x ready reaction mix, and 5 x BigDye sequencing buffer in a total volume of 10 µl. PCR cycling program was performed with an initial denaturation step at 95 °C for 5 min. This was followed by 30 cycles with 30 s at 95 °C, 10 s at 55 °C, and 4 min at 60 °C. Sequencing reaction mix was purified according to DyeEx® 2.0 spin protocol for dye-terminator removal. Centrifugation steps were performed at 750 x g and room temperature. Resin of the spin column was resuspended, the cap of the column was loosened a bit, and the bottom closure was removed. The column was centrifuged for 3 min and the flow-through was discarded. The complete sequencing reaction was added to the gel bed dropwise. The centrifugation step was repeated and 20 µl H_2O ad iniectabilia was added to the purified DNA in the flow-through and mix was pipetted to a MicroAmp 96-well plate. Sanger sequencing was performed on an ABI3500.

3.3 Virology methods and peptide treatment

3.3.1 Fluorescence-activated cell sorting (FACS) for CAR expression

Before virus infection and vector transduction experiments, CHO-CAR cells were sorted for high CAR expression levels. Therefore, cells were harvested with Accutase and washed with FACS-buffer (0.5 % BSA in PBS with 1 mM sodium azide). Cells were stained with anti-CAR PE-labelled antibody (clone E1-1) diluted 1:300 in FACS-buffer for 30 min at 4 °C. Cells were washed twice with PBS, fixed with 2 % PFA in PBS for 20 min at 4 °C, washed again and resuspended in FACS-buffer. FACS was performed with an Attune Nxt Acoustic Focusing Cytometer. All samples were measured in technical triplicate.

3.3.2 Ad5-GFP transduction and CVB3 infection

Cells were seeded in Nunclon 96-well plates (2×10^4 cells per well) and challenged the next day with Ad5-GFP or CVB3. Adequate multiplicities of infection (MOIs) have been determined in pilot experiments.

Cells were transduced with Ad5-GFP with MOI=100 for 72 h at 37 °C. After transduction, cells were stained for CAR, fixed, and analysed as described above (3.3.1).

For CVB3 infection, cells were challenged with MOI=1 overnight at 37 °C. For detection of intracellular CVB3-surface protein VP1, cells had to be permeabilised. Therefore, cells were harvested and fixed as described above (3.3.1) and incubated in Perm-buffer (0.5 % saponin in FACS-buffer) for 15 min at 4 °C. Cells were stained with anti-enteroviral VP1 antibody diluted 1:300 in Perm-buffer for 30 min at 4 °C, washed twice with Perm-buffer and incubated for 30 min at 4 °C with secondary anti-mouse FITC-labelled antibody diluted 1:300 in Perm-buffer. Cells were washed and resuspended in FACS-buffer. To determine CAR surface levels, cells from the same passage that was infected with CVB3 were stained for CAR as described above (3.3.1).

CAR surface levels as well as GFP and VP1 levels were determined by flow cytometry using the Attune® Nxt Acoustic Focusing Cytometer. Events were gated for ´Cells´ and ´Singlets´. Gating strategies are visualised in Figure 17 in Appendix. Transduction and infection rates were defined as percentage of GFP- or FITC-positive cells. CAR level was defined as percentage of PE-positive cells. All samples were measured in technical triplicate.

3.3.3 Peptide treatment of A549 cells for adenovector entry inhibition

Peptides were dissolved in water to a concentration of 1 µg/µl. Peptides CAR3 and CAR4 had to be dissolved in water containing 0.55 % ammonium bicarbonate (ABC).

Experiment procedures were derived from publications that used other viruses and cells (ALHOOT ET AL. 2013; YIN ET AL. 2017). A549 cells were seeded in a Nunclon 96-well plate (2 x 10^4 cells per well). The next day, cells and adenovectors were pre-treated with synthetic peptides for 1 h at 37 °C. As control, water (or 0.55 % ABC for CAR3 and CAR4) was added to cells and vectors instead of peptides. Peptides were diluted in DMEM with concentrations as indicated in the text and 50 µl was added per well of the 96-well plate. Ad5-GFP vectors (MOI=1000) were added to 30 µl DMEM-peptide solution. After 1 h, 20 µl prewarmed DMEM was added to the vector-peptide solution and the total volume of 50 µl was added to the cells. Cells were challenged with Ad5-GFP in presence of peptides for 1 h at 37 °C. Then, cells were washed with medium and cultivated overnight with 100 µl DMEM containing 10 % FBS. GFP expression was analysed the next day with flow cytometry as described above (3.3.2). All samples were measured in technical triplicate. For subsequent experiments, cells were transduced with MOI=500 for 1 h or with MOI=1000 for 30 min.

3.3.4 Peptide cytotoxicity tests

2 x 10^4 A549 cells were seeded per well of a Nunclon 96-well plate. The next day, medium was aspirated and 100 µl DMEM including peptides (concentrations as indicated in the text) was added per well for 2 h at 37 °C. Afterwards, peptide-containing medium was aspirated and cells were incubated for 4 h at 37 °C with 100 µl DMEM (containing 10 % FBS) and 25 µl tetrazolium salt 3-(4,5-dimethylthiazol-2-yl)-2,5-diphenyltetrazolium bromide (MTT) solution (5 mg/ml in PBS). Reduction by mitochondria was stopped by adding 100 µl extraction buffer (20 % w/v sodium dodecyl sulfate (SDS), 50 % dimethylformamide, pH 4.7). After overnight incubation at 37 °C, solution was mixed and debris was pelleted at 900 x g for 3 min. 100 µl of the supernatant was transferred to a new plate and formazan dye absorbance was measured at 560 nm. Higher absorbance indicates higher cell viability, because only viable cells reduce MTT. All samples were measured in technical triplicate.

Another viability test was performed by staining dead cells with fixable viability dye (FixVi). Therefore, cells were treated for 1 h with peptides (10 or 100 µM) in DMEM

and incubated with FixVi diluted 1:100 in FACS buffer for 30 min at 4 °C. Afterwards, cells were washed, fixed, and analysed by flow cytometry as described above (3.3.1). Results were expressed as percentage of dead cells (positive for Cy7-signal). All samples were measured in technical triplicate.

3.4 Protein expression and analysis

3.4.1 BL21 *E. coli* transformation, scale up protein expression, and inclusion body preparation

Transformation of BL21 *E. coli* for protein expression was performed as described in the manual with minor changes. A vial of OneShot® BL21 (DE3) cells was thawed on ice and 5 ng DNA (vector pCXADR-pET100 coding for full-length human CAR with a C-terminal His tag) was added. Mixture was kept on ice for 30 min followed by a heat-shock for 30 sec at 42 °C. Then, super optimal broth with catabolite repression (S.O.C.)-medium was added and bacteria were incubated at 37 °C for 1 h with shaking. Transformed bacteria were grown overnight with shaking in 10 ml 2 % lysogeny broth medium with 100 µg/ml carbenicillin and 1 % glucose (LB-carbenicillin).

The next day, 100 ml LB-carbenicillin was inoculated with the overnight culture and incubated at 37 °C with shaking. When an optical density (measured at 600 nm) of 0.5 - 0.8 was reached, expression was induced with 1 mM isopropyl β-d-1-thiogalactopyranoside (IPTG). After 4 h, bacteria were pelleted at 4000 x g and 4 °C.

Pellet was resuspended at room temperature with shaking in 5 ml lysis buffer (50 mM potassium phosphate, 400 mM NaCl, 10 % glycerol, 0.5 % Triton X-100, 100 mM KCl, 10 mM imidazole, 1 mM EDTA, 1 mM β-mercaptoethanol in H_2O, pH 7,8) including 100 mg/ml lysozyme. Cells were lysed by freezing them in liquid nitrogen, thawing them in a 42 °C water bath, and sonicating them for 20 sec. These steps were repeated two times and lysate was pelleted for 20 min at 4000 x g and 4 °C. Pellet was resuspended in 1 ml wash buffer 1 (50 mM Tris-HCl, 100 mM NaCl, 1 mM EDTA, 1 mM β-mercaptoethanol, 2 % Triton X-100, pH 8.0) and sonicated three times for 10 sec to remove *E. coli* membrane. After centrifugation for 20 min at 4000 x g and 4 °C, pellet was washed in 1 ml wash buffer 2 (as wash buffer 1, but without Triton X-100) and sonicated again three times for 10 sec. Inclusion bodies with recombinant human full-length CAR were pelleted for 20 min at 4000 x g and 4 °C and resolved

overnight at room temperature with shaking in 400 µl urea buffer (8 M urea, 50 mM Tris-HCl in H_2O, pH 8.0). Protein concentration was determined with a BCA assay (3.4.8).

3.4.2 Protease activity tests with synthetic substrates

Protease kinetics were measured for 1 h at 37 °C with artificial substrates and a TECAN plate reader. NE and PR3 cleave substrate MeOSuc-AAPV-pNA (50 mM in DMSO). CG cleaves substrate Suc-AAPF-pNA (50 mM in DMSO). Substrates were diluted to 25 mM with 200 mM Tris-HCl, pH 8.8. Assay mixture was prepared with appropriate protease assay buffer (Table 8) to obtain an end concentration of 1 mM. 100 µl of substrate mix was added to the protease (1 ng/µl) in a clear 96-well plate and release of chromophor pNA was monitored at 410 nm.

MMP-3 and MMP-10 cleave fluorogenic substrate II Mca-RPKPVE-Nval-WRK(Dnp)-NH_2 (4.8 mM in DMSO), whereas the other MMP catalytic domains cleave substrate IX Mca-KPLGL-Dpa-AR-NH_2 (6.2 mM in DMSO). Substrates were diluted to a concentration of 10 µM in 100 µl appropriate protease assay buffer (Table 8) and added per well of a black non-binding 96-well plate containing 1 ng/µl protease. Fluorescence from unquenched fluorophores was measured with excitation at 320 nm and emission at 405 nm.

3.4.3 Protease treatment of whole cell lysates or recombinant proteins expressed by *E. coli* and mammalian cells

Samples were mixed with proteases in protease assay buffers and incubated at 37 °C for different time points. Protease assay buffers were used with 3-fold ion strength to obtain an 1-fold concentration in the mixtures. As controls, protease reconstitution buffers instead of proteases, or protease inhibitors were added. For some experiments, pure proteases without substrates were incubated in protease assay buffers. Samples were either directly used for LDS-PAGE analysis (3.4.9) or deglycosylated with PNGase F before (3.4.4).

CHO-CAR cell lysates containing 20 µg total protein were digested with 100 ng/µl proteases. For MMPs, 1 µl EDTA (500 mM) was added as inhibitor. Serine proteases were inhibited with 1 µl PMSF (100 mM) solved in ethanol. 1 µl ethanol was added to the other samples as control. To exclude influence on cleavage by the alcohol, samples

were also digested without ethanol. Sample volume was filled up to 3 µl with assay buffer (3-fold ion strength). For Western blotting, 5.5 µg total protein lysate were loaded per lane.

E. coli BL21 inclusion body preparations containing 500 µg total protein were diluted 1:100 in protease assay buffer and mixed with proteases (100 ng/µl). For MMPs, 1 µl 500 mM EDTA was added as inhibitor. Serine proteases were inhibited with 1 µl 100 mM PMSF solved in ethanol. 1 µl ethanol was added to the other samples as control. Sample volume was filled up to 3 µl with assay buffer (3-fold ion strength) suitable for each protease. For Western blotting, 2.5 µg *E. coli* protein preparations were loaded per lane.

Recombinant human or mouse CAR extracellular domain (rhECD and rmECD 266 ng/µl) were mixed with 100 ng/µl proteases and sample volume was filled up with protease assay buffer (3-fold ion strength). For undigested control samples, protease reconstitution buffer was added instead of the protease. For NE digest, concentration and time series were performed as indicated in the text. For Western blotting and silver staining, 100 ng rhECD was loaded per lane. For colloidal blue staining and subsequent preparation for MS, 1 µg rhECD was loaded per lane. Recombinant human integrin αvβ5 and DAF (266 ng/µl) were treated with 100 ng/µl NE in NE assay buffer (3-fold ion strength). For silver staining, 200 ng integrin and 100 ng DAF were loaded per lane.

3.4.4 Deglycosylation

Samples containing 400 ng rhECD were treated with PNGase F (glycerol-free) under denaturing or non-denaturing conditions. Samples were denatured with 0.5 µl 10 x denaturing buffer (5 % SDS, 0.4 M DTT) in 5 µl total reaction volume for 10 min at 100 °C. Then, 1 µl 2 x GlycoBuffer2 (50 mM sodium phosphate, pH 7.5), 1 µl 10 % Nonidet P40, 0.5 µl PNGase F, and H_2O were added for a total reaction volume of 10 µl. Sample was deglycosylated at 37 °C for 1 h. For non-denaturing conditions, sample with 400 ng rhECD was mixed with 1 µl GlycoBuffer2 and 5 µl PNGase F. Sample was deglycosylated for 24 h at 37 °C, because glycostructures of non-denatured proteins are often less accessible to PNGase F and need longer incubation times.

For subsequent mass spectrometry analysis, 1 µg rhECD was mixed with 2 µl 5 x buffer and 0.5 µl Rapid^{TM} PNGase F in a total reaction volume of 2 µl. Sample was de-

glycosylated for 10 min at 50 °C. Rapid™ PNGase F completely deglycosylates proteins without addition of SDS and DTT, which would interfere with mass spectrometry.

3.4.5 NE treatment of recombinant human extracellular CAR domain (rhECD) bound to nickel nitrilotriacetic acid (NiNTA) resin

All centrifugation steps were performed at 700 x g for 2 min. 40 µl NiNTA resin was pelleted and supernatant was discarded. Resin was washed twice with 80 µl wash buffer (25 mM imidazole in PBS, pH 7.4). 5 µl rhECD (400 ng/µl) was mixed with 75 µl NE assay buffer (Table 8) and added to NiNTA resin. Binding was allowed for 30 min at room temperature with occasional shaking. After centrifugation, supernatant with unbound rhECD was removed and resin was washed twice with 80 µl NE assay buffer. Then, NE was added at a concentration of 100 ng/µl in 40 µl NE assay buffer. Cleavage was performed for 3 h at 37 °C with occasional shaking. Supernatant was saved and resin was washed twice with 80 µl NE assay buffer. Afterwards, some samples were reduced by adding 12.5 mM DTT (concentration was tested in preliminary studies) in NE assay buffer for 15 min and supernatant was saved. Resin was washed twice with 80 µl NE assay buffer. Proteins still bound to NiNTA after NE digest and reducing were eluted by washing the resin with 40 µl native elution buffer (250 mM imidazole in PBS, pH 7.4) and collecting the supernatant. Supernatants were concentrated by acetone precipitation (3.4.6).

3.4.6 Acetone precipitation

Conditioned cell culture media (3.1.7) and supernatants from NiNTA resin (3.4.5) were precipitated by mixing them 1:9 with ice-cold acetone and overnight incubation at -20 °C. Proteins were pelleted at 13000 x g for 20 min at 4 °C, supernatant was discarded, and acetone was allowed to evaporate. Pellets were resolved in 5 µl 4 x NuPAGE™ LDS sample buffer. Complete volume of precipitated conditioned cell culture medium was loaded onto the gel for subsequent Western blot. For NiNTA supernatants, 2 µl (supernatants recovered after NE digest or reducing conditions) or 1 µl (elution samples) were loaded onto the gel.

3.4.7 Surface plasmon resonance (SPR) spectroscopy

SPR was measured with a Biacore™ system at an assay temperature of 25 °C. NTA chip was loaded with nickel ions three times for 1 min each, before 3 µg/ml rhECD was

captured for 2 min. Then, NE (100 ng/µl) or NE reconstitution buffer as control was injected for 2 min. rhECD as well as NE (or NE reconstitution buffer) were diluted in NE assay buffer (Table 8).

3.4.8 Bicinchoninic acid (BCA) assay

Samples were measured in duplicate per dilution. 10 µl sample (undiluted or diluted) was added per well of a 96-well plate. 200 µl 0.08 % (w/v) copper(II) sulfate in BCA was added per well. Biuret reaction was measured after incubation at 37 °C for 30 min with a TECAN plate reader at 562 nm. BSA dilutions were used as standards.

3.4.9 Lithium dodecyl sulphate - polyacrylamide gel electrophoresis (LDS-PAGE), silver and colloidal blue staining, and Western blot

Samples were mixed with DTT (50 mM) and NuPAGE™ LDS sample buffer (1x). Then, proteins were denatured for 5 min at 70 °C and subsequently separated on a NuPAGE 4-12 % BisTris gel for 35 min at 200 V with running buffer (2.5 mM 2-(N-morpholino)ethanesulfonic acid (MES), 2.5 mM Tris, 0.005 % SDS, 50 µM EDTA, 0.25 % antioxidant, pH 7.3). Gels were stained either with the Colloidal Blue Staining Kit or with the Silver Staining Kit according to the manuals. Per gel, a volume of 10 ml was used.

For Western blotting, proteins were transferred onto a polyvinylidene fluoride (PVDF) membrane for 1 h at 160 mA with transfer buffer (1.25 mM bicine, 1.25 mM BisTris, 50 µM EDTA, 10 % methanol, 0.1 % antioxidant, pH 7.2). Membrane was blocked with 5 % non-fat milk in TBST (25 mM Tris-HCl, 500 mM NaCl, 0.5 % Tween 20, pH 7.5) for 1 h at room temperature, washed 3 times for 5 min with TBST, and incubated with antibodies in TBST with times and dilutions as indicated in Table 18. Between incubations with primary and secondary antibodies, membrane was washed three times 5 min with TBST.

Table 18: Antibody incubation times and dilutions used for Western blots. Room temperature (RT), horseradish peroxidise (HRP), alkaline phosphatase (AP)

Antibody	Supplier, Cat.-No.	Time and temperature	Dilution
rabbit anti-CAR N-terminus	abcam, ab189216	overnight 4 °C + 4 h RT	1:5000
rabbit anti-CAR C-terminus	Sigma, HPA030411	overnight 4 °C + 4 h RT	1:20000
rabbit anti-vinculin	ABclonal, A14193	overnight 4 °C + 4 h RT	1:20000
rabbit anti-His tag HRP-conjugated	abcam, ab1187	1 h RT	1:2000
goat anti-rabbit AP-conjugated	DAKO, D0487	1 h RT	1:1000
donkey anti-rabbit HRP-conjugated	Amersham, NA934V	1 h RT	1:5000

To detect alkaline phosphatase (AP) signals, membrane was washed for 5 min with AP-buffer (0.1 M Tris-HCl, 0.1 M NaCl, 5 mM $MgCl_2$, pH 9.5) and protein bands were revealed with AP Chromogenic Substrate. To detect horseradish peroxidase (HRP) signals, membrane was incubated with ECL substrate and signals were detected with an ECL Chemostar detection system. If necessary, membranes were stripped by two 10 min washing steps with stripping buffer (200 mM glycine, 3.5 mM SDS, 1 % Tween 20, pH 2.2), followed by two 10 min washes with PBS and two 5 min washes with TBST. Then, membranes were blocked again and reprobed.

3.4.10 Mass spectrometry and database searches

Protein bands were cut from colloidal-blue-stained gel and destained by washing with 30 % acetonitrile (ACN) in 100 µM ABC buffer. Gel pieces were dried in a vacuum concentrator and digested with trypsin gold at a final concentration of 10 ng/µl in 3 mM Tris-HCl buffer, pH 8.8 overnight at room temperature and 200 rpm. Digestion was stopped by adding 1 % trifluoroacetic acid (TFA). Gel pieces were incubated in LC-MS grade water with 0.1 % TFA and 50 % ACN for 45 min at room temperature and 400 rpm, and supernatant with extracted peptides was collected. This step was repeated once. Samples were dried in a vacuum concentrator and resuspended in 10 µl of LC-MS grade water with 0.1 % TFA and 2.5 % ACN. Particles were removed by high-speed centrifugation at 13300 x g and 4 °C for 5 min.

nanoLC-MS/MS was performed with an UltiMate 3000 RSLC Dionex system. Peptides were separated by an Acclaim PepMap 100 C18 pre-column cartridge and desalted on a 25-cm Acclaim PepMap 100 C18-LC-column. Effective gradient (15 or 35 min) was 4–30 % or 4–35 % solvent B (80 % ACN, 1 % TFA) with a flow rate of 300 nl/min. Online ESI-Orbitrap mass spectrometry measurements were carried out by a Q Exactive Plus instrument in data dependent top 10 acquisition mode. MS scan range was 350–2000 m/z with a resolution of 70000 and the dynamic exclusion time of precursors for MS/MS was set to 5 or 15 sec. Fragment ions were scanned with a resolution of 17500 and fragmented with normalised collision energy of 28.

Peptide identification was performed with Proteome Discoverer 2.4. Amino acid sequences of human CAR´s extracellular domain (Uniprot P78310, amino acids 20 to 237 and C-terminal 6xHis tag) as well as human NE (Uniprot P08246) were used as template for peptide spectrum matching. Furthermore, the randomly shuffled sequences

(generated with Sequence Manipulation Suite) were added for exclusion of unspecific findings. Semi-tryptic digest was chosen with maximum two missed cleavage sites. Oxidation of methionine and N-terminal acetylation were set as variable modifications. For PNGase F treated samples, deamidation of asparagine and glutamine was included as variable modification. False discovery rate of 0.01 was selected and a minimum of two peptide spectrum matches (PSMs) was set as filter. Peptide search was performed separately for deglycosylated and glycosylated samples, respectively, and results were merged in one consensus file.

3.5 Statistics

Statistics were performed with GraphPad Prism 6. All data are expressed as mean±SEM. P-values <0.05 were considered statistically significant.

4 RESULTS

4.1 Influence of CAR genetic variants on CAR subcellular localisation, cell adhesion, cell proliferation, and virus internalisation

4.1.1 Characterisation of CAR expressing polyclonal CHO cell lines

CHO-K1 cells were stably transfected with vectors coding for wild type CAR and CAR variants (Table 1). Genomic DNA of CHO cell lines was isolated and targeted point mutations in *CXADR* sequence were verified by Sanger sequencing (data not shown).

Subcellular localisation did not differ among the CAR variant forms. All variants were expressed at cell-cell contacts (Figure 14). Punctuate CAR staining in cytoplasm may result from CAR processing in ER or Golgi apparatus.

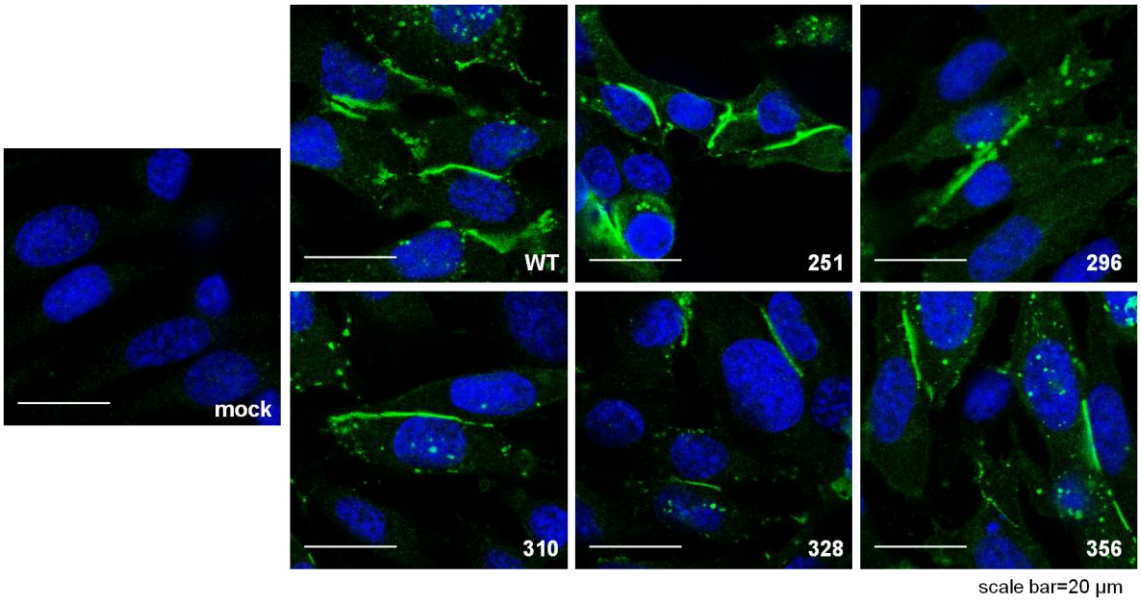

Figure 14: CAR variants localised at cell-cell-contacts. Immunofluorescence staining with anti-CAR antibody H300 of CHO-CAR and CHO mock cells showed the same expression pattern for CAR WT and CAR variants. As expected, CHO mock cells were CAR-negative. Images are representative.

Proliferation rate was determined by measuring the amount of viable cells with a commercial assay and by cell counting. Cell adhesion rate was derived from the amount of cell aggregates over a time span of 5 hours. CAR variants influenced neither cell adhesion nor proliferation rates. Mock transfected cells also did not differ significantly from CAR expressing cell lines (Figure 15).

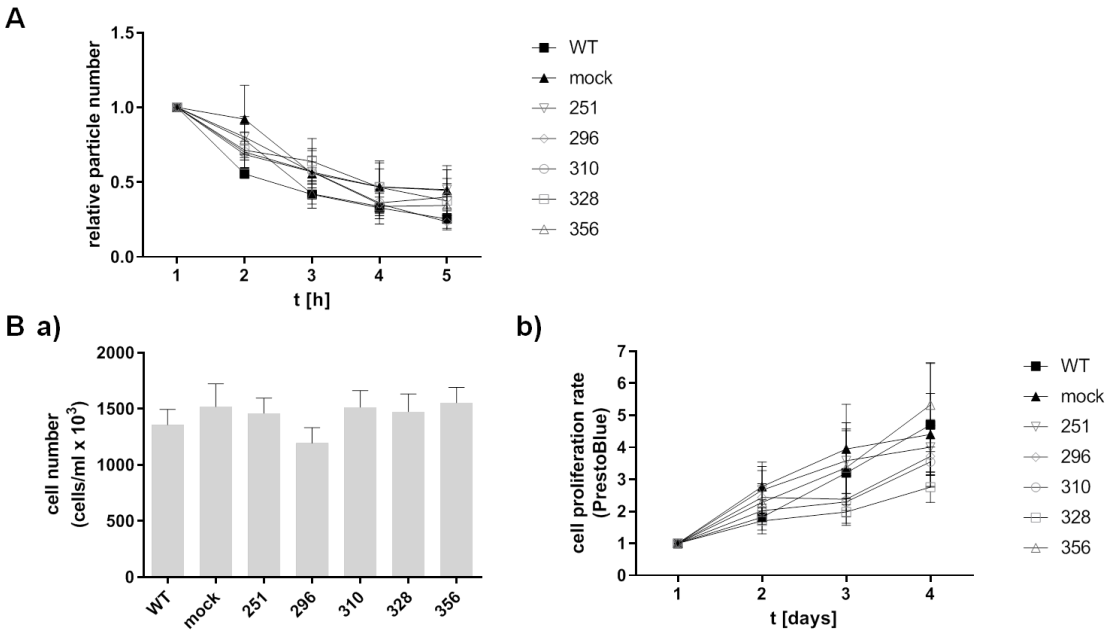

Figure 15: Adhesion and proliferation properties of polyclonal CHO-CAR (CAR wild type and variants) and CHO mock cells did not differ significantly. A) Cell adhesion was determined by counting the number of particles in a cell suspension over a period of 5 h. Single cells as well as cell clumps were counted as one particle. With time, cells adhered and single cells became less frequent leading to a decreased total particle number. Particle number at time point 1 h was set as 1 for each cell line. Graphs show mean±SEM (n=5). Cells expressing CAR variants and mock cells did not differ significantly from CHO-CAR WT cells (two-way ANOVA with Dunnett´s multiple comparisons test). B) Cell proliferation was measured by (a) determining the cell concentration at each subculturing day and by (b) using a commercial assay. At each subculturing day, cells were harvested and resuspended in 4 mL medium. Cell number per milliliter was determined using a hemocytometer. Bars show mean±SEM (n=12). Cell numbers during subculturing did not differ significantly among the cell lines (one-way ANOVA with Dunnett´s multiple comparisons test). The PrestoBlue assay measures cell numbers by detecting a fluorescent dye, which is formed by reduction of resazurin by viable cells. Each day after seeding, resazurin was added to the cells and fluorescence signal was measured. Signal at day 1 was set as 1 for each cell line. Mean±SEM is shown (n=5). Proliferation rates did not differ significantly among the cell lines (mixed effect model test).

4.1.2 Coxsackievirus infection and adenovector transduction

CAR expression levels in polyclonal CHO-CAR cell lines were not uniform as was observed for total and surface protein (Figure 3 in Appendix). After cell sorting, at least 91.5 % of the cell population were CAR-positive in all cell lines (Figure 4 in Appendix). Sorted polyclonal cells with uniform CAR surface expression were then challenged with adenoviral vectors coding for GFP (Ad5-GFP) and Coxsackieviruses B3 (CVB3). Transduction and infection rates were expressed as cells positive for GFP or coxsackieviral VP-1 protein as determined by flow cytometry. No striking difference in cell susceptibility to Ad5-GFP transduction or CVB3 infection was observed among the variants. CHO mock cells were not susceptible as expected (Figure 16).

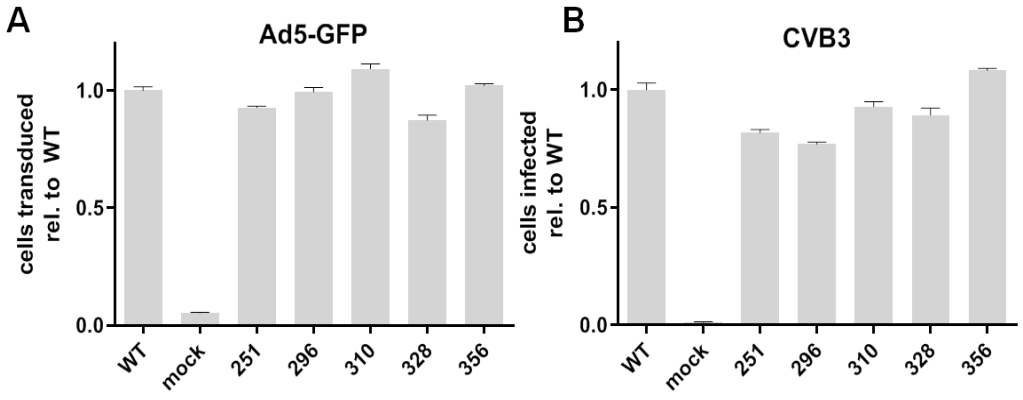

Figure 16: Polyclonal CHO cells expressing CAR variants did not differ prominently in their susceptibility to Ad5-GFP transduction or CVB3 infection. A) Ad5-GFP MOI=100 (ANOVA with multiple comparisons with CAR-WT: mock ****, 251 *, 296 ns, 310 **, 328 ***, 356 ns) B) CVB3 MOI=1 (ANOVA with multiple comparisons with CAR-WT: mock ****, 251 ****, 296 ****, 310 ns, 328 **, 356 *)

4.2 Adenovector transduction inhibition by synthetic peptides based on CAR D1 or adenoviral knob

4.2.1 Rationale of peptide design

Peptide sequences stem from CAR D1 domain as well as from the adenoviral knob. Amino acids involved in D1-knob interaction were determined by analysis of CAR D1-Ad12 knob crystal structure or CAR-CAR homodimerisation (Figures 8 and 2). Buried surface area scores of the interfaces were determined with the Proteins, Interfaces, Structures and Assemblies (PISA) tool. Residues, which are inaccessible for the solvent, since they are exposed to the ligand, have high buried surface area scores and are probably involved in contact formation. PISA results are presented in Tables 1-4 in Appendix. Furthermore, information from the literature about residues involved in interactions was taken into account (see 1.1.1.2 and 1.1.4.3).

Seven peptides based on CAR D1 domain were designed (Figure 17). Cysteine at position 120 was replaced with a threonine in peptides CAR2, CAR6, and CAR7 to exclude unwanted disulfide bond formation. Threonine is a frequent amino acid in beta-sheets (CHOU & FASMAN 1978). Peptide CAR2 skips a large sequence in order to connect three beta sheets. In peptide CAR7, a glycine replaces leucine 139, since glycine is often present in turns (CHOU & FASMAN 1978) and the peptide was planned to be cyclised. However, this was not feasible during synthesis process.

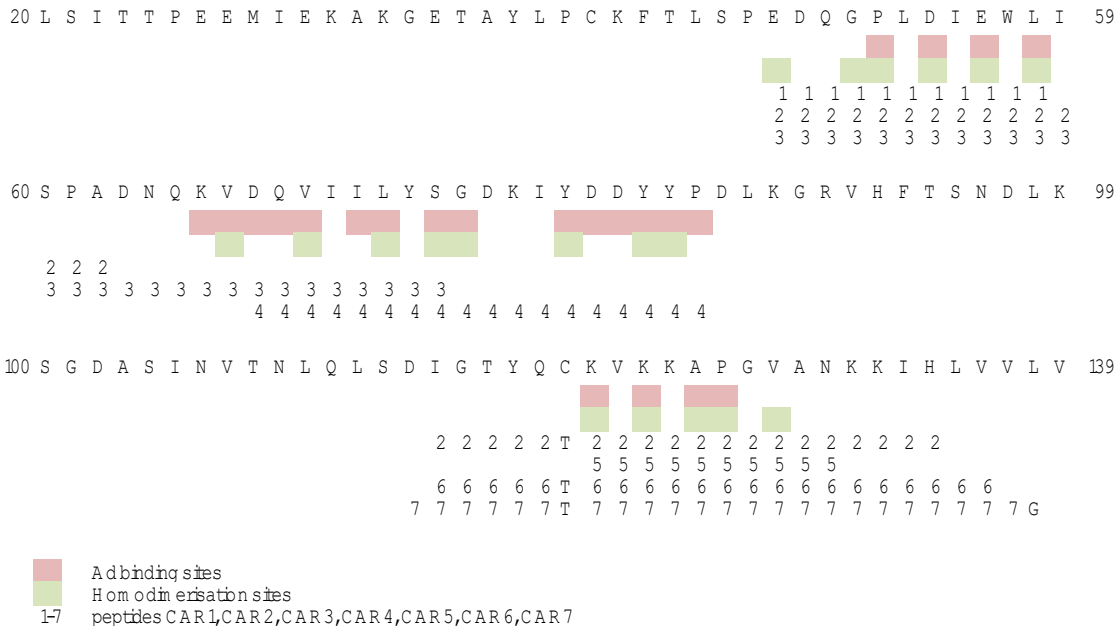

Figure 17: CAR ECD sequence with Ad binding and homodimerisation sites. Part of CAR ECD (amino acids 20 to 139; UniProt accession number P78310) is depicted with coloured amino acids important for CAR-Ad knob interaction (magenta) and for CAR homodimerisation (green). Numbers indicate the sequences of the seven synthesised peptides used in this work (CAR1-CAR7).

For peptides derived from Ad knob motifs, amino acid sequences of Ad5 and Ad12 knob were aligned (Figure 5 in Appendix). Crystal structure was determined for Ad12-CAR complex (Figure 8). I designed peptides that matched the Ad5 sequence (Figure 18), because I used Ad5-GFP for transduction experiments.

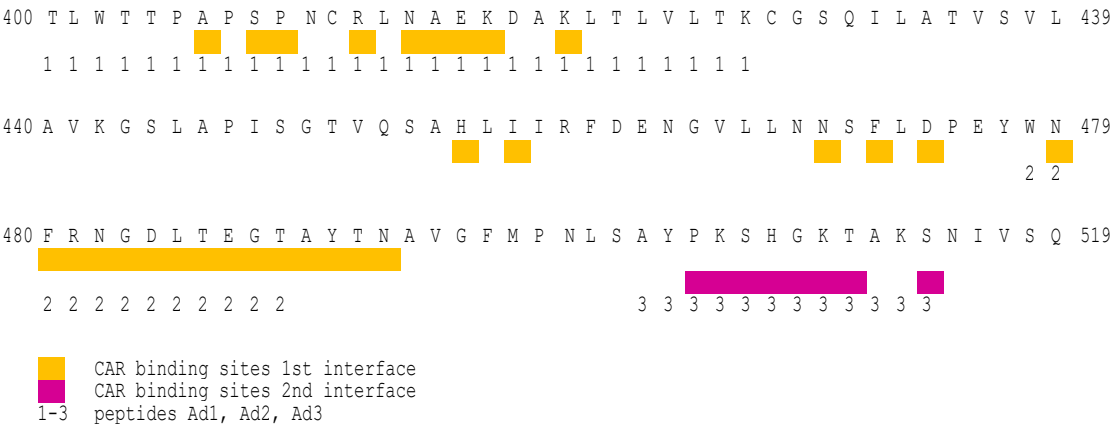

Figure 18: Ad5 knob sequence with CAR binding sites. Part of the Ad5 fiber that comprises the knob (amino acids 400 to 519; Uniprot accession number P11818) is depicted with coloured amino acids that are important for CAR-knob interaction. Amino acids involved in the binding to CAR D1 are coloured (Figure 8 interface 1 in orange, interface 2 magenta). Numbers indicate the sequences of the three synthesised peptides used in this work (Ad1-Ad3).

Location of sequences in CAR D1 and Ad5 knob corresponding to synthesised peptides is visualised in Figure 19. Compare Figures 2 and 8 for corresponding positions of interaction sites.

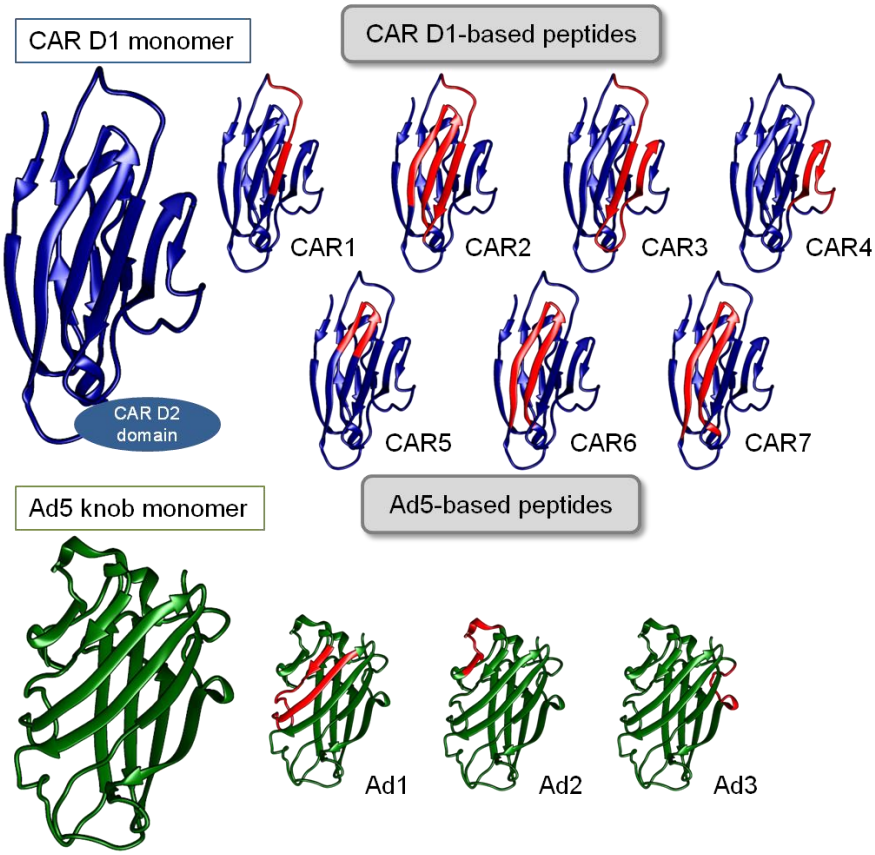

Figure 19: Potential entry-inhibitor peptides designed for this study. For peptides based on CAR D1 (CAR1-CAR7), sequences correspond to the amino acid motifs involved in Ad knob binding and CAR homodimerisation (top). Peptides based on Ad5 knob monomer (Ad1-Ad3) comprise the CAR-binding sites (bottom). Localisation of the peptide sequences in CAR D1 monomer (PDB ID: 1RSF (JIANG ET AL. 2004)) and Ad5 knob monomer (PDB ID: 4ATZ (DREIER ET AL. 2013)) is coloured in red.

4.2.2 Peptide treatment for adenovector entry inhibition

Some peptides were tested for their cytotoxicity. None of the tested peptides was toxic to A549 cells, when added in concentrations up to 100 µM. However, addition of seven different peptides in a concentration of 10 µM each was slightly toxic (Figure 6 in Appendix).

Adenoviral vectors expressing GFP (Ad5-GFP) and A549 cells were preincubated with synthetic peptides for 1 h at 37 °C. Then, cells were challenged with Ad vectors (MOI=1000) in the presence of peptides for 1 h. Afterwards, medium was aspirated, cells were washed and GFP expression was determined with flow cytometry the next

day. No peptide showed a significant dose-dependent inhibitory effect on Ad5-GFP transduction rate. The peptide mix also did not reduce transduction efficiency significantly (Figure 20). No dose-dependent inhibition could be observed, when lower MOI (500) or shorter transduction time (30 min) were tried (Figure 7 in Appendix).

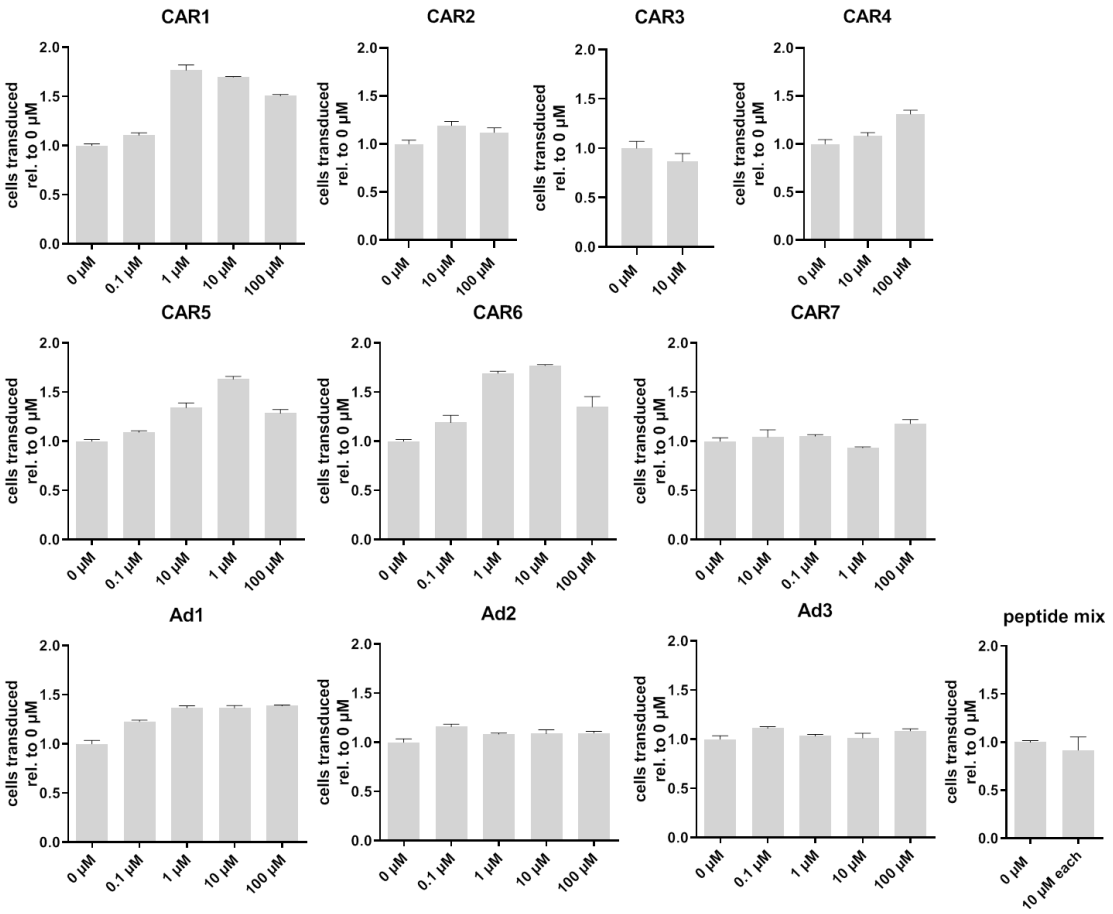

Figure 20: Peptide treatment did not decrease transduction efficiency. Ad5 vectors and A549 cells were preincubated with peptides at indicated concentrations for 1 h. Furthermore, a peptide mix of CAR1, CAR2, CAR4, CAR5, CAR6, CAR7, and Ad1 (each peptide in a concentration of 10 µM) was tested. Ad5-peptide mixtures were added to the cell culture medium (MOI=1000). Cells were challenged with Ad5 vectors for 1 h, before cell culture medium was exchanged and transgene expression was determined the next day (GFP readout by flow cytometry). Transduction efficiency is normalised to samples without peptide addition (0 µM). No striking dose-dependent decrease in Ad5 transduction could be observed for a single peptide or the peptide mix. Each experiment was performed as technical triplicate and bars show mean±SEM.

4.3 Proteolysis of soluble and membranous full-length CAR or CAR ECD by MMPs and neutrophil serine proteases

4.3.1 Human CAR expressed by *E. coli*

Human neutrophil serine proteases (NE, PR3, and CG) as well as catalytic domains of several human MMPs were tested for their potential to cleave human CAR expressed by *E. coli* (Figure 21). General activity of proteases was confirmed with artificial substrates (Figure 8 in Appendix). Recombinant CAR with an N-terminal His tag and an Xpress epitope ran at a height between 38 and 49 kDa in the gel, which corresponds to its calculated molecular weight of 42 kDa. All proteases cleaved CAR´s N-terminus within overnight digestion. MMP-9 and MMP-11 digest resulted in cleavage products that were recognised by the anti-CAR N-terminus antibody and ran at about 34-38 kDa. All other proteases proteolysed CAR so that the epitope (amino acids 20-50 in mature CAR) was not recognised by the antibody anymore.

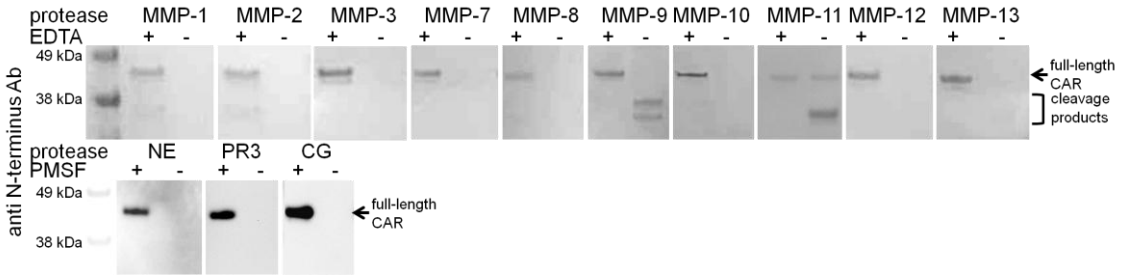

Figure 21: Human CAR expressed by *E. coli* was cleaved by catalytic MMP domains and serine proteases. Inclusion body preparations from *E. coli* expressing human CAR were treated overnight with proteases (100 ng/µl). Blots were probed with anti-CAR N-terminus antibody. Human CAR expressed by *E. coli* was cleaved by MMPs and serine proteases. MMP-9 and MMP-11 had distinct cleavage pattern, whereas the other MMP catalytic domains and serine proteases cleaved the antibody´s epitope and no product was recognised by anti-CAR N-terminus antibody. Addition of protease inhibitors (EDTA for MMPs and PMSF for serine proteases) inhibited proteolysis.

4.3.2 Human CAR ECD expressed by HEK-293 cells

4.3.2.1 Overnight digest by MMPs and serine proteases

Compared to proteins expressed by eukaryotic cells, *E. coli* expressed proteins are not posttranslationally modified. Since mammalian CAR is glycosylated at two asparagine residues in its ECD, these modifications may have implications for putative shedding events. Therefore, I tested recombinant human CAR extracellular domain (rhECD) with a C-terminal 6xHis tag expressed by HEK-293 cells and detected cleavage products

with an anti-CAR N-terminus antibody and with an anti-His tag antibody via Western blotting. Full-length rhECD ran at a height of about 30 kDa, which is in line with its calculated molecular weight of 24.8 kDa plus about 3 kDa per sugar moiety (EXCOFFON ET AL. 2007; HONDA ET AL. 2000). Furthermore, a smaller protein, which was recognised by both antibodies, occurred at a slightly lower molecular weight. This might be a glycoform of the full-length rhECD, since it disappeared upon deglycosylation (Figure 9 in Appendix).

Most MMP catalytic domains did not cleave rhECD within overnight incubation (Figure 22). An exception was MMP-3, which cleaved rhECD and created two products recognised by anti-CAR N-terminus and anti-His tag antibody, respectively.

To test, whether proteases were recognised by antibodies, only MMP-3, MMP-9, and MMP-11 were loaded. Corresponding controls for serine proteases are depicted in Figures 23 and 24. MMP-9 and MMP-11 catalytic domains were recognised by the anti-His tag antibody as monomers and dimers. Molecular weight is 39 kDa for MMP-9 and 19.3 kDa for MMP-11 according to the manufacturer´s data sheets.

Digest with serine proteases resulted in distinct cleavage pattern within overnight digest. All products were recognised by the anti-CAR N-terminus antibody, but not by the anti-His tag antibody, suggesting that proteases cleaved the C-terminal part of the ECD. For further analyses, I focused on serine proteases, since MMP-3 cleavage was not as extensive.

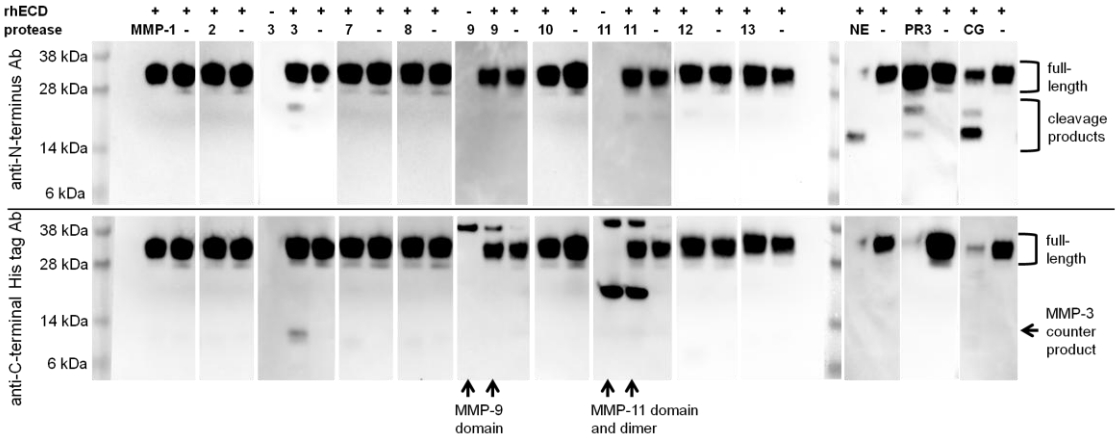

Figure 22: Human recombinant CAR extracellular domain (rhECD) expressed by HEK-293 cells was cleaved by MMP-3 and serine proteases. During overnight treatment, MMP-3, PR3, CG, and NE cleaved rhECD and products were recognised by anti-N-terminus antibody or anti-His tag antibody. MMP-9 and MMP-11 catalytic domains contain a His tag and were recognised by anti-His tag antibody as monomers and dimers.

4.3.2.2 *Time and concentration series of serine protease digests*

rhECD was incubated with PR3, CG (Figure 23), or NE (Figure 24) at 37 °C for different time points and samples were visualised by probing blots with anti-CAR N-terminus antibody and anti-His tag antibody. As controls, rhECD or protease alone were incubated overnight at 37 °C. Proteases are not recognised by the antibodies.

PR3 cleaved rhECD close to its His tag. The cleavage product ran at the same height as full-length rhECD and was not recognised by anti-His tag antibody. The cleaved His tag was not detected as it was probably too small to be visualised in a gel with this polyacrylamide gradient. Furthermore, two cleavage products were recognised by the anti-N-terminus antibody but not by the anti-His tag antibody. This was also the case for CG digest. Both proteases needed several hours to cleave rhECD and cleavage was not completed after overnight incubation. Subtle differences in apparent protein quantities may be explained by uneven gel loading.

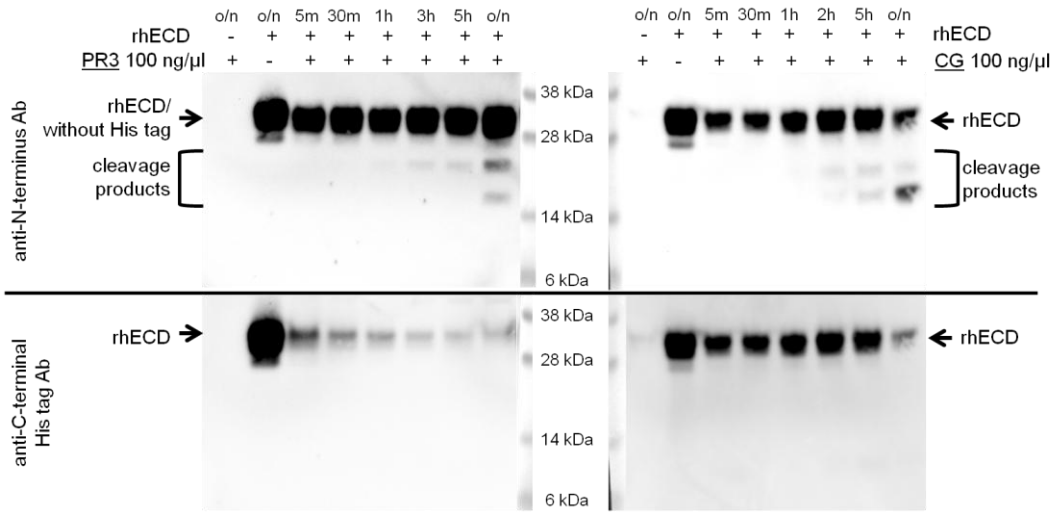

Figure 23: Time series of PR3 and CG cleavage of rhECD. Proteases were added to rhECD with a concentration of 100 ng/µl for time spans indicated on top. PR3 cleaved the His tag within 5 min resulting in a product running at about the same height as full-length rhECD. Both PR3 and CG digests resulted in a distinct cleavage pattern within hours of treatment. Products were recognised by anti-N-terminus antibody, but not anti-His tag antibody.

For NE, time and concentration series were performed. As PR3, NE cleaved rhECD close to its His tag. Compared to PR3 and CG however, NE cleaved rhECD faster and more extensively. Within 5 minutes, a smaller product occurred, which was subsequently cleaved to a secondary product. Due to the time-dependent occurrence of these cleavage products, I designated them intermediate and end product. Both of them were

recognised by the anti-N-terminus antibody, but not by the anti-His tag antibody, indicating that cleavage sites are located at the C-terminal D2 domain of CAR. Interestingly, intermediate and end product also occurred, when a concentration series was performed with NE. Therefore, products formed time- and dose-dependently. When low NE concentrations were used, the His tag was not cleaved off of full-length rhECD. Therefore, cleavage that resulted in the intermediate product also yielded a counter product, which was recognised by anti-His tag antibody.

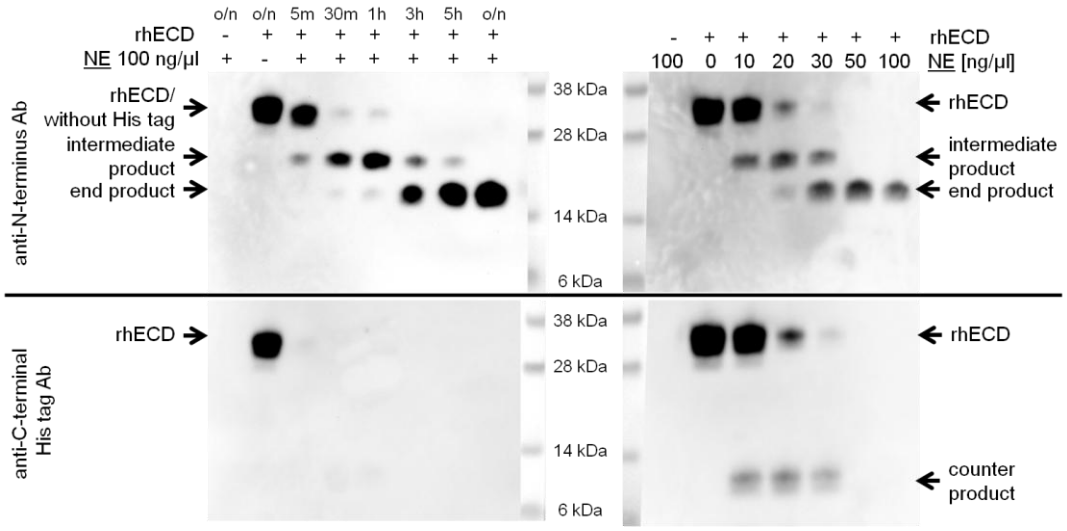

Figure 24: Time and concentration series of NE digest of rhECD. NE (100 ng/µl) cleaved the His tag within 5 minutes resulting in a product that ran at about the same height as full-length rhECD. NE digest resulted in two distinct cleavage products, an intermediate and an end product. This pattern was observed with both increasing incubation times and NE concentrations. Lower NE concentrations (10-30 ng/µl) did not remove the His tag from rhECD after overnight incubation. Therefore, a C-terminal counter product recognised by anti-His tag antibody occurred.

To compare sizes of rhECD digest end products, overnight treated samples were visualised in a silver-stained gel (Figure 25). CG end product was slightly larger than products from NE and PR3 digest. Since end products were recognised by the anti-N-terminus antibody in Western blots, they included CAR´s D1 domain. No other cleavage products with lower molecular weights were detected with silver staining. Therefore, serine proteases seemed to digest CAR´s D2 domain extensively.

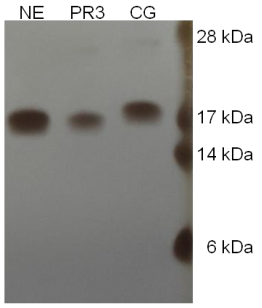

Figure 25: Size comparison of NE, PR3, and CG digest end products. Silver-stained gel of overnight digested rhECD samples treated with 100 ng/µl protease.

4.3.2.3 Determination of NE cleavage sites in rhECD by nLC-MS/MS

Estimated molecular weights of rhECD full-length as well as NE digestion products in their glycosylated and deglycosylated states were determined with a silver-stained gel (Figure 26). Different migration pattern of glycosylated and deglycosylated proteins indicate that full-length rhECD as well as the intermediate product contain both N-glycosylation sites and that the end product contains only one sugar moiety.

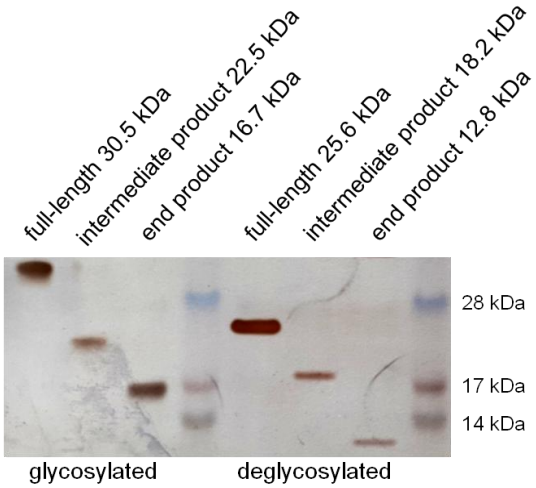

Figure 26: Silver-stained gel of glycosylated and deglycosylated NE digest products. Deglycosylation of rhECD full-length and NE digest products results in different migration pattern in the polyacrylamide gel. Estimated molecular weights are listed.

Glycosylated as well as deglycosylated proteins were in-gel digested with trypsin. Tryptic peptides were analysed with nLC-MS/MS (Table 5 in Appendix) and coverage is visualised in Figure 27. Full-length rhECD was completely covered by peptides (magenta). The intermediate product (green) comprised full D1 domain and a large part of the D2 domain. Accordingly, it contained both glycosylated asparagine residues. The end product included mainly the membrane-distal D1 domain and only one asparagine

residue. Since NE cleaves preferentially after aliphatic amino acids like valine, alanine, and isoleucine (FU ET AL. 2018), valines at positions 129 and 199 seemed to be suitable cleavage sites. Intermediate product that comprises amino acids 1 to 199 has a calculated molecular weight of 22.1 kDa. The end product (amino acid 1 to 129) has a calculated molecular weight of 14.3 kDa. Both sizes fit quite well to the sizes of deglycosylated proteins in the polyacrylamide gel (Figure 26).

CG end product was also analysed with nLC-MS/MS, but with less repeated measurements (Table 5 in Appendix). Therefore, coverage was not as high as for NE products (Figure 10 in Appendix).

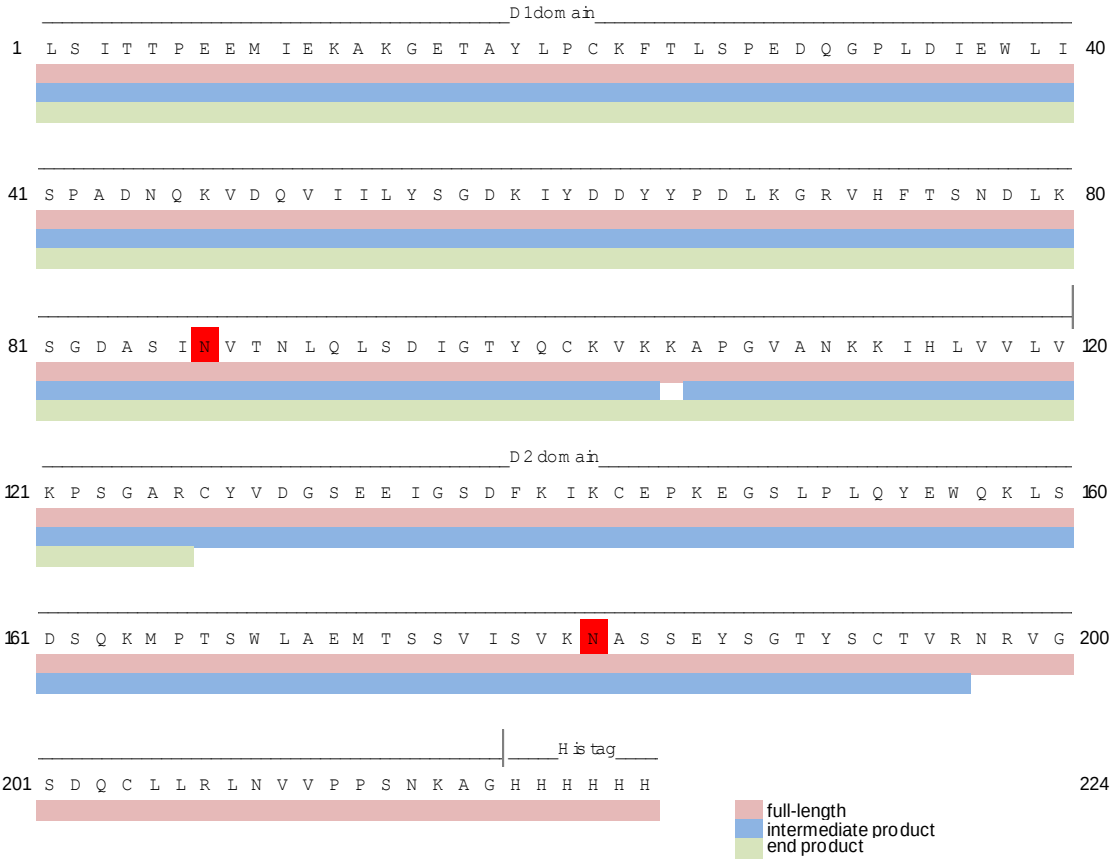

Figure 27: Sequences of full-length rhECD, intermediate and end product of NE digest covered by peptides (nLC-MS/MS). Full-length rhECD sequence was completely covered by peptides (magenta). The intermediate product (blue) contained the complete membrane-distal D1 domain and a large part of the membrane-proximal D2 domain. The end product (green) included D1 domain and a small part of D2 domain. N-glycosylation sites are marked in red.

4.3.2.4 Role of disulfide bonds and N-glycosylation in NE cleavage

The importance of the tertiary structure on the susceptibility of rhECD to NE proteolysis was assessed by reducing disulfide bonds either before or after NE digest (Figure

28). As seen before (Figure 24), NE digest of rhECD in its native conformation resulted in the intermediate and end product (Figure 28A). Interestingly, reduced disulfide bonds led to a cleavage pattern that was also observed for lower NE concentrations (Figure 24), i.e. the intermediate and the counter product. Furthermore, the His tag was not cleaved (Figure 28B). Therefore, reduced disulfide bonds and a disrupted tertiary structure of rhECD seemed to mask two cleavage sites (for cleavage of the His tag and the end product). When samples were run under non-reducing conditions in the gel (Figure 28C and D), the same cleavage pattern were observed. Native intermediate product did not migrate properly into the gel (Figure 28C).

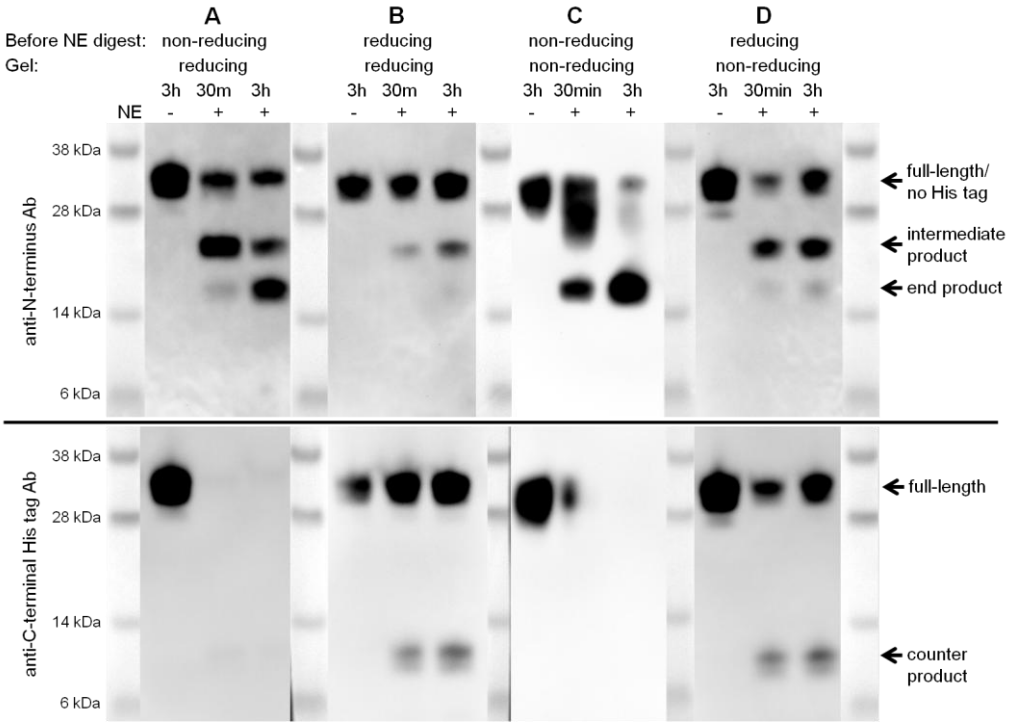

Figure 28: Tertiary structure of rhECD facilitated access of NE to the cleavage site of the end product. rhECD was digested for 30 min or 3 h with NE. As control, no protease was added. A and B) Sample buffer for polyacrylamide gel runs included DTT. C and D) Sample buffer did not include DTT. A) Native rhECD digest with NE results in the intermediate and end product. B) Disulfide bonds were reduced by DTT before NE digest. His tag was not cleaved off resulting in the counter product recognised by anti-His tag antibody. After 3 h NE digest, the end product did not occur. The same pattern was observed, when samples were run without DTT in the sample buffer (C and D).

Furthermore, the role of N-glycosylation in NE-mediated cleavage was investigated. Therefore, sugars were removed either before or after NE digest with PNGase F under non-denaturing conditions. Glycosylated rhECD was cleaved into the intermediate and end product (Figure 29A) and deglycosylated cleavage products migrated at lower molecular levels (Figure 29B) as demonstrated before (Figure 26). rhECD was incubated

overnight either with PNGase F buffer alone or with PNGase F in buffer at 37 °C (Figure 29C and D). Overnight incubation at 37 °C seemed to alter the tertiary structure of rhECD, although the non-reducing buffer format was used. The digestion pattern was the same as for rhECD with reduced disulfide bonds (Figure 28B). PNGase F did not deglycosylate rhECD to a full extent, when rhECD was not pre-digested by NE (compare Figure 29B and D). Only one oligosaccharide entity seemed to be removed for a large fraction of full-length rhECD. Besides, already within 30 min digestion time, the end product (glycosylated and deglycosylated) occurred. Loss of sugar moieties seemed to alter the presentation of cleavage sites to NE. However, since rhECD was present in an altered conformation after overnight incubation with PNGase F buffer (Figure 29C), no final statement could be made about the exact role of rhECD glycosylation.

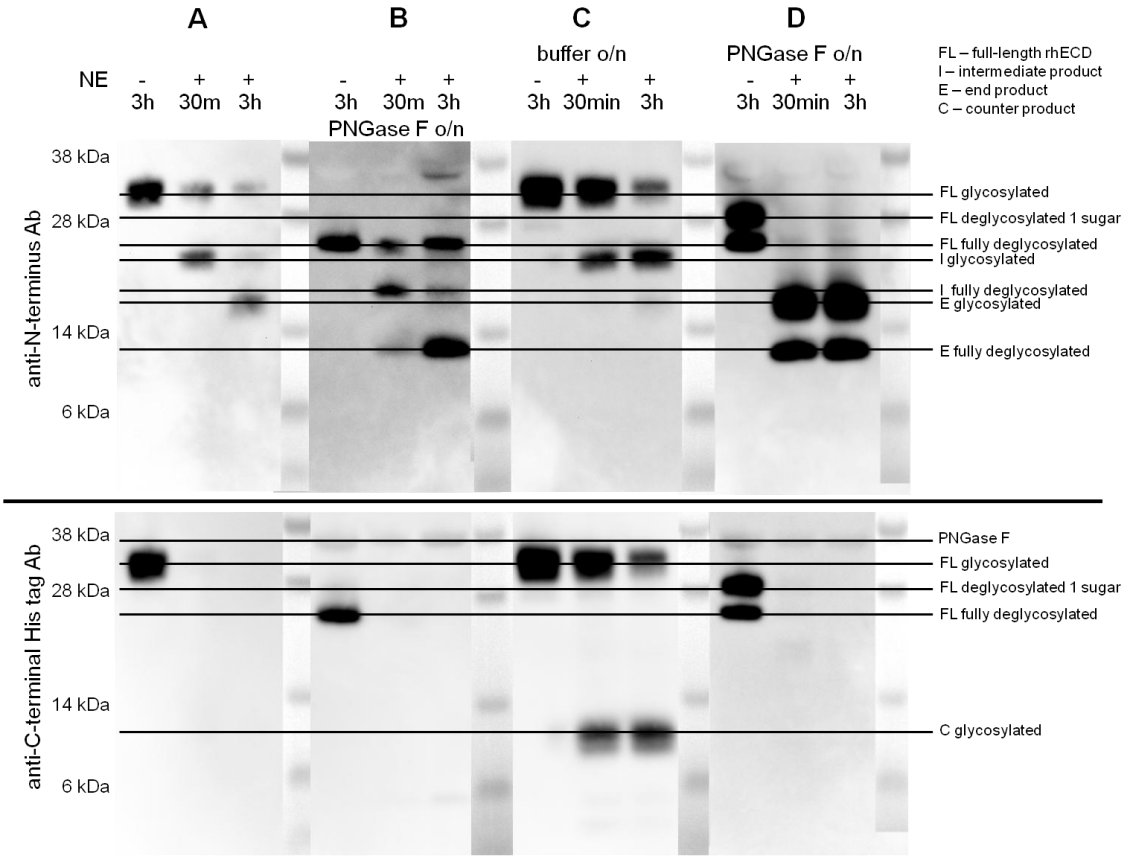

Figure 29: Sugar moieties protected rhECD from proteolysis at the second cleavage site by NE. rhECD was digested for 30 min or 3 h with NE. As control, no protease was added. Furthermore, rhECD was deglycosylated either before or after NE digest. A) rhECD full-length (FL) in its glycosylated form was digested by NE. Intermediate (I) and end (E) product occurred. B) After NE digest, products were deglycosylated. C) rhECD was incubated with PNGase F buffer overnight before NE digest. Intermediate and counter (C) products occurred, but not end product. D) rhECD was deglycosylated by PNGase F and treated with NE afterwards. Missing sugar moieties allowed faster cleavage and end product occurred already within 30 min incubation time.

4.3.2.5 NE cleavage of rhECD bound to nickel NiNTA resin

To mimic a situation, in which CAR´s extracellular domain is present on a surface as it would be on a cell membrane, rhECD was coupled to NiNTA beads and NE was added for 3 h. I wanted to test, whether orientation on a surface alters conformation and thereby susceptibility of rhECD towards proteolysis. After NE digest (Figure 30A), both end product and rhECD without the His tag were observed in the supernatant. The source of the end product must therefore not necessarily be bound rhECD, but could also be soluble rhECD without His tag. To test whether disulfide bonds stabilised cleavage products, 12.5 mM DTT was added to NiNTA resin after NE digest (Figure 30B). This DTT concentration reduced nickel and full-length rhECD eluted from the resin. However, when lower DTT concentrations were used, no products were released from NE treated samples (data not shown). Elution from bound rhECD and cleavage products showed that intermediate and end product were still attached to NiNTA resin despite DTT treatment (Figure 30C). Disulfide bonds did not seem to be responsible for attachment of the products to the resin, which was in line with observations for unbound rhECD (Figure 28). Cleavage products may remain associated by other chemical bonds, for example salt bridges, hydrogen bonds, or van der Waals forces.

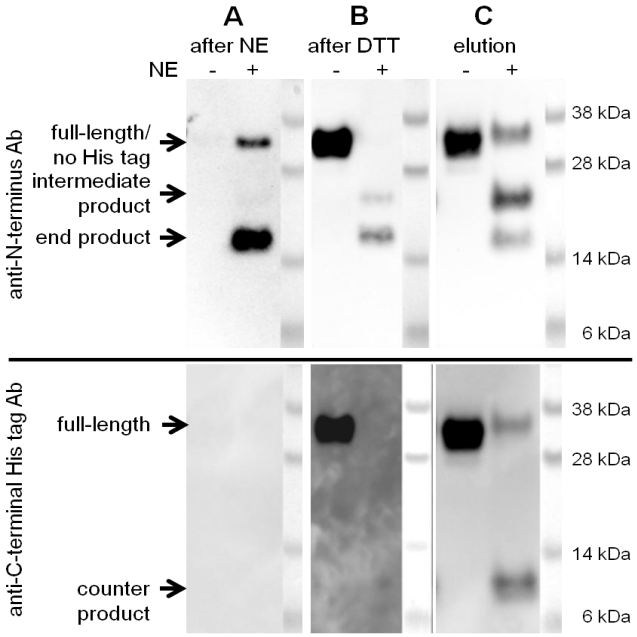

Figure 30: rhECD bound to NiNTA was cleaved by NE. A) NE (100 ng/µl) was added for 3 h to rhECD bound to NiNTA resin and the end product occurred in the supernatant. B) Reduction of disulfide bonds released intermediate and end products from the resin, but also full-length rhECD due to the reduction of nickel. C) Full-length rhECD and cleavage products were still attached to NiNTA resin and were washed out with elution buffer.

Moreover, surface plasmon resonance (SPR) spectroscopy was used to mimic proteolysis of membranous CAR ECD. However, rhECD did not bind stably to the nickel loaded NTA sensor chip. Within one to three minutes, rhECD `bled out` to an extent that no mass decrease could be observed by addition of NE (data not shown).

4.3.3 NE cleavage of murine CAR ECD

For possible future studies regarding shedding experiments *in vivo*, behaviour of murine CAR upon NE digest was investigated. Alignment of human and murine CAR D2 domain (Figure 11 in Appendix) showed high similarity between the species. Time series of NE digest was performed with recombinant murine extracellular CAR domain (rmECD) expressed by HEK-293 cells with a C-terminal His tag (Figure 31). As in rhECD (Figure 24), the His tag was cleaved off of rmECD and two N-terminal cleavage products occur. In contrast to rhECD, the larger product was not a prerequisite for occurrence of the smaller product in rmECD. The smaller product occurred within 5 min incubation time with NE and increased in quantity over time. The larger product occurred within 30 min incubation time and remained present in the sample even after overnight incubation time. Obviously, cleavage of human and murine CAR ECD by NE differed, although proposed cleavage sites of NE in human CAR (valine 129 and 199) also exist in murine CAR D2 domain (Figure 11 in Appendix).

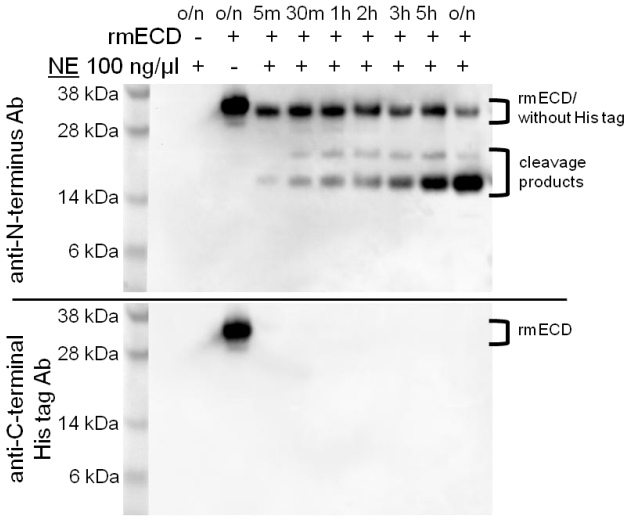

Figure 31: Time series of NE digest of rmECD. NE (100 ng/µl) cleaved the His tag within 5 minutes resulting in a product that ran at about the same height as full-length rmECD. NE digest resulted in two distinct cleavage products. The smaller product increased with time. The larger product occurred within 30 min, but did not change in quantity within longer incubation times.

4.3.4 Human CAR expressed by CHO-K1 cells

To test proteolysis of full-length human CAR expressed by eukaryotic cells, whole cell lysate of CHO-CAR cells was treated with various MMPs and serine proteases. As control, inhibitors (EDTA for MMPs and PMSF for serine proteases) were added. CAR products were detected with anti-CAR N-terminus and C-terminus antibodies (Figure 32). Full-length CAR ran at a height of about 48 kDa. N- and C-terminus antibodies recognised cleavage products of MMP and PR3 digests, which ran at heights of 38 to 45 kDa. This suggests that cleavage occurred in the intracellular domain of CAR but left the C-terminal antibody epitope intact. NE and CG, however, digested CAR extensively and no cleavage product was recognised by either N- or C-terminus antibodies. PMSF was solubilised in ethanol. Therefore, ethanol without PMSF was added as control. To test, if ethanol itself influenced CAR´s conformation and thereby protease digest, no ethanol was added to the reactions. Cleavage pattern of NE and PR3 were the same (Figure 12 in Appendix).

Differences in serine protease cleavage between rhECD (Figure 22) and CAR expressed by CHO-K1 cells (Figure 32) could be explained with the preparation procedure of cell lysates. Lysis buffer contained 1 % Nonidet P40 detergent. When rhECD was denatured with SDS, DTT, and Nonidet P40, overnight treatment with NE also resulted in extensive proteolysis (Figure 13 in Appendix). Denatured CAR was therefore highly susceptible to unlimited proteolysis, whereas CAR ECD in its native conformation was cleaved into two distinct products by NE. This was also observed for rhECD with reduced disulfide bonds (Figure 28).

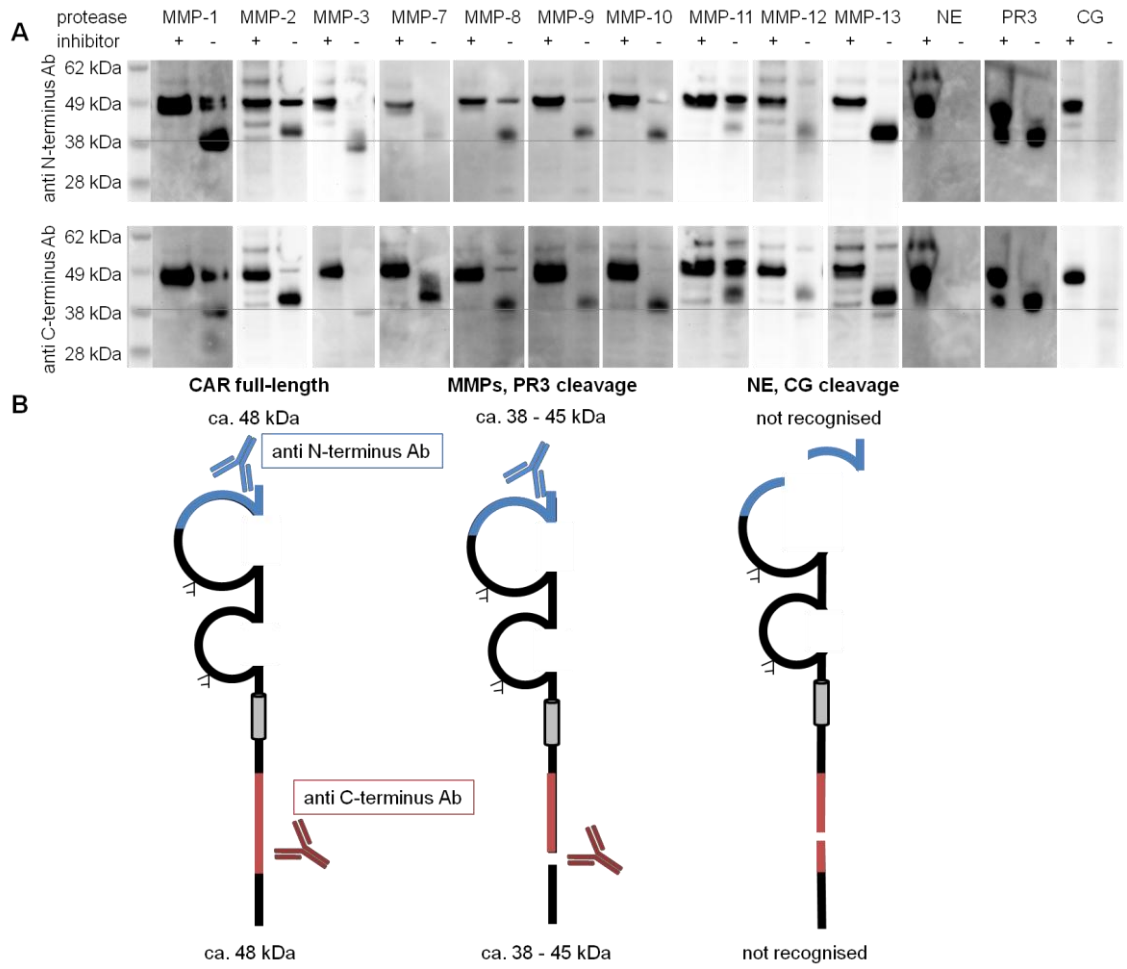

Figure 32: Human CAR expressed by CHO-K1 cells was cleaved by catalytic MMP domains and serine proteases. A) Western blots with N- and C-terminal anti-CAR antibodies. B) Schematic representation of CAR cleavage. Whole cell lysates from CHO-CAR cells were treated overnight with proteases (100 ng/µl). Proteolysis was inhibited by EDTA for MMP domains and PMSF for serine proteases. Catalytic MMP domains and PR3 digested CAR at its C-terminus. The cleavage products ran at heights of about 38 to 43 kDa and both anti-CAR antibodies recognised them. NE and CG digested CAR so that anti-CAR antibodies did not recognise cleavage products.

4.3.5 Membranous CAR in mammalian epithelial cells

4.3.5.1 CAR expression in investigated mammalian cell lines

To test CAR cleavage by NE not only in solution or bound to an artificial surface, six mammalian epithelial cell lines from different tissue origin were tested. Cells express human CAR either exogenously (CHO-CAR) or endogenously (A549, HeLa, HEK-293, HepG2, and SW13). CAR expression was confirmed by flow cytometry and immunofluorescence microscopy (Figure 33). Expression levels as well as localisation of CAR varied between the cell lines. Localisation coincided with cell-cell contacts. For

example, A549 cells displayed a discontinous ´chickenwire´ outline of cell-cell contacts, whereas HepG2 cells tended to form strong clusters with large contact sites.

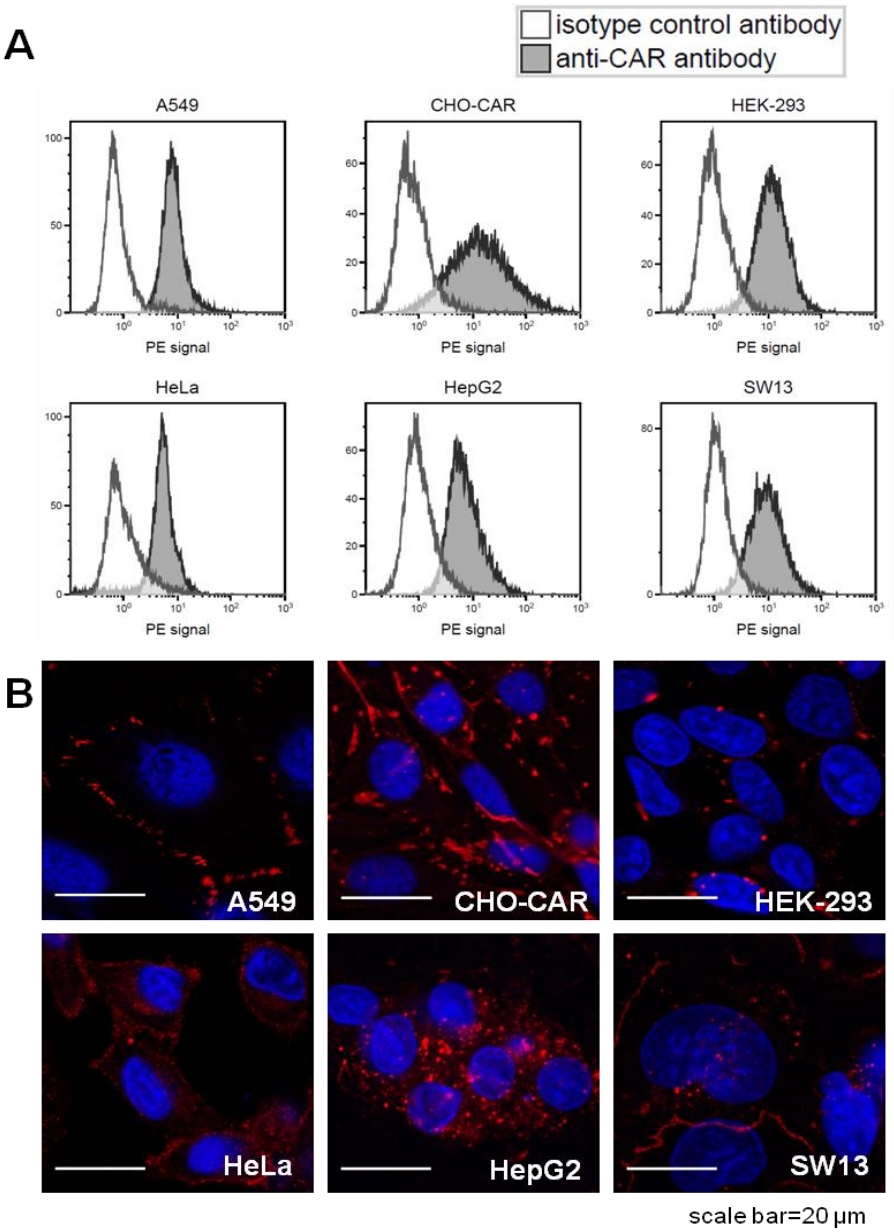

Figure 33: CAR was expressed at the cell surface of all six investigated epithelial cell lines. A) Cells were stained with anti-CAR or isotype control antibody and analysed by flow cytometry. Histograms are representative. B) CAR was localised at cell-cell-contacts in epithelial cells. Immunofluorescence staining showed different expression pattern in human and hamster epithelial cell lines. Endogenous CAR as well as CAR overexpressed in CHO cells was located at cell junctions, however, shapes of membrane contact sites differed among the cell lines. Images are representative. HeLa was stained with RmcB antibody and other cells were stained with 3C100 antibody. As expected, CHO mock cells were not stained by these anti-CAR antibodies (Figure 14 in Appendix).

4.3.5.2 *Changes of cell morphology and cleavage of virus coreceptors through NE treatment*

NE was added to cells in the presence of Ham´s F-12, but without the addition of FBS to prevent NE cleavage of serum proteins. NE activity in Ham´s was confirmed with an artificial substrate and rhECD (Figure 15 in Appendix).

Since NE does not display a high substrate specificity (KORKMAZ ET AL. 2007), it alters cell morphology by cleavage of several surface proteins. Cells were detached from the cell culture vessel by treatment with NE in a time-dependent manner (Figure 34).

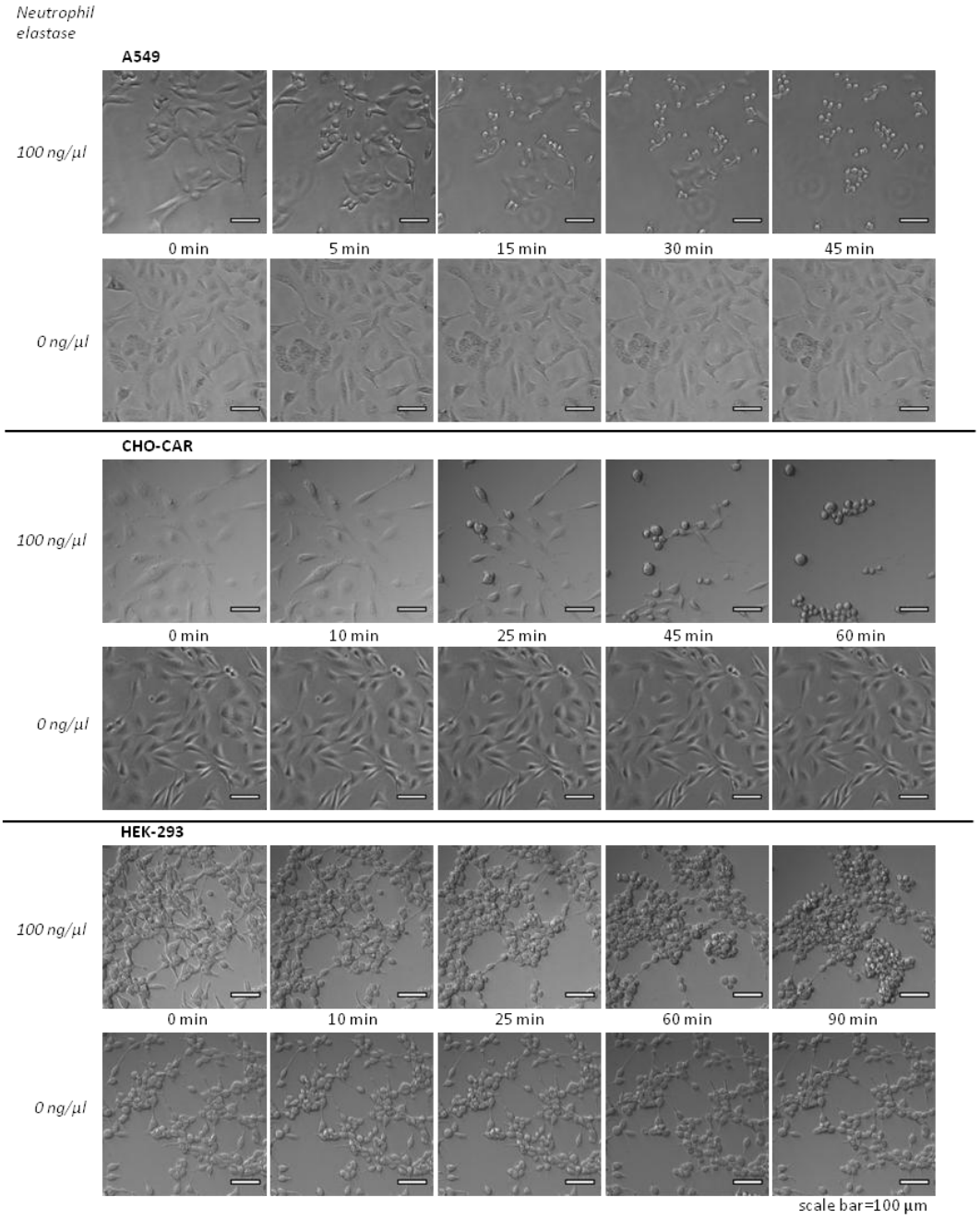

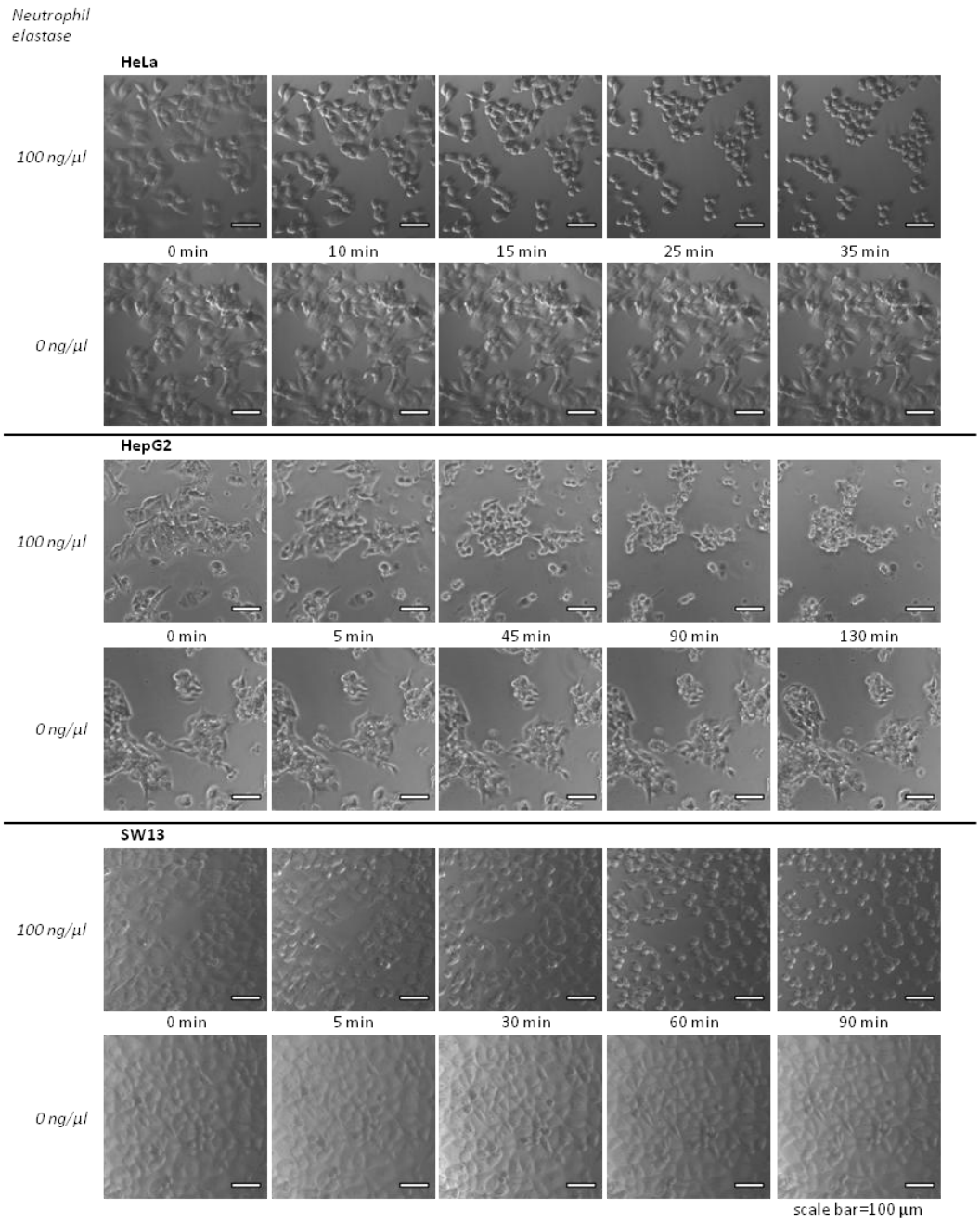

Figure 34: NE treatment detached cells from the culture vessel surface. NE was added to the six cell lines (A549, CHO-CAR, HEK-293, HeLa, HepG2, and SW13) at a concentration of 100 ng/µl in Ham´s F-12 medium and cell dissociation after different time points was documented. As a control, NE reconstitution buffer without NE was added (0 ng/µl).

Since NE detached cells from the vessel surface, I tested whether it also permeabilised CHO-CAR cells for antibodies used for flow cytometry (Figure 35). If the antibody stained intracellular CAR, this would conceal a possible CAR-shedding effect after NE treatment. Intracellular vimentin was stained in all permeabilised cells, whereas only a few non-permeabilised cells were stained. The same low staining level was observed for

cells treated with NE for 5 h, indicating that cells were not permeabilised for antibodies. Statistics for this experiment are visualised in Figure 16 in Appendix.

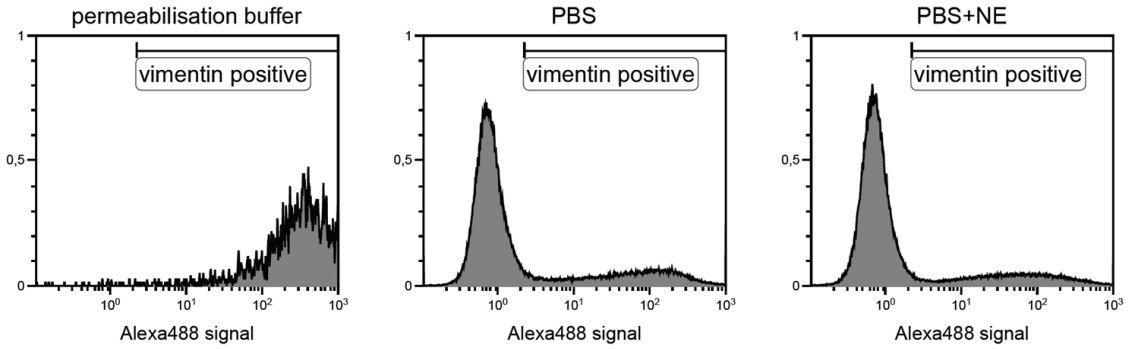

Figure 35: Cells were not permeabilised for antibodies by 5 h NE treatment. When permeabilised with saponin (permeabilisation buffer), CHO-CAR cells were stained intracellularly by anti-vimentin antibody. When not permeabilised (PBS), only a small fraction of cells was stained. This was also the case for non-permeabilised, but NE-treated cells (PBS+NE), indicating that NE treatment did not permeabilise cells for anti-vimentin antibody.

Cells changed their morphology upon NE treatment as was observed by flow cytometry. Events recorded after 2 h NE treatment showed lower forward scatter (FS) and side scatter (SS) signals than events of an untreated sample (Figure 36A). Events representing large and highly granular cells became less frequent and events representing small cells increased (88.92 % in untreated and 99.00 % in treated samples).

To exclude cell debris and cell doublets from the analysis, events were gated. For visualisation of gating strategies, see Figure 17 in Appendix. Upon NE treatment, events representing singlet cells increased significantly, indicating that cell clumps dispersed. This was in line with the observation that cell adhesion to the cell culture vessel decreased (Figure 34). NE addition did not result in significantly more cell debris in the samples (Figure 36B).

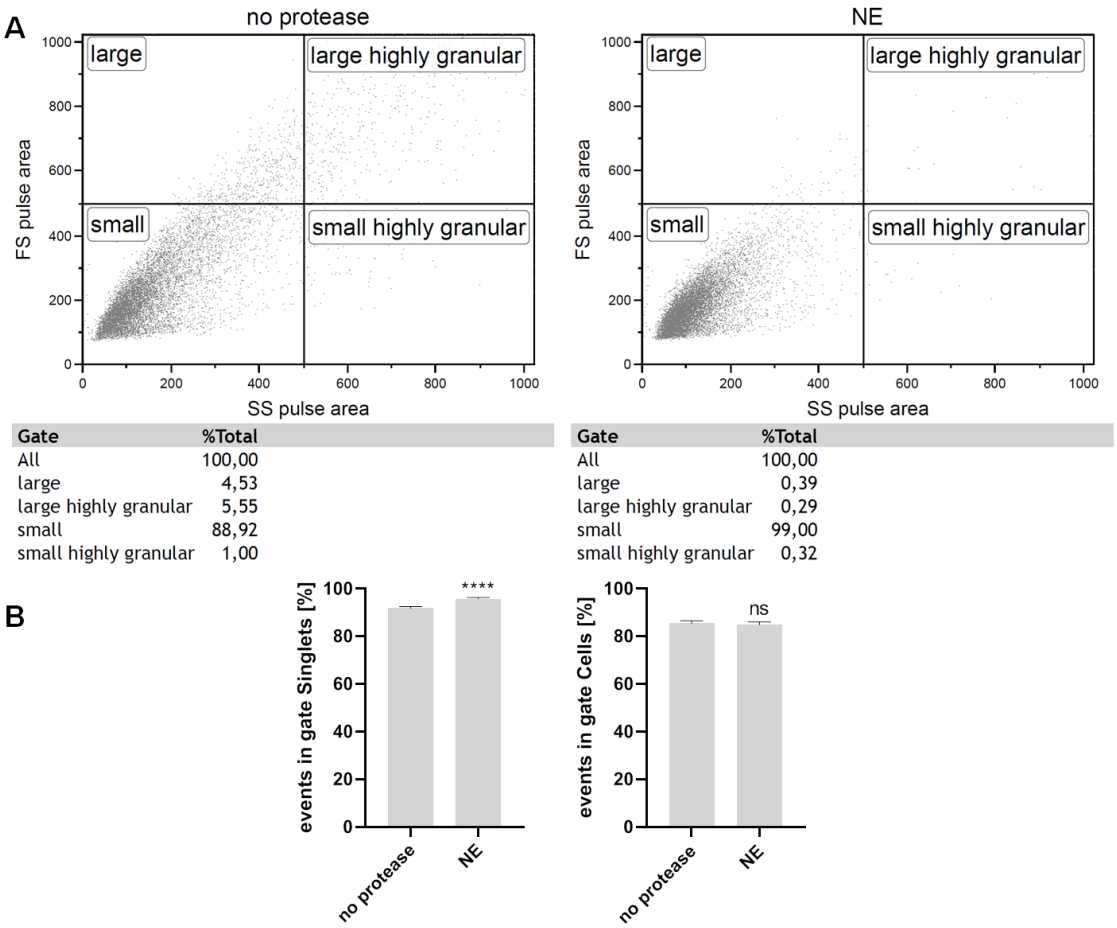

Figure 36: NE treatment changed cell morphology. A) Example dot plots (forward scatter (FS) versus side scatter (SS) pulse areas). Upon NE treatment (2 h, 100 ng/µl) of CHO-CAR cells, events representing small and less granular cells became more frequent. B) All measurements performed for the experiment presented in Figure 38 were analysed for the percentage of events in gates "Cells" and "Singlets" (n=248). NE treatment did not decrease event number in gate "Cells", implicating that no debris was formed. However, NE treatment increased event number in gate "Singlets" significantly (t test), implicating that cell aggregates dispersed.

Next, I was interested in NE´s influence on virus coreceptors. Adenoviruses use integrins as entry receptors and Coxsackieviruses use DAF as attachment receptor. Recombinant human integrin αvβ5 and DAF were treated with NE in a time series (Figure 37). Integrin heterodimer αvβ5 was digested already within 5 min and proteolysis was nearly complete within 1 h. NE cleavage of DAF was not completed after overnight incubation.

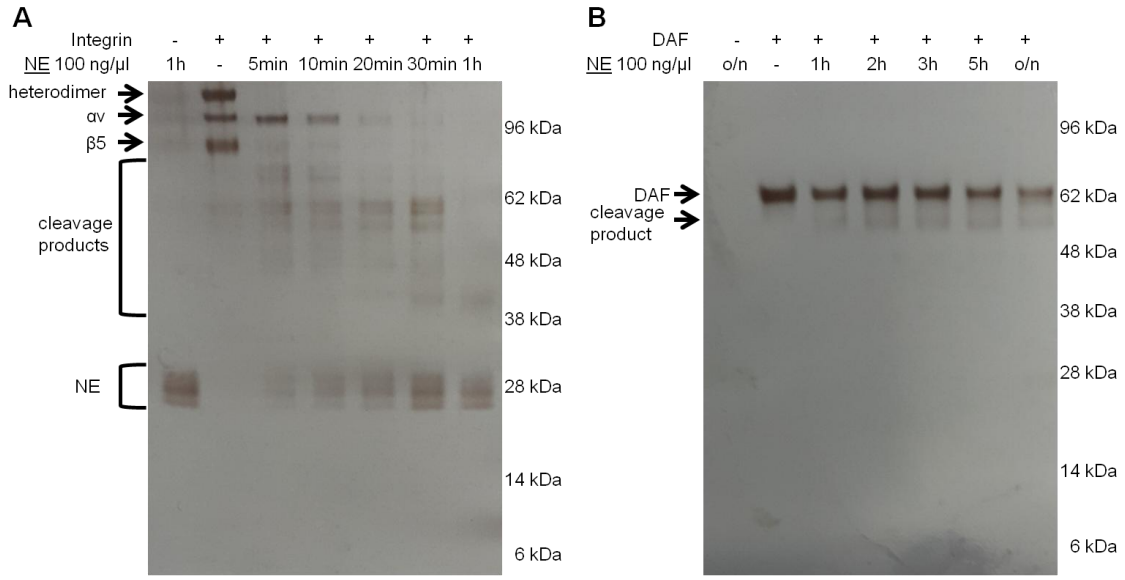

Figure 37: Recombinant human integrin and DAF were cleaved by NE. A) Integrin αvβ5 was cleaved by NE in a time-dependent manner resulting in several cleavage products. Integrin heterodimer and monomers αv and β5 ran at 200, 115, and 85 kDa, respectively. NE ran as a triplet at about 28 kDa in the silver-stained gel. B) DAF cleavage by NE was not completed after overnight incubation.

4.3.5.3 Cleavage of membranous CAR by NE

Treatment of CAR expressing cells with NE and subsequent analysis of cell´s membrane-organelle fractions by Western blot revealed a significant decrease in total CAR protein level (data not shown). Uniform loading quantities were ensured by BCA assays and a loading control. Since vinculin level also decreased with NE treatment, it could not be used as a proper loading control. Thus, Western blot was dismissed as a suitable technique to observe differences in CAR levels. In precipitated supernatants of NE treated CHO-CAR cells, no CAR cleavage product could be observed in Western blots probed with anti-CAR N-terminus antibody (data not shown). Lysates of NE-treated CHO-CAR cells did not contain cleavage products that were recognised by anti-CAR C-terminus antibody in Western blots (data not shown).

Instead, I tested CAR surface levels in correlation to NE treatment. Epithelial cell lines expressing CAR were treated with NE (100 ng/µl) for different time points and CAR surface level was monitored using flow cytometry (Figure 38). In all cell lines, except for HEK-293 cells, a time-dependent decrease in CAR surface level upon NE treatment was observed. In A549 and HepG2 cells, this decrease was not significant, but implied. Incubation times were adjusted for the varying resistance of each cell line towards NE treatment. Longer treatment periods resulted in cell rupture.

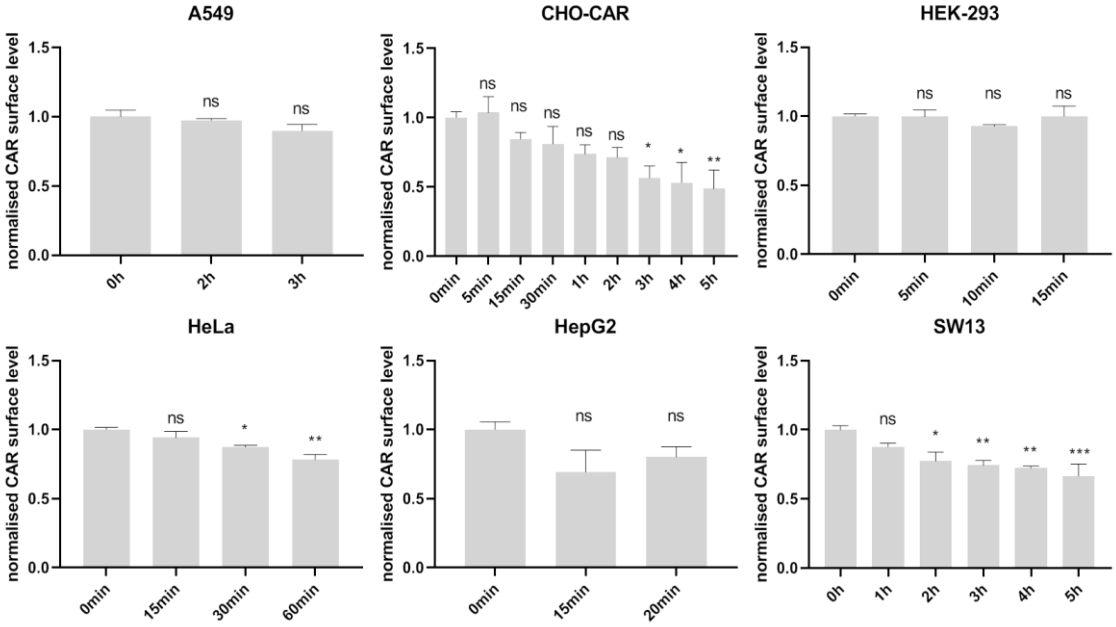

Figure 38: CAR surface expression decreased in most of the tested epithelial cell lines upon NE treatment. Cells were incubated for different time points with or without NE and stained for CAR. CAR surface levels (geometric mean, gates "Cells" and "Singlets") of NE-treated cells were normalised to CAR levels of untreated cells. Furthermore, relative CAR levels at time point t=0 were set as 1. Significances were calculated with ANOVA with multiple comparisons. Experiment was repeated three times (A549, HeLa, HepG2), four times (CHO-CAR, HEK-293), or five times (SW13).

Flow cytometry data were analysed by multiple strategies, but none had major implications for the outcome of the experiment. Flow cytometry data can be presented either as geometric mean or as median to measure the central tendency of lognormal distributions. I chose the geometric mean, since the median could not reflect the occurrence of a CAR-negative subpopulation upon NE treatment in HepG2 cells (Figure 18 in Appendix). Besides, events were gated for "Cells" and "Singlets" (Figure 17 in Appendix). However, when none or only one of these gates was applied, no major difference could be observed in NE-dependent CAR level decrease (Figure 19 in Appendix).

When not normalised to time point t=0, CAR signals of NE-treated cells exceeded those of untreated cells at short incubation periods (Figure 20 in Appendix). This observation may be due to the experimental design regarding time point t=0. There, NE was also added to the cells, but directly removed by pelleting and washing cells. Nevertheless, cells were in contact with NE for 4 minutes during centrifugation. This may be sufficient to open cell-cell contacts and cleave other proteins, thereby facilitating anti-CAR antibody binding to uncleaved CAR. Interestingly, trypsin treatment of cells for up to 10 min also increased CAR signal determined by flow cytometry (data not shown).

To test whether disulfide bonds prevented shedding of CAR´s ECD by maintaining CAR´s tertiary structure despite proteolysis, cells were treated with DTT (50 mM) after NE digest and CAR levels were measured with flow cytometry (Figure 39). CAR levels of CHO-CAR and SW13 decreased slightly more pronounced compared to non-reducing conditions (Figure 38). NE effect on CAR levels of HEK-293 cells was not influenced by reducing conditions. Higher DTT concentrations resulted in disrupted cells that could not be analysed with flow cytometry (data not shown). High DTT concentrations cause cell apoptosis (TARTIER ET AL. 2000).

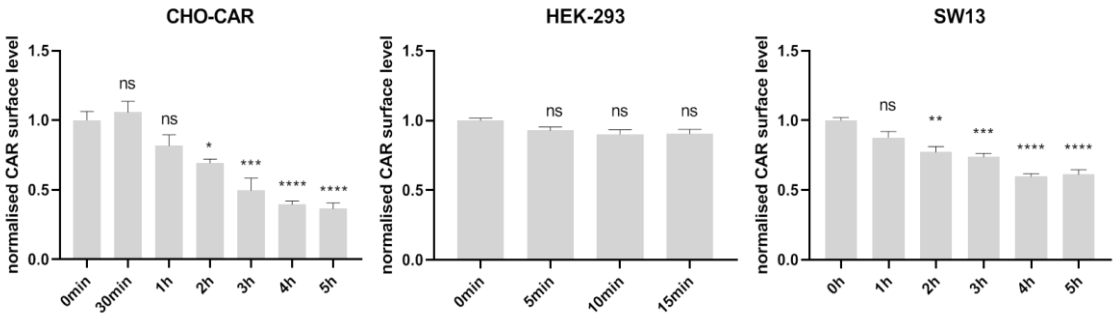

Figure 39: CAR surface expression in three epithelial cell lines upon NE treatment and reducing conditions. Cells were incubated for different time points with or without NE and kept under reducing conditions after NE treatment. CAR surface levels (geometric mean, gates "Cells" and "Singlets") of NE-treated cells were normalised to CAR levels of untreated cells. Furthermore, relative CAR levels at time point t=0 were set to 1. Significances were calculated with ANOVA with multiple comparisons. Experiment was repeated three times (CHO-CAR, SW13) or four times (HEK-293).

As another technique to monitor CAR surface levels, immunofluorescence staining of non-fixed and non-permeabilised cells was performed. This method allowed exclusive staining of extracellular proteins (Figure 21 in Appendix). Thereby, signals from intracellular CAR that would not be accessible for NE did not distort the results. Anti-CAR antibody RmcB recognises CAR ECD only when both immunoglobulin domains are present (PINKERT ET AL. 2016).

CHO-CAR cells were treated with NE, stained for CAR, and analysed via confocal microscopy (Figure 40). In untreated samples, CAR was expressed at cell-cell contacts. Upon NE treatment, cell aggregates loosened and CAR levels decreased significantly. NE-dependent reduction of cell adhesion was also observed via brightfield microscopy (Figure 34) and flow cytometry (Figure 36).

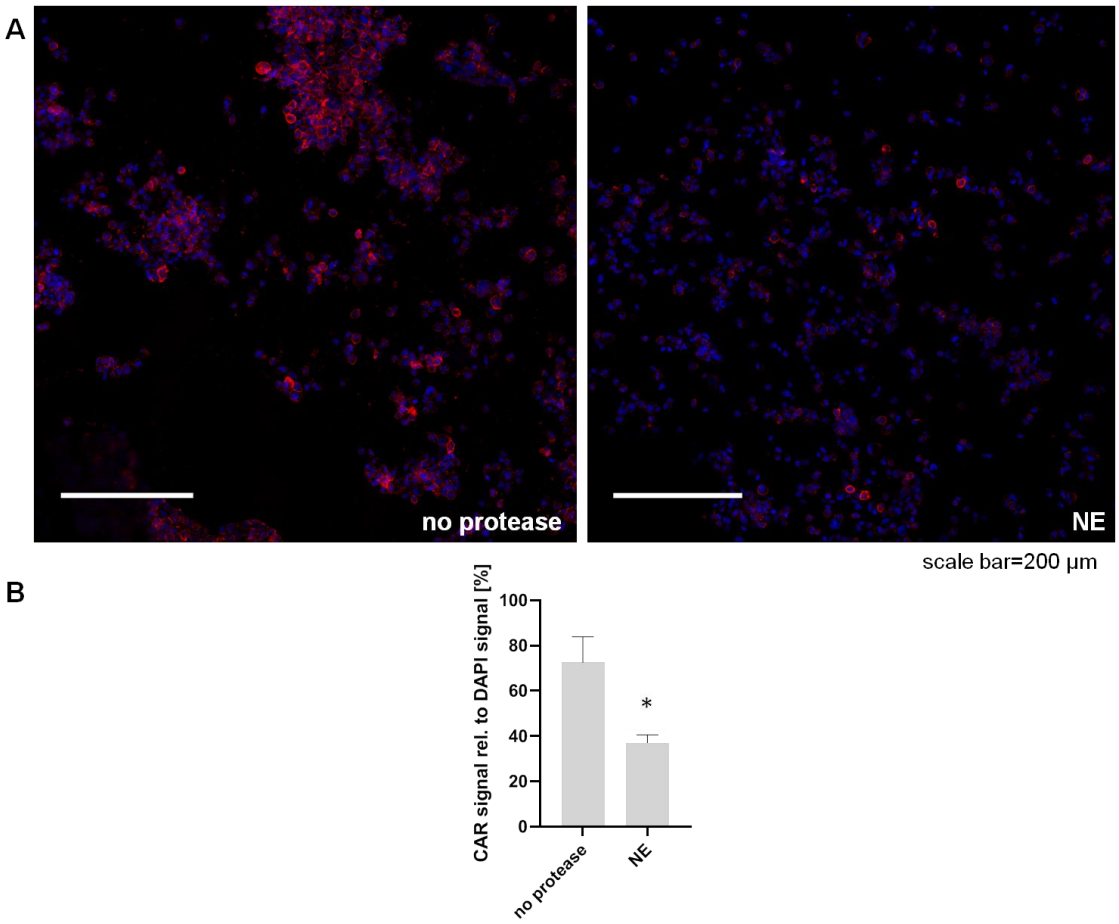

Figure 40: CAR surface level on CHO-CAR cells decreased upon NE treatment as determined by immunofluorescence staining. Cells were treated with NE (100 ng/µl) for 3 h and stained for extracellular CAR. A) Representative fluorescence images of untreated (no protease) and treated (NE) cells stained with DAPI (blue) and anti-CAR antibody RmcB (red). B) Decrease of CAR level upon NE treatment was statistically significant (t test). Experiment was performed 3 times.

5 DISCUSSION

5.1 Natural CAR variants have no impact on CAR´s subcellular localisation, cell adhesion, cell proliferation, and virus internalisation

No disease-causing variant in *CXADR* coding sequence has been found until now. An exception is a nucleotide exchange in exon 7 that results in a synonymous variant in CAR´s main isoform CAREx7 and in a missense mutation in isoform CAREx8. It might be associated with hypertension (SHETTY ET AL. 2012). I aimed to characterise the five *CXADR* missense variants that are most frequent in human population (Table 1). Since CAR´s transmembrane and intracellular domains influence CAR intracellular signalling and CAR localisation as well as cell properties, I hypothesised that virus attachment and entry may also be altered by variants in these domains. This could be mediated by affecting overall tertiary structure of CAR´s intracellular domain or the motifs important for posttranslational modifications and intracellular signalling (Figure 3). Therefore, next to the variants´ influence on vector transduction and cell properties, I also tested CAR´s subcellular localisation.

Notably, CAR expression levels differed significantly among stably transfected polyclonal CHO-CAR cell lines (Figure 3 in Appendix). I observed this in two different transfection experiments (data not shown), but I did not test for uniform transfection efficiency, for example by co-transfecting a GFP-coding plasmid or by assessing the transgene copy number. It would be interesting to determine, if variants influence CAR expression levels like other cytoplasmic variations (see 1.1.1.3). Monoclonal cell lines could be selected for uniform CAR expression, but they might introduce bias regarding cell properties. Cells expanded from one single cell might bear random characteristics interfering with the research question. Therefore, I decided to use the polyclonal cell lines and sort them by FACS to obtain a uniform CAR expression level (Figure 4 in Appendix).

None of the variants had a major effect on the receptor´s ability to mediate virus internalisation into CHO cells (Figure 16). The minor differences that were observed would probably not be physiologically relevant. It can be assumed that these variants do not modify CAR´s TMD or CPD, which would have led to differences in virus inter-

nalisation or cell-cell adhesion. Accordingly, the receptor variants showed regular membrane localisation and did not influence cell adhesion or proliferation (Figures 14 and 15). These results correspond with studies using GPI-anchored CAR ECD, which was able to mediate virus uptake independently of TMD and CPD (VAN'T HOF & CRYSTAL 2001; OKEGAWA ET AL. 2001; WALTERS ET AL. 2001; WANG & BERGELSON 1999).

Readout parameters (GFP and VP1 expression in CHO-CAR cells) reflect transduction or infection rate, since protein expression by the host cell is a prerequisite for measurement. Other key steps in virus infection are cell attachment and cell entry. Attachment rate could be determined with labelled viruses (e.g. fluorescent or radioactive) and readout directly after infection. Virus genome amount in cells directly after infection is a parameter for virus entry (INGEMARSDOTTER ET AL. 2015). As I used replication-deficient adenovectors, GFP expression resembles virus attachment and entry rates. Coxsackievirus attachment and entry rates could differ from the results obtained for infection rates, although normally one would assume a linear correlation between these parameters.

According to American College of Medical Genetics and Genomics (ACMG) criteria, the examined variants are classified as variants of unknown significance, because functional data are missing. *In silico* programs like MutationTaster2, PolyPhen-2, PROVEAN, FATHMM, and SNPs&GO predict variant p.Pro356Ser to be pathogenic, but I did not observe changes in CAR´s functionality, which is in line with an earlier study (EXCOFFON ET AL. 2006).

The five variants also affect other splice isoforms apart from CAREx7. Amino acid changes are identical for CAREx8, except for c.1066C>T (p.Pro356Ser in CAREx7), which is spliced out in CAREx8. c.886G>A (p.Gly296Ser in CAREx7) and c.983G>A (p.Arg328His in CAREx7) are also missense mutations in CAR isoforms CAR2/7, CAR3/7, and CAR4/7. Because no specific *in vivo* functions of CAR isoforms have been described so far (see 1.1.2.1), the role of these variants cannot be defined.

The five CAR missense variants might be classified as rare polymorphisms without pathological relevance, because I could not identify a functionally modified receptor. However, I cannot exclude other mechanisms by which the variants may influence CAR´s physiological function in general. For example, CAR-mediated multiprotein complexes could not form (COYNE ET AL. 2004), or localisation in polarised cells may

differ (WALTERS ET AL. 2001). I used non-polar CHO cells as a model system, since they allow correct posttranslational modifications like glycosylation, which are important for CAR´s function. Furthermore, CHO cells do not express CAR endogenously so that infection rate depends exclusively on exogenously expressed human CAR.

Another relatively common variant c.43G>C, p.Asp15His (rs563708764) with a MAF of 0.06 % is located in CAR´s signal peptide. I did not investigate this variant, because it would not affect virus intake directly, but may change CAR expression, localisation, or trafficking. Investigations regarding these mechanisms were out of the scope of this work. Variants in signal peptides were shown to inhibit processing and secretion of the affected proteins (ARNOLD ET AL. 1990; LINDERT ET AL. 2018; RAJPAR 2002). Besides, nucleotide guanine 43 is a splice donor site for *CXADR* exon 1. According to *in silico* program Human Splicing Finder, this variant most probably affects splicing. Translation would probably terminate after 16 amino acids due to a premature stop codon. However, because this variant is common in human population, it probably does not impair CAR´s functions. Homozygous loss-of-function mutations would lead to premature death of the affected individual as was shown for CAR KO mice (ASHER ET AL. 2005; DORNER ET AL. 2005). It might be promising to investigate CAR variants found in embryonic developmental disorders rather variants present in normal control collectives like gnomAD that might not represent severe or lethal CAR variants.

Variant p.Gln119His is the most common variant in human population that is located in CAR´s ECD. However, with a MAF of 0.0052 %, it is very rare and amino acid glutamine 119 is not involved in homodimer formation (Figure 17). This underlines the high evolutionary constraints on CAR´s ECD.

Until now, no pathogenic CAR variants have been identified in cardiomyopathies, cancer, hearing loss, or myocardial infarction (see 1.4.1). In my study, I also did not identify a pathogenic effect of frequent CAR variants. This is in line with the hypothesis that mutations might be incompatible with CAR´s indispensible physiological role in tissue differentiation during embryogenesis.

5.2 Peptides based on CAR D1 or adenoviral knob do not inhibit adenovector transduction

In this work, synthetic peptides derived from CAR D1 domain and adenovirus knob domain were tested for their inhibitory effects on adenovector internalisation into lung epithelial cells. Neither single peptides nor a mix of seven different peptides inhibited vector transduction (Figure 20). Adenoviruses can displace CAR molecules from the homodimer binding and open cell-cell contacts (WALTERS ET AL. 2002). Dissociation constants are in nanomolar range for CAR D1-Ad interaction (KIRBY ET AL. 2000) and in micromolar range for CAR D1 homodimer formation (VAN RAAIJ ET AL. 2000). This makes the CAR-adenovirus interaction 1000-fold stronger than the CAR-CAR binding. Peptides may disrupt CAR homodimers and facilitate access of adenovectors to CAR monomers. Affinities of peptides to target proteins could be measured with SPR spectrometry (TAMAMURA ET AL. 1996; WANG ET AL. 2003). In addition, peptides may adhere to each other rather than bind to target proteins. This would be especially important for CAR D1-based peptides, which might resemble homodimer formation.

Next to CAR, Ad5 uses heparan sulfate-glycosaminoglycans as attachment sites in A549 cells. Cells remained permissive, when Ad-CAR interaction was inhibited with an anti-CAR antibody (DECHECCHI ET AL. 2001). However, if peptides blocked Ad-CAR interaction successfully, one would expect a noticeable dose-dependent inhibitory effect anyway.

I designed peptides that based on Ad5 knob domain. 3D structure of CAR complex was determined for Ad12 and amino acids involved in CAR-binding are not well conserved between the serotypes (Figure 5 in Appendix). However, binding sites of Ad5 mostly overlap with these in Ad12 as determined by site-directed mutagenesis (see 4.2.1). Therefore, I assumed that at least the CAR-based peptides should work as efficiently against Ad5 as against Ad12.

Peptides are susceptible to proteolysis and can be endocytosed, which would weaken their entry inhibitory effect (LÜ ET AL. 2014). In order to stabilise peptide conformation, I tried to cover beta sheets in the protein structures and some peptides were cyclised. However, I did not test for peptide stability and proteolytic processing. D-amino acids could be incorporated to increase resistance towards proteolysis (HAACK ET AL. 1997).

I did not expect to design the most effective inhibitor peptide, but I attempted to find a candidate to develop peptides that are more effective. Screening for peptides with antiviral effects is often performed with high-throughput methods like phage display libraries (LÜ ET AL. 2014), Förster resonance energy transfer and fluorescence lifetime imaging microscopy (MARGINEANU ET AL. 2016), or yeast-two-hybrid assays (YANG, WU, & FIELDS 1995). I designed peptides that cover known interfaces from the CAR-Ad interaction. Other approaches include testing a library of overlapping sequences covering the target protein (YIN ET AL. 2017) or designing suitable peptides with *in silico* programs (ALHOOT ET AL. 2013; BAIG ET AL. 2020; UNAL, GURSOY, & ERMAN 2010). In general, a systematic and high-throughput screening of inhibitory peptides is a task for the research-based pharmaceutical industry.

5.3 CAR is a putative target protein for NE-mediated shedding

5.3.1 NE processes human CAR *in vitro* in a physiologically relevant manner

Immune cells, which are recruited to inflammatory sites during myocarditis, secrete proteases. Neutrophil serine proteases (CG, NE, and PR3) and MMPs facilitate immune cell migration by cleaving ECM components and CAMs (MITTAL ET AL. 2016B; PHAM 2006). Furthermore, they target chemokines, cytokines (BANK & ANSORGE 2001), growth factors, and cell surface receptors (KORKMAZ ET AL. 2010).

I tested proteolysis of human CAR with various *in vitro* models. CAR expressed by *E. coli* was processed by all tested proteases (Figure 21). MMP-9 and MMP-11 cleaved *E. coli* CAR probably in the intracellular domain. Products were recognised by the anti-CAR N-terminus antibody and were too large to comprise only CAR´s ECD (maximum 28 kDa). *E. coli* proteins are not posttranslationally modified, which renders them particularly prone to proteolysis. To circumvent this limitation, recombinant human CAR ECD (rhECD) expressed by human cells was used. None of the investigated MMPs, except MMP-3, proteolysed rhECD (Figure 22). Catalytic domains instead of full-length MMPs were used though. Deletion of the hemopexin-like domain reduces the natural collagenase activity of the proteases, whereas other target proteins are cleaved normally (BODE ET AL. 1999; KNÄUPER ET AL. 1997; MURPHY & KNÄUPER 1997; SILLER-LÓPEZ ET

AL. 2000). Whether full-length MMPs show a different activity towards rhECD, remains to be elucidated.

Serine proteases and MMP-3 proteolysed rhECD resulting in distinct cleavage pattern (Figures 22, 23, and 24). MMP-3, CG, and PR3 showed lower activity towards rhECD than NE. For NE, cleavage occurred in a time- and dose-dependent manner that suggested physiological relevance. *In vivo*, NE concentrations can locally be very high and exceed concentrations of their inhibitors. Inhibitors of high molecular weight are excluded from microenvironments located between PMN and tissue. Proteolytic activity is very high at the pericellular zone (CAMPBELL & CAMPBELL 1988; CAMPBELL ET AL. 1999). One neutrophil contains 1.1-1.6 pg NE (CAMPBELL, SILVERMAN, & CAMPBELL 1989; DAMIANO ET AL. 1988), which can be released from secretory granules in quantum bursts of very high amounts (5.3 mM) (LIOU & CAMPBELL 1995). In my experiments, cleavage of soluble rhECD occurred within 5 minutes with 100 ng/µl NE and after overnight incubation with 10 ng/µl NE (10-100 mg/l) (Figure 24). Possible *in vivo* NE concentration of 5.3 mM or 150 g/l (with NE molecular weight 28.5 kDa) exceeds the effective concentrations in my *in vitro* experiments more than 1500-fold. Therefore, I propose that NE concentrations *in vivo* would be sufficient to process CAR.

Potential cleavage sites were determined based on the sizes of digest products in polyacrylamide gels (Figure 25), glycosylation patterns (Figure 26), and MS/MS data (Figure 27). NE and PR3 prefer valine, alanine, or isoleucine at the position upstream of the proteolytic cleavage site, whereas CG has a chymotrypsin-like activity and prefers phenylalanine or tyrosine (FU ET AL. 2018). These substrate preferences were resembled by rhECD proteolysis: NE and PR3 products were very similar in size, indicating that both proteases may cleave rhECD at the same position. In my experiments, PR3 was less active than NE (Figure 22 and Figure 8 in Appendix), which was in line with previous results (FU ET AL. 2018). CG cleavage results in a larger product (Figure 25). Analysis with nLC-MS/MS could not characterise a cleavage site for CG, because sequence coverage was insufficient (Figure 10 in Appendix). For NE digest products, sequence coverage was sufficient to predict valines 129 and 199 as potential cleavage sites (Figure 41). In full-length CAR sequence (Figure 1 in Appendix), these are valines 148 and 218, which are conserved among species (e.g. mouse, cow, and rat). In order to determine the exact cleavage site of NE in CAR ECD, site-directed mutagenesis of poten-

tial cleavage sites could be performed. Besides, peptides with neo-N-termini due to proteolysis can be identified via mass spectrometry with TAILS or COFRADIC (NIEDERMAIER & HUESGEN 2019).

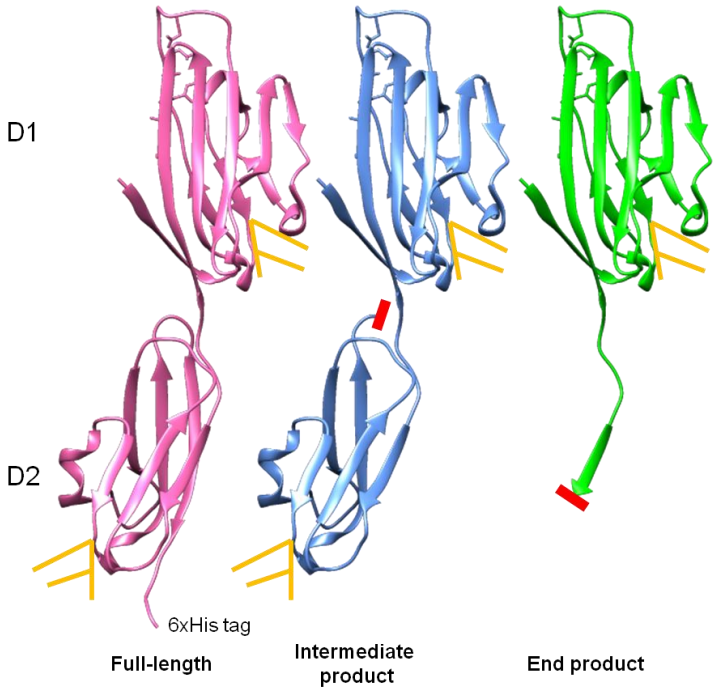

Figure 41: Proposed model of NE cleavage of CAR extracellular domain. Full-length extracellular domain of CAR (magenta) consisting of immunoglobulin domains D1 and D2 with two N-glycosylation sites (yellow branches) is cleaved by NE at two distinct sites (V129 and V199, marked with red lines) resulting in an intermediate and an end product (blue and green). Both products include CAR´s D1 domain, which could be involved in virus inhibition, if present in the interstitium in soluble form. 3D model is based on murine CAR extracellular domain and was modified from PDB ID: 3JZ7 (PATZKE ET AL. 2010).

CAR expressed by CHO cells was cleaved differently than rhECD (Figures 22 and 32), probably because it was denatured due to detergent in cell lysis buffer. MMPs and PR3 cleaved CAR expressed by CHO cells intracellularly. CG and NE cleavage sites were located in CAR´s intracellular and extracellular domains. Intracellular CAR proteolysis was observed in apoptotic Jurkat cells and cleavage site was defined as glycine 303 (CRAWFORD ET AL. 2013). This adds evidence to the idea that intracellular CAR domain is susceptible towards proteolysis. When undigested CHO lysates were stained with anti-CAR N-terminus antibody, multiple bands were detected. These may represent dimers, glycoforms, or proteolysed forms of full-length CAR. CHO cells express many proteases endogenously, which may process CAR (BEE ET AL. 2015; GAO ET AL. 2011; PARK ET AL. 2017; ROBERT ET AL. 2009). To circumvent endogenous proteolysis as

much as possible, I prepared CHO-CAR lysate often and froze it at -80 °C for storage. I did not add protease inhibitors to allow proteolysis by exogenously added proteases.

rhECD seemed to be the most suitable substrate to test proteolysis in solution, because it was present in its native form and displayed all posttranslational modifications. However, *in vitro* experiments with proteases and substrates in solution cannot reflect physiological conditions. Particularly, a transmembrane protein as CAR likely behaves differently, when not expressed on a cell surface but as ECD in solution. Thus, I wanted to test surface-bound rhECD. However, rhECD binding was instable in both NiNTA resin and SPR. Anyway, NE could attack rhECD that was fixed onto NiNTA resin and release cleavage products (Figure 30). To improve SPR measurements, binding stability could be enhanced by using a longer His tag or by binding via biotin/streptavidin.

To resemble a physiologically relevant situation, NE was added to mammalian cells. I planned to determine total CAR levels with Western blotting, but I could not normalise protein quantities with an appropriate loading control. NE processed vinculin, which was described before (BAKOLITSA ET AL. 1999). When I searched for another suitable loading control, I found that NE processes many frequently used proteins: F-actin (METZLER ET AL. 2014), GAPDH (KNECHT & ROCHE 1986), histones (ZHOU ET AL. 2014), laminin (MYDEL ET AL. 2008), and tubulin (ANDERSON 1979). In order to use Western blots for quantitation of total CAR level, protocols have to be optimised either by finding a loading control protein that is not cleaved by NE or by preventing NE access to the cytoplasm, for example with shorter incubation times.

I showed a decrease in CAR surface levels upon NE treatment with immunofluorescence microscopy (Figure 40) and flow cytometry (Figure 38). Decrease occurred in most cell lines and was time-dependent. Differences in CAR decrease rates among the cell lines may be explained by different NE treatment times. HEK-293 cells, for example, tolerated only 15 minutes NE treatment, before they lysed. Other cell lines like CHO-CAR or SW13 could be incubated for 5 hours with NE.

Within short incubation times, NE treatment resulted in increased CAR signals compared to untreated cells (Figure 20 in Appendix). Anti-CAR antibody could have gained better access to CAR through NE digest. Cell-cell contacts could have been disrupted or the antibody epitope could have been exposed by cleavage of other proteins. Trypsin

treatment of cells also facilitated CAR recognition by the antibody in flow cytometry (data not shown).

Reducing conditions had no strong impact on CAR level decrease (Figure 39), suggesting that NE cleavage products did not adhere to the cells via disulfide bonds as was observed for tryptic digest products (CARSON 2000). By reducing rhECD and its NE digestion products, also no additional products occurred (Figure 28).

5.3.2 Possible implications of NE-mediated CAR-shedding *in vivo*

Only 2 % of cell surface proteins are processed via ectodomain shedding (HAYASHIDA ET AL. 2010). Not all proteolytic events seen in *in vitro* experiments must occur *in vivo*, where substrate and sheddase are controlled spatially and temporarily. Protease inhibitors, other NE substrates, and CAR localisation may hamper CAR-shedding in tissues. Localisation in lipid rafts inhibits proteolysis of transmembrane proteins (BAE, YANG, & REZAIE 2008). Furthermore, glycosylation and phosphorylation inhibit proteolysis by altering the protein´s conformation and by blocking cleavage sites for proteases (BOON ET AL. 2019; HAVUKAINEN ET AL. 2012; RUSSELL, OLDHAM, & DAVIS 2009). Dimerisation or binding to other interaction partners or antibodies can protect proteins from shedding (HARTMANN ET AL. 2015; LI ET AL. 2019; SAHNI ET AL. 2000). NE cleavage of rhECD was influenced by N-glycosylation (Figure 29) as well as tertiary structure (Figure 28). Interestingly, both features of rhECD seemed to enable NE cleavage at the two distinct sites. Denatured CAR was completely processed by NE. This was observed for CAR expressed by *E. coli* in urea buffer (Figure 21), denatured rhECD (Figure 13 in Appendix), or CAR from CHO cells in detergent containing buffer (Figure 32). Glycosylation of rhECD protected a cleavage site from NE activity (Figure 29). It was not elucidated, whether membranous CAR would be influenced by oligosaccharides the same way as CAR in solution.

Murine CAR is a target protein for ADAM10-mediated shedding (HOURI, HUANG, & NALBANTOGLU 2013). Cleavage sites are located in the sequence MLRL (amino acids 224-227; LLRL in human CAR). If human CAR was also a target for ADAM10, this would regulate CAR´s turnover and physiological functions. However, since ADAM10 is a membrane-bound sheddase, turnover rate and inducibility would probably differ from shedding by NE. A soluble protease that is released at high concentrations from

infiltrating neutrophils would have more profound and faster effects on the myocardial tissue than ADAM10 that is transcriptionally regulated.

CAR ectodomain shedding through NE might be a defense mechanism against active viral infections during myocarditis and other viral-induced inflammatory diseases. Adenoviruses and Coxsackieviruses infect multiple organs next to the heart, for example respiratory tract, digestive tract, kidney, or pancreas (see 1.1.4.2 and 1.1.4.3). CAR-shedding as a sequela of inflammatory response could also occur during infectious diseases of these organs. Both CAR cleavage products contain complete D1 domain (Figure 41) and would function as biologically active fragments. They would be able to trap viruses and block unshed, membranous CAR for viruses. Virus traps were tested *in vitro* and *in vivo*: Soluble CAR proteins comprising either D1 domain alone (FREIMUTH ET AL. 1999) or complete ECD (GOODFELLOW ET AL. 2005; ROELVINK ET AL. 1998) inhibited Coxsackie- and adenovirus infections *in vitro*. Besides, CAR ECD fused to Ig-Fc portion was a suitable therapeutic agent against virus infections. In some studies, significant treatment effects were only observed, when soluble CAR was given prophylactically or concomitantly with virus inoculation (LIM ET AL. 2006; PINKERT ET AL. 2019; YANAGAWA ET AL. 2004; ZHANG ET AL. 2013). Other studies, however, showed a decrease in virus titers in myocarditis models also for post-infection treatment (PINKERT ET AL. 2009; STEIN ET AL. 2015). Therefore, it remains to be elucidated to which extent shed CAR ECD would decrease ongoing infections. Reduction of CAR surface levels through shedding could resemble CAR knockdown in *in vivo* experiments, where virus infections were ameliorated in heart and pancreas (KALLEWAARD ET AL. 2009; SHI ET AL. 2009). Shedding would probably not remove all CAR ECDs from the tissues surface. However, due to the biological activities of shed soluble ECD, a positive effect would be expected also for incomplete shedding. Furthermore, Coxsackie- and adenoviruses bind in a positive cooperative manner (HE ET AL. 2001; LORTAT-JACOB ET AL. 2001). One virion binds multiple receptors (Figures 6 and 7), which leads to a higher stability of interaction. If surface CAR would be reduced drastically by shedding, scattered remaining receptors probably could not mediate stable virus interactions. Strikingly, NE treatment of HeLa cells resulted in less CVB attachment (ZAJAC & CROWELL 1965). At the time this study was conducted, CAR had not been characterised, so authors did not investigate CAR levels.

Next to CAR, other CAMs are target proteins for NE-mediated shedding: E-cadherin (GINZBERG ET AL. 2001), ICAM-1 (CHAMPAGNE ET AL. 1998), and VCAM-1 (LÉVESQUE ET AL. 2001). As CAR, ICAM-1 and VCAM-1 are virus receptors (GREVE ET AL. 1989; HUBER 1994). Soluble ICAM-1 levels in nasal fluids increased upon rhinovirus inoculation, but had no protective effect (WINTHER ET AL. 2002). In an *in vitro* model, rhinoviruses upregulated membranous ICAM-1 and downregulated soluble ICAM-1 (WHITEMAN ET AL. 2003).

NE does not have a high substrate specifity (KORKMAZ, MOREAU, & GAUTHIER 2008) and can be used as dissociation agent (PHILLIPS 1972; WESTLIN & GIMBRONE 1993). It is capable of removing the glycocalyx (PICKLES ET AL. 2000) and opening cell-cell contacts (GINZBERG ET AL. 2001), which could improve access to CAR for viruses. I observed cell detachment from culture vessels (Figure 34), changes in cell morphology (Figure 36), and cleavage of recombinant human integrin (Figure 37) upon NE treatment. Interestingly, integrin was more susceptible towards NE digest than DAF. In CAR, DAF, and integrin αvβ5, 17.9, 13.8, and 17.4 % of amino acids are alanine, valine, or isoleucine, which are preferred by NE. DAF and integrins are glycosylated (LEHMANN ET AL. 1996; REDDY, CARAS, & KRIEGER 1989), which may protect them from proteolytic cleavage. Proteolysis of integrins as adenovirus co-receptors would be another interesting mechanism to investigate in cells.

A treatment that takes advantage of CAR-shedding by NE would probably lead to massive side effects due to the unspecific substrate spectrum of NE. Administration or downregulation of NE will affect its role in immune response and tissue remodelling. Inhibition of NE activity even increased survival rate in myocardial infarction and encephalomyocarditis virus-induced myocarditis (OHTA ET AL. 2004; ZAIDI ET AL. 1999). If a designed recombinant protease that targets CAR specifically could be administered, this may have beneficial effects for the outcome of myocarditis. Until now, only a few proteases have been used as drugs, because positive and undesirable consequences are difficult to balance (CRAIK, PAGE, & MADISON 2011). CAR-shedding itself may have detrimental effects for the host. On the one hand, CAR is downregulated postnatally (see 1.1.3.2) suggesting that it might not play a major role in tissue homeostasis in adult organisms. On the other hand, CAR is involved in tissue remodelling after injury, and tissue integrity, cell adhesiveness, and leukocyte migration could be impaired by CAR-shedding (see 1.1.3.1).

5.3.3 Possible future investigations

For further investigations of NE-mediated CAR-shedding, epithelial cells could be treated with conditioned media of NE secreting neutrophils and CAR surface expression levels could be monitored. Most importantly, the effect of CAR-shedding on virus infection is to be investigated. Due to the unspecific activity of NE, cells may be damaged and virus entry may even be facilitated as was shown in preliminary studies (data not shown). Thereby, proof of principle may be difficult to obtain. *In vivo* experiments may also face challenges. NE up- or downregulation during myocarditis alter multiple parameters, which will probably induce massive bias. As an example, NE-induced signalling activates several other proteases, which in turn influence disease outcome (GERAGHTY ET AL. 2007). Statements regarding CAR-shedding alone will therefore be challenging to obtain. If *in vivo* investigations are to be performed in mice, one has to bear in mind that human NE and murine NE differ in their activity profiles (WIESNER ET AL. 2005). For murine CAR ECD treated with human NE, similar product sizes as for human ECD were determined, but time-dependent occurrence of the products differed (Figures 24 and 31).

Soluble CAR fragments could be searched in serum of patients suffering from myocarditis, DCM, cystic fibrosis, or intestinal inflammation. Large cohort studies (e.g. Kooperative Gesundheitsforschung in der Region Augsburg, Heinz Nixdorf Recall Studie, or Gutenberg Gesundheitsstudie) include individuals, who suffer from diabetes, cardiovascular diseases, and lung diseases. Currently no routine mass spectrometry analyses of blood or urine samples are performed (personal communications). Interestingly, in pleural effusions of lung cancer patients, CAR ECD was detected, but it was not clear, if it stemmed from shedding or alternative splicing (BERNAL ET AL. 2002).

Murine cytoplasmic CAR domain is processed by RIP following ADAM-10 mediated shedding (HOURI, HUANG, & NALBANTOGLU 2013). To investigate CAR´s C-terminal fragment that remains in the cell membrane after NE-mediated shedding, CAR could be overexpressed in CHO cells with a C-terminal His tag. Follow-up of the shed extracellular CAR domain fragments in cell culture supernatant could be facilitated by biotinylation of CAR´s N-terminus.

Next to CG, NE, PR3, and MMPs, other soluble proteases could be potential CAR sheddases. Secondary granules of neutrophils also contain urokinase-type plasminogen

activator (OWEN ET AL. 1995). Chymase and tryptase are expressed in secretory granules of mast cells (PEJLER ET AL. 2010), which are present in inflamed tissue during myocarditis (HIGUCHI ET AL. 2008). Secreted calpains increase during reovirus-induced myocarditis (DEBIASI ET AL. 2001) and are important in cardiac remodelling events (LETAVERNIER ET AL. 2012). Furthermore, cathepsins B, K, L, and S degrade ECM components *in vivo* and are found in cardiac tissue upon injury (CHENG ET AL. 2012).

5.4 Conclusion

With this thesis, I elucidate three different mechanisms that influence CAR´s pathophysiological function as a virus receptor.

First, the most frequent genetic CAR variants in human population did not influence cell´s susceptibility towards virus infections. This adds evidence to the idea that pathogenic variants in CAR are very rare, presumably due to CAR´s highly important role during embryogenesis.

Second, synthetic peptides based on CAR D1 or adenovirus knob were inefficient adenovector entry inhibitors. Peptide affinity to CAR D1 or adenovirus knob might be too low to achieve a potent inhibitory effect.

Third, I showed for the first time that the virus receptor CAR is a putative target protein for neutrophil elastase-mediated shedding. This characterises a new mechanism of host defense against Coxsackie- and adenovirus infections.

REFERENCES

Aden, D.P., Fogel, A., Plotkin, S., Damjanov, I., Knowles, B.B. (1979). Controlled synthesis of HBsAg in a differentiated human liver carcinoma-derived cell line. Nature *282*, 615–616.

Adzhubei, I.A., Schmidt, S., Peshkin, L., Ramensky, V.E., Gerasimova, A., Bork, P., Kondrashov, A.S., Sunyaev, S.R. (2010). A method and server for predicting damaging missense mutations. Nature Methods *7*, 248–249.

Ahn, J., Jee, Y., Seo, I., Yoon, S.Y., Kim, D., Kim, Y.K., Lee, H. (2008). Primary neurons become less susceptible to Coxsackievirus B5 following maturation: The correlation with the decreased level of CAR expression on cell surface. Journal of Medical Virology *80*, 434–440.

Alhoot, M.A., Rathinam, A.K., Wang, S.M., Manikam, R., Sekaran, S.D. (2013). Inhibition of dengue virus entry into target cells using synthetic antiviral peptides. International Journal of Medical Sciences *10*, 719–729.

Anders, M., Christian, C., McMahon, M., McCormick, F., Korn, W.M. (2003). Inhibition of the Raf/MEK/ERK pathway up-regulates expression of the Coxsackievirus and adenovirus receptor in cancer cells. Cancer Research *63*, 2088–2095.

Anderson, P.J. (1979). The structure and amount of tubulin in cells and tissues. The Journal of Biological Chemistry *254*, 2168–2171.

Anderson, D.H., Johnson, L.V., Hageman, G.S. (1995). Vitronectin receptor expression and distribution at the photoreceptor-retinal pigment epithelial interface. The Journal of Comparative Neurology *360*, 1–16.

Andersson, B., Tomko, R.P., Edwards, K., Mirza, M., Darban, H., Öncü, D., Sonnhammer, E., Sollerbrant, K., Philipson, L. (2000). Putative regulatory domains in the human and mouse CVADR genes. Gene Function & Disease *1*, 82–86.

Arnberg, N. (2012). Adenovirus receptors: Implications for targeting of viral vectors. Trends in Pharmacological Sciences *33*, 442–448.

Arnold, A., Horst, S.A., Gardella, T.J., Baba, H., Levine, M.A., Kronenberg, H.M. (1990). Mutation of the signal peptide-encoding region of the preproparathyroid hormone gene in familial isolated hypoparathyroidism. Journal of Clinical Investigation *86*, 1084–1087.

Asher, D.R., Cerny, A.M., Weiler, S.R., Horner, J.W., Keeler, M.L., Neptune, M.A., Jones, S.N., Bronson, R.T., DePinho, R.A., Finberg, R.W. (2005). Coxsackievirus and adenovirus receptor is essential for cardiomyocyte development. Genesis *42*, 77–85.

Auer, D., Reimer, D., Porto, V., Fleischer, M., Roessler, J., Wiedemair, A., Marth, C., Müller-Holzner, E., Daxenbichler, G., Zeimet, A.G. (2009). Expression of Coxsackie-adenovirus receptor is related to estrogen sensitivity in breast cancer. Breast Cancer Research and Treatment *116*, 103–111.

Bae, J.-S., Yang, L., Rezaie, A.R. (2008). Lipid raft localization regulates the cleavage specificity of protease activated receptor 1 in endothelial cells. Journal of Thrombosis and Haemostasis *6*, 954–961.

Bagheri, N., Shiina, M., Lauffenburger, D.A., Korn, W.M. (2011). A dynamical systems model for combinatorial cancer therapy enhances oncolytic adenovirus efficacy by MEK-inhibition. PLOS Computational Biology *7*, e1001085.

Baig, M., Alagumuthu, M., Rajpoot, S., Saqib, U. (2020). Identification of a potential peptide inhibitor of SARS-CoV-2 targeting its entry into the host cells. Drugs in R&D *20*, 161–169.

Bakolitsa, C., Pereda, J.M. de, Bagshaw, C.R., Critchley, D.R., Liddington, R.C. (1999). Crystal structure of the vinculin tail suggests a pathway for activation. Cell *99*, 603–613.

Bank, U., Ansorge, S. (2001). More than destructive: Neutrophil-derived serine proteases in cytokine bioactivity control. Journal of Leukocyte Biology *69*, 197–206.

Bastian, A., Schäfer, H. (2001). Human alpha-defensin 1 (HNP-1) inhibits adenoviral infection in vitro. Regulatory Peptides *101*, 157–161.

Beauparlant, S.L., Read, P.W., Di Cristofano, A. (2004). In vivo adenovirus-mediated gene transduction into mouse endometrial glands: A novel tool to model endometrial cancer in the mouse. Gynecologic Oncology *94*, 713–718.

Bee, J.S., Tie, L., Johnson, D., Dimitrova, M.N., Jusino, K.C., Afdahl, C.D. (2015). Trace levels of the CHO host cell protease cathepsin D caused particle formation in a monoclonal antibody product. Biotechnology Progress *31*, 1360–1369.

Bergelson, J.M., Cunningham, J.A., Droguett, G., Kurt-Jones, E.A., Krithivas, A., Hong, J.S., Horwitz, M., Crowell, R., Finberg, R. (1997). Isolation of a common receptor for Coxsackie B viruses and adenoviruses 2 and 5. Science *275*, 1320–1323.

Bergelson, J.M., Krithivas, A., Celi, L., Droguett, G., Horwitz, M., Wickham, T.J., Crowell, R.L., Finberg, R. (1998). The murine CAR homolog is a receptor for Coxsackie B viruses and adenoviruses. Journal of Virology *72*, 415–419.

Berman, H.M., Westbrook, J., Feng, Z., Gilliland, G., Bhat, T.N., Weissig, H., Shindyalov, I.N., Bourne, P.E. (2000). The Protein Data Bank. Nucleic Acids Research *28*, 235–242.

Bernal, R.M., Sharma, S., Gardner, B.K., Douglas, J.T., Bergelson, J.M., Dubinett, S.M., Batra, R.K. (2002). Soluble Coxsackievirus adenovirus receptor is a putative inhibitor of adenoviral gene transfer in the tumor milieu. Clinical Cancer Research *8*, 1915–1923.

Bewley, M.C., Springer, K., Zhang, Y.-B.Z., Freimuth, P., Flanagan, J.M. (1999). Structural analysis of the mechanism of adenovirus binding to its human cellular receptor, CAR. Science *286*, 1579–1583.

Bischof, C.A. (2018). Expression des Coxsackie- und Adenovirusrezeptors in kardialen Myxomen. Bachelor thesis. Universität Bielefeld.

Blauwet, L.A., Cooper, L.T. (2010). Myocarditis. Progress in Cardiovascular Diseases *52*, 274–288.

Bode, W., Fernandez-Catalan, C., Grams, H.T., F., Maskos, H.N., K. (1999). Structural properties of matrix metalloproteinases. Cellular and Molecular Life Sciences *55*, 639–652.

Boon, L., Ugarte-Berzal, E., Martens, E., Vandooren, J., Rybakin, V., Colau, D., Gordon-Alonso, M., Bruggen, P. van der, Stöcker, W., Becker-Pauly, C., et al. (2019). Propeptide glycosylation and galectin-3 binding decrease proteolytic activation of human proMMP-9/progelatinase B. The FEBS Journal *286*, 930–945.

Bowles, K.R., Gibson, J., Wu, J., Shaffer, L.G., Towbin, J.A., Bowles, N.E. (1999). Genomic organization and chromosomal localization of the human Coxsackievirus B-adenovirus receptor gene. Human Genetics *105*, 354–359.

Bowles, N.E., Javier Fuentes-Garcia, F., Makar, K.A., Li, H., Gibson, J., Soto, F., Schwimmbeck, P.L., Schultheiss, H.-P., Pauschinger, M. (2002). Analysis of the Coxsackievirus B-adenovirus receptor gene in patients with myocarditis or dilated cardiomyopathy. Molecular Genetics and Metabolism *77*, 257–259.

Bowles, N.E., Ni, J., Kearney, D.L., Pauschinger, M., Schultheiss, H.-P., McCarthy, R., Hare, J., Bricker, J.T., Bowles, K.R., Towbin, J.A. (2003). Detection of viruses in myocardial tissues by polymerase chain reaction. Journal of the American College of Cardiology *42*, 466–472.

Bruder, J.T., Kovesdi, I. (1997). Adenovirus infection stimulates the Raf/MAPK signaling pathway and induces interleukin-8 expression. Journal of Virology *71*, 398–404.

Brüning, A., Runnebaum, I.B. (2003). CAR is a cell–cell adhesion protein in human cancer cells and is expressionally modulated by dexamethasone, TNFα, and TGFβ. Gene Therapy *10*, 198–205.

Brüning, A., Runnebaum, I.B. (2004). The Coxsackie adenovirus receptor inhibits cancer cell migration. Experimental Cell Research *298*, 624–631.

Bugert, P., Elmas, E., Stach, K., Weiss, C., Kälsch, T., Dobrev, D., Borggrefe, M. (2011). No evidence for an association between the rs2824292 variant at chromosome 21q21 and ventricular fibrillation during acute myocardial infarction in a German population. Clinical Chemistry and Laboratory Medicine *49*, 1237–1239.

Burckhardt, C.J., Suomalainen, M., Schoenenberger, P., Boucke, K., Hemmi, S., Greber, U.F. (2011). Drifting motions of the adenovirus receptor CAR and immobile integrins initiate virus uncoating and membrane lytic protein exposure. Cell Host & Microbe *10*, 105–117.

Burian, J., Buser, P., Eriksson, U. (2005). Myocarditis: The immunologist´s view on pathogenesis and treatment. Swiss Med Wkly *135*, 359–364.

Caforio, A.L.P., Pankuweit, S., Arbustini, E., Basso, C., Gimeno-Blanes, J., Felix, S.B., Fu, M., Helio, T., Heymans, S., Jahns, R., et al. (2013). Current state of knowledge on aetiology, diagnosis, management, and therapy of myocarditis: A position statement of the European Society of Cardiology Working Group on Myocardial and Pericardial Diseases. European Heart Journal *34*, 2636–2648.

Campbell, E.J., Campbell, M.A. (1988). Pericellular proteolysis by neutrophils in the presence of proteinase inhibitors: Effects of substrate opsonization. Journal of Cell Biology *106*, 667–676.

Campbell, E.J., Silverman, E.K., Campbell, M.A. (1989). Elastase and cathepsin G of human monocytes. Quantification of cellular content, release in response to stimuli, and heterogeneity in elastase-mediated proteolytic activity. Journal of Immunology (Baltimore, Md.: 1950) *143*, 2961–2968.

Campbell, E.J., Campbell, M.A., Boukedes, S.S., Owen, C.A. (1999). Quantum proteolysis by neutrophils: Implications for pulmonary emphysema in alpha 1-antitrypsin deficiency. The Journal of Clinical Investigation *104*, 337–344.

Capriotti, E., Calabrese, R., Fariselli, P., Martelli, P.L., Altman, R.B., Casadio, R. (2013). WS-SNPs&GO: A web server for predicting the deleterious effect of human protein variants using functional annotation. BMC Genomics *14*, S6.

Carson, S.D. (2000). Limited proteolysis of the Coxsackievirus and adenovirus receptor (CAR) on HeLa cells exposed to trypsin. FEBS Letters *484*, 149–152.

Carson, S.D., Hobbs, J.T., Tracy, S.M., Chapman, N.M. (1999). Expression of the Coxsackievirus and adenovirus receptor in cultured human umbilical vein endothelial cells: Regulation in response to cell density. Journal of Virology *73*, 7077–7079.

Caruso, L., Yuen, S., Smith, J., Husain, M., Opavsky, M.A. (2010). Cardiomyocyte-targeted overexpression of the Coxsackie–adenovirus receptor causes a cardiomyopathy in association with β-catenin signaling. Journal of Molecular and Cellular Cardiology *48*, 1194–1205.

Carvajal-Gonzalez, J.M., Gravotta, D., Mattera, R., Diaz, F., Perez Bay, A., Roman, A.C., Schreiner, R.P., Thuenauer, R., Bonifacino, J.S., Rodriguez-Boulan, E. (2012). Basolateral sorting of the Coxsackie and adenovirus receptor through interaction of a canonical YXX motif with the clathrin adaptors AP-1A and AP-1B. Proceedings of the National Academy of Sciences *109*, 3820–3825.

Champagne, B., Tremblay, P., Cantin, A., St Pierre, Y. (1998). Proteolytic cleavage of ICAM-1 by human neutrophil elastase. Journal of Immunology (Baltimore, Md.: 1950) *161*, 6398–6405.

Chen, J.-W., Zhou, B., Yu, Q.-C., Shin, S.J., Jiao, K., Schneider, M.D., Scott Baldwin, H., Bergelson, J.M. (2006). Cardiomyocyte-specific deletion of the Coxsackievirus and adenovirus receptor results in hyperplasia of the embryonic left ventricle and abnormalities of sinuatrial valves. Circulation Research *98*, 923–930.

Chen, Z., Wang, Q., Sun, J., Gu, A., Jin, M., Shen, Z., Qiu, Z., Wang, J., Wang, X., Zhan, Z., et al. (2013). Expression of the Coxsackie and adenovirus receptor in human lung cancers. Tumor Biology *34*, 17–24.

Cheng, X.W., Shi, G.-P., Kuzuya, M., Sasaki, T., Okumura, K., Murohara, T. (2012). Role for cysteine protease cathepsins in heart disease: Focus on biology and mechanisms with clinical implication. Circulation *125*, 1551–1562.

Cheung, C., Luo, H., Yanagawa, B., Leong, H.S., Samarasekera, D., Lai, J.C.K., Suarez, A., Zhang, J., McManus, B.M. (2006). Matrix metalloproteinases and tissue inhibitors of metalloproteinases in Coxsackievirus-induced myocarditis. Cardiovascular Pathology *15*, 63–74.

Choi, Y., Sims, G.E., Murphy, S., Miller, J.R., Chan, A.P. (2012). Predicting the functional effect of amino acid substitutions and Indels. PLOS ONE *7*, e46688.

Chou, P.Y., Fasman, G.D. (1978). Empirical predictions of protein conformation. Annual Review of Biochemistry *47*, 251–276.

Chrétien, I., Robert, J., Marcuz, A., Garcia-Sanz, J.A., Courtet, M., du Pasquier, L. (1996). CTX, a novel molecule specifically expressed on the surface of cortical thymocytes in Xenopus. European Journal of Immunology *26*, 780–791.

Chrétien, I., Marcuz, A., Courtet, M., Katevuo, K., Vainio, O., Heath, J.K., White, S.J., du Pasquier, L. (1998). CTX, a Xenopus thymocyte receptor, defines a molecular family conserved throughout vertebrates. European Journal of Immunology *28*, 4094–4104.

Chung, J., Kim, K.H., An, S.H., Lee, S., Lim, B.-K., Kang, S.W., Kwon, K. (2019). Coxsackievirus and adenovirus receptor mediates the responses of endothelial cells to fluid shear stress. Experimental & Molecular Medicine *51*, 144.

Chung Moh, M., Hoon Lee, L., Shen, S. (2005). Cloning and characterization of hepaCAM, a novel Ig-like cell adhesion molecule suppressed in human hepatocellular carcinoma. Journal of Hepatology *42*, 833–841.

Cleutjens, J.P., Kandala, J.C., Guarda, E., Guntaka, R.V., Weber, K.T. (1995). Regulation of collagen degradation in the rat myocardium after infarction. Journal of Molecular and Cellular Cardiology *27*, 1281–1292.

Cohen, C.J., Shieh, J.T.C., Pickles, R.J., Okegawa, T., Hsieh, J.-T., Bergelson, J.M. (2001a). The Coxsackievirus and adenovirus receptor is a transmembrane component of the tight junction. Proceedings of the National Academy of Sciences *98*, 15191–15196.

Cohen, C.J., Gaetz, J., Ohman, T., Bergelson, J.M. (2001b). Multiple regions within the Coxsackievirus and adenovirus receptor cytoplasmic domain are required for basolateral sorting. Journal of Biological Chemistry *276*, 25392–25398.

Cohen, C.J., Xiang, Z.Q., Gao, G.-P., Ertl, H.C.J., Wilson, J.M., Bergelson, J.M. (2002). Chimpanzee adenovirus CV-68 adapted as a gene delivery vector interacts with the Coxsackievirus and adenovirus receptor. Journal of General Virology *83*, 151–155.

Coker, M.L., Doscher, M.A., Thomas, C.V., Galis, Z.S., Spinale, F.G. (1999). Matrix metalloproteinase synthesis and expression in isolated LV myocyte preparations. The American Journal of Physiology *277*, H777-787.

Cole, A.M., Hong, T., Boo, L.M., Nguyen, T., Zhao, C., Bristol, G., Zack, J.A., Waring, A.J., Yang, O.O., Lehrer, R.I. (2002). Retrocyclin: A primate peptide that protects cells from infection by T- and M-tropic strains of HIV-1. Proceedings of the National Academy of Sciences of the United States of America *99*, 1813–1818.

Conant, K., Daniele, S., Bozzelli, P.L., Abdi, T., Edwards, A., Szklarczyk, A., Olchefske, I., Ottenheimer, D., Maguire-Zeiss, K. (2017). Matrix metalloproteinase activity stimulates N-cadherin shedding and the soluble N-cadherin ectodomain promotes classical microglial activation. Journal of Neuroinflammation *14*.

Coyne, C.B., Bergelson, J.M. (2005). CAR: A virus receptor within the tight junction. Advanced Drug Delivery Reviews *57*, 869–882.

Coyne, C.B., Voelker, T., Pichla, S.L., Bergelson, J.M. (2004). The Coxsackievirus and adenovirus receptor interacts with the multi-PDZ domain protein-1 (MUPP-1) within the tight junction. Journal of Biological Chemistry *279*, 48079–48084.

Craik, C.S., Page, M.J., Madison, E.L. (2011). Proteases as therapeutics. The Biochemical Journal *435*, 1–16.

Crawford, E.D., Seaman, J.E., Agard, N., Hsu, G.W., Julien, O., Mahrus, S., Nguyen, H., Shimbo, K., Yoshihara, H.A.I., Zhuang, M., et al. (2013). The DegraBase: A database of proteolysis in healthy and apoptotic human cells. Molecular & Cellular Proteomics *12*, 813–824.

Damiano, V.V., Kucich, U., Murer, E., Laudenslager, N., Weinbaum, G. (1988). Ultrastructural quantitation of peroxidase- and elastase-containing granules in human neutrophils. The American Journal of Pathology *131*, 235–245.

DeBiasi, R.L., Edelstein, C.L., Sherry, B., Tyler, K.L. (2001). Calpain inhibition protects against virus-induced apoptotic myocardial injury. Journal of Virology *75*, 351–361.

Dechecchi, M.C., Melotti, P., Bonizzato, A., Santacatterina, M., Chilosi, M., Cabrini, G. (2001). Heparan sulfate glycosaminoglycans are receptors sufficient to mediate the initial binding of adenovirus types 2 and 5. Journal of Virology *75*, 8772–8780.

Deng, X., Jia, C., Chen, F., Liu, J., Zhou, Z. (2013). Effects of heat stress on the expression of the Coxsackievirus and adenovirus receptor in mouse skin keratinocytes. Experimental and Therapeutic Medicine *6*, 1029–1033.

Dermody, T.S., Kirchner, E., Guglielmi, K.M., Stehle, T. (2009). Immunoglobulin superfamily virus receptors and the evolution of adaptive immunity. PLOS Pathogens *5*, e1000481.

Desmet, F.-O., Hamroun, D., Lalande, M., Collod-Béroud, G., Claustres, M., Béroud, C. (2009). Human Splicing Finder: An online bioinformatics tool to predict splicing signals. Nucleic Acids Research *37*, e67.

Doolan, A., Langlois, N., Semsarian, C. (2004). Causes of sudden cardiac death in young Australians. The Medical Journal of Australia *180*, 110–112.

Dörner, A., Xiong, D., Couch, K., Yajima, T., Knowlton, K.U. (2004). Alternatively spliced soluble Coxsackie-adenovirus receptors inhibit Coxsackievirus infection. Journal of Biological Chemistry *279*, 18497–18503.

Dörner, A., Grunert, H.-P., Lindig, V., Chandrasekharan, K., Fechner, H., Knowlton, K.U., Isik, A., Pauschinger, M., Zeichhardt, H., Schultheiss, H.-P. (2006). Treatment of Coxsackievirus-B3-infected BALB/c mice with the soluble Coxsackie adenovirus receptor CAR4/7 aggravates cardiac injury. Journal of Molecular Medicine *84*, 842–851.

Dorner, A.A., Wegmann, F., Butz, S., Wolburg-Buchholz, K., Wolburg, H., Mack, A., Nasdala, I., August, B., Westermann, J., Rathjen, F.G., et al. (2005). Coxsackievirus-adenovirus receptor (CAR) is essential for early embryonic cardiac development. Journal of Cell Science *118*, 3509–3521.

Dreier, B., Honegger, A., Hess, C., Nagy-Davidescu, G., Mittl, P.R.E., Grütter, M.G., Belousova, N., Mikheeva, G., Krasnykh, V., Plückthun, A. (2013). Development of a generic adenovirus delivery system based on structure-guided design of bispecific trimeric DARPin adapters. Proceedings of the National Academy of Sciences *110*, E869-877.

Ebnet, K., Susuki, A., Ohno, S., Vestweber, D. (2004). Junctional adhesion molecules (JAMs): More molecules with dual functions? Journal of Cell Science *117*, 19–29.

Eckart, R.E., Scoville, S.L., Campbell, C.L., Shry, E.A., Stajduhar, K.C., Potter, R.N., Pearse, L.A., Virmani, R. (2004). Sudden death in young adults: A 25-year review of autopsies in military recruits. Annals of Internal Medicine *141*, 829–834.

Excoffon, K.J.D.A., Moninger, T., Zabner, J. (2003). The Coxsackie B virus and adenovirus receptor resides in a distinct membrane microdomain. Journal of Virology *77*, 2559–2567.

Excoffon, K.J.D.A., Hruska-Hageman, A., Klotz, M., Traver, G.L. (2004). A role for the PDZ-binding domain of the Coxsackie B virus and adenovirus receptor (CAR) in cell adhesion and growth. Journal of Cell Science *117*, 4401–4409.

Excoffon, K.J.D.A., Traver, G.L., Zabner, J. (2005). The role of the extracellular domain in the biology of the Coxsackievirus and adenovirus receptor. American Journal of Respiratory Cell and Molecular Biology *32*, 498–503.

Excoffon, K.J.D.A., Avenarius, M.R., Hansen, M.R., Kimberling, W.J., Najmabadi, H., Smith, R.J.H., Zabner, J. (2006). The Coxsackievirus and adenovirus receptor: A new adhesion protein in cochlear development. Hearing Research *215*, 1–9.

Excoffon, K.J.D.A., Gansemer, N., Traver, G., Zabner, J. (2007). Functional effects of Coxsackievirus and adenovirus receptor glycosylation on homophilic adhesion and adenoviral infection. Journal of Virology *81*, 5573–5578.

Excoffon, K.J.D.A., Gansemer, N.D., Mobily, M.E., Karp, P.H., Parekh, K.R., Zabner, J. (2010). Isoform-specific regulation and localization of the Coxsackie and adenovirus receptor in human airway epithelia. PLOS ONE *5*, e9909.

Fabre-Lafay, S., Garrido-Urbani, S., Reymond, N., Gonçalves, A., Dubreuil, P., Lopez, M. (2005). Nectin-4, a new serological breast cancer marker, is a substrate for tumor necrosis factor-alpha-converting enzyme (TACE)/ADAM-17. The Journal of Biological Chemistry *280*, 19543–19550.

Farmer, C., Morton, P.E., Snippe, M., Santis, G., Parsons, M. (2009). Coxsackie adenovirus receptor (CAR) regulates integrin function through activation of p44/42 MAPK. Experimental Cell Research *315*, 2637–2647.

Fätkenheuer, G., Pozniak, A.L., Johnson, M.A., Plettenberg, A., Staszewski, S., Hoepelman, A.I.M., Saag, M.S., Goebel, F.D., Rockstroh, J.K., Dezube, B.J., et al. (2005). Efficacy of short-term monotherapy with maraviroc, a new CCR5 antagonist, in patients infected with HIV-1. Nature Medicine *11*, 1170–1172.

Fechner, H., Haack, A., Wang, H., Eizema, K., Pauschinger, M., Schoemaker, R.G., van Veghel, R., Houtsmuller, A.B., Schultheiss, H.-P., Lamers, J.M.J., et al. (1999). Expression of Coxsackie adenovirus receptor and alphav-integrin does not correlate with adenovector targeting in vivo indicating anatomical vector barriers. Gene Therapy *6*, 1520–1535.

Fechner, H., Noutsias, M., Tschöpe, C., Hinze, K., Wang, X., Escher, F., Pauschinger, M., Dekkers, D., Vetter, R., Paul, M., et al. (2003). Induction of Coxsackievirus-adenovirus-receptor expression during myocardial tissue formation and remodeling: Identification of a cell-to-cell contact-dependent regulatory mechanism. Circulation *107*, 876–882.

Fechner, H., Pinkert, S., Wang, X., Sipo, I., Suckau, L., Kurreck, J., Dörner, A., Sollerbrant, K., Zeichhardt, H., Grunert, H.-P., et al. (2007). Coxsackievirus B3 and adenovirus infections of cardiac cells are efficiently inhibited by vector-mediated RNA interference targeting their common receptor. Gene Therapy *14*, 960–971.

Fechner, H., Pinkert, S., Geisler, A., Poller, W., Kurreck, J. (2011). Pharmacological and biological antiviral therapeutics for cardiac Coxsackievirus infections. Molecules *16*, 8475–8503.

Fok, P.T., Huang, K.-C., Holland, P.C., Nalbantoglu, J. (2007). The Coxsackie and adenovirus receptor binds microtubules and plays a role in cell migration. Journal of Biological Chemistry *282*, 7512–7521.

Freiberg, F., Sauter, M., Pinkert, S., Govindarajan, T., Kaldrack, J., Thakkar, M., Fechner, H., Klingel, K., Gotthardt, M. (2014). Interspecies differences in virus uptake versus cardiac function of the Coxsackievirus and adenovirus receptor. Journal of Virology *88*, 7345–7356.

Freimuth, P., Springer, K., Berard, C., Hainfeld, J., Bewley, M., Flanagan, J.M. (1999). Coxsackievirus and adenovirus receptor amino-terminal immunoglobulin V-related domain binds adenovirus type 2 and fiber knob from adenovirus type 12. Journal of Virology *73*, 1392–1398.

Fu, Z., Thorpe, M., Akula, S., Chahal, G., Hellman, L.T. (2018). Extended cleavage specificity of human neutrophil elastase, human proteinase 3, and their distant ortholog clawed frog PR3—Three elastases with similar primary but different extended specificities and stability. Frontiers in Immunology *9*.

Funke, C., Farr, M., Werner, B., Dittmann, S., Überla, K., Piper, C., Niehaus, K., Horstkotte, D. (2010). Antiviral effect of Bosentan and Valsartan during Coxsackievirus B3 infection of human endothelial cells. Journal of General Virology *91*, 1959–1970.

Gao, Y., Lui, W.-Y. (2014). Synergistic effect of interferon-gamma and tumor necrosis factor-alpha on Coxsackievirus and adenovirus receptor expression: An explanation of cell sloughing during testicular inflammation in mice1. Biology of Reproduction *90*, 1–12.

Gao, S.X., Zhang, Y., Stansberry-Perkins, K., Buko, A., Bai, S., Nguyen, V., Brader, M.L. (2011). Fragmentation of a highly purified monoclonal antibody attributed to residual CHO cell protease activity. Biotechnology and Bioengineering *108*, 977–982.

Garton, K.J., Gough, P.J., Raines, E.W. (2006). Emerging roles for ectodomain shedding in the regulation of inflammatory responses. Journal of Leukocyte Biology *79*, 1105–1116.

Geraghty, P., Rogan, M.P., Greene, C.M., Boxio, R.M.M., Poiriert, T., O'Mahony, M., Belaaouaj, A., O'Neill, S.J., Taggart, C.C., McElvaney, N.G. (2007). Neutrophil elastase up-regulates cathepsin B and matrix metalloprotease-2 expression. Journal of Immunology (Baltimore, Md.: 1950) *178*, 5871–5878.

Ginzberg, H.H., Cherapanov, V., Dong, Q., Cantin, A., McCulloch, C.A.G., Shannon, P.T., Downey, G.P. (2001). Neutrophil-mediated epithelial injury during transmigration: Role of elastase. American Journal of Physiology-Gastrointestinal and Liver Physiology *281*, G705-717.

Goldsmith, M.E., Aguila, A., Steadman, K., Martinez, A., Steinberg, S.M., Alley, M.C., Waud, W.R., Bates, S.E., Fojo, T. (2007). The histone deacetylase inhibitor FK228 given prior to adenovirus infection can boost infection in melanoma xenograft model systems. Molecular Cancer Therapeutics *6*, 496–505.

Goodfellow, I.G., Evans, D.J., Blom, A.M., Kerrigan, D., Miners, J.S., Morgan, B.P., Spiller, O.B. (2005). Inhibition of Coxsackie B virus infection by soluble forms of its receptors: Binding affinities, altered particle formation, and competition with cellular receptors. Journal of Virology *79*, 12016–12024.

Graham, F.L., Smiley, J., Russell, W.C., Nairn, R. (1977). Characteristics of a human cell line transformed by DNA from human adenovirus type 5. The Journal of General Virology *36*, 59–74.

Greve, J.M., Davis, G., Meyer, A.M., Forte, C.P., Yost, S.C., Marlor, C.W., Kamarck, M.E., McClelland, A. (1989). The major human rhinovirus receptor is ICAM-1. Cell *56*, 839–847.

Gye, M.C., Oh, Y.S., Lee, J.E., Shim, S., Choi, K.J., Ahn, H.S. (2011). Expression of Coxsackievirus and adenovirus receptor isoforms in developing mouse bladder uroepithelium. Urology *77*, 1009.e9-18.

Haack, T., González, Ma.J., Sánchez, Y., Giralt, E. (1997). D-Amino acids in protein de novo design. II. Protein-diastereomerism versus protein-enantiomerism. Letters in Peptide Science *4*, 377–386.

Hartmann, M., Parra, L.M., Ruschel, A., Lindner, C., Morrison, H., Herrlich, A., Herrlich, P. (2015). Inside-out regulation of ectodomain cleavage of Cluster-of-Differentiation-44 (CD44) and of neuregulin-1 requires substrate dimerization. Journal of Biological Chemistry *290*, 17041–17054.

Havukainen, H., Underhaug, J., Wolschin, F., Amdam, G., Halskau, O. (2012). A vitellogenin polyserine cleavage site: Highly disordered conformation protected from proteolysis by phosphorylation. Journal of Experimental Biology *215*, 1837–1846.

Hayashida, K., Bartlett, A.H., Chen, Y., Park, P.W. (2010). Molecular and cellular mechanisms of ectodomain shedding. The Anatomical Record: Advances in Integrative Anatomy and Evolutionary Biology *293*, 925–937.

He, Y., Chipman, P.R., Howitt, J., Bator, C.M., Whitt, M.A., Baker, T.S., Kuhn, R.J., Anderson, C.W., Freimuth, P., Rossmann, M.G. (2001). Interaction of Coxsackievirus B3 with the full length Coxsackievirus-adenovirus receptor. Nature Structural Biology *8*, 874–878.

Heath, J.K., White, S.J., Johnstone, C.N., Catimel, B., Simpson, R.J., Moritz, R.L., Tu, G.F., Ji, H., Whitehead, R.H., Groenen, L.C., et al. (1997). The human A33 antigen is a transmembrane glycoprotein and a novel member of the immunoglobulin superfamily. Proceedings of the National Academy of Sciences USA *94*, 469–474.

Herrmann, L. (2016). Shedding of the human Coxsackie- and adenovirus receptor in cell culture. Master thesis. Westfälische Wilhelms-Universität.

Hidaka, C., Milano, E., Leopold, P.L., Bergelson, J.M., Hackett, N.R., Finberg, R.W., Wickham, T.J., Kovesdi, I., Roelvink, P., Crystal, R.G. (1999). CAR-dependent and CAR-independent pathways of adenovirus vector–mediated gene transfer and expression in human fibroblasts. Journal of Clinical Investigation *103*, 579–587.

Higuchi, H., Hara, M., Yamamoto, K., Miyamoto, T., Kinoshita, M., Yamada, T., Uchiyama, K., Matsumori, A. (2008). Mast cells play a critical role in the pathogenesis of viral myocarditis. Circulation *118*, 363–372.

Hirata, K., Ishida, T., Penta, K., Rezaee, M., Yang, E., Wohlgemuth, J., Quertermous, T. (2001). Cloning of an immunoglobulin family adhesion molecule selectively expressed by endothelial cells. Journal of Biological Chemistry *276*, 16223–16231.

van't Hof, W., Crystal, R.G. (2001). Manipulation of the cytoplasmic and transmembrane domains alters cell surface levels of the Coxsackie–adenovirus receptor and changes the efficiency of adenovirus infection. Human Gene Therapy *12*, 25–34.

van't Hof, W., Crystal, R.G. (2002). Fatty acid modification of the Coxsackievirus and adenovirus receptor. Journal of Virology *76*, 6382–6386.

Honda, T., Saitoh, H., Masuko, M., Katagiri-Abe, T., Tominaga, K., Kozakai, I., Kobayashi, K., Kumanishi, T., Watanabe, Y.G., Odani, S., et al. (2000). The Coxsackievirus-adenovirus receptor protein as a cell adhesion molecule in the developing mouse brain. Molecular Brain Research *77*, 19–28.

Horne, W.S., Wiethoff, C.M., Cui, C., Wilcoxen, K.M., Amorin, M., Ghadiri, M.R., Nemerow, G.R. (2005). Antiviral cyclic D,L-α-peptides: Targeting a general biochemical pathway in virus infections. Bioorganic & Medicinal Chemistry *13*, 5145–5153.

Hotta, Y., Honda, T., Naito, M., Kuwano, R. (2003). Developmental distribution of Coxsackie virus and adenovirus receptor localized in the nervous system. Developmental Brain Research *143*, 1–13.

Houri, N., Huang, K.-C., Nalbantoglu, J. (2013). The Coxsackievirus and adenovirus receptor (CAR) undergoes ectodomain shedding and regulated intramembrane proteolysis (RIP). PLOS ONE *8*, e73296.

Huang, K., Ru, B., Zhang, Y., Chan, W.-L., Chow, S.-C., Zhang, J., Lo, C., Lui, W.-Y. (2019). Sertoli cell-specific Coxsackievirus and adenovirus receptor knockout regulates cell adhesion and gene transcription via β-catenin inactivation and Cdc42 activation. FASEB Journal: Official Publication of the Federation of American Societies for Experimental Biology 7588–7602.

Huang, K.-C., Yasruel, Z., Guérin, C., Holland, P.C., Nalbantoglu, J. (2007). Interaction of the Coxsackie and adenovirus receptor (CAR) with the cytoskeleton: Binding to actin. FEBS Letters *581*, 2702–2708.

Huber, S.A. (1994). VCAM-1 is a receptor for encephalomyocarditis virus on murine vascular endothelial cells. Journal of Virology *68*, 3453–3458.

Huber, M., Watson, K.A., Selinka, H.C., Carthy, C.M., Klingel, K., McManus, B.M., Kandolf, R. (1999). Cleavage of RasGAP and phosphorylation of mitogen-activated protein kinase in the course of Coxsackievirus B3 replication. Journal of Virology *73*, 3587–3594.

Hübschmann, M.V., Skladchikova, G., Bock, E., Berezin, V. (2005). Neural cell adhesion molecule function is regulated by metalloproteinase-mediated ectodomain release. Journal of Neuroscience Research *80*, 826–837.

Hung, S.-C., Lu, C.-Y., Shyue, S.-K., Liu, H.-C., Ho, L.L.-T. (2004). Lineage differentiation-associated loss of adenoviral susceptibility and Coxsackie-adenovirus receptor expression in human mesenchymal stem cells. Stem Cells *22*, 1321–1329.

Hutchin, M.E., Pickles, R.J., Yarbrough, W.G. (2000). Efficiency of adenovirus-mediated gene transfer to oropharyngeal epithelial cells correlates with cellular differentiation and human Coxsackie and adenovirus receptor expression. Human Gene Therapy *11*, 2365–2375.

Ilan, N., Mohsenin, A., Cheung, L., Madri, J.A. (2001). PECAM-1 shedding during apoptosis generates a membrane-anchored truncated molecule with unique signaling characteristics. FASEB Journal: Official Publication of the Federation of American Societies for Experimental Biology *15*, 362–372.

Ingemarsdotter, C.K., Tookman, L.A., Browne, A., Pirlo, K., Cutts, R., Chelela, C., Khurrum, K.F., Leung, E.Y.L., Dowson, S., Webber, L., et al. (2015). Paclitaxel resistance increases oncolytic adenovirus efficacy via upregulated CAR expression and dysfunctional cell cycle control. Molecular Oncology *9*, 791–805.

Ito, M., Kodama, M., Masuko, M., Yamaura, M., Fuse, K., Uesugi, Y., Hirono, S., Okura, Y., Kato, K., Hotta, Y., et al. (2000). Expression of Coxsackievirus and adenovirus receptor in hearts of rats with experimental autoimmune myocarditis. Circulation Research *86*, 275–280.

James, S.L., Abate, D., Abate, K.H., Abay, S.M., Abbafati, C., Abbasi, N., Abbastabar, H., Abd-Allah, F., Abdela, J., Abdelalim, A., et al. (2018). Global, regional, and national incidence, prevalence, and years lived with disability for 354 diseases and injuries for 195 countries and territories, 1990–2017: A systematic analysis for the Global Burden of Disease Study 2017. The Lancet *392*, 1789–1858.

Jenssen, H., Hamill, P., Hancock, R.E.W. (2006). Peptide antimicrobial agents. Clinical Microbiology Reviews *19*, 491–511.

Jeong, Y., Ock, S.-A., Yoo, J.G., Yu, D.-Y., Choi, I. (2019). The Cxadr-Adam10 complex plays pivotal roles in tight junction integrity and early trophoblast development in mice. Molecular Reproduction and Development *86*, 1628–1638.

Jiang, S., Caffrey, M. (2007). Solution structure of the Coxsackievirus and adenovirus receptor domain 2. Protein Science *16*, 539–542.

Jiang, S., Jacobs, A., Laue, T.M., Caffrey, M. (2004). Solution structure of the Coxsackievirus and adenovirus receptor domain 1. Biochemistry *43*, 1847–1853.

Kallewaard, N.L., Zhang, L., Chen, J.-W., Guttenberg, M., Sanchez, M.D., Bergelson, J.M. (2009). Tissue-specific deletion of the Coxsackievirus and adenovirus receptor protects mice from virus-induced pancreatitis and myocarditis. Cell Host & Microbe *6*, 91–98.

Karczewski, K.J., Francioli, L.C., Tiao, G., Cummings, B.B., Alföldi, J., Wang, Q., Collins, R.L., Laricchia, K.M., Ganna, A., Birnbaum, D.P., et al. (2020). The mutational constraint spectrum quantified from variation in 141,456 humans. Nature *581*, 434–443.

Kashimura, T., Kodama, M., Hotta, Y., Hosoya, J., Yoshida, K., Ozawa, T., Watanabe, R., Okura, Y., Kato, K., Hanawa, H., et al. (2004). Spatiotemporal changes of Coxsackievirus and adenovirus receptor in rat hearts during postnatal development and in cultured cardiomyocytes of neonatal rats. Euopean Journal of Pathology *444*, 283–292.

Kasuga, I., Hogg, J.C., Paré, P.D., Hayashi, S., Sedgwick, E.G., Ruan, J., Wallace, A.M., He, J.-Q., Zhang, X., Sandford, A.J. (2009). Role of genetic susceptibility to latent adenoviral infection and decreased lung function. Respiratory Medicine *103*, 1672–1680.

Kaur, T., Mishra, B., Saikia, U.N., Sharma, M., Bahl, A., Ratho, R.K. (2012). Expression of Coxsackievirus and adenovirus receptor and its cellular localization in myocardial tissues of dilated cardiomyopathy. Experimental and Clinical Cardiology *17*, 183–186.

van Kilsdonk, J.W.J., van Kempen, L.C.L.T., van Muijen, G.N.P., Ruiter, D.J., Swart, G.W.M. (2010). Soluble adhesion molecules in human cancers: Sources and fates. European Journal of Cell Biology *89*, 415–427.

Kindermann, I., Kindermann, M., Kandolf, R., Klingel, K., Bültmann, B., Müller, T., Lindinger, A., Böhm, M. (2008). Predictors of outcome in patients with suspected myocarditis. Circulation *118*, 639–648.

Kirby, I., Davison, E., Beavil, A.J., Soh, C.P.C., Wickham, T.J., Roelvink, P.W., Kovesdi, I., Sutton, B.J., Santis, G. (2000). Identification of contact residues and definition of the CAR-binding site of adenovirus type 5 fiber protein. Journal of Virology *74*, 2804–2813.

Kitazono, M., Rao, V.K., Robey, R., Aikou, T., Bates, S., Fojo, T., Goldsmith, M.E. (2002). Histone deacetylase inhibitor FR901228 enhances adenovirus infection of hematopoietic cells. Blood *99*, 2248–2251.

Knäuper, V., Cowell, S., Smith, B., López-Otin, C., O'Shea, M., Morris, H., Zardi, L., Murphy, G. (1997). The role of the C-terminal domain of human collagenase-3 (MMP-13) in the activation of procollagenase-3, substrate specificity, and tissue inhibitor of metalloproteinase interaction. The Journal of Biological Chemistry *272*, 7608–7616.

Knecht, E., Roche, E. (1986). The reduction-oxidation status may influence the degradation of glyceraldehyde-3-phosphate dehydrogenase. FEBS *206*, 339–342.

Kobayashi, T., Matsugo, H., Maruyama, J., Kamiki, H., Takada, A., Maeda, K., Takenaka-Uema, A., Tohya, Y., Murakami, S., Horimoto, T. (2019). Characterization of a novel species of adenovirus from Japanese microbat and role of CXADR as its entry factor. Scientific Reports *9*, 573.

Koenen, R.R., Pruessmeyer, J., Soehnlein, O., Fraemohs, L., Zernecke, A., Schwarz, N., Reiss, K., Sarabi, A., Lindbom, L., Hackeng, T.M., et al. (2009). Regulated release and functional modulation of junctional adhesion molecule A by disintegrin metalloproteinases. Blood *113*, 4799–4809.

Kolawole, A.O., Sharma, P., Yan, R., Lewis, K.J.E., Xu, Z., Hostetler, H.A., Excoffon, K.J.D.A. (2012). The PDZ1 and PDZ3 domains of MAGI-1 regulate the eight-exon isoform of the Coxsackievirus and adenovirus receptor. Journal of Virology *86*, 9244–9254.

Korkmaz, B., Hajjar, E., Kalupov, T., Reuter, N., Brillard-Bourdet, M., Moreau, T., Juliano, L., Gauthier, F. (2007). Influence of charge distribution at the active site surface on the substrate specificity of human neutrophil protease 3 and elastase. A kinetic and molecular modeling analysis. The Journal of Biological Chemistry *282*, 1989–1997.

Korkmaz, B., Moreau, T., Gauthier, F. (2008). Neutrophil elastase, proteinase 3 and cathepsin G: Physicochemical properties, activity and physiopathological functions. Biochimie *90*, 227–242.

Korkmaz, B., Horwitz, M.S., Jenne, D.E., Gauthier, F. (2010). Neutrophil elastase, proteinase 3, and cathepsin G as therapeutic targets in human diseases. Pharmacological Reviews *62*, 726–759.

Kotha, P.L.N., Sharma, P., Kolawole, A.O., Yan, R., Alghamri, M.S., Brockman, T.L., Gomez-Cambronero, J., Excoffon, K.J.D.A. (2015). Adenovirus entry from the apical surface of polarized epithelia is facilitated by the host innate immune response. PLOS Pathogens *11*, e1004696.

Krissinel, E., Henrick, K. (2007). Inference of macromolecular assemblies from crystalline state. Journal of Molecular Biology *372*, 774–797.

Krivega, M., Geens, M., van de Velde, H. (2014). CAR expression in human embryos and hESC illustrates its role in pluripotency and tight junctions. Reproduction *148*, 531–544.

Kühl, U., Pauschinger, M., Noutsias, M., Seeberg, B., Bock, T., Lassner, D., Poller, W., Kandolf, R., Schultheiss, H.-P. (2005). High prevalence of viral genomes and multiple viral infections in the myocardium of adults with "idiopathic" left ventricular dysfunction. Circulation *111*, 887–893.

Kwon, J., Kim, N.-H., Choi, I. (2016). CXADR is required for AJ and TJ assembly during porcine blastocyst formation. Reproduction *151*, 297–304.

Lacher, M.D., Tiirikainen, M.I., Saunier, E.F., Christian, C., Anders, M., Oft, M., Balmain, A., Akhurst, R.J., Korn, W.M. (2006). Transforming growth factor-receptor inhibition enhances adenoviral infectability of carcinoma cells via up-regulation of Coxsackie and adenovirus receptor in conjunction with reversal of epithelial-mesenchymal transition. Cancer Research *66*, 1648–1657.

Lacher, M.D., Shiina, M., Chang, P., Keller, D., Tiirikainen, M.I., Korn, W.M. (2011). ZEB1 limits adenoviral infectability by transcriptionally repressing the Coxsackie virus and adenovirus Receptor. Molecular Cancer *10*, 1–16.

Law, L.K., Davidson, B.L. (2005). What does it take to bind CAR? Molecular Therapy *12*, 599–609.

Lee, J.K., Zaidi, S.H.E., Liu, P., Dawood, F., L.Cheah, A.Y., Wen, W.-H., Saiki, Y., Rabinovitch, M. (1998). A serine elastase inhibitor reduces inflammation and fibrosis and preserves cardiac function after experimentally-induced murine myocarditis. Nature Medicine *4*, 1383–1391.

Lehmann, M., El Battari, A., Abadie, B., Martin, J.M., Marvaldi, J. (1996). Role of alpha v beta 5 and alpha v beta 6 integrin glycosylation in the adhesion of a colonic adenocarcinoma cell line (HT29-D4). Journal of Cellular Biochemistry *61*, 266–277.

Leibovitz, A., McCombs, W.M., Johnston, D., McCoy, C.E., Stinson, J.C. (1973). New human cancer cell culture lines. I. SW-13, small-cell carcinoma of the adrenal cortex. Journal of the National Cancer Institute *51*, 691–697.

Letavernier, E., Zafrani, L., Perez, J., Letavernier, B., Haymann, J.-P., Baud, L. (2012). The role of calpains in myocardial remodelling and heart failure. Cardiovascular Research *96*, 38–45.

Lévesque, J.P., Takamatsu, Y., Nilsson, S.K., Haylock, D.N., Simmons, P.J. (2001). Vascular cell adhesion molecule-1 (CD106) is cleaved by neutrophil proteases in the bone marrow following hematopoietic progenitor cell mobilization by granulocyte colony-stimulating factor. Blood *98*, 1289–1297.

Levitt, N.H., Crowell, R.L. (1967). Comparative studies of the regeneration of HeLa cell receptors for poliovirus T1 and Coxsackievirus B3. Journal of Virology *1*, 693–700.

Li, C., Gu, H., Yu, M., Yang, P., Zhang, M., Ba, H., Yin, Y., Wang, J., Yin, B., Zhou, X., et al. (2019). Inhibition of transmembrane TNF-α shedding by a specific antibody protects against septic shock. Cell Death & Disease *10*, 1–17.

Li, J., Schwimmbeck, P.L., Tschope, C., Leschka, S., Husmann, L., Rutschow, S., Reichenbach, F., Noutsias, M., Kobalz, U., Poller, W., et al. (2002). Collagen degradation in a murine myocarditis model: Relevance of matrix metalloproteinase in association with inflammatory induction. Cadiovascular Research *56*, 235–247.

Lieber, M., Smith, B., Szakal, A., Nelson-Rees, W., Todaro, G. (1976). A continuous tumor-cell line from a human lung carcinoma with properties of type II alveolar epithelial cells. International Journal of Cancer *17*, 62–70.

Lim, B.-K., Choi, J., Nam, J., Gil, C., Shin, J., Yun, S., Kim, D., Jeon, E. (2006). Virus receptor trap neutralizes Coxsackievirus in experimental murine viral myocarditis. Cardiovascular Research *71*, 517–526.

Lim, B.-K., Xiong, D., Dorner, A., Youn, T.-J., Yung, A., Liu, T.I., Gu, Y., Dalton, N.D., Wright, A.T., Evans, S.M., et al. (2008). Coxsackievirus and adenovirus receptor (CAR) mediates atrioventricular-node function and connexin 45 localization in the murine heart. Journal of Clinical Investigation *118*, 2758–2770.

Lindert, U., Gnoli, M., Maioli, M., Bedeschi, M.F., Sangiorgi, L., Rohrbach, M., Giunta, C. (2018). Insight into the pathology of a COL1A1 signal peptide heterozygous mutation leading to severe osteogenesis imperfecta. Calcified Tissue International *102*, 373–379.

Lindner, D., Li, J., Savvatis, K., Klingel, K., Blankenberg, S., Tschöpe, C., Westermann, D. (2014). Cardiac fibroblasts aggravate viral myocarditis: Cell specific Coxsackievirus B3 replication. Mediators of Inflammation *519528*, 1–14.

Liou, T.G., Campbell, E.J. (1995). Nonisotropic enzyme-inhibitor interactions: A novel nonoxidative mechanism for quantum proteolysis by human neutrophils. Biochemistry *34*, 16171–16177.

Lisewski, U., Shi, Y., Wrackmeyer, U., Fischer, R., Chen, C., Schirdewan, A., Juttner, R., Rathjen, F., Poller, W., Radke, M.H., et al. (2008). The tight junction protein CAR regulates cardiac conduction and cell-cell communication. Journal of Experimental Medicine *205*, 2369–2379.

Liu, P.P., Mason, J.W. (2001). Advances in the understanding of myocarditis. Circulation *104*, 1076–1082.

Liu, Q., Su, X., Yu, Y., Liu, Y. (2013). Correlation between virus persistent infection and cardiac function in patients with dilated cardiomyopathy. Journal of Zhejiang University. Science. B *14*, 749–753.

Lortat-Jacob, H., Chouin, E., Cusack, S., van Raaij, M.J. (2001). Kinetic analysis of adenovirus fiber binding to its receptor reveals an avidity mechanism for trimeric receptor-ligand interactions. Journal of Biological Chemistry *276*, 9009–9015.

Lü, X., Yao, M., Zhang, J.-M., Yang, J., Lei, Y.-F., Huang, X.-J., Jia, Z.-S., Ma, L., Lan, H.-Y., Xu, Z.-K., et al. (2014). Identification of peptides that bind hepatitis C virus envelope protein E2 and inhibit viral cellular entry from a phage-display peptide library. International Journal of Molecular Medicine *33*, 1312–1318.

Lynch, J.P., Kajon, A.E. (2016). Adenovirus: Epidemiology, global spread of novel serotypes, and advances in treatment and prevention. Seminars in Respiratory and Critical Care Medicine *37*, 586–602.

Lyons, P.D., Benveniste, E.N. (1998). Cleavage of membrane-associated ICAM-1 from astrocytes: Involvement of a metalloprotease. Glia *22*, 103–112.

Marchant, D., McManus, B.M. (2009). Matrix metalloproteinases in the pathogenesis of viral heart disease. Trends in Cardiovascular Medicine *19*, 21–26.

Maretzky, T., Schulte, M., Ludwig, A., Rose-John, S., Blobel, C., Hartmann, D., Altevogt, P., Saftig, P., Reiss, K. (2005). L1 is sequentially processed by two differently activated metalloproteases and presenilin/gamma-secretase and regulates neural cell adhesion, cell migration, and neurite outgrowth. Molecular and Cellular Biology *25*, 9040–9053.

Margineanu, A., Chan, J.J., Kelly, D.J., Warren, S.C., Flatters, D., Kumar, S., Katan, M., Dunsby, C.W., French, P.M.W. (2016). Screening for protein-protein interactions using Förster resonance energy transfer (FRET) and fluorescence lifetime imaging microscopy (FLIM). Scientific Reports *6*, 28186.

Maron, B.J. (2003). Sudden death in young athletes. New England Journal of Medicine *349*, 1064–1075.

Marsman, R.F.J., Bezzina, C.R., Freiberg, F., Verkerk, A.O., Adriaens, M.E., Podliesna, S., Chen, C., Purfürst, B., Spallek, B., Koopmann, T.T., et al. (2014). Coxsackie and adenovirus receptor is a modifier of cardiac conduction and arrhythmia vulnerability in the setting of myocardial ischemia. Journal of the American College of Cardiology *63*, 549–559.

Martino, T.A., Petric, M., Weingartl, H., Bergelson, J.M., Opavsky, M.A., Richardson, C.D., Modlin, J.F., Finberg, R.W., Kain, K.C., Willis, N., et al. (2000). The Coxsackie-adenovirus receptor (CAR) is used by reference strains and clinical isolates representing all six serotypes of Coxsackievirus group B and by swine vesicular disease virus. Virology *271*, 99–108.

Mason, J.W., O'Connell, J.B., Herskowitz, A., Rose, N.R., McManus, B.M., Billingham, M.E., Moon, T.E. (1995). A clinical trial of immunosuppressive therapy for myocarditis. New England Journal of Medicine *333*, 269–275.

McGuire, J.K., Li, Q., Parks, W.C. (2003). Matrilysin (matrix metalloproteinase-7) mediates E-cadherin ectodomain shedding in injured lung epithelium. The American Journal of Pathology *162*, 1831–1843.

Metzler, K.D., Goosmann, C., Lubojemska, A., Zychlinsky, A., Papayannopoulos, V. (2014). A myeloperoxidase-containing complex regulates neutrophil elastase release and actin dynamics during NETosis. Cell Reports *8*, 883–896.

Milstone, A.M., Petrella, J., Sanchez, M.D., Mahmud, M., Whitbeck, J.C., Bergelson, J.M. (2005). Interaction with Coxsackievirus and adenovirus receptor, but not with decay-accelerating factor (DAF), induces A-particle formation in a DAF-binding Coxsackievirus B3 isolate. Journal of Virology *79*, 655–660.

Mirza, M., Raschperger, E., Philipson, L., Pettersson, R.F., Sollerbrant, K. (2005). The cell surface protein Coxsackie- and adenovirus receptor (CAR) directly associates with the ligand-of-Numb protein-X2 (LNX2). Experimental Cell Research *309*, 110–120.

Mirza, M., Hreinsson, J., Strand, M.-L., Hovatta, O., Söder, O., Philipson, L., Pettersson, R.F., Sollerbrant, K. (2006). Coxsackievirus and adenovirus receptor (CAR) is expressed in male germ cells and forms a complex with the differentiation factor JAM-C in mouse testis. Experimental Cell Research *312*, 817–830.

Mirza, M., Pang, M.F., Zaini, M.A., Haiko, P., Tammela, T., Alitalo, K., Philipson, L., Fuxe, J., Sollerbrant, K. (2012). Essential role of the Coxsackie- adenovirus receptor (CAR) in development of the lymphatic system in mice. PLOS ONE *7*, e37523.

Mittal, R., Patel, A.P., Debs, L.H., Nguyen, D., Patel, K., Grati, M., Mittal, J., Yan, D., Chapagain, P., Liu, X.Z. (2016a). Intricate functions of matrix metalloproteinases in physiological and pathological conditions: Role of MMPs in health and disease. Journal of Cellular Physiology *231*, 2599–2621.

Mittal, R., Patel, A.P., Debs, L.H., Nguyen, D., Patel, K., Grati, M., Mittal, J., Yan, D., Chapagain, P., Liu, X.Z. (2016b). Intricate functions of matrix metalloproteinases in physiological and pathological conditions: Role of MMPs in health and disease. Journal of Cellular Physiology *231*, 2599–2621.

Morton, P.E., Hicks, A., Nastos, T., Santis, G., Parsons, M. (2013). CAR regulates epithelial cell junction stability through control of E-cadherin trafficking. Scientific Reports *3*, 1–13.

Morton, P.E., Hicks, A., Ortiz-Zapater, E., Raghavan, S., Pike, R., Noble, A., Woodfin, A., Jenkins, G., Rayner, E., Santis, G., et al. (2016). TNFα promotes CAR-dependent migration of leukocytes across epithelial monolayers. Scientific Reports *6*, 26321.

Motrescu, E.R., Rio, M.-C. (2008). Cancer cells, adipocytes and matrix metalloproteinase 11: A vicious tumor progression cycle. Biological Chemistry *389*, 1037–1041.

Muckelbauer, J.K., Kremer, M., Minor, I., Diana, G., Dutko, F.J., Groarke, J., Pevear, D.C., Rossmann, M.G. (1995). The structure of Coxsackievirus B3 at 3.5 A resolution. Structure *3*, 653–667.

Muehlenbachs, A., Bhatnagar, J., Zaki, S.R. (2015). Tissue tropism, pathology and pathogenesis of enterovirus infection. The Journal of Pathology *235*, 217–228.

Murakami, T., Nakajima, T., Koyanagi, Y., Tachibana, K., Fujii, N., Tamamura, H., Yoshida, N., Waki, M., Matsumoto, A., Yoshie, O., et al. (1997). A small molecule CXCR4 inhibitor that blocks T cell line–tropic HIV-1 infection. The Journal of Experimental Medicine *186*, 1389–1393.

Murphy, G., Knäuper, V. (1997). Relating matrix metalloproteinase structure to function: Why the "hemopexin" domain? Matrix Biology: Journal of the International Society for Matrix Biology *15*, 511–518.

Murphy, G., Murthy, A., Khokha, R. (2008). Clipping, shedding and RIPping keep immunity on cue. Trends in Immunology *29*, 75–82.

Mydel, P., Shipley, J.M., Adair-Kirk, T.L., Kelley, D.G., Broekelmann, T.J., Mecham, R.P., Senior, R.M. (2008). Neutrophil elastase cleaves laminin-332 (laminin-5) generating peptides that are chemotactic for neutrophils. The Journal of Biological Chemistry *283*, 9513–9522.

Nagano, O., Murakami, D., Hartmann, D., de Strooper, B., Saftig, P., Iwatsubo, T., Nakajima, M., Shinohara, M., Saya, H. (2004). Cell–matrix interaction via CD44 is independently regulated by different metalloproteinases activated in response to extracellular Ca2+ influx and PKC activation. The Journal of Cell Biology *165*, 893–902.

Nalbantoglu, J., Pari, G., Karpati, G., Holland, P.C. (1999). Expression of the primary Coxsackie and adenovirus receptor is downregulated during skeletal muscle maturation and limits the efficacy of adenovirus-mediated gene delivery to muscle cells. Human Gene Therapy *10*, 1009–1019.

Nalbantoglu, J., Larochelle, N., Wolf, E., Karpati, G., Lochmuller, H., Holland, P.C. (2001). Muscle-specific overexpression of the adenovirus primary receptor CAR overcomes low efficiency of gene transfer to mature skeletal muscle. Journal of Virology *75*, 4276–4282.

Nasuno, A., Toba, K., Ozawa, T., Hanawa, H., Osman, Y., Hotta, Y., Yoshida, K., Saigawa, T., Kato, K., Kuwano, R., et al. (2004). Expression of Coxsackievirus and adenovirus receptor in neointima of the rat carotid artery. Cardiovascular Pathology *13*, 79–84.

Naus, S., Richter, M., Wildeboer, D., Moss, M., Schachner, M., Bartsch, J.W. (2004). Ectodomain shedding of the neural recognition molecule CHL1 by the metalloprotease-disintegrin ADAM8 promotes neurite outgrowth and puppresses neuronal cell death. Journal of Biological Chemistry *279*, 16083–16090.

Nicklin, S.A., Wu, E., Nemerow, G.R., Baker, A.H. (2005). The influence of adenovirus fiber structure and function on vector development for gene therapy. Molecular Therapy *12*, 384–393.

Niedermaier, S., Huesgen, P.F. (2019). Positional proteomics for identification of secreted proteoforms released by site-specific processing of membrane proteins. Biochimica et Biophysica Acta (BBA) - Proteins and Proteomics *1867*, 140138.

Niu, L., Li, C., Wang, Z., Xu, H., An, X. (2017). Effects of the MAPK pathway and the expression of CAR in a murine model of viral myocarditis. Experimental and Therapeutic Medicine *13*, 230–234.

Noutsias, M., Fechner, H., de Jonge, H., Wang, X., Dekkers, D., Houtsmuller, A.B., Pauschinger, M., Bergelson, J., Warraich, R., Yacoub, M., et al. (2001). Human Coxsackie-adenovirus receptor is colocalized with integrins alphav beta3 and alphav beta5 on the cardiomyocyte sarcolemma and upregulated in dilated cardiomyopathy: Implications for cardiotropic viral infections. Circulation *104*, 275–280.

Novak, K. (2002). Metastasis: CAR problems. Nature Reviews Cancer *2*.

Oberscheidt, V. (2014). Untersuchungen zum Shedding des rekombinanten Coxsackie-Adenovirus-Rezeptor. Master thesis. Bielefeld.

Ohta, K., Nakajima, T., Cheah, A.Y.L., Zaidi, S.H.E., Kaviani, N., Dawood, F., You, X.-M., Liu, P., Husain, M., Rabinovitch, M. (2004). Elafin-overexpressing mice have improved cardiac function after myocardial infarction. American Journal of Physiology. Heart and Circulatory Physiology *287*, H286-292.

Okegawa, T., Li, Y., Pong, R.-C., Bergelson, J.M., Zhou, J., Hsieh, J.-T. (2000). The dual impact of Coxsackie and adenovirus receptor expression on human prostate cancer gene therapy. Cancer Research *60*, 5031–5036.

Okegawa, T., Pong, R.-C., Li, Yingming, Bergelson, J.M., Sagalowsky, A.I., Hsieh, J.-T. (2001). The mechanism of the growth-inhibitory effect of Coxsackie and adenovirus receptor (CAR) on human bladder cancer: A functional analysis of CAR protein structure. Cancer Research *61*, 6592–6600.

Okegawa, T., Sayne, J.R., Nutahara, K., Pong, R.-C., Saboorian, H., Kabbani, W., Higashihara, E., Hsieh, J.-T. (2007). A histone deacetylase inhibitor enhances adenoviral infection of renal cancer cells. The Journal of Urology *177*, 1148–1156.

Opavsky, M.A., Martino, T., Rabinovitch, M., Penninger, J., Richardson, C., Petric, M., Trinidad, C., Butcher, L., Chan, J., Liu, P.P. (2002). Enhanced ERK-1/2 activation in mice susceptible to Coxsackievirus-induced myocarditis. The Journal of Clinical Investigation *109*, 1561–1569.

Owen, C.A., Campbell, E.J. (1999). The cell biology of leukocyte-mediated proteolysis. Journal of Leukocyte Biology *65*, 137–150.

Owen, C.A., Campbell, M.A., Sannes, P.L., Boukedes, S.S., Campbell, E.J. (1995). Cell surface-bound elastase and cathepsin G on human neutrophils: A novel, non-oxidative mechanism by which neutrophils focus and preserve catalytic activity of serine proteinases. The Journal of Cell Biology *131*, 775–789.

Park, J.H., Jin, J.H., Lim, M.S., An, H.J., Kim, J.W., Lee, G.M. (2017). Proteomic analysis of host cell protein dynamics in the culture supernatants of antibody-producing CHO cells. Scientific Reports *7*, 44246.

Parks, W.C., Wilson, C.L., López-Boado, Y.S. (2004). Matrix metalloproteinases as modulators of inflammation and innate immunity. Nature Reviews Immunology *4*, 617–629.

Patzke, C., Max, K.E.A., Behlke, J., Schreiber, J., Schmidt, H., Dorner, A.A., Kroger, S., Henning, M., Otto, A., Heinemann, U., et al. (2010). The Coxsackievirus-adenovirus receptor reveals complex homophilic and heterophilic interactions on neural cells. Journal of Neuroscience *30*, 2897–2910.

Pazirandeh, A., Sultana, T., Mirza, M., Rozell, B., Hultenby, K., Wallis, K., Vennström, B., Davis, B., Arner, A., Heuchel, R., et al. (2011). Multiple phenotypes in adult mice following inactivation of the Coxsackievirus and adenovirus receptor (CAR) gene. PLOS ONE *6*, e20203.

Pejler, G., Ronnberg, E., Waern, I., Wernersson, S. (2010). Mast cell proteases: Multifaceted regulators of inflammatory disease. Blood *115*, 4981–4990.

Petrella, J., Cohen, C.J., Gaetz, J., Bergelson, J.M. (2002). A zebrafish Coxsackievirus and adenovirus receptor homologue interacts with Coxsackie B virus and adenovirus. Journal of Virology *76*, 10503–10506.

Pettersen, E.F., Goddard, T.D., Huang, C.C., Couch, G.S., Greenblatt, D.M., Meng, E.C., Ferrin, T.E. (2004). UCSF Chimera-A visualization system for exploratory research and analysis. Journal of Computational Chemistry *25*, 1605–1612.

Pham, C.T.N. (2006). Neutrophil serine proteases: Specific regulators of inflammation. Nature Reviews Immunology *6*, 541–550.

Phillips, H.J. (1972). Dissociation of single cells from lung or kidney tissue with elastase. In Vitro *8*, 101–105.

Pickles, R.J., Fahrner, J.A., Petrella, J.M., Boucher, R.C., Bergelson, J.M. (2000). Retargeting the Coxsackievirus and adenovirus receptor to the apical surface of polarized epithelial cells reveals the glycocalyx as a barrier to adenovirus-mediated gene transfer. Journal of Virology *74*, 6050–6057.

Pinkert, S., Westermann, D., Wang, X., Klingel, K., Dörner, A., Savvatis, K., Grossl, T., Krohn, S., Tschope, C., Zeichhardt, H., et al. (2009). Prevention of cardiac dysfunction in acute Coxsackievirus B3 cardiomyopathy by inducible expression of a soluble Coxsackievirus-adenovirus receptor. Circulation *120*, 2358–2366.

Pinkert, S., Röger, C., Kurreck, J., Bergelson, J., Fechner, H. (2016). The Coxsackievirus and adenovirus receptor: Glycosylation and the extracellular D2 domain are not required for Coxsackievirus B3 infection. Journal of Virology *90*, 5601–5610.

Pinkert, S., Dieringer, B., Klopfleisch, R., Savvatis, K., Van Linthout, S., Pryshliak, M., Tschöpe, C., Klingel, K., Kurreck, J., Beling, A., et al. (2019). Early treatment of Coxsackievirus B3-infected animals with soluble Coxsackievirus-adenovirus receptor inhibits development of chronic Coxsackievirus B3 cardiomyopathy. Circulation. Heart Failure *12*, e005250.

Pong, R.-C., Lai, Y.-J., Chen, H., Okegawa, T., Frenkel, E., Sagalowsky, A.I., Hsieh, J.-T. (2003). Epigenetic regulation of Coxsackie and adenovirus receptor (CAR) gene promotor in urogenital cancer cells. Cancer Research *63*, 8680–8686.

Puck, T.T., Cieciura, S.J., Robinson, A. (1958). Genetics of somatic mammalian cells. III. Long-term cultivation of euploid cells from human and animal subjects. Journal of Experimental Medicine *108*, 945–956.

Qin, M., Chen, S., Yu, T., Escuadro, B., Sharma, S., Batra, R.K. (2003). Coxsackievirus adenovirus receptor expression predicts the efficiency of adenoviral gene transfer into non-small cell lung cancer xenografts. Clinical Cancer Research *9*, 4992–4999.

Qureshi, A., Thakur, N., Tandon, H., Kumar, M. (2014). AVPdb: A database of experimentally validated antiviral peptides targeting medically important viruses. Nucleic Acids Research *42*, D1147-1153.

van Raaij, M.J., Chouin, E., van der Zandt, H., Bergelson, J.M., Cusack, S. (2000). Dimeric structure of the Coxsackievirus and adenovirus receptor D1 domain at 1.7 Å resolution. Structure *8*, 1147–1155.

Rabquer, B.J., Amin, M.A., Teegala, N., Shaheen, M.K., Tsou, P.-S., Ruth, J.H., Lesch, C.A., Imhof, B.A., Koch, A.E. (2010). Junctional adhesion molecule-C is a soluble mediator of angiogenesis. The Journal of Immunology *185*, 1777–1785.

Rajpar, M.H. (2002). Mutation of the signal peptide region of the bicistronic gene DSPP affects translocation to the endoplasmic reticulum and results in defective dentine biomineralization. Human Molecular Genetics *11*, 2559–2565.

Raschperger, E., Engstrom, U., Pettersson, R.F., Fuxe, J. (2004). CLMP, a novel member of the CTX family and a new component of epithelial tight junctions. Journal of Biological Chemistry *279*, 796–804.

Raschperger, E., Thyberg, J., Pettersson, S., Philipson, L., Fuxe, J., Pettersson, R.F. (2006). The Coxsackie- and adenovirus receptor (CAR) is an in vivo marker for epithelial tight junctions, with a potential role in regulating permeability and tissue homeostasis. Experimental Cell Research *312*, 1566–1580.

Raschperger, E., Neve, E.P.A., Wernerson, A., Hultenby, K., Pettersson, R.F., Majumdar, A. (2008). The Coxsackie and adenovirus receptor (CAR) is required for renal epithelial differentiation within the zebrafish pronephros. Developmental Biology *313*, 455–464.

Rebel, V.I., Hartnett, S., Denham, J., Chan, M., Finberg, R., Sieff, C.A. (2000). Maturation and lineage-specific expression of the Coxsackie and adenovirus receptor in hematopoietic cells. Stem Cells *18*, 176–182.

Reddy, P., Caras, I., Krieger, M. (1989). Effects of O-linked glycosylation on the cell surface expression and stability of decay-accelerating factor, a glycophospholipid-anchored membrane protein. The Journal of Biological Chemistry *264*, 17329–17336.

Reeh, M., Bockhorn, M., Görgens, D., Vieth, M., Hoffmann, T., Simon, R., Izbicki, J.R., Sauter, G., Schumacher, U., Anders, M. (2013). Presence of the Coxsackievirus and adenovirus receptor (CAR) in human neoplasms: A multitumour array analysis. British Journal of Cancer *109*, 1848–1858.

Reimer, D., Steppan, I., Wiedemair, A., Concin, N., Hofstetter, G., Marth, C., Müller-Holzner, E., Zeimet, A.G. (2007). Soluble isoforms but not the transmembrane form of Coxsackie-adenovirus receptor are of clinical relevance in epithelial ovarian cancer. International Journal of Cancer *120*, 2568–2575.

Reiss, K., Saftig, P. (2009). The "A disintegrin and metalloprotease" (ADAM) family of sheddases: Physiological and cellular functions. Seminars in Cell & Developmental Biology *20*, 126–137.

Riabi, S., Harrath, R., Gaâloul, I., Hamzeh-Cognasse, H., Délezay, O., Aouni, M., Pozzetto, B. (2014). Flow cytometry analysis of Coxsackievirus B receptors expression in human CaCo-2 cells. Central European Journal of Biology *9*, 699–707.

Robert, F., Bierau, H., Rossi, M., Agugiaro, D., Soranzo, T., Broly, H., Mitchell-Logean, C. (2009). Degradation of an Fc-fusion recombinant protein by host cell proteases: Identification of a CHO cathepsin D protease. Biotechnology and Bioengineering *104*, 1132–1141.

Roelvink, P.W., Lizonova, A., Lee, J.G.M., Li, Y., Bergelson, J.M., Finberg, R., Brough, D.E., Kovesdi, I., Wickham, T.J. (1998). The Coxsackievirus-adenovirus receptor protein can function as a cellular attachment protein for adenovirus serotypes from subgroups A, C, D, E, and F. Journal of Virology *72*, 7909–7915.

Röger, C., Pozzuto, T., Klopfleisch, R., Kurreck, J., Pinkert, S., Fechner, H. (2015). Expression of an engineered soluble Coxsackievirus and adenovirus receptor by a dimeric AAV9 vector inhibits adenovirus infection in mice. Gene Therapy *22*, 458–466.

Ruppert, V., Meyer, T., Pankuweit, S., Jonsdottir, T., Maisch, B. (2008). Activation of STAT1 transcription factor precedes up-regulation of Coxsackievirus–adenovirus receptor during viral myocarditis. Cardiovascular Pathology *17*, 81–92.

Russell, D., Oldham, N.J., Davis, B.G. (2009). Site-selective chemical protein glycosylation protects from autolysis and proteolytic degradation. Carbohydrate Research *344*, 1508–1514.

Rutschow, S., Li, J., Schultheiss, H., Pauschinger, M. (2006). Myocardial proteases and matrix remodeling in inflammatory heart disease. Cardiovascular Research *69*, 646–656.

Sahni, A., Baker, C.A., Sporn, L.A., Francis, C.W. (2000). Fibrinogen and fibrin protect fibroblast growth factor-2 from proteolytic degradation. Thrombosis and Haemostasis *83*, 736–741.

Santis, G., Legrand, V., Hong, S.S., Davison, E., Kirby, I., Imler, J.L., Finberg, R.W., Bergelson, J.M., Mehtali, M., Boulanger, P. (1999). Molecular determinants of adenovirus serotype 5 fibre binding to its cellular receptor CAR. Journal of General Virology *80*, 1519–1527.

Sasse, A., Wallich, M., Ding, Z., Goedecke, A., Schrader, J. (2003). Coxsackie-and-adenovirus receptor mRNA expression in human heart failure. Journal of Gene Medicine *5*, 876–882.

Schell, C., Kretz, O., Bregenzer, A., Rogg, M., Helmstädter, M., Lisewski, U., Gotthardt, M., Tharaux, P.-L., Huber, T.B., Grahammer, F. (2015). Podocyte-specific deletion of murine CXADR does not impair podocyte development, function or stress response. PLOS ONE *10*, e0129424.

Scherer, W.F., Syverton, J.T., Gey, G.O. (1953). Studies on the propagation in vitro of poliomyelitis viruses. IV. Viral multiplication in a stable strain of human malignant epithelial cells (strain HeLa) derived from an epidermoid carcinoma of the cervix. Journal of Experimental Medicine *97*, 695–710.

Schmidt, M.R., Piekos, B., Cabatingan, M.S., Woodland, R.T. (2000). Expression of a human Coxsackie/adenovirus receptor transgene permits adenovirus infection of primary lymphocytes. Journal of Immunology *165*, 4112–4119.

Schwarz, J.M., Cooper, D.N., Schuelke, M., Seelow, D. (2014). MutationTaster2: Mutation prediction for the deep-sequencing age. Nature Methods *11*, 361–362.

Segura-Pacheco, B., Avalos, B., Rangel, E., Velazquez, D., Cabrera, G. (2007). HDAC inhibitor valproic acid upregulates CAR in vitro and in vivo. Genetic Vaccines and Therapy *5*, 1–8.

Shafren, D.R., Bates, R.C., Agrez, M.V., Herd, R.L., Bums, G.F., Barry, R.D. (1995). Coxsackieviruses B1, B3, and B5 use decay accelerating factor as a receptor for cell attachment. Journal of Virology *69*, 3873–3877.

Shafren, D.R., Williams, D.T., Barry, R.D. (1997). A decay-accelerating factor-binding strain of Coxsackievirus B3 requires the Coxsackievirus-adenovirus receptor protein to mediate lytic infection of rhabdomyosarcoma cells. Journal of Virology *71*, 9844–9848.

Sharma, M., Mishra, B., Saikia, U.N., Bahl, A., Ratho, R.K., Talwar, K.K. (2016). Role of Coxsackievirus and adenovirus receptor (CAR) expression and viral load of adenovirus and enterovirus in patients with dilated cardiomyopathy. Archives of Virology *161*, 87–94.

Sharma, P., Kolawole, A.O., Wiltshire, S.M., Frondorf, K., Excoffon, K.J.D.A. (2012). Accessibility of the Coxsackievirus and adenovirus receptor and its importance in adenovirus gene transduction efficiency. The Journal of General Virology *93*, 155–158.

Shauer, A., Gotsman, I., Keren, A., Zwas, D.R., Hellman, Y., Durst, R., Admon, D. (2013). Acute viral myocarditis: Current concepts in diagnosis and treatment. The Israel Medical Association Journal: IMAJ *15*, 180–185.

Shaw, C.A., Holland, P.C., Sinnreich, M., Allen, C., Sollerbrant, K., Karpati, G., Nalbantoglu, J. (2004). Isoform-specific expression of the Coxsackie and adenovirus receptor (CAR) in neuromuscular junction and cardiac intercalated discs. BMC Cell Biology *5*, 1–8.

Shaw, C.A., Larochelle, N., Dudley, R.W.R., Lochmuller, H., Danialou, G., Petrof, B.J., Karpati, G., Holland, P.C., Nalbantoglu, J. (2006). Simultaneous dystrophin and dysferlin deficiencies associated with high-level expression of the Coxsackie and adenovirus receptor in transgenic mice. The American Journal of Pathology *169*, 2148–2160.

Shetty, P.B., Tang, H., Tayo, B.O., Morrison, A.C., Hanis, C.L., Rao, D.C., Young, J.H., Fox, E.R., Boerwinkle, E., Cooper, R.S., et al. (2012). Variants in CXADR and F2RL1 are associated with blood pressure and obesity in African-Americans in regions identified through admixture mapping. Journal of Hypertension *30*, 1970–1976.

Shi, Y., Chen, C., Lisewski, U., Wrackmeyer, U., Radke, M., Westermann, D., Sauter, M., Tschöpe, C., Poller, W., Klingel, K., et al. (2009). Cardiac deletion of the Coxsackievirus-adenovirus receptor abolishes Coxsackievirus B3 infection and prevents myocarditis in vivo. Journal of the American College of Cardiology *53*, 1219–1226.

Shieh, J.T.C., Bergelson, J.M. (2002). Interaction with decay-accelerating factor facilitates Coxsackievirus B infection of polarized epithelial cells. Journal of Virology *76*, 9474–9480.

Shihab, H.A., Gough, J., Cooper, D.N., Stenson, P.D., Barker, G.L.A., Edwards, K.J., Day, I.N.M., Gaunt, T.R. (2013). Predicting the functional, molecular, and phenotypic consequences of amino acid substitutions using hidden Markov models. Human Mutation *34*, 57–65.

Siller-López, F., García-Bañuelos, J., Hasty, K.A., Segura, J., Ramos-Márquez, M., Qoronfleh, M.W., Aguilar-Cordova, E., Armendáriz-Borunda, J. (2000). Truncated active matrix metalloproteinase-8 gene expression in HepG2 cells is active against native type I collagen. Journal of Hepatology *33*, 758–763.

Singh, R.J.R., Mason, J.C., Lidington, E.A., Edwards, D.R., Nuttall, R.K., Khokha, R., Knauper, V., Murphy, G., Gavrilovic, J. (2005). Cytokine stimulated vascular cell adhesion molecule-1 (VCAM-1) ectodomain release is regulated by TIMP-3. Cardiovascular Research *67*, 39–49.

Sinnreich, M., Shaw, C.A., Pari, G., Nalbantoglu, J., Holland, P.C., Karpati, G. (2005). Localization of Coxsackie virus and adenovirus receptor (CAR) in normal and regenerating human muscle. Neuromuscular Disorders *15*, 541–548.

Smith, J.G., Nemerow, G.R. (2008). Mechanism of adenovirus neutralization by human alpha-defensins. Cell Host & Microbe *3*, 11–19.

Sollerbrant, K., Raschperger, E., Mirza, M., Engström, U., Philipson, L., Ljungdahl, P.O., Pettersson, R.F. (2003). The Coxsackievirus and adenovirus receptor (CAR) forms a complex with the PDZ domain-containing protein Ligand-of-Numb protein-X (LNX). Journal of Biological Chemistry *278*, 7439–7444.

Soudais, C., Boutin, S., Hong, S.S., Chillon, M., Danos, O., Bergelson, J.M., Boulanger, P., Kremer, E.J. (2000). Canine adenovirus type 2 attachment and internalisation: Coxsackievirus-adenovirus receptor, alternative receptors, and an RGD-independent pathway. Journal of Virology *74*, 10639–10649.

Stecker, K., Koschel, A., Wiedenmann, B., Anders, M. (2009). Loss of Coxsackie and adenovirus receptor downregulates α-catenin expression. British Journal of Cancer *101*, 1574–1579.

Stecker, K., Vieth, M., Koschel, A., Wiedenmann, B., Röcken, C., Anders, M. (2011). Impact of the Coxsackievirus and adenovirus receptor on the adenoma–carcinoma sequence of colon cancer. British Journal of Cancer *104*, 1426–1433.

Stein, E.A., Pinkert, S., Becher, P.M., Geisler, A., Zeichhardt, H., Klopfleisch, R., Poller, W., Tschöpe, C., Lassner, D., Fechner, H., et al. (2015). Combination of RNA interference and virus receptor trap exerts additive antiviral activity in Coxsackievirus B3-induced myocarditis in mice. The Journal of Infectious Diseases *211*, 613–622.

Su, L., Fu, L., Li, X., Zhang, Y., Li, Z., Wu, X., Li, Y., Bai, X., Hu, D. (2016). Loss of CAR promotes migration and proliferation of HaCaT cells, and accelerates wound healing in rats via Src-p38 MAPK pathway. Scientific Reports *6*, 1–13.

Sun, F., Li, Y., Jia, T., Ling, Y., Liang, L., Liu, G., Chen, H., Chen, S. (2012). Differential expression of Coxsackievirus and adenovirus receptor on alveolar epithelial cells between fetal and adult mice determines their different susceptibility to Coxsackievirus B infection. Archives of Virology *157*, 1101–1111.

Suzu, S., Hayashi, Y., Harumi, T., Nomaguchi, K., Yamada, M., Hayasawa, H., Motoyoshi, K. (2002). Molecular cloning of a novel immunoglobulin superfamily gene preferentially expressed by brain and testis. Biochemical and Biophysical Research Communications *296*, 1215–1221.

Tallone, T., Malin, S., Samuelsson, A., Wilbertz, J., Miyahara, M., Okamoto, K., Poellinger, L., Philipson, L., Pettersson, S. (2001). A mouse model for adenovirus gene delivery. Proceedings of the National Academy of Sciences *98*, 7910–7915.

Tamamura, H., Otaka, A., Murakami, T., Ishihara, T., Ibuka, T., Waki, M., Matsumoto, A., Yamamoto, N., Fujii, N. (1996). Interaction of an anti-HIV peptide, T22, with gp120 and CD4. Biochemical and Biophysical Research Communications *219*, 555–559.

Tamanini, A., Nicolis, E., Bonizzato, A., Bezzerri, V., Melotti, P., Assael, B.M., Cabrini, G. (2006). Interaction of adenovirus type 5 fiber with the Coxsackievirus and adenovirus receptor activates inflammatory response in human respiratory cells. Journal of Virology *80*, 11241–11254.

Tan, P.K., Bergelson, J.M., Michou, A.-I., Cotton, M. (2001). Defining CAR as a cellular receptor for the avian adenovirus CELO using a genetic analysis of the two viral fibre proteins. Journal of General Virology *82*, 1465–1472.

Tartier, L., McCarey, Y.L., Biaglow, J.E., Kochevar, I.E., Held, K.D. (2000). Apoptosis induced by dithiothreitol in HL-60 cells shows early activation of caspase 3 and is independent of mitochondria. Cell Death & Differentiation *7*, 1002–1010.

Tatrai, E., Bedi, K., Kovalszky, I., Hartyanszky, I., Laszik, A., Acsady, G., Sotonyi, P., Hubay, M. (2011). No mutation but high mRNA expression of Coxsackie-adenovirus receptor was observed in both dilated and ischemic cardiomyopathy. Forensic Science International *212*, 216–222.

Thoelen, I., Keyaerts, E., Lindberg, M., van Ranst, M. (2001a). Characterization of a cDNA encoding the bovine Coxsackie and adenovirus receptor. Biochemical and Biophysical Research Communications *288*, 805–808.

Thoelen, I., Magnusson, C., Tågerud, S., Polacek, C., Lindberg, M., van Ranst, M. (2001b). Identification of alternative splice products encoded by the human Coxsackie-adenovirus receptor gene. Biochemical and Biophysical Research Communications *287*, 216–222.

Thoelen, I., Duson, G., Wollants, E., van Rast, M. (2002). Analysis of genetic heterogeneity in the HCAR adenovirus-binding Ig1 domain in a Caucasian Flemish population. BMC Genetics *3*, 1–3.

Toivonen, R., Mäyränpää, M.I., Kovanen, P.T., Savontaus, M. (2010). Dilated cardiomyopathy alters the expression patterns of CAR and other adenoviral receptors in human heart. Histochemistry and Cell Biology *133*, 349–357.

Tomko, R.P., Xu, R., Philipson, L. (1997). HCAR and MCAR: The human and mouse cellular receptors for subgroup C adenoviruses and group B Coxsackieviruses. Proceedings of the National Academy of Sciences *94*, 3352–3356.

Tomko, R.P., Johansson, C.B., Totrov, M., Abagyan, R., Frisén, J., Philipson, L. (2000). Expression of the adenovirus receptor and its interaction with the fiber knob. Experimental Cell Research *255*, 47–55.

Unal, E.B., Gursoy, A., Erman, B. (2010). VitAL: Viterbi Algorithm for de novo peptide design. PLoS ONE *5*, e10926.

Venkatraman, G., Behrens, M., Pyrski, M., Margolis, F.L. (2005). Expression of Coxsackie-adenovirus receptor (CAR) in the developing mouse olfactory system. Journal of Neurocytology *34*, 295–305.

Verdino, P., Witherden, D.A., Havran, W.L., Wilson, I.A. (2010). The molecular interaction of CAR and JAML recruits the central cell signal transducer PI3K. Science *329*, 1210–1214.

Vincent, T., Pettersson, R.F., Crystal, R.G., Leopold, P.L. (2004). Cytokine-mediated downregulation of Coxsackievirus-adenovirus receptor in endothelial cells. Journal of Virology *78*, 8047–8058.

Vincent, T., Neve, E.P.A., Johnson, J.R., Kukalev, A., Rojo, F., Albanell, J., Pietras, K., Virtanen, I., Philipson, L., Leopold, P.L., et al. (2009). A SNAIL1–SMAD3/4 transcriptional repressor complex promotes TGF-β mediated epithelial–mesenchymal transition. Nature Cell Biology *11*, 943–950.

Walters, R.W., Grunst, T., Bergelson, J.M., Finberg, R.W., Welsh, M.J., Zabner, J. (1999). Basolateral localization of fiber receptors limits adenovirus infection from the apical surface of airway epithelia. Journal of Biological Chemistry *274*, 10219–10226.

Walters, R.W., van't Hof, W., Yi, S.M.P., Schroth, M.K., Zabner, J., Crystal, R.G., Welsh, M.J. (2001). Apical localization of the Coxsackie-adenovirus receptor by glycosyl-phosphatidylinositol modification is sufficient for adenovirus-mediated gene transfer through the apical surface of human airway epithelia. Journal of Virology *75*, 7703–7711.

Walters, R.W., Freimuth, P., Moninger, T.O., Ganske, I., Zabner, J., Welsh, M.J. (2002). Adenovirus fiber disrupts CAR-mediated intercellular adhesion allowing virus escape. Cell *110*, 789–799.

Wan, Y.Y., Leon, R.P., Marks, R., Cham, C.M., Schaack, J., Gajewski, T.F., DeGregori, J. (2000). Transgenic expression of the Coxsackie/adenovirus receptor enables adenoviral-mediated gene delivery in naive T cells. Proceedings of the National Academy of Sciences USA *97*, 13784–13789.

Wang, X., Bergelson, J.M. (1999). Coxsackievirus and adenovirus receptor cytoplasmic and transmembrane domains are not essential for Coxsackievirus and adenovirus infection. Journal of Virology *73*, 2559–2562.

Wang, W., Cole, A.M., Hong, T., Waring, A.J., Lehrer, R.I. (2003). Retrocyclin, an antiretroviral theta-defensin, is a lectin. Journal of Immunology (Baltimore, Md.: 1950) *170*, 4708–4716.

Weber, D.A., Sumagin, R., McCall, I.C., Leoni, G., Neumann, P.A., Andargachew, R., Brazil, J.C., Medina-Contreras, O., Denning, T.L., Nusrat, A., et al. (2014). Neutrophil-derived JAML inhibits repair of intestinal epithelial injury during acute inflammation. Mucosal Immunology *7*, 1221–1232.

Werner, B., Dittmann, S., Funke, C., Überla, K., Piper, C., Niehaus, K., Horstkotte, D., Farr, M. (2014). Effect of lovastatin on Coxsackievirus B3 infection in human endothelial cells. Inflammation Research *63*, 267–276.

Westlin, W.F., Gimbrone, M.A. (1993). Neutrophil-mediated damage to human vascular endothelium. Role of cytokine activation. The American Journal of Pathology *142*, 117–128.

Whiteman, S.C., Bianco, A., Knight, R.A., Spiteri, M.A. (2003). Human rhinovirus selectively modulates membranous and soluble forms of its intercellular adhesion molecule–1 (ICAM-1) receptor to promote epithelial cell infectivity. Journal of Biological Chemistry *278*, 11954–11961.

Wickham, T.J., Mathias, P., Cheresh, D.A., Nemerow, G.R. (1993). Integrins αvβ3 and αvβ5 promote adenovirus internalization but not virus attachment. Cell *73*, 309–319.

Wiesner, O., Litwiller, R.D., Hummel, A.M., Viss, M.A., McDonald, C.J., Jenne, D.E., Fass, D.N., Specks, U. (2005). Differences between human proteinase 3 and neutrophil elastase and their murine homologues are relevant for murine model experiments. FEBS Letters *579*, 5305–5312.

Winther, B., Arruda, E., Witek, T.J., Marlin, S.D., Tsianco, M.M., Innes, D.J., Hayden, F.G. (2002). Expression of ICAM-1 in nasal epithelium and levels of soluble ICAM-1 in nasal lavage fluid during human experimental rhinovirus infection. Archives of Otolaryngology–Head & Neck Surgery *128*, 131–136.

Witherden, D.A., Verdino, P., Rieder, S.E., Garijo, O., Mills, R.E., Teyton, L., Fischer, W.H., Wilson, I.A., Havran, W.L. (2010). The junctional adhesion molecule JAML is a costimulatory receptor for epithelial T cell activation. Science *329*, 1205–1210.

Wright, H.L., Moots, R.J., Bucknall, R.C., Edwards, S.W. (2010). Neutrophil function in inflammation and inflammatory diseases. Rheumatology *49*, 1618–1631.

Yanagawa, B., Spiller, O.B., Proctor, D.G., Choy, J., Luo, H., Zhang, H.M., Suarez, A., Yang, D., McManus, B.M. (2004). Soluble recombinant Coxsackievirus and adenovirus receptor abrogates Coxsackievirus B3–mediated pancreatitis and myocarditis in mice. Journal of Infectious Diseases *189*, 1431–1439.

Yang, M., Wu, Z., Fields, S. (1995). Protein-peptide interactions analyzed with the yeast two-hybrid system. Nucleic Acids Research *23*, 1152–1156.

Yasin, B., Wang, W., Pang, M., Cheshenko, N., Hong, T., Waring, A.J., Herold, B.C., Wagar, E.A., Lehrer, R.I. (2004). Theta defensins protect cells from infection by herpes simplex virus by inhibiting viral adhesion and entry. Journal of Virology *78*, 5147–5156.

Yin, P., Zhang, Ling, Ye, F., Deng, Y., Lu, S., Li, Y.-P., Zhang, Leiliang, Tan, W. (2017). A screen for inhibitory peptides of hepatitis C virus identifies a novel entry inhibitor targeting E1 and E2. Scientific Reports *7*, 1–10.

You, Z., Fischer, D.C., Tong, X., Hasenburg, A., Aguilar-Cordova, E., Kieback, D.G. (2001). Coxsackievirus–adenovirus receptor expression in ovarian cancer cell lines is associated with increased adenovirus transduction efficiency and transgene expression. Cancer Gene Therapy *8*, 168–175.

Yuen, S., Smith, J., Caruso, L., Balan, M., Opavsky, M.A. (2011). The Coxsackie–adenovirus receptor induces an inflammatory cardiomyopathy independent of viral infection. Journal of Molecular and Cellular Cardiology *50*, 826–840.

Zabner, J., Freimuth, P., Puga, A., Fabrega, A., Welsh, M.J. (1997). Lack of high affinity fiber receptor activity explains the resistance of ciliated airway epithelia to adenovirus infection. Journal of Clinical Investigation *100*, 1144–1149.

Zabner, J., Winter, M., Excoffon, K.J.D.A., Stoltz, D., Ries, D., Shasby, S., Shasby, M. (2003). Histamine alters E-cadherin cell adhesion to increase human airway epithelial permeability. Journal of Applied Physiology *95*, 394–401.

Zaidi, S.H., Hui, C.C., Cheah, A.Y., You, X.M., Husain, M., Rabinovitch, M. (1999). Targeted overexpression of elafin protects mice against cardiac dysfunction and mortality following viral myocarditis. The Journal of Clinical Investigation *103*, 1211–1219.

Zajac, I., Crowell, R.L. (1965). Effect of enzymes on the interaction of enteroviruses with living HeLa cells. Journal of Bacteriology *89*, 574–582.

Zen, K., Liu, Y., McCall, I., Wu, T., Lee, W., Babbin, B., Nusrat, A., Parkos, C. (2005). Neutrophil migration across tight junctions is mediated by adhesive interactions between epithelial Coxsackie and adenovirus receptor and a junctional adhesion molecule-like protein on neutrophils. Molecular Biology of the Cell *16*, 2694–2703.

Zhang, Y., Bergelson, J.M. (2005). Adenovirus receptors. Journal of Virology *79*, 12125–12131.

Zhang, K., Yu, H., Xie, W., Xu, Z., Zhou, S., Huang, C., Sheng, H., He, X., Xiong, J., Qian, G. (2013). Expression of Coxsackievirus and adenovirus receptor (CAR)-Fc fusion protein in Pichia pastoris and characterization of its anti-Coxsackievirus activity. Journal of Biotechnology *164*, 461–468.

Zhou, P., Wu, E., Alam, H.B., Li, Y. (2014). Histone cleavage as a mechanism for epigenetic regulation: Current insights and perspectives. Current Molecular Medicine *14*, 1164–1172.

Zussy, C., Loustalot, F., Junyent, F., Gardoni, F., Bories, C., Valero, J., Desarmenien, M.G., Bernex, F., Henaff, D., Bayo-Puxan, N., et al. (2016). Coxsackievirus adenovirus receptor loss impairs adult neurogenesis, synapse content, and hippocampus plasticity. Journal of Neuroscience *36*, 9558–9571.

APPENDIX

1 General

CAR immature protein sequence comprises a signal sequence, two extracellular domains, a transmembrane domain, and a cytoplasmic tail.

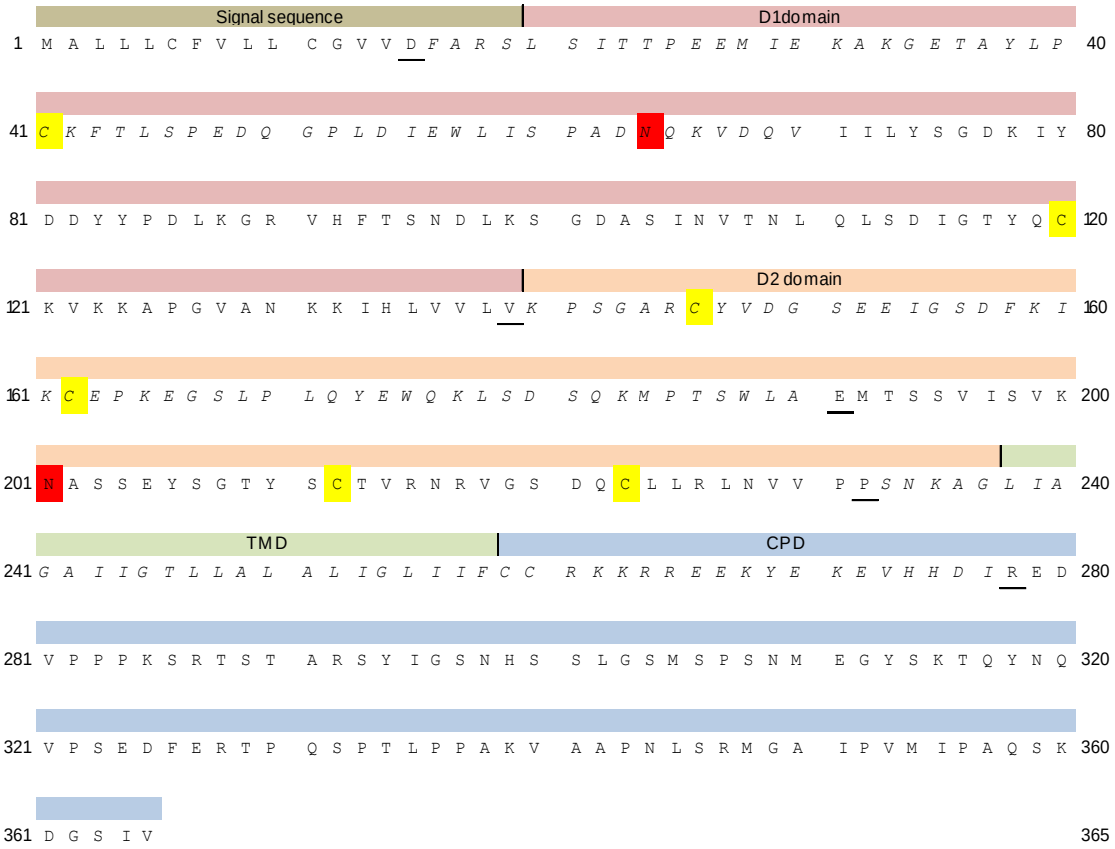

Figure 1: Human CAR amino acid sequence (Uniprot P78310). CAR comprises a signal sequence, an extracellular domain (D1 and D2 Ig-domains), a transmembrane (TMD), and a cytoplasmic domain (CPD). Cysteines involved in disulfide bond formation are marked in yellow and glycosylated asparagines are coloured in red. Alternating exons are italicised and residues that overlap splice sites are underlined.

Coxsackieviruses bind several motifs in CAR ECD.

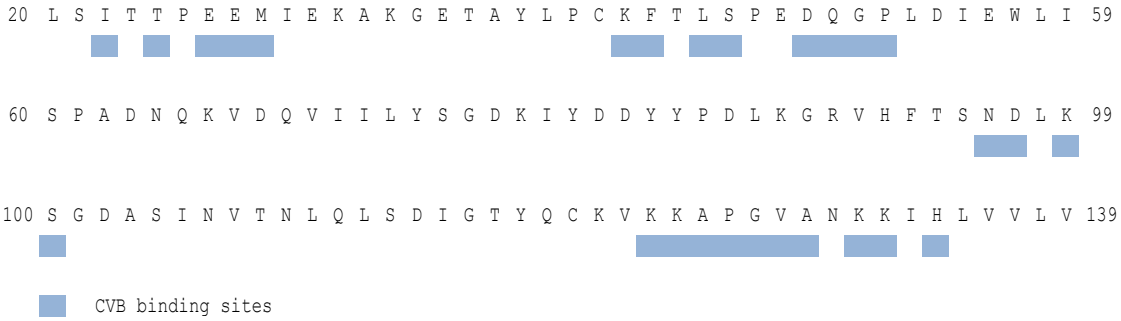

Figure 2: CAR ECD sequence with CVB3 binding sites. Part of CAR ECD (amino acids 20 to 140; UniProt accession number P78310) is depicted with coloured amino acids important for CAR-CVB3 interaction (HE ET AL. 2001).

2 CAR genetic variants

CAR total protein levels and surface protein levels differed significantly among CHO cell lines expressing CAR variants and CAR WT. Total protein and surface protein levels of each cell line corresponded.

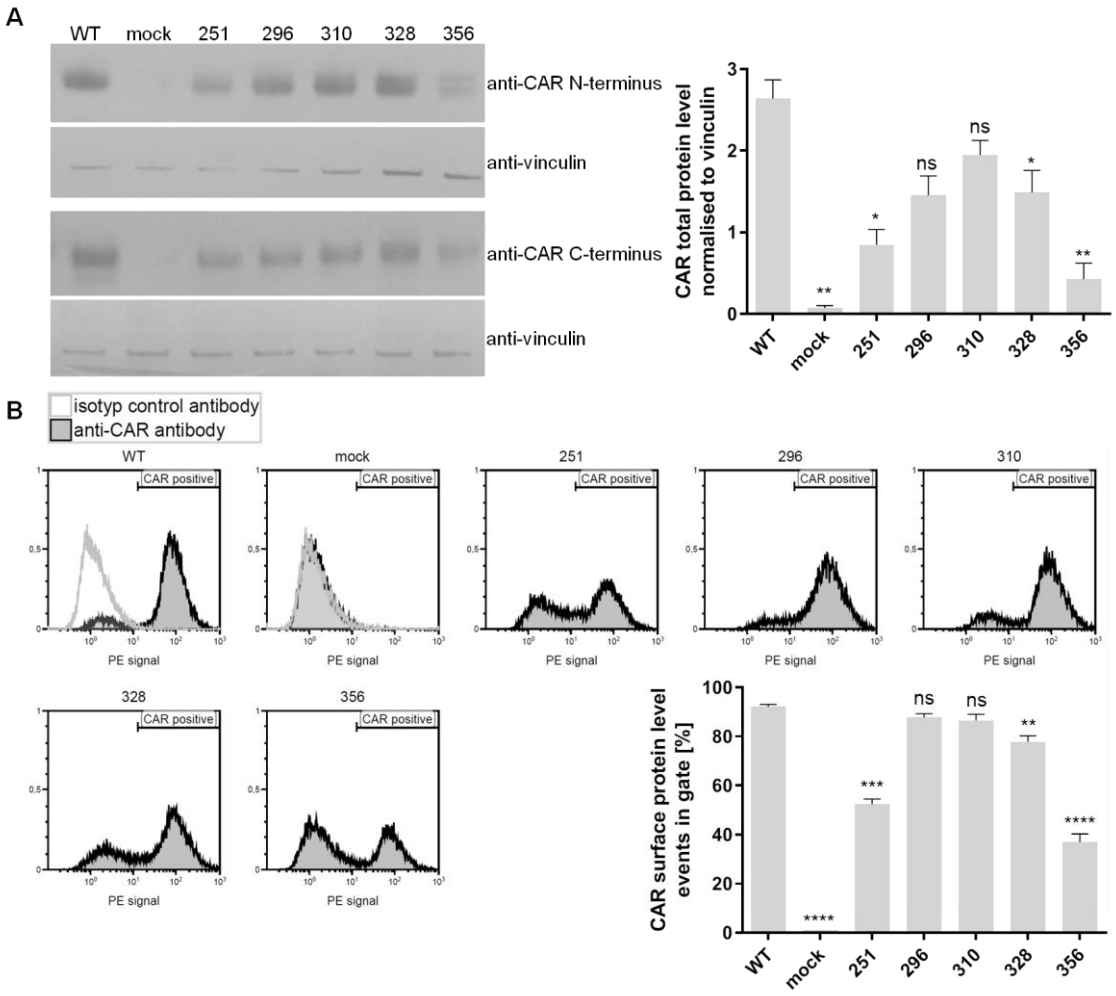

Figure 3: CAR protein expression levels in polyclonal CHO-CAR and CHO mock cells. A) CAR total protein expression levels determined by Western blot. Cells were lysed at two different time points and lysates were blotted with antibodies against CAR´s N- or C-terminus. Representative blots are shown. CAR signals were normalised to vinculin signals. Bars show mean±SEM. Except CAR 296 and CAR 310, all variants were expressed at significantly lower levels as CAR WT (ANOVA with multiple comparisons). B) CAR surface expression levels determined by flow cytometry. Cells were stained with anti-CAR antibody and 10000 events were recorded at six different days. The CAR-positive gate was set to include 1 % false positive events for mock cells. CAR WT and mock cells were stained with isotype control antibody as controls. Representative histograms are shown. The number of CAR-positive events was normalised to CHO-CAR WT cells. Bars show mean±SEM. All variants were expressed at significantly lower levels as CAR WT, except CAR 296 and CAR 310 (ANOVA with multiple comparisons).

Polyclonal CHO-CAR cells were sorted by flow cytometry. Afterwards, the cell lines expressed uniform CAR levels.

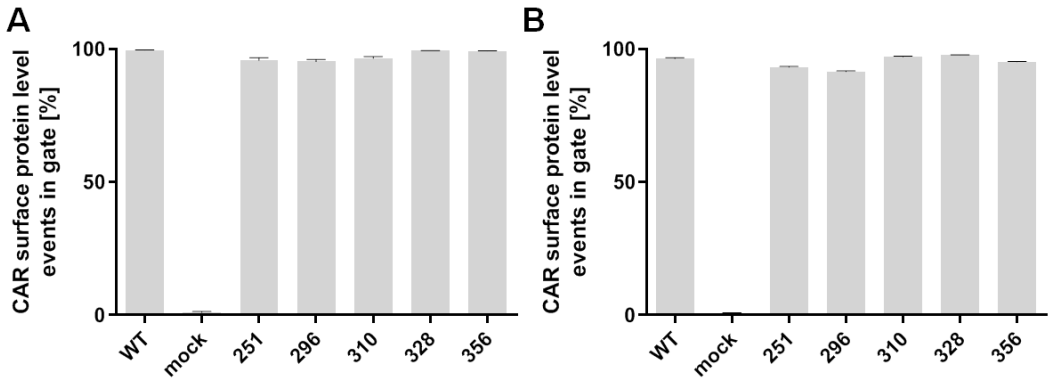

Figure 4: CAR surface expression levels in polyclonal CHO-CAR and CHO mock cells after sorting. A) Subculture of cells, which was transduced with adenovectors. B) Subculture of cells, which was infected with coxsackieviruses B3. CAR was stained with antibody E1-1 PE and each cell line was measured in triplicate. The number of CAR-positive events was normalised to CHO-CAR WT cells. Bars show mean±SEM. Differences in CAR surface expression levels were still significant (ANOVA with multiple comparisons), but not as striking as before sorting: Subculture for Ad5-GFP transduction - mock ****, 251 ****, 296 ****, 310 ns, 328 **, 356 **. Subculture for CVB3 infection - mock ****, 251 **, 296 ***, 310 **, 328 ns, 356 ns.

3 Peptides for virus entry inhibition

For CAR homodimer and Ad12 knob-CAR D1 interactions, buried surface area scores were determined with PISA. CAR homodimer can form in an antiparallel and a parallel manner. Ad12 knob-CAR interaction is characterised by two interfaces. Amino acid motifs involved in protein-protein interactions are coloured.

Table 1: PISA buried surface area scores for CAR D1 antiparallel homodimerisation (PDB ID: 1EAJ).

CAR b	score	CAR a	score
		A:PHE 16	0
		A:ALA 17	0
		A:ARG 18	0
		A:SER 19	1
B:LEU 20	0	A:LEU 20	0
B:SER 21	0	A:SER 21	0
B:ILE 22	0	A:ILE 22	0
B:THR 23	0	A:THR 23	0
B:THR 24	0	A:THR 24	0
B:PRO 25	0	A:PRO 25	0
B:GLU 26	0	A:GLU 26	0
B:GLU 27	0	A:GLU 27	0
B:MET 28	0	A:MET 28	0
B:ILE 29	0	A:ILE 29	0
B:GLU 30	0	A:GLU 30	0
B:LYS 31	0	A:LYS 31	0
B:ALA 32	0	A:ALA 32	0
B:LYS 33	0	A:LYS 33	0
B:GLY 34	0	A:GLY 34	0
B:GLU 35	0	A:GLU 35	0
B:THR 36	0	A:THR 36	0
B:ALA 37	0	A:ALA 37	0
B:TYR 38	0	A:TYR 38	0
B:LEU 39	0	A:LEU 39	0
B:PRO 40	0	A:PRO 40	0
B:CYS 41	0	A:CYS 41	0
B:LYS 42	0	A:LYS 42	0
B:PHE 43	0	A:PHE 43	0
B:THR 44	0	A:THR 44	0
B:LEU 45	0	A:LEU 45	0
B:SER 46	0	A:SER 46	0
B:PRO 47	0	A:PRO 47	0
B:GLU 48	3	A:GLU 48	3
B:ASP 49	1	A:ASP 49	1
B:GLN 50	1	A:GLN 50	1
B:GLY 51	4	A:GLY 51	4
B:PRO 52	6	A:PRO 52	6
B:LEU 53	0	A:LEU 53	0
B:ASP 54	8	A:ASP 54	9
B:ILE 55	0	A:ILE 55	0
B:GLU 56	6	A:GLU 56	6
B:TRP 57	0	A:TRP 57	0
B:LEU 58	1	A:LEU 58	1
B:ILE 59	0	A:ILE 59	0
B:SER 60	0	A:SER 60	0
B:PRO 61	0	A:PRO 61	0
B:ALA 62	0	A:ALA 62	0
B:ASP 63	0	A:ASP 63	0
B:ASN 64	0	A:ASN 64	0
B:GLN 65	0	A:GLN 65	0
B:LYS 66	0	A:LYS 66	0
B:VAL 67	0	A:VAL 67	0
B:ASP 68	0	A:ASP 68	1
B:GLN 69	0	A:GLN 69	0
B:VAL 70	5	A:VAL 70	6
B:ILE 71	0	A:ILE 71	0
B:ILE 72	0	A:ILE 72	0
B:LEU 73	10	A:LEU 73	10
B:TYR 74	0	A:TYR 74	0
B:SER 75	9	A:SER 75	10
B:GLY 76	5	A:GLY 76	5
B:ASP 77	0	A:ASP 77	0
B:LYS 78	0	A:LYS 78	0
B:ILE 79	0	A:ILE 79	0
B:TYR 80	6	A:TYR 80	6
B:ASP 81	0	A:ASP 81	0
B:ASP 82	0	A:ASP 82	0
B:TYR 83	4	A:TYR 83	4
B:TYR 84	7	A:TYR 84	7
B:PRO 85	0	A:PRO 85	0
B:ASP 86	0	A:ASP 86	0
B:LEU 87	0	A:LEU 87	0
B:LYS 88	0	A:LYS 88	0
B:GLY 89	0	A:GLY 89	0
B:ARG 90	0	A:ARG 90	0
B:VAL 91	0	A:VAL 91	0
B:HIS 92	0	A:HIS 92	0
B:PHE 93	0	A:PHE 93	0
B:THR 94	0	A:THR 94	0
B:SER 95	0	A:SER 95	0
B:ASN 96	0	A:ASN 96	0
B:ASP 97	0	A:ASP 97	0
B:LEU 98	0	A:LEU 98	0
B:LYS 99	0	A:LYS 99	0
B:SER 100	0	A:SER 100	0
B:GLY 101	0	A:GLY 101	0
B:ASP 102	0	A:ASP 102	0
B:ALA 103	0	A:ALA 103	0
B:SER 104	0	A:SER 104	0
B:ILE 105	0	A:ILE 105	0
B:ASN 106	0	A:ASN 106	0
B:VAL 107	0	A:VAL 107	0
B:THR 108	0	A:THR 108	0
B:ASN 109	0	A:ASN 109	0
B:LEU 110	0	A:LEU 110	0
B:GLN 111	0	A:GLN 111	0
B:LEU 112	0	A:LEU 112	0
B:SER 113	0	A:SER 113	0
B:ASP 114	0	A:ASP 114	0
B:ILE 115	0	A:ILE 115	0
B:GLY 116	0	A:GLY 116	0
B:THR 117	0	A:THR 117	0
B:TYR 118	0	A:TYR 118	0
B:GLN 119	0	A:GLN 119	0
B:CYS 120	0	A:CYS 120	0
B:LYS 121	4	A:LYS 121	4
B:VAL 122	0	A:VAL 122	0
B:LYS 123	8	A:LYS 123	8
B:LYS 124	0	A:LYS 124	0
B:ALA 125	10	A:ALA 125	10
B:PRO 126	10	A:PRO 126	9
B:GLY 127	5	A:GLY 127	4
B:VAL 128	5	A:VAL 128	5
B:ALA 129	0	A:ALA 129	0
B:ASN 130	0	A:ASN 130	0
B:LYS 131	0	A:LYS 131	0
B:LYS 132	0	A:LYS 132	0
B:ILE 133	0	A:ILE 133	0
B:HIS 134	0	A:HIS 134	0
B:LEU 135	0	A:LEU 135	0
B:VAL 136	0	A:VAL 136	0
B:VAL 137	0	A:VAL 137	0
B:LEU 138	0	A:LEU 138	0
B:VAL 139	0	A:VAL 139	0

Table 2: PISA buried surface area scores for CAR D1 parallel homodimerisation (PDB ID: 3JZ7).

CAR b	score	CAR a	score	CAR b	score	CAR a	score	CAR b	score	CAR a	score
A:PRO 25	0	A:PRO 25	0	A:SER 95	0	A:SER 95	0	A:LYS 165	0	A:LYS 165	0
A:GLU 26	0	A:GLU 26	0	A:ASN 96	0	A:ASN 96	0	A:GLU 166	0	A:GLU 166	0
A:GLN 27	0	A:GLN 27	0	A:ASP 97	0	A:ASP 97	0	A:GLY 167	0	A:GLY 167	0
A:ARG 28	0	A:ARG 28	0	A:VAL 98	0	A:VAL 98	0	A:SER 168	0	A:SER 168	0
A:ILE 29	0	A:ILE 29	0	A:LYS 99	0	A:LYS 99	0	A:LEU 169	0	A:LEU 169	0
A:GLU 30	0	A:GLU 30	0	A:SER 100	0	A:SER 100	0	A:PRO 170	0	A:PRO 170	0
A:LYS 31	0	A:LYS 31	0	A:GLY 101	0	A:GLY 101	0	A:LEU 171	0	A:LEU 171	0
A:ALA 32	0	A:ALA 32	0	A:ASP 102	0	A:ASP 102	0	A:GLN 172	0	A:GLN 172	0
A:LYS 33	0	A:LYS 33	0	A:ALA 103	0	A:ALA 103	0	A:PHE 173	0	A:PHE 173	0
A:GLY 34	0	A:GLY 34	0	A:SER 104	0	A:SER 104	0	A:GLU 174	0	A:GLU 174	0
A:GLU 35	0	A:GLU 35	0	A:ILE 105	0	A:ILE 105	0	A:TRP 175	0	A:TRP 175	0
A:THR 36	0	A:THR 36	0	A:ASN 106	0	A:ASN 106	0	A:GLN 176	0	A:GLN 176	0
A:ALA 37	0	A:ALA 37	0	A:VAL 107	0	A:VAL 107	0	A:LYS 177	0	A:LYS 177	0
A:TYR 38	0	A:TYR 38	0	A:THR 108	0	A:THR 108	0	A:LEU 178	0	A:LEU 178	0
A:LEU 39	0	A:LEU 39	0	A:ASN 109	0	A:ASN 109	0	A:SER 179	0	A:SER 179	0
A:PRO 40	0	A:PRO 40	0	A:LEU 110	0	A:LEU 110	0	A:ASP 180	0	A:ASP 180	0
A:CYS 41	0	A:CYS 41	0	A:GLN 111	0	A:GLN 111	0	A:SER 181	0	A:SER 181	0
A:LYS 42	0	A:LYS 42	0	A:LEU 112	0	A:LEU 112	0	A:GLN 182	0	A:GLN 182	0
A:PHE 43	0	A:PHE 43	0	A:SER 113	0	A:SER 113	0	A:THR 183	0	A:THR 183	0
A:THR 44	0	A:THR 44	0	A:ASP 114	0	A:ASP 114	0	A:MET 184	0	A:MET 184	0
A:LEU 45	0	A:LEU 45	0	A:ILE 115	0	A:ILE 115	0	A:PRO 185	0	A:PRO 185	0
A:SER 46	0	A:SER 46	0	A:GLY 116	0	A:GLY 116	0	A:THR 186	0	A:THR 186	0
A:PRO 47	0	A:PRO 47	0	A:THR 117	0	A:THR 117	0	A:PRO 187	0	A:PRO 187	0
A:GLU 48	0	A:GLU 48	0	A:TYR 118	0	A:TYR 118	0	A:TRP 188	0	A:TRP 188	0
A:ASP 49	0	A:ASP 49	0	A:GLN 119	2	A:GLN 119	2	A:LEU 189	0	A:LEU 189	0
A:GLN 50	1	A:GLN 50	1	A:CYS 120	0	A:CYS 120	0	A:ALA 190	0	A:ALA 190	0
A:GLY 51	7	A:GLY 51	7	A:LYS 121	6	A:LYS 121	6	A:GLU 191	0	A:GLU 191	0
A:PRO 52	7	A:PRO 52	7	A:VAL 122	0	A:VAL 122	0	A:MET 192	0	A:MET 192	0
A:LEU 53	0	A:LEU 53	0	A:LYS 123	9	A:LYS 123	9	A:THR 193	0	A:THR 193	0
A:ASP 54	10	A:ASP 54	10	A:LYS 124	0	A:LYS 124	0	A:SER 194	0	A:SER 194	0
A:ILE 55	11	A:ILE 55	11	A:ALA 125	10	A:ALA 125	11	A:PRO 195	0	A:PRO 195	0
A:GLU 56	8	A:GLU 56	8	A:PRO 126	5	A:PRO 126	5	A:VAL 196	0	A:VAL 196	0
A:TRP 57	0	A:TRP 57	0	A:GLY 127	0	A:GLY 127	0	A:ILE 197	0	A:ILE 197	0
A:LEU 58	5	A:LEU 58	4	A:VAL 128	5	A:VAL 128	5	A:SER 198	0	A:SER 198	0
A:ILE 59	0	A:ILE 59	0	A:ALA 129	0	A:ALA 129	0	A:VAL 199	0	A:VAL 199	0
A:SER 60	0	A:SER 60	0	A:ASN 130	1	A:ASN 130	1	A:LYS 200	0	A:LYS 200	0
A:PRO 61	0	A:PRO 61	0	A:LYS 131	0	A:LYS 131	0	A:ASN 201	0	A:ASN 201	0
A:SER 62	0	A:SER 62	0	A:LYS 132	1	A:LYS 132	1	A:ALA 202	0	A:ALA 202	0
A:ASP 63	0	A:ASP 63	0	A:PHE 133	0	A:PHE 133	0	A:SER 203	0	A:SER 203	0
A:ASN 64	0	A:ASN 64	0	A:LEU 134	0	A:LEU 134	0	A:SER 204	0	A:SER 204	0
A:GLN 65	0	A:GLN 65	0	A:LEU 135	0	A:LEU 135	0	A:GLU 205	0	A:GLU 205	0
A:ILE 66	0	A:ILE 66	0	A:THR 136	0	A:THR 136	0	A:TYR 206	0	A:TYR 206	0
A:VAL 67	0	A:VAL 67	0	A:VAL 137	0	A:VAL 137	0	A:SER 207	0	A:SER 207	0
A:ASP 68	2	A:ASP 68	2	A:LEU 138	0	A:LEU 138	0	A:GLY 208	0	A:GLY 208	0
A:GLN 69	0	A:GLN 69	0	A:VAL 139	0	A:VAL 139	0	A:THR 209	0	A:THR 209	0
A:VAL 70	7	A:VAL 70	7	A:LYS 140	0	A:LYS 140	0	A:TYR 210	0	A:TYR 210	0
A:ILE 71	0	A:ILE 71	0	A:PRO 141	0	A:PRO 141	0	A:SER 211	0	A:SER 211	0
A:ILE 72	0	A:ILE 72	0	A:SER 142	0	A:SER 142	0	A:CYS 212	0	A:CYS 212	0
A:LEU 73	10	A:LEU 73	10	A:GLY 143	0	A:GLY 143	0	A:THR 213	0	A:THR 213	0
A:TYR 74	0	A:TYR 74	0	A:THR 144	0	A:THR 144	0	A:VAL 214	0	A:VAL 214	0
A:SER 75	10	A:SER 75	10	A:ARG 145	0	A:ARG 145	0	A:GLN 215	0	A:GLN 215	0
A:GLY 76	5	A:GLY 76	5	A:CYS 146	0	A:CYS 146	0	A:ASN 216	0	A:ASN 216	0
A:ASP 77	0	A:ASP 77	0	A:PHE 147	0	A:PHE 147	0	A:ARG 217	0	A:ARG 217	0
A:LYS 78	0	A:LYS 78	0	A:VAL 148	0	A:VAL 148	0	A:VAL 218	0	A:VAL 218	0
A:ILE 79	0	A:ILE 79	0	A:ASP 149	0	A:ASP 149	0	A:GLY 219	0	A:GLY 219	0
A:TYR 80	6	A:TYR 80	6	A:GLY 150	0	A:GLY 150	0	A:SER 220	0	A:SER 220	0
A:ASP 81	0	A:ASP 81	0	A:SER 151	0	A:SER 151	0	A:ASP 221	0	A:ASP 221	0
A:ASN 82	0	A:ASN 82	0	A:GLU 152	0	A:GLU 152	0	A:GLN 222	0	A:GLN 222	0
A:TYR 83	5	A:TYR 83	5	A:GLU 153	0	A:GLU 153	0	A:CYS 223	0	A:CYS 223	0
A:TYR 84	0	A:TYR 84	0	A:ILE 154	0	A:ILE 154	0	A:MET 224	0	A:MET 224	0
A:PRO 85	0	A:PRO 85	0	A:GLY 155	0	A:GLY 155	0	A:LEU 225	0	A:LEU 225	0
A:ASP 86	0	A:ASP 86	0	A:ASN 156	0	A:ASN 156	0	A:ARG 226	0	A:ARG 226	0
A:LEU 87	0	A:LEU 87	0	A:ASP 157	0	A:ASP 157	0	A:LEU 227	0	A:LEU 227	0
A:LYS 88	0	A:LYS 88	0	A:PHE 158	0	A:PHE 158	0	A:ASP 228	0	A:ASP 228	0
A:GLY 89	0	A:GLY 89	0	A:LYS 159	0	A:LYS 159	0	A:VAL 229	0	A:VAL 229	0
A:ARG 90	0	A:ARG 90	0	A:LEU 160	0	A:LEU 160	0	A:VAL 230	0	A:VAL 230	0
A:VAL 91	0	A:VAL 91	0	A:LYS 161	0	A:LYS 161	0	A:PRO 231	0	A:PRO 231	0
A:HIS 92	0	A:HIS 92	0	A:CYS 162	0	A:CYS 162	0	A:PRO 232	0	A:PRO 232	0
A:PHE 93	0	A:PHE 93	0	A:GLU 163	0	A:GLU 163	0	A:SER 233	0	A:SER 233	0
A:THR 94	0	A:THR 94	0	A:PRO 164	0	A:PRO 164	0				

Table 3: PISA buried surface area scores for CAR D1-Ad12 knob binding interface 1 (PDB ID: 1KAC).

CAR	score	Ad12	score
B:GLY 23	0	A:THR 403	0
B:ILE 24	0	A:PRO 404	0
B:THR 25	0	A:TYR 405	0
B:THR 26	0	A:ASP 406	0
B:PRO 27	0	A:PRO 407	0
B:GLU 28	0	A:LEU 408	0
B:GLU 29	0	A:THR 409	0
B:MET 30	0	A:LEU 410	0
B:ILE 31	0	A:TRP 411	0
B:GLU 32	0	A:THR 412	0
B:LYS 33	0	A:THR 413	4
B:ALA 34	0	A:PRO 414	0
B:LYS 35	0	A:ASP 415	6
B:GLY 36	0	A:PRO 416	2
B:GLU 37	0	A:PRO 417	9
B:THR 38	0	A:PRO 418	10
B:ALA 39	0	A:ASN 419	0
B:TYR 40	0	A:CYS 420	0
B:LEU 41	0	A:SER 421	0
B:PRO 42	0	A:LEU 422	0
B:CYS 43	0	A:ILE 423	0
B:LYS 44	0	A:GLN 424	0
B:PHE 45	0	A:GLU 425	2
B:THR 46	0	A:LEU 426	10
B:LEU 47	0	A:ASP 427	0
B:SER 48	0	A:ALA 428	0
B:PRO 49	0	A:LYS 429	7
B:GLU 50	1	A:LEU 430	0
B:ASP 51	0	A:THR 431	0
B:GLN 52	2	A:LEU 432	0
B:GLY 53	6	A:CYS 433	0
B:PRO 54	4	A:LEU 434	0
B:LEU 55	0	A:THR 435	0
B:ASP 56	7	A:LYS 436	0
B:ILE 57	0	A:ASN 437	0
B:GLU 58	10	A:GLY 438	0
B:TRP 59	0	A:SER 439	0
B:LEU 60	7	A:ILE 440	0
B:ILE 61	0	A:VAL 441	0
B:SER 62	0	A:ASN 442	0
B:PRO 63	0	A:GLY 443	0
B:ALA 64	0	A:ILE 444	0
B:ASP 65	0	A:VAL 445	0
B:ASN 66	0	A:SER 446	0
B:GLN 67	0	A:LEU 447	0
B:LYS 68	0	A:VAL 448	0
B:VAL 69	0	A:GLY 449	0
B:ASP 70	1	A:VAL 450	7
B:GLN 71	1	A:LYS 451	8
B:VAL 72	9	A:GLY 452	0
B:ILE 73	0	A:ASN 453	0
B:ILE 74	0	A:LEU 454	0
B:LEU 75	10	A:LEU 455	2
B:TYR 76	0	A:ASN 456	0
B:SER 77	9	A:ILE 457	0
B:GLY 78	5	A:GLN 458	0
B:ASP 79	0	A:SER 459	0
B:LYS 80	0	A:THR 460	0
B:ILE 81	0	A:THR 461	0
B:TYR 82	7	A:THR 462	0
B:ASP 83	2	A:THR 463	0
B:ASP 84	2	A:VAL 464	0
B:TYR 85	9	A:GLY 465	0
B:TYR 86	0	A:VAL 466	0
B:PRO 87	1	A:HIS 467	0
B:ASP 88	0	A:LEU 468	0

CAR	score	Ad12	score
B:LEU 89	0	A:VAL 469	0
B:LYS 90	0	A:PHE 470	0
B:GLY 91	0	A:ASP 471	0
B:ARG 92	0	A:GLU 472	0
B:VAL 93	0	A:GLN 473	0
B:HIS 94	0	A:GLY 474	0
B:PHE 95	0	A:ARG 475	0
B:THR 96	0	A:LEU 476	0
B:SER 97	0	A:ILE 477	0
B:ASN 98	0	A:THR 478	0
B:ASP 99	0	A:SER 479	0
B:LEU 100	0	A:THR 480	0
B:LYS 101	0	A:PRO 481	0
B:SER 102	0	A:THR 482	0
B:GLY 103	0	A:ALA 483	0
B:ASP 104	0	A:LEU 484	0
B:ALA 105	0	A:VAL 485	1
B:SER 106	0	A:PRO 486	0
B:ILE 107	0	A:GLN 487	8
B:ASN 108	0	A:ALA 488	1
B:VAL 109	0	A:SER 489	3
B:THR 110	0	A:TRP 490	0
B:ASN 111	0	A:GLY 491	0
B:LEU 112	0	A:TYR 492	0
B:GLN 113	0	A:ARG 493	0
B:LEU 114	0	A:GLN 494	5
B:SER 115	0	A:GLY 495	0
B:ASP 116	0	A:GLN 496	2
B:ILE 117	0	A:SER 497	9
B:GLY 118	0	A:VAL 498	8
B:THR 119	0	A:SER 499	3
B:TYR 120	0	A:THR 500	6
B:GLN 121	0	A:ASN 501	0
B:CYS 122	0	A:THR 502	0
B:LYS 123	6	A:VAL 503	0
B:VAL 124	0	A:THR 504	0
B:LYS 125	7	A:ASN 505	0
B:LYS 126	0	A:GLY 506	0
B:ALA 127	8	A:LEU 507	0
B:PRO 128	8	A:GLY 508	0
B:GLY 129	1	A:PHE 509	0
B:VAL 130	4	A:MET 510	0
B:ALA 131	0	A:PRO 511	0
B:ASN 132	0	A:ASN 512	0
B:LYS 133	0	A:VAL 513	0
B:LYS 134	0	A:SER 514	0
B:ILE 135	0	A:ALA 515	0
B:HIS 136	0	A:TYR 516	0
B:LEU 137	0	A:PRO 517	0
B:VAL 138	0	A:ARG 518	0
B:VAL 139	0	A:PRO 519	0
B:LEU 140	0	A:ASN 520	0
B:VAL 141	0	A:ALA 521	0
B:LYS 142	0	A:SER 522	0
B:PRO 143	0	A:GLU 523	0
B:SER 144	0	A:ALA 524	0
B:GLY 145	0	A:LYS 525	0
B:ALA 146	0	A:SER 526	0
		A:GLN 527	0
		A:MET 528	0
		A:VAL 529	0
		A:SER 530	0
		A:LEU 531	0
		A:THR 532	0
		A:TYR 533	0
		A:LEU 534	0

Table 4: PISA buried surface area scores for CAR D1-Ad12 knob binding interface 2 (PDB ID: 1KAC).

CAR	score	Ad12	score
B:GLY 23	0	A:THR 403	0
B:ILE 24	0	A:PRO 404	0
B:THR 25	0	A:TYR 405	0
B:THR 26	0	A:ASP 406	0
B:PRO 27	0	A:PRO 407	0
B:GLU 28	0	A:LEU 408	0
B:GLU 29	0	A:THR 409	0
B:MET 30	0	A:LEU 410	0
B:ILE 31	0	A:TRP 411	0
B:GLU 32	0	A:THR 412	0
B:LYS 33	0	A:THR 413	0
B:ALA 34	0	A:PRO 414	0
B:LYS 35	0	A:ASP 415	0
B:GLY 36	0	A:PRO 416	0
B:GLU 37	0	A:PRO 417	0
B:THR 38	0	A:PRO 418	0
B:ALA 39	0	A:ASN 419	0
B:TYR 40	0	A:CYS 420	0
B:LEU 41	0	A:SER 421	0
B:PRO 42	0	A:LEU 422	0
B:CYS 43	0	A:ILE 423	0
B:LYS 44	0	A:GLN 424	0
B:PHE 45	0	A:GLU 425	0
B:THR 46	0	A:LEU 426	0
B:LEU 47	0	A:ASP 427	0
B:SER 48	0	A:ALA 428	0
B:PRO 49	0	A:LYS 429	0
B:GLU 50	0	A:LEU 430	0
B:ASP 51	0	A:THR 431	0
B:GLN 52	0	A:LEU 432	0
B:GLY 53	0	A:CYS 433	0
B:PRO 54	0	A:LEU 434	0
B:LEU 55	0	A:THR 435	0
B:ASP 56	0	A:LYS 436	0
B:ILE 57	0	A:ASN 437	0
B:GLU 58	0	A:GLY 438	0
B:TRP 59	0	A:SER 439	0
B:LEU 60	0	A:ILE 440	0
B:ILE 61	0	A:VAL 441	0
B:SER 62	0	A:ASN 442	0
B:PRO 63	0	A:GLY 443	0
B:ALA 64	0	A:ILE 444	0
B:ASP 65	0	A:VAL 445	0
B:ASN 66	0	A:SER 446	0
B:GLN 67	1	A:LEU 447	0
B:LYS 68	1	A:VAL 448	0
B:VAL 69	8	A:GLY 449	0
B:ASP 70	5	A:VAL 450	0
B:GLN 71	1	A:LYS 451	0
B:VAL 72	0	A:GLY 452	0
B:ILE 73	0	A:ASN 453	0
B:ILE 74	0	A:LEU 454	0
B:LEU 75	0	A:LEU 455	0
B:TYR 76	0	A:ASN 456	0
B:SER 77	0	A:ILE 457	0
B:GLY 78	0	A:GLN 458	0
B:ASP 79	0	A:SER 459	0
B:LYS 80	0	A:THR 460	0
B:ILE 81	0	A:THR 461	0
B:TYR 82	0	A:THR 462	0
B:ASP 83	0	A:THR 463	0
B:ASP 84	0	A:VAL 464	0
B:TYR 85	0	A:GLY 465	0
B:TYR 86	0	A:VAL 466	0
B:PRO 87	0	A:HIS 467	0
B:ASP 88	0	A:LEU 468	0

CAR	score	Ad12	score
B:LEU 89	0	A:VAL 469	0
B:LYS 90	0	A:PHE 470	0
B:GLY 91	0	A:ASP 471	0
B:ARG 92	0	A:GLU 472	0
B:VAL 93	0	A:GLN 473	0
B:HIS 94	0	A:GLY 474	0
B:PHE 95	0	A:ARG 475	0
B:THR 96	0	A:LEU 476	0
B:SER 97	0	A:ILE 477	0
B:ASN 98	0	A:THR 478	0
B:ASP 99	0	A:SER 479	0
B:LEU 100	0	A:THR 480	0
B:LYS 101	0	A:PRO 481	0
B:SER 102	0	A:THR 482	0
B:GLY 103	0	A:ALA 483	0
B:ASP 104	0	A:LEU 484	0
B:ALA 105	0	A:VAL 485	0
B:SER 106	0	A:PRO 486	0
B:ILE 107	0	A:GLN 487	0
B:ASN 108	0	A:ALA 488	0
B:VAL 109	0	A:SER 489	0
B:THR 110	0	A:TRP 490	0
B:ASN 111	0	A:GLY 491	0
B:LEU 112	0	A:TYR 492	0
B:GLN 113	0	A:ARG 493	0
B:LEU 114	0	A:GLN 494	0
B:SER 115	0	A:GLY 495	0
B:ASP 116	0	A:GLN 496	0
B:ILE 117	0	A:SER 497	0
B:GLY 118	0	A:VAL 498	0
B:THR 119	0	A:SER 499	0
B:TYR 120	0	A:THR 500	0
B:GLN 121	0	A:ASN 501	0
B:CYS 122	0	A:THR 502	0
B:LYS 123	1	A:VAL 503	0
B:VAL 124	0	A:THR 504	0
B:LYS 125	0	A:ASN 505	0
B:LYS 126	0	A:GLY 506	0
B:ALA 127	0	A:LEU 507	0
B:PRO 128	0	A:GLY 508	0
B:GLY 129	0	A:PHE 509	0
B:VAL 130	0	A:MET 510	0
B:ALA 131	0	A:PRO 511	0
B:ASN 132	0	A:ASN 512	0
B:LYS 133	0	A:VAL 513	0
B:LYS 134	1	A:SER 514	1
B:ILE 135	0	A:ALA 515	0
B:HIS 136	0	A:TYR 516	0
B:LEU 137	0	A:PRO 517	3
B:VAL 138	0	A:ARG 518	0
B:VAL 139	0	A:PRO 519	2
B:LEU 140	0	A:ASN 520	8
B:VAL 141	0	A:ALA 521	0
B:LYS 142	0	A:SER 522	1
B:PRO 143	0	A:GLU 523	4
B:SER 144	0	A:ALA 524	0
B:GLY 145	0	A:LYS 525	0
B:ALA 146	0	A:SER 526	0
		A:GLN 527	0
		A:MET 528	0
		A:VAL 529	0
		A:SER 530	0
		A:LEU 531	0
		A:THR 532	0
		A:TYR 533	0
		A:LEU 534	0

Ad5 and Ad12 knob amino acid sequences are homologous.

Figure 5: Alignment of Ad5 and Ad12 knob sequences. Fiber knob sequences (Uniprot accession numbers P11818 and P36711) are depicted with coloured amino acids that are important for CAR-knob interaction. Amino acids involved in CAR D1 binding are coloured (Figure 8 interface 1 orange, interface 2 magenta).

CAR-based peptides, Ad1, and a mix of seven different peptides (CAR1, 2, 4, 5, 6, 7, and Ad1) were tested for their cytotoxicity using an MTT assay and FixVi staining.

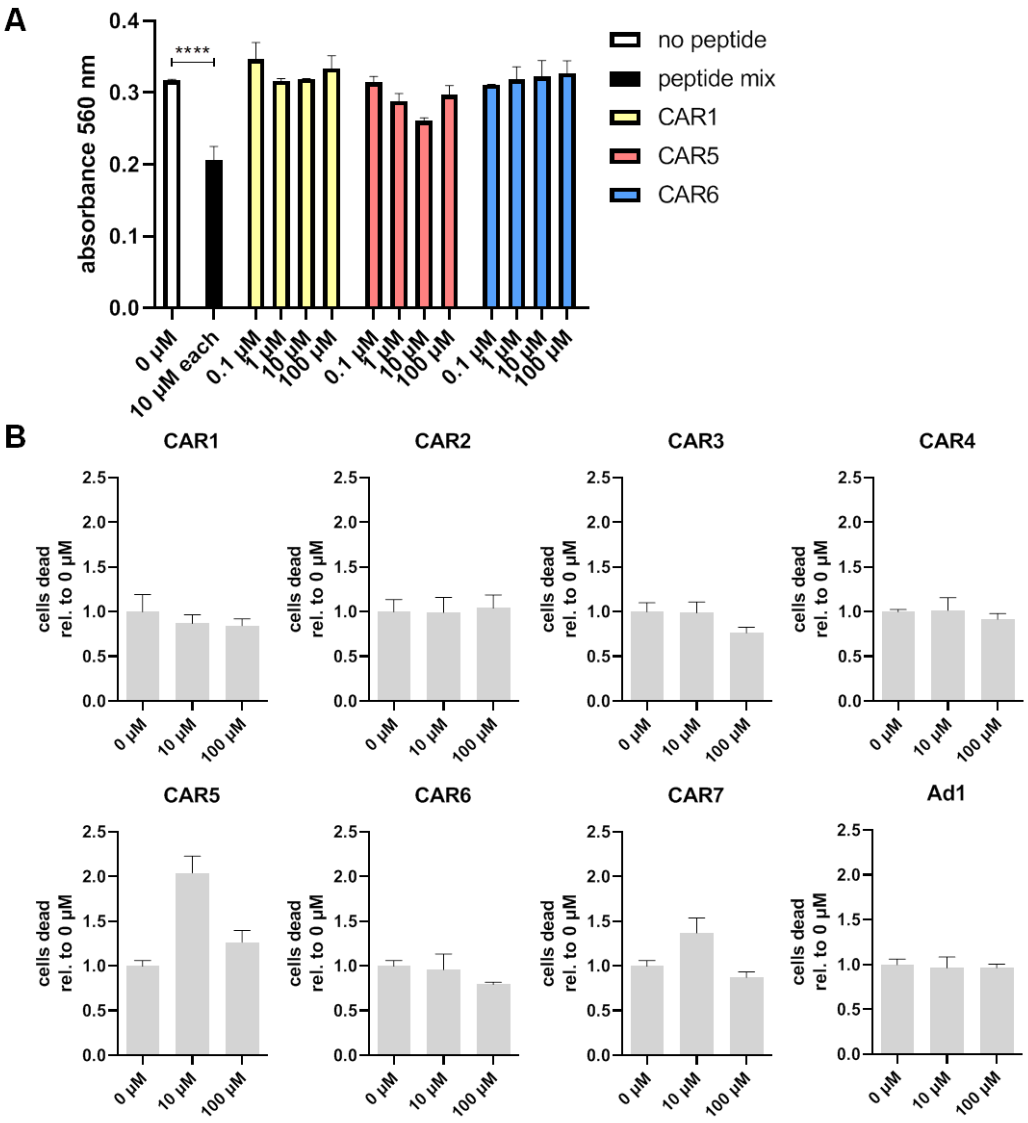

Figure 6: Tests for peptide cytotoxicity. A) MTT assay for A549 cell viability test after 2 h treatment with a mix of CAR1, 2, 4, 5, 6, 7, and Ad1 (each peptide in a concentration of 10 µM) and one of the peptides CAR1, 5, 6 (concentration ranged from 0.1 to 100 µM). As control, no peptide was added (0 µM). MTT reduction by mitochondria was measured at 560 nm to detect the formazan product. Less formazan dye indicates less reduction by mitochondria, thereby less viable cells. Only the peptide mix resulted in a significant decrease in cell viability compared to cells that were not treated with peptides (ANOVA with multiple comparisons). Each condition was measured as technical triplicate and bars show mean±SEM. B) Flow cytometry analysis for A549 cell viability after 1 h peptide treatment (10 and 10 µM) using FixVi staining. No striking dose-dependent effect on cell viability was observed for the peptides. Each condition was measured as technical triplicate and bars show mean±SEM.

Peptides also did not inhibit adenovector transduction, when cells were challenged with MOI=500 for 1 h or with MOI=1000 for 30 min.

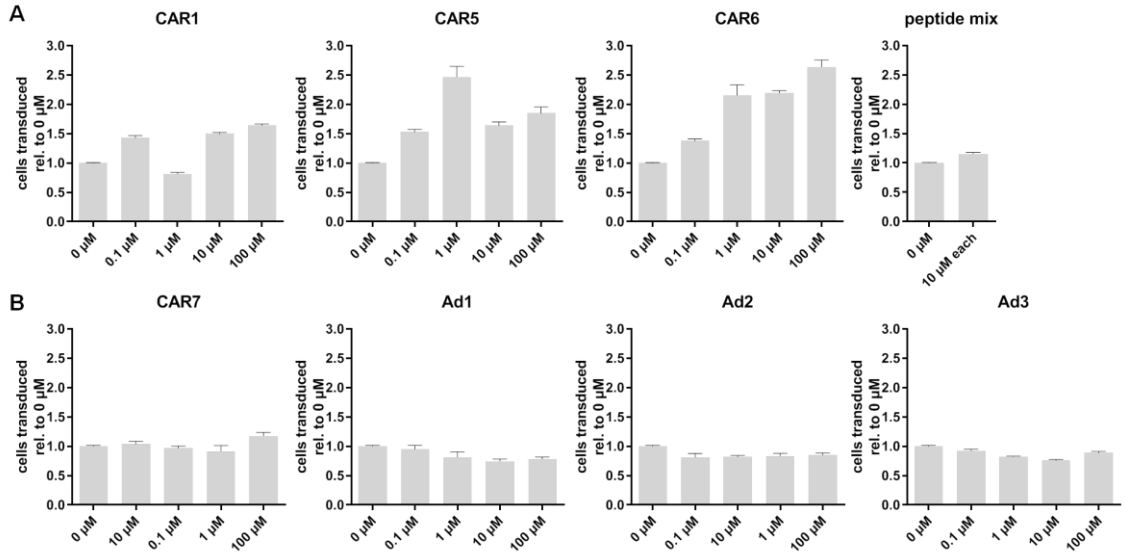

Figure 7: Peptide treatment of Ad5-GFP and A549 cells did not decrease transduction efficiency, when cells were challenged with a lower MOI or for a shorter period of time. Ad5 vectors and A549 cells were preincubated with peptides at indicated concentrations for 1 h. Ad5-peptide mixtures were then added to the cell culture medium with a MOI of 500 for 1 h (A), or with a MOI of 1000 for 30 min (B), before cell culture medium was exchanged. Transgene expression was determined the next day (GFP readout with flow cytometry). Transduction efficiency was normalised to probes without peptide addition (0 µM). Furthermore, a mix of peptides CAR1, CAR2, CAR4, CAR5, CAR6, CAR7, and Ad1 (each peptide in a concentration of 10 µM) was added to cells and vectors. No obvious dose-dependent decrease in Ad5-GFP transduction could be observed for a single peptide or the peptide mix. Each experiment was performed as technical triplicate and bars show mean±SEM.

4 CAR-shedding

MMP catalytic domains and serine proteases were active and cleaved artificial substrates. MMP-11 activity was severely reduced compared to other MMPs, however, it is known to have an unique substrate preference and to cleave normal MMP substrates only ineffectively (MOTRESCU & RIO 2008).

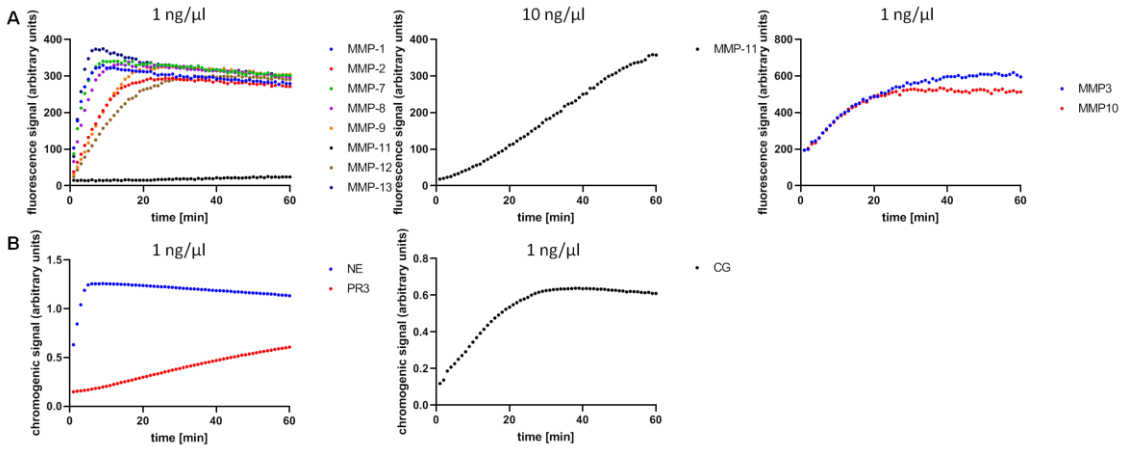

Figure 8: Substrate tests for protease activity. MMPs and serine proteases were active at a concentration of 1 ng/µl, except MMP-11, which showed only a low activity at 1 ng/µl, but was more active at 10 ng/µl. A) MMP-3 and MMP-10 needed another fluorescent substrate as the other MMP domains. B) CG cleaved another chromogenic substrate as NE and PR3.

rhECD ran as a double band in the gel with a smaller, and less abundant product. This band might represent a differentially glycosylated form of full-length rhECD, since it disappeared upon deglycosylation.

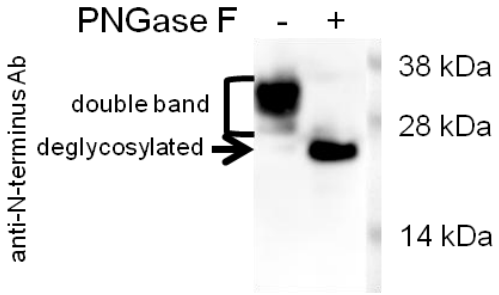

Figure 9: Deglycosylation of rhECD results in a sharper band in Western blot compared to glycosylated rhECD

rhECD was digested with NE. Some samples were deglycosylated with PNGase F. Proteins were loaded on a polyacrylamide gel and tryptically in-gel digested. Tryptic peptides were identified using nLC-MS/MS.

Table 5: Peptides identified by nLC-MS/MS. For each peptide, its position in the protein sequence, its modifications, and the number of peptide spectrum matches (PSMs) are listed. For NE digests, full-length rhECD, intermediate and end products were analysed. For CG digests, full-length rhECD and end product were measured. Peptides only found in deglycosylated samples are marked in grey.

Peptide sequence	Position	Modification	Found in sample [#PSMs]				
			NE digest			CG digest	
			full-length rhECD (n=5)	intermediate product (n=4)	end product (n=5)	full-length rhECD (n=2)	end product (n=2)
[-].LSITTPEEMIEK.[A]	1-12	1xOxidation [M 9]	239	144	104	149	32
		1xAcetyl [N-Term]	200	143	149	104	57
		1xAcetyl [N-Term]; 1xOxidation [M 9]	20	13	17	9	4
			25	31	32	7	9
[-].LSITTPEEMIEKAK.[G]	1-14	1xOxidation [M 9]	32	25	38	12	13
		1xAcetyl [N-Term]	50	52	55	15	26
		1xAcetyl [N-Term]; 1xOxidation [M 9]		2	5		
					2		
[K].AKGETAYLPCK.[F]	13-23		13	7	2		
[K].FTLSPEDQGPLD.[I]	24-35				2		
[K].FTLSPEDQGPLDIEWLISPADNQK.[V]	24-47		147	14	15	110	
[F].TLSPEDQGPLDIEWLISPADNQK.[V]	25-47		3			3	
[L].DIEWLISPADNQK.[V]	35-47		2				
[D].IEWLISPADNQK.[V]	36-47				4		
[K].VDQVIILYSGDK.[I]	48-59		65	36	35	24	12
[K].VDQVIILYSGDKIYDD.[Y]	48-63				2		
[K].VDQVIILYSGDKIYDDYYPDLK.[G]	48-69		257	47	60	205	13
[K].VDQVIILYSGDKIYDDYYPDLKGR.[V]	48-71		58	30	44	55	2
[D].QVIILYSGDKIYDDYYPDLK.[G]	50-69		2				
[L].YSGDKIYDDYYPDLK.[G]	55-69		11	10	7	4	2
[Y].SGDKIYDDYYPDLK.[G]	56-69		15	17	10	7	3
[Y].SGDKIYDDYYPDLKGR.[V]	56-71		3	5	5	2	
[K].IYDDYYPDLK.[G]	60-69		9	4		8	2
[K].IYDDYYPDLKGR.[V]	60-71		17	11	16	10	8
[K].GRVHFTSNDLK.[S]	70-80		43	33	34	14	9
[R].VHFTSNDLK.[S]	72-80		144	82	55	93	23
[V].HFTSNDLK.[S]	73-80		4	3		2	
[K].SGDASINVTNLQLSDIGTYQCK.[V]	81-102	1xDeamidated [N/Q]	9	10	8	22	2
		2xDeamidated [N/Q; N/Q]	2				
[K].SGDASINVTNLQLSDIGTYQCKVK.[K]	81-104	1xDeamidated [N/Q]		3			
[K].VKKAPGVANK.[K]	103-112		4			4	

Peptide sequence	Position	Modification	Found in sample [#PSMs]				
			NE digest			CG digest	
			full-length rhECD (n=5)	intermediate product (n=4)	end product (n=5)	full-length rhECD (n=2)	end product (n=2)
[K].APGVANKKIHLVVLVKP.[S]	106-122				12		
[K].APGVANKKIHLVVLVKPSGAR.[C]	106-126		20	4		8	
[A].PGVANKK.[I]	107-113			2		4	
[K].KIHLVVLVK.[P]	113-121					3	
[K].KIHLVVLVKP.[S]	113-122				34		
[K].KIHLVVLVKPSGA.[R]	113-125					3	
[K].KIHLVVLVKPSGAR.[C]	113-126		318	64		109	
[K].IHLVVLVKPSGA.[R]	114-125				2		
[K].IHLVVLVKPSGAR.[C]	114-126		200	71	2	119	21
[H].LVVLVKPSGAR.[C]	116-126					2	
[R].CYVDGSEEIGSDFK.[I]	127-140		18	9			
[K].IKCEPKEGSLPLQYEWQK.[L]	141-158		5	2		7	
[K].EGSLPLQYEWQK.[L]	147-158		189	122		85	
[K].EGSLPLQYEWQKLSDSQK.[M]	147-164		10	4		2	
[K].LSDSQKMPTSWLAEMTSSVISVK.[N]	159-181		9			5	
		1xOxidation [M]	23			10	
		2xOxidation [M7; M15]	21			7	
[K].MPTSWLAEMTSSVISVK.[N]	165-181		128			111	
		1xOxidation [M]	195			123	
		2xOxidation [M1; M9]	118	2		51	
[W].LAEMTSSVISVK.[N]	170-181		2			0	
		1xOxidation [M4]	5			4	
[K].NASSEYSGTYSCTVR.[N]	182-196		2			0	
		1xDeamidated [N1]	34	4		8	
[K].NASSEYSGTYSCTVRNR.[V]	182-198	1xDeamidated [N1]	4			0	
[R].NRVGSDQCLLR.[L]	197-207		7			5	
[R].VGSDQCLLR.[L]	199-207		13			11	
[R].VGSDQCLLRLNVVPPSNK.[A]	199-216		3			0	
[R].LNVVPPSNKAGHHHHHH.[-]	208-224		31			7	
		1xDeamidated [N8]	2			8	

rhECD and end product of CG digest were analysed with nLC-MS/MS. Peptides are listed in Table 5 in Appendix.

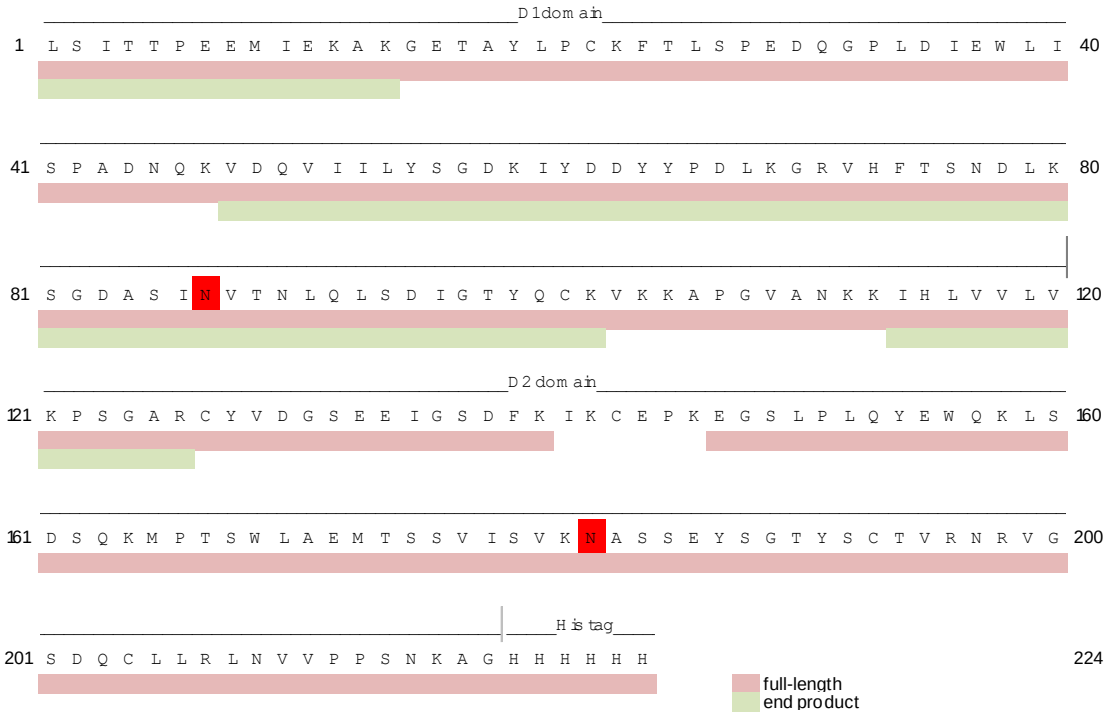

Figure 10: Sequences of full-length rhECD end product of CG digest covered by peptides (nLC-MS/MS). Coverage of full-length CAR is coloured in red, coverage of the end product is coloured in green. The end product consists of D1 domain and a small part of D2 domain. N-glycosylation sites are marked in red.

Amino acids sequences of human and murine extracellular CAR D2 domains are 88 % identical.

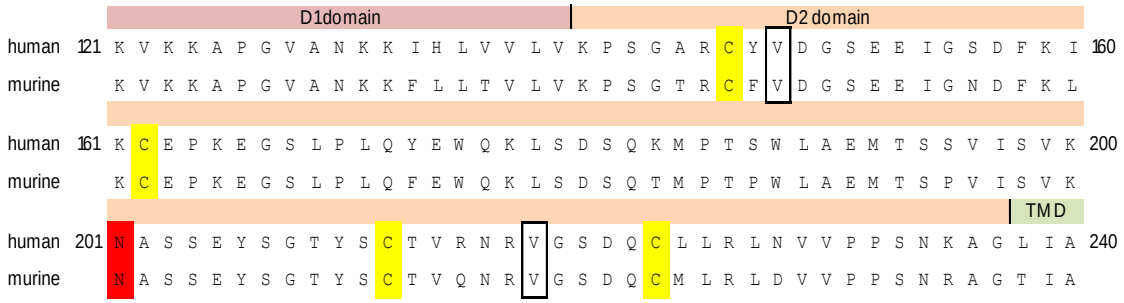

Figure 11: Alignment of human and murine CAR D2 domain. Human CAR (Uniprot accession number P78310) and murine CAR (Uniprot accession number P97792) are 88 % identical in their D2 domains. Possible sites for NE cleavage are framed. Glycosylation site is marked in red and cysteines involved in disulfide bonds are marked in yellow.

When no ethanol was added to CHO-CAR lysate, NE and PR3 digest resulted in the same pattern as when ethanol was present in the sample.

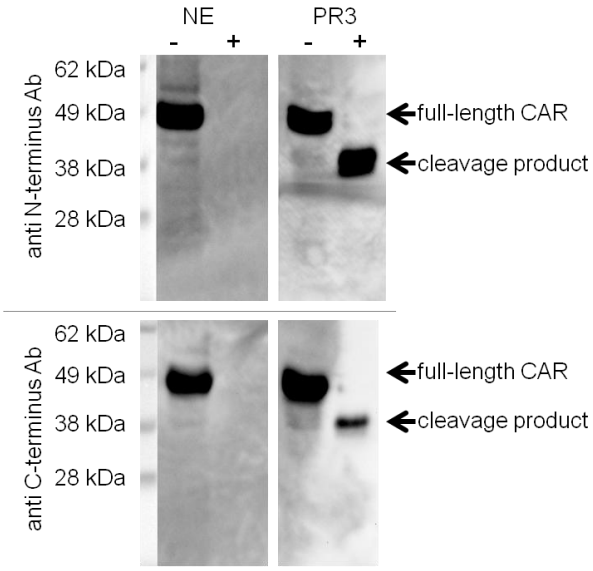

Figure 12: Ethanol addition did not influence NE and PR3 digest of human CAR expressed by CHO cells. Lysates of CHO cells were digested overnight with proteases without the addition of ethanol. Cleavage was visualised with N- and C-terminal anti-CAR antibodies. Cleavage products correspond to these seen in Figure 32.

Denatured rhECD was proteolysed extensively within 30 min NE treatment.

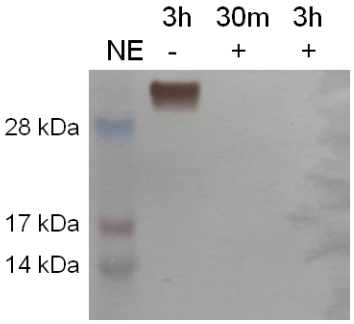

Figure 13: Denatured rhECD was cleaved extensively by NE. Incubation of rhECD with PNGase F denaturing buffer (0.5 % SDS, 40 mM DTT, 1 % Nonidet P40) resulted in extensiv proteolysis by NE already within 30 min as seen in a silver-stained gel.

Anti-CAR antibodies 3C100 or RmcB did not stain CHO mock cells unspecifically.

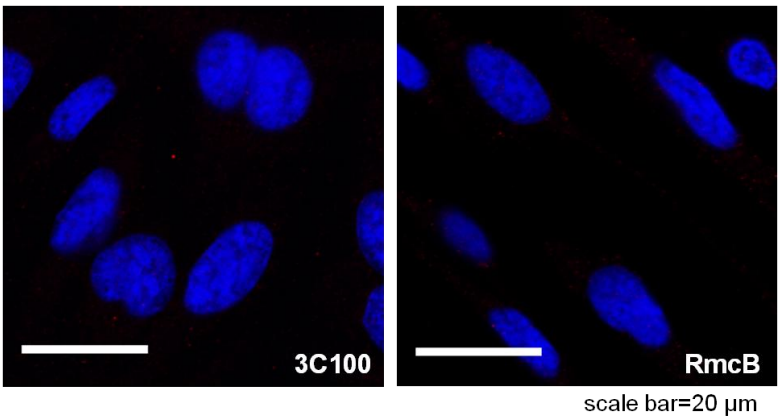

Figure 14: CHO mock cells were not stained by anti-CAR antibodies 3C100 and RmcB. Monoclonal CHO mock cells were stained with 3C100 or RmcB and secondary anti-mouse Cy3-conjugated antibody. As expected, no fluorescence signal was detected.

NE was active in Ham´s F-12. rhECD seemed to alter its conformation in Ham´s F-12, since the counter product occurred within 5 min NE treatment (100 ng/µl). This was in contrast to results observed for time series performed with NE assay buffer (Figure 24). Ham´s F-12 contains less NaCl than NE assay buffer (130 mM vs. 500 mM) and is more acidic (7.07-7.4 vs. 7.5), which may influence NE activity.

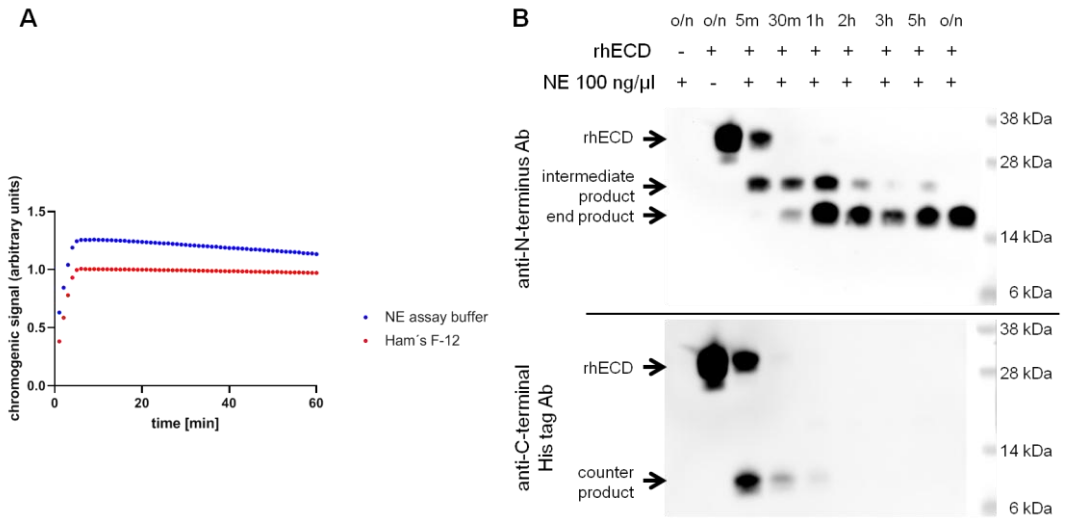

Figure 15: NE was active in Ham´s F-12 medium. A) NE activity was tested with artificial chromogenic substrate in NE assay buffer or Ham´s F-12 medium. B) rhECD was digested with NE in Ham´s F-12 medium.

NE treatment did not permeabilise CHO-CAR cells for anti-vimentin antibody.

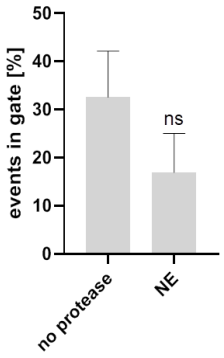

Figure 16: Cells were not permeabilised for antibodies by NE treatment. Cells were treated with NE for 5 h and stained for vimentin. As a control, NE reconstitution buffer was added to cells. The experiment was performed four times and percentage of events in the vimentin-positive gate (defined as including 99 % of events in a permeabilised sample) are shown as mean±SEM. NE treatment did not increase vimentin staining signal, but on the contrary, seemed to decrease vimentin signal albeit non-significantly (t test).

Flow cytometry events can be gated to exclude cell debris and doublet cells. Forward scatter (FS) represents cell size and side scatter (SS) represents cell granularity. Small, less granular events are defined as debris. A doublet event is a single event that actually consists of two independent particles. A pulse can be defined by its area, its height, and its width. By plotting pulse area versus pulse height of FS, one can identify doublets by gating events that do not show a linear relationship between those parameters. Pulse area and pulse width are larger for doublet events than they are for singlet events.

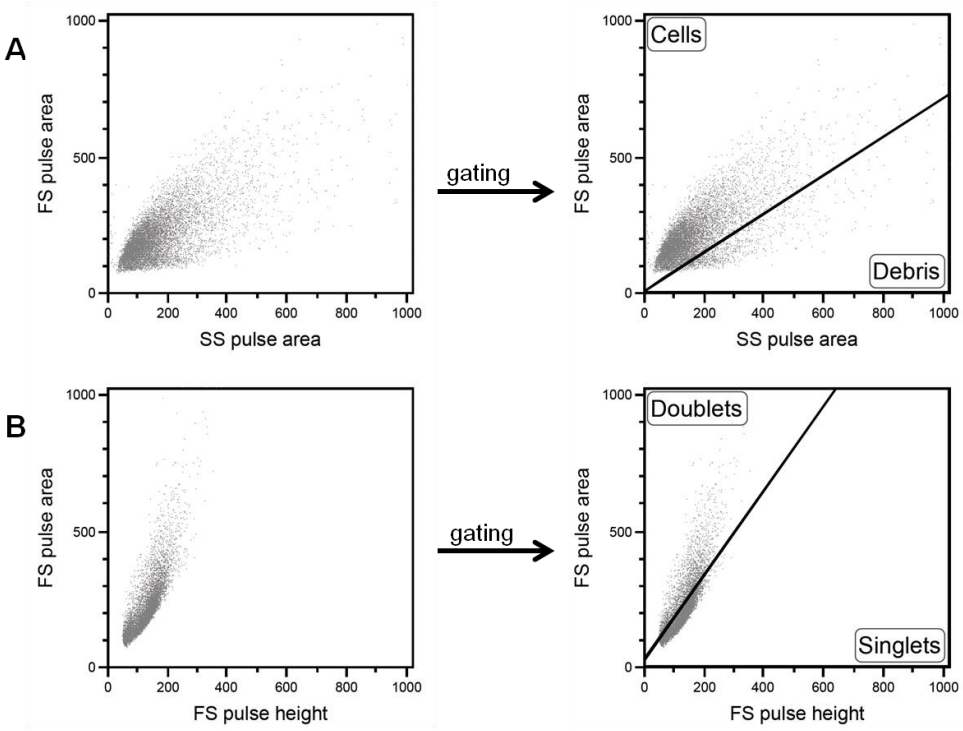

Figure 17: Gating strategies for flow cytometry. Representative dot plots of CHO-CAR cells. A) In order to exclude debris, events were gated by displaying pulse areas of forward scatter (FS) and side scatter (SS). B) Doublet events were excluded in a plot of FS pulse area versus FS pulse height.

Median would be no suitable measurement for CAR surface expression as seen with HepG2 cells. In this example, CAR level decreased by 23 %, when median values were measured, but by 57 %, when geometric mean values were examined.

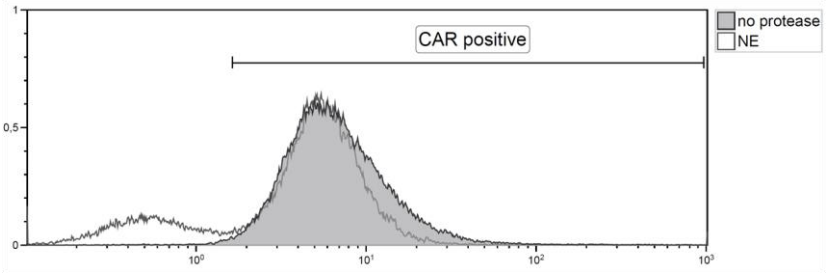

Figure 18: NE treatment of HepG2 cells results in a CAR-negative subpopulation. Cells were treated with NE in NE reconstitution buffer (100 ng/µl) or with reconstitution buffer alone (no protease) for 15 min and stained for CAR.

Gating of flow cytometry events did not influence decrease of CAR surface level.

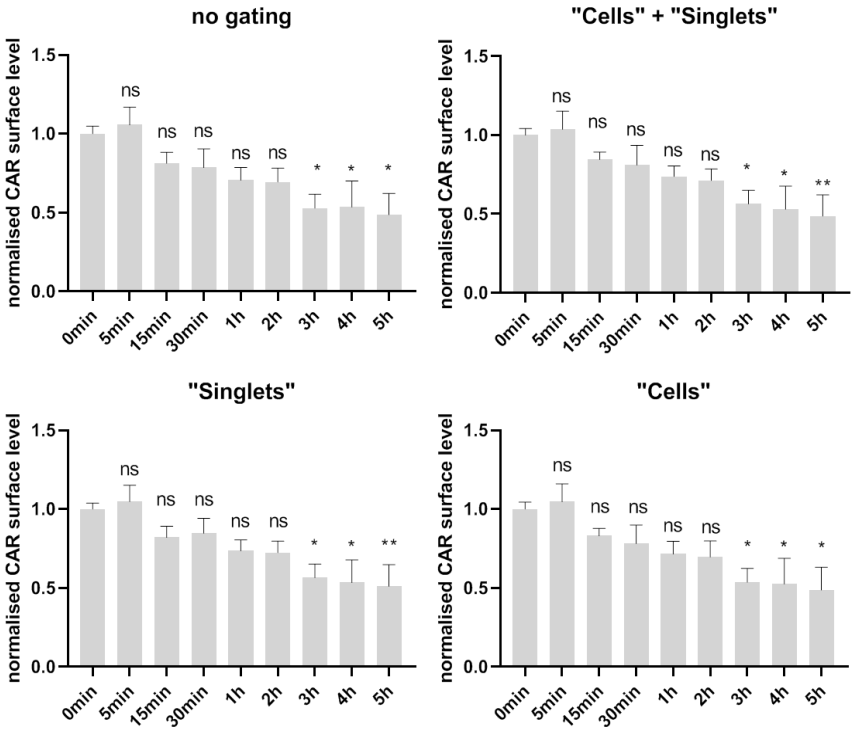

Figure 19: Gating strategies had no major influence on results of CAR surface level decrease in CHO-CAR cells upon NE treatment. Cells were incubated for different incubation times with or without NE and stained for CAR. CAR surface levels (geometric mean) of NE-treated cells were normalised to CAR levels of untreated cells. Furthermore, relative CAR levels of time point t=0 were set as 1. Gating for “Singlets”, “Cells”, or both had no major influence on data points compared to ungated events (ANOVA with multiple comparisons).

CAR signals measured by flow cytometry of NE treated CHO-CAR cells exceeded those of untreated cells at short incubation periods. Anti-CAR antibody seemed to have better access to CAR.

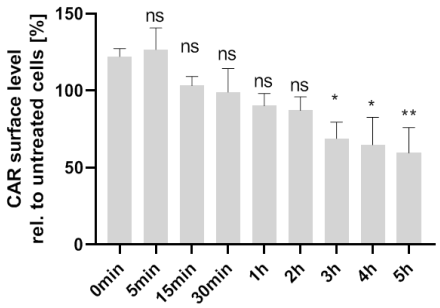

Figure 20: CAR surface expression in CHO-CAR upon NE treatment facilitated antibody recognition. Cells were incubated for different time points with or without NE and stained for CAR. CAR surface levels (geometric mean, gates "Cells" and "Singlets") of NE-treated cells were normalised to CAR levels of untreated cells. Significances were calculated with ANOVA with multiple comparisons. Addition of NE to cells for short time points results in better CAR-recognition by anti-CAR antibody compared to cells that were not treated with NE.

Immunofluorescence staining of non-permeabilised cells visualised only extracellular, but not intracellular proteins.

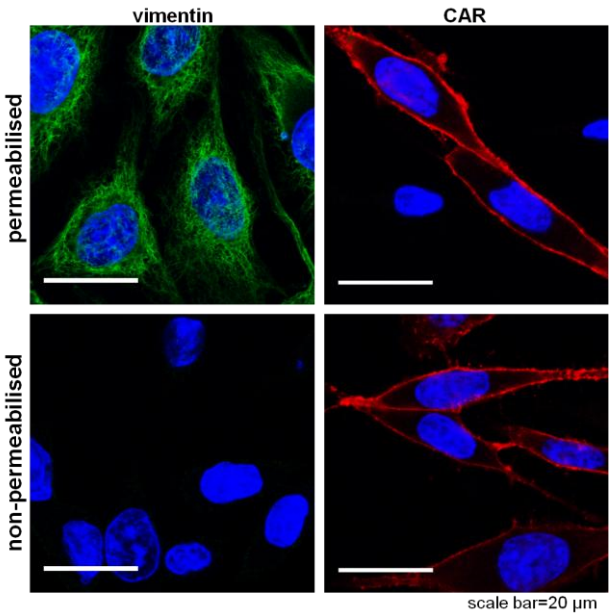

Figure 21: Immunofluorescence staining distinguished between intracellular and extracellular localisation of a protein. CHO-CAR cells were either permeabilised (top row) or non-permeabilised (bottom row) before anti-vimentin (green) or anti-CAR (red) staining. As expected, intracellular vimentin was not stained, when cells were not permeabilised. In contrast, CAR that is expressed intracellularly, but also on the cell surface was stained in both permeabilised and non-permeabilised cells.

DANKSAGUNG

Ohne die Unterstützung zahlreicher Personen hätte die vorliegende Arbeit nicht realisiert werden können. Für die vielfältig erfahrene Hilfe möchte ich mich an dieser Stelle sehr herzlich bedanken.

Ich danke Herrn Prof. Dr. Volker Rudolph für die Möglichkeit, diese Dissertation am HDZ anfertigen zu dürfen.

Mein besonderer Dank gilt meinem Doktorvater Herrn Prof. Dr. Karsten Niehaus für die wissenschaftliche Betreuung meiner Arbeit und seine wertvollen Anregungen.

Ich danke Herrn Dr. Martin Farr sehr für die interessante Promotionsthematik, seine stete Hilfsbereitschaft und sein großes Engagement. Der konstruktive Austausch und die regelmäßigen Gespräche mit ihm waren stets eine große Hilfe. Durch seine fachlichen Hinweise und tatkräftige Unterstützung hat er wesentlich zum erfolgreichen Abschluss dieser Arbeit beigetragen.

Für die regelmäßigen Gespräche auf fachlicher und persönlicher Ebene danke ich sehr den Mitarbeiterinnen und Mitarbeitern der Arbeitsgruppen im ZFE des HDZ.

Für vielfältige Unterstützung bin ich besonders den externen Arbeitsgruppen dankbar, mit denen ich zusammenarbeiten durfte:

Am Virologischen Institut in Erlangen wurden meine Forschungen durch Herrn Prof. Dr. Matthias Tenbusch, Pascal Irrgang und Dr. Dennis Lapuente entscheidend unterstützt. Besonders danken möchte ich Herrn Adrian Filip, der mit seiner Bachelorarbeit die Infektions- und Transduktionsversuche entscheidend vorangebracht hat.

Sehr danken möchte ich auch Herrn Dr. Raimund Hoffrogge, Frau Larissa Leßmann und Frau Louise Schelletter der Arbeitsgruppe Zellkulturtechnik der Technischen Fakultät der Universität Bielefeld für ihre große Unterstützung bei der Massenspektrometrie und ihr großes Engagement.

Ein besonderer Dank gilt auch Herrn Prof. Dr. Hartmut Niemann von der Fakultät für Chemie der Universität Bielefeld, der mir wertvolle Hilfestellung zum Peptiddesign gegeben hat.

Herr Prof. Dr. Friedrich Herberg, Herr Philipp Henning und Frau Dr. Vanya Uzunova danke ich dafür, dass sie mir die SPR-Messungen in der Universität Kassel ermöglicht haben.

SELBSTSTÄNDIGKEITSERKLÄRUNG

Ich habe diese Dissertation selbst angefertigt, keine Textabschnitte von Dritten oder eigener Prüfungsarbeiten ohne Kennzeichnung übernommen und alle von mir benutzten Hilfsmittel und Quellen in meiner Arbeit angegeben.

Ich habe diese Dissertation noch nicht als Prüfungsarbeit für eine staatliche oder andere wissenschaftliche Prüfung eingereicht.

Ich habe weder die gleiche noch eine in wesentlichen Teilen ähnliche noch eine andere Abhandlung bei einer anderen Hochschule als Dissertation eingereicht.

Bielefeld, 04.12.2020

Leonie Herrmann

Gedruckt auf alterungsbeständigem Papier DIN ISO 9706